Hydrodynamic modeling of RHIC BES

Chun Shen

Brookhaven National Lab

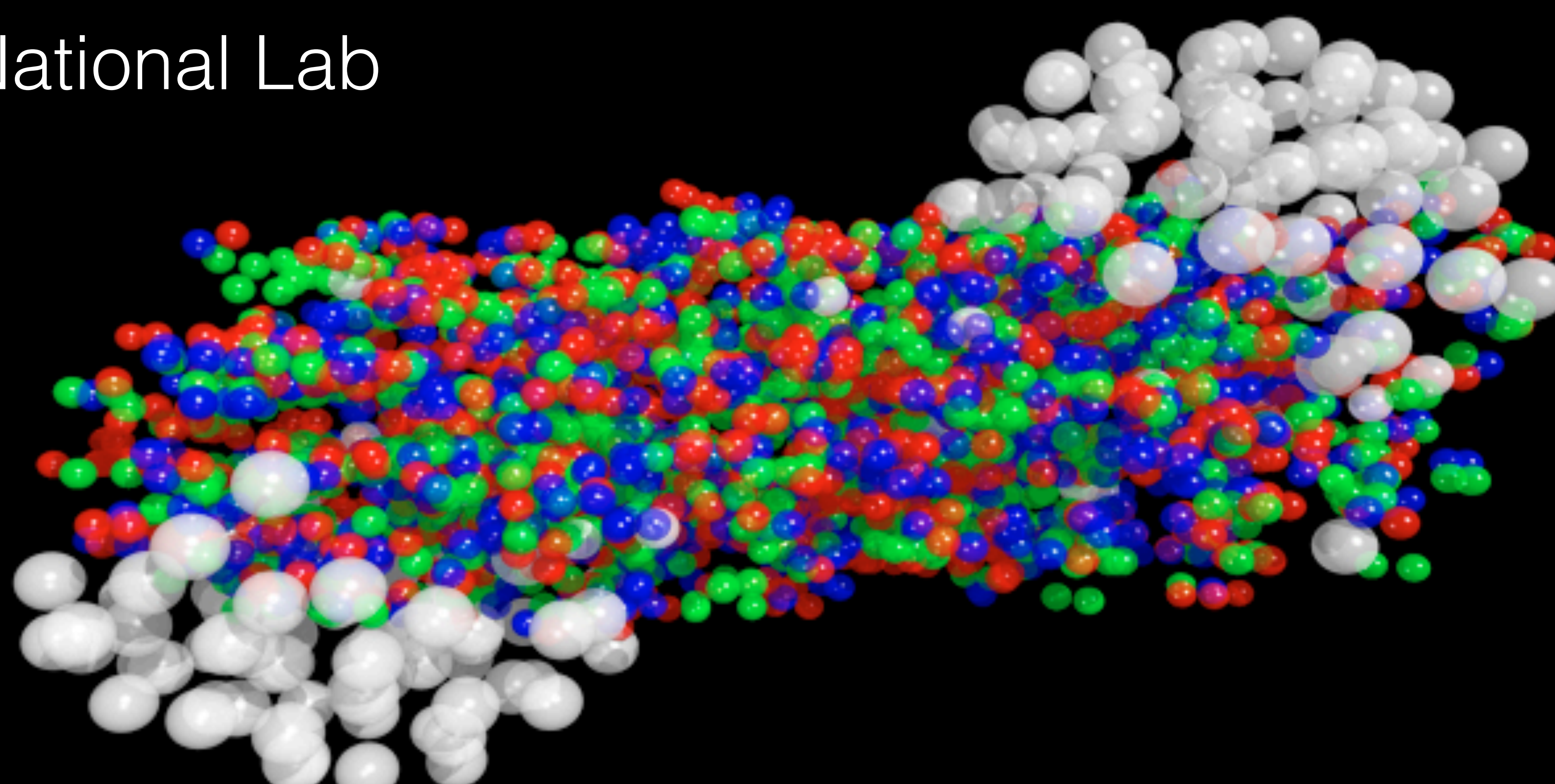

Relativistic Heavy-Ion Collisions

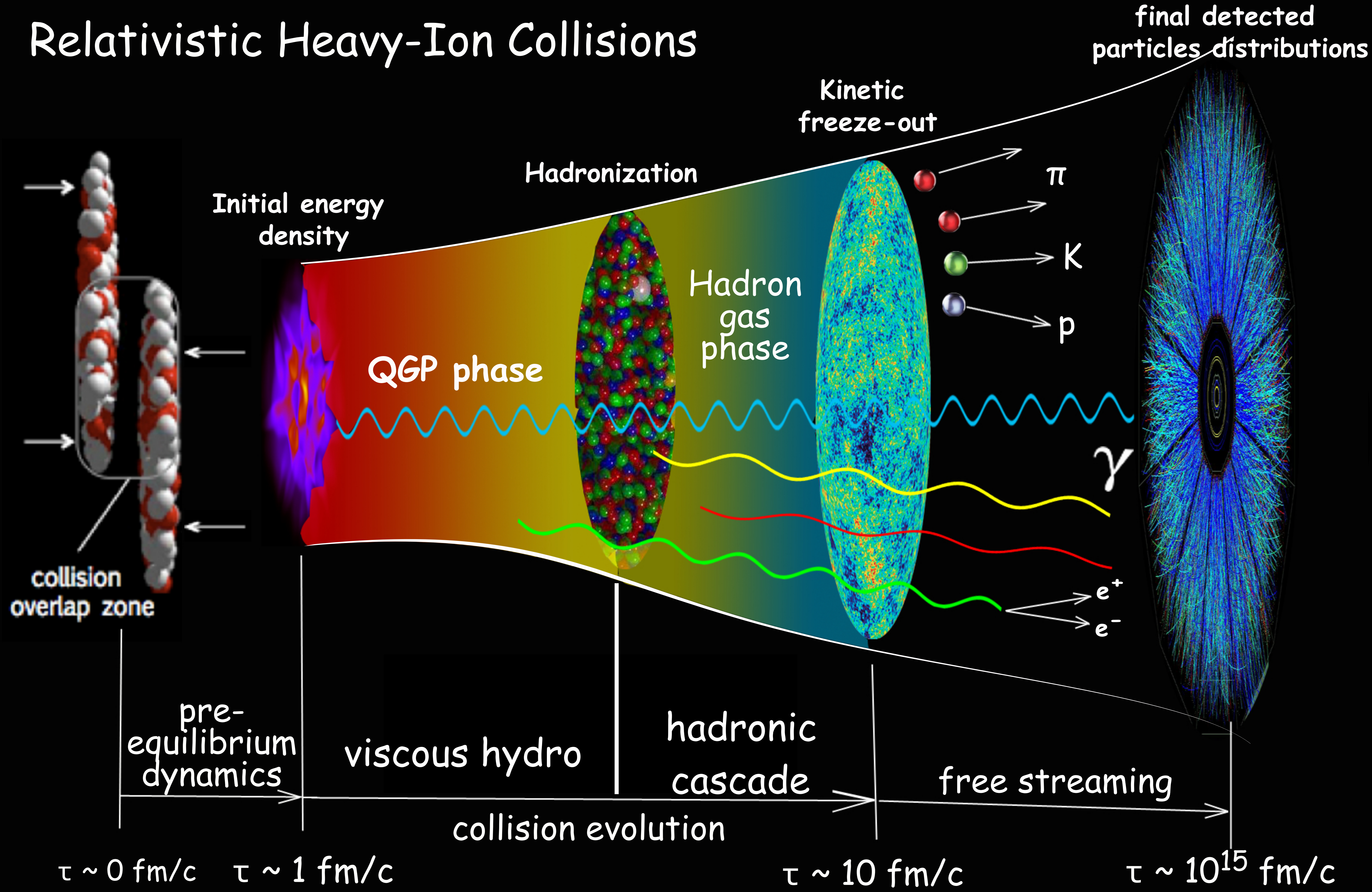

Exploring the phases of QCD

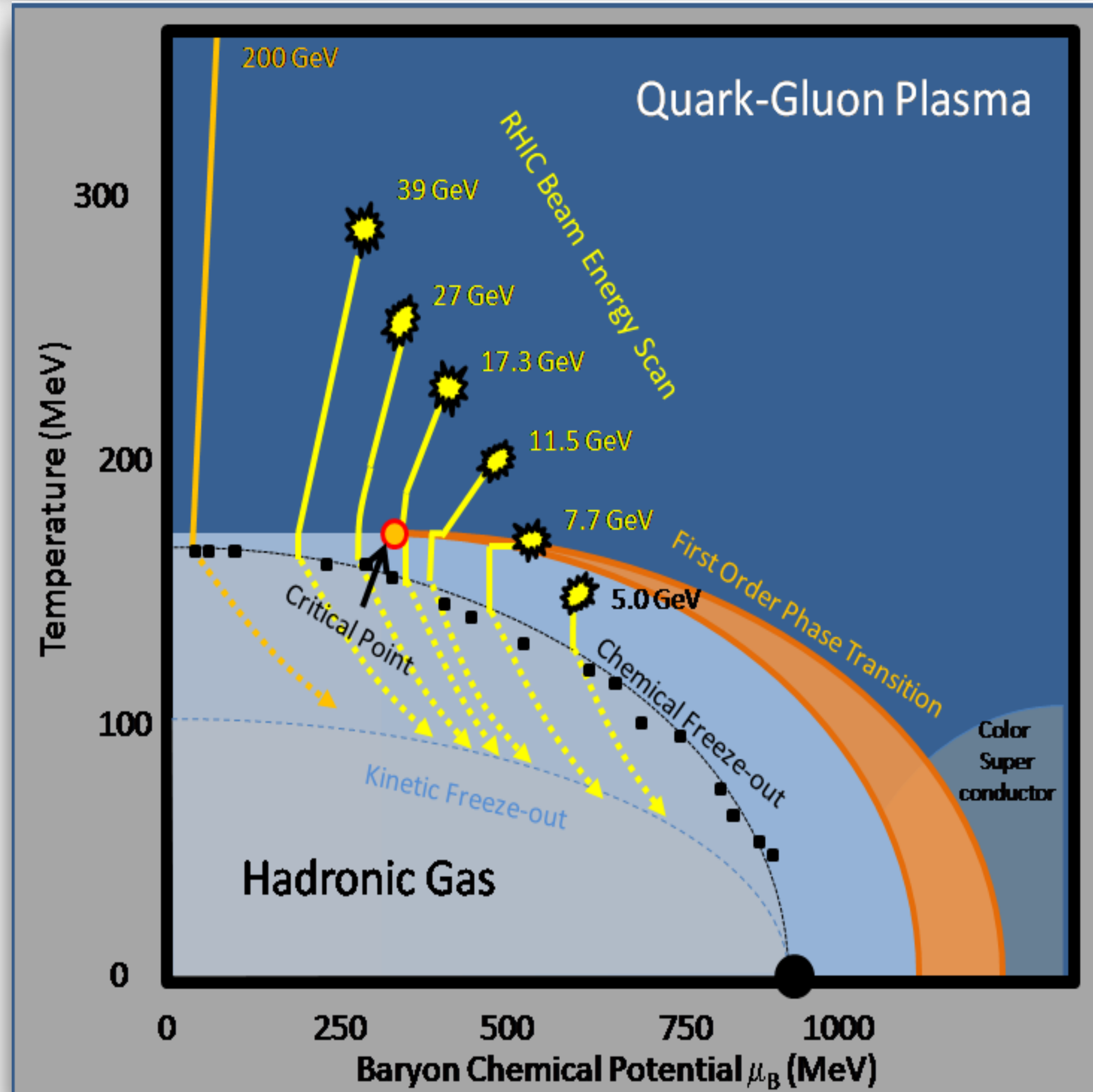

Exploring the phases of QCD

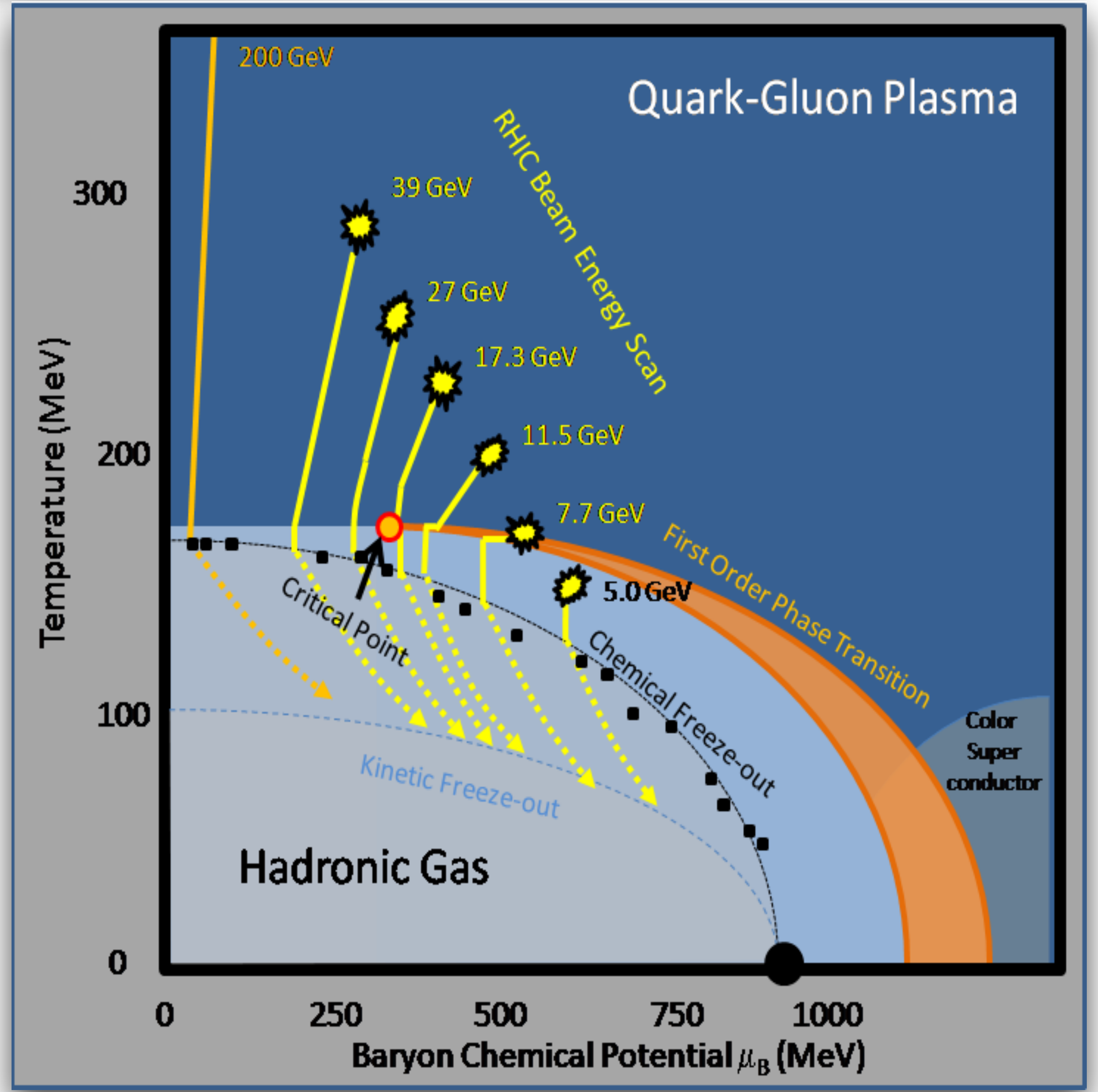

- Event-by-event fluctuating initial conditions
- (3+1)-d dissipative hydrodynamic modelling of the QGP
- Microscopic description for hadronic phase

Exploring the phases of QCD

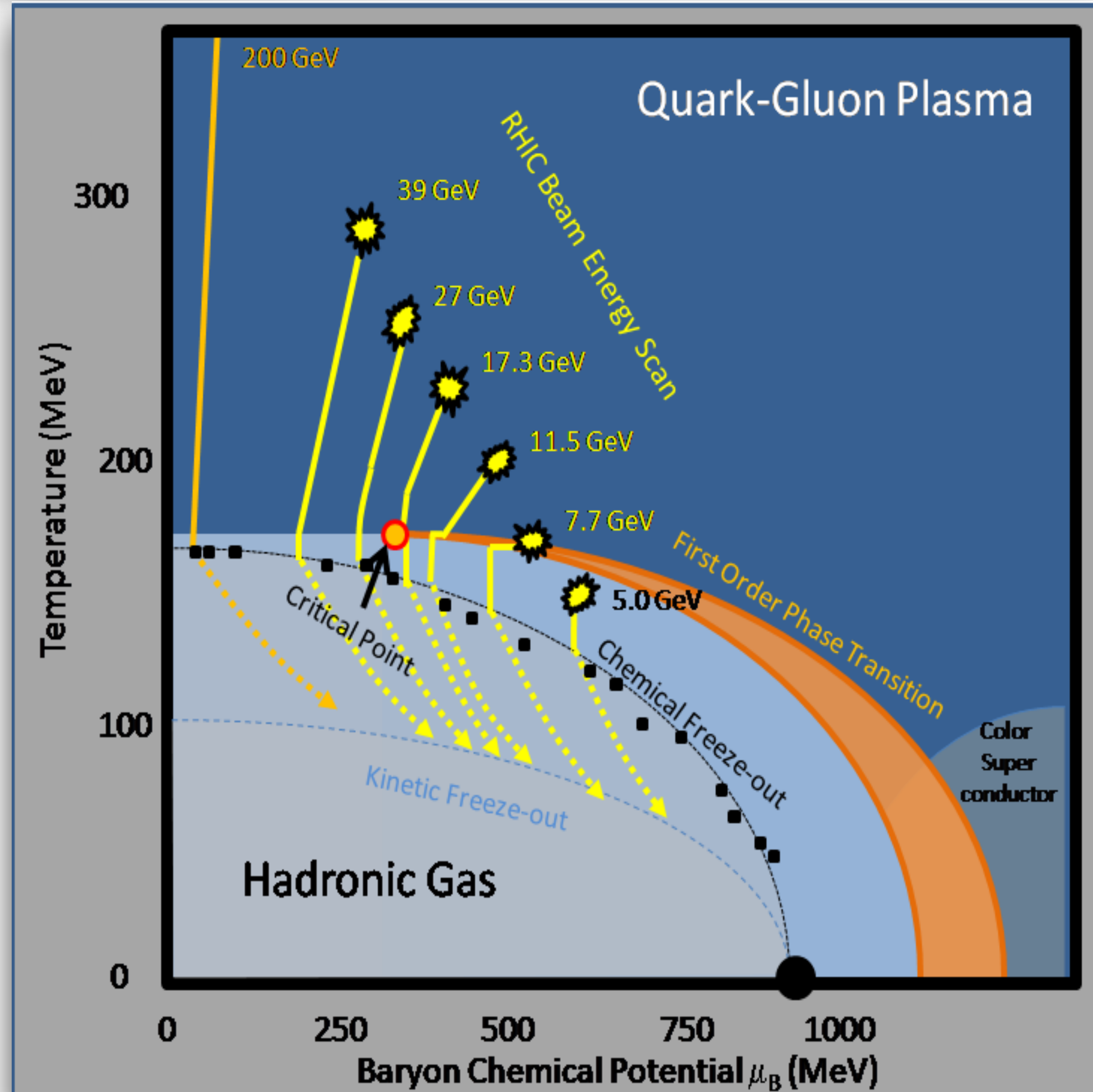

- Event-by-event fluctuating initial conditions

  Glauber-LEXUS

- (3+1)-d dissipative hydrodynamic modelling of the QGP

  MUSIC

- Microscopic description for hadronic phase

  UrQMD/JAM

When to start hydrodynamics?

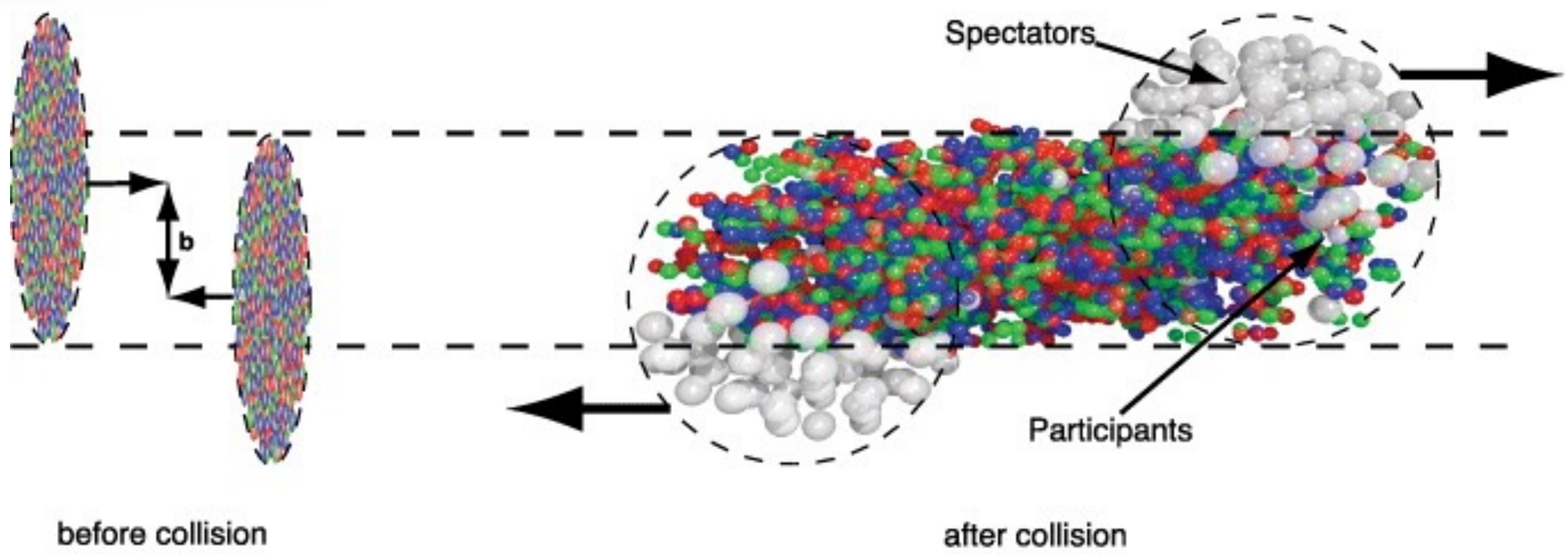

Two nuclei overlapping time

$$\tau \sim \frac{2R}{\gamma v_z}$$

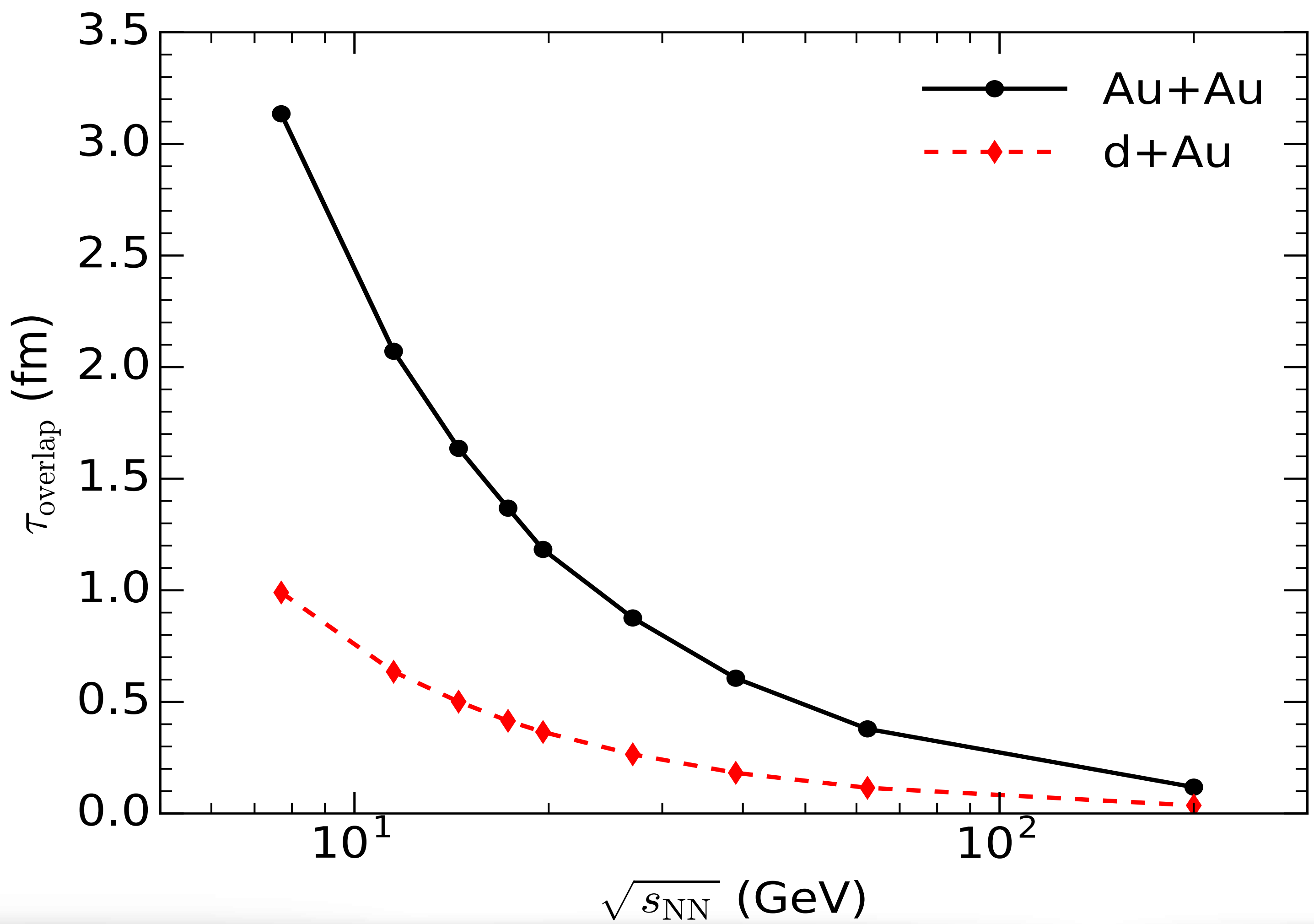

- Nuclei overlapping time is large at low collision energy
- Pre-equilibrium dynamics can play an important role

Go beyond the Bjorken approximation

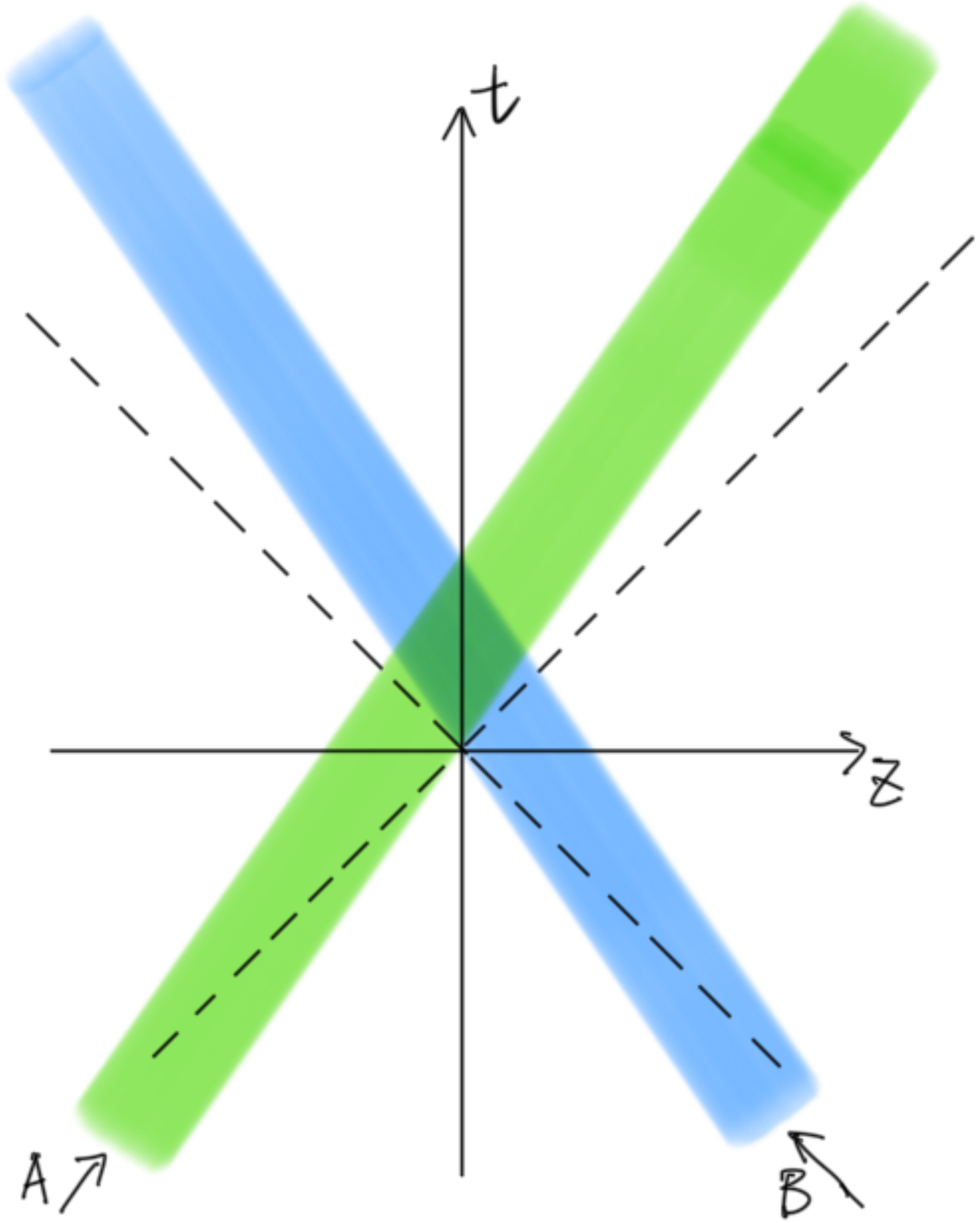

- The finite widths of the colliding nuclei are taken into account

Go beyond the Bjorken approximation

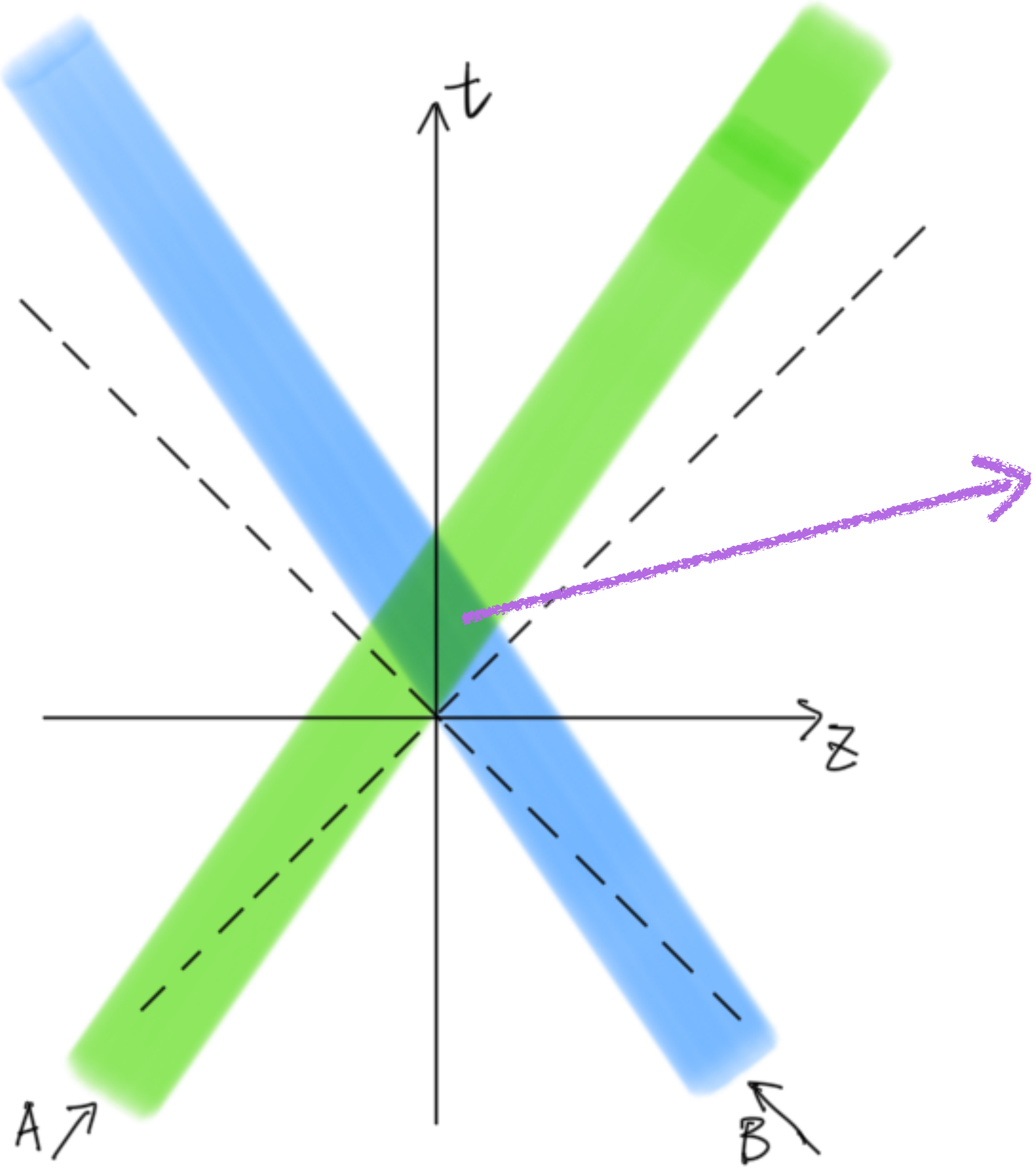

- The finite widths of the colliding nuclei are taken into account

The interaction zone is not point like

$$y \neq \eta_s$$

The 3D MCGlauber-LEXUS model

C. Shen, B. Schenke, in preparation

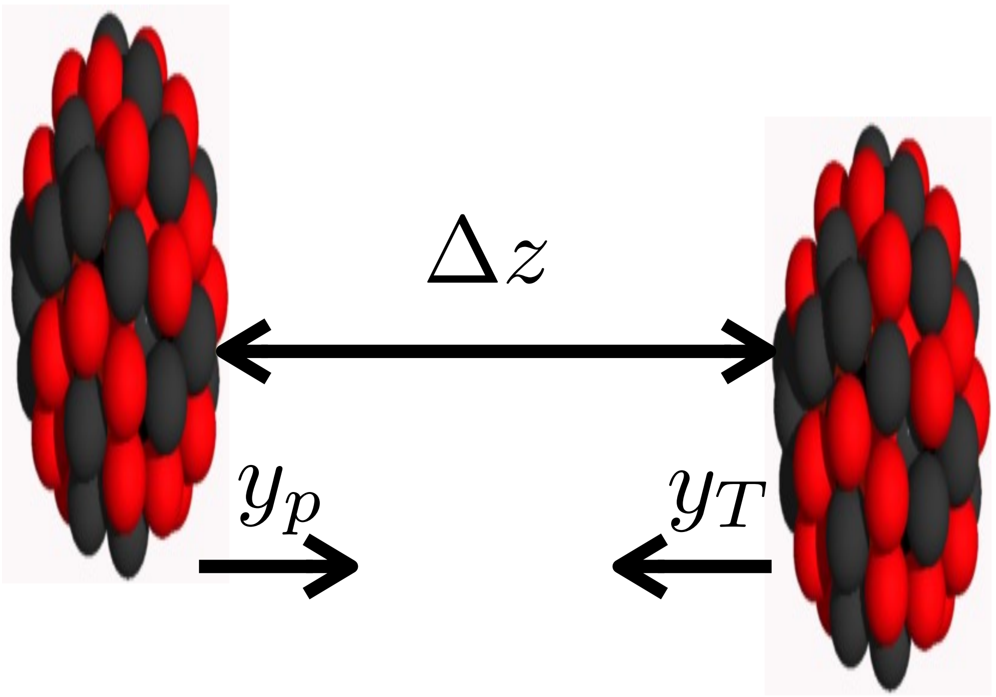

- Collision time and 3D spatial position are determined for every binary collision

The 3D MCGlauber-LEXUS model

C. Shen, B. Schenke, in preparation

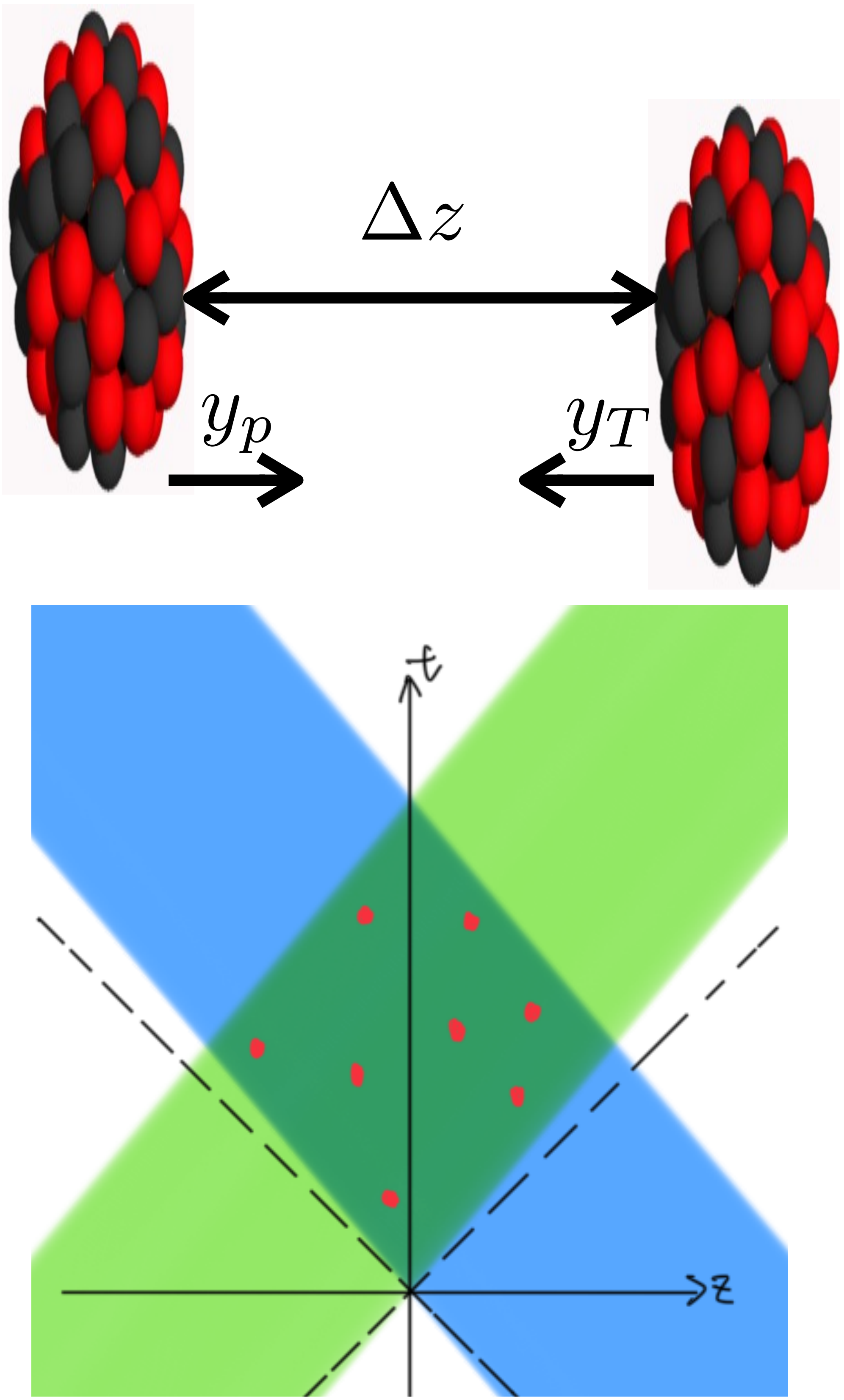

- Collision time and 3D spatial position are determined for every binary collision
- QCD strings are randomly produced from collision points

The 3D MCGlauber-LEXUS model

C. Shen, B. Schenke, in preparation

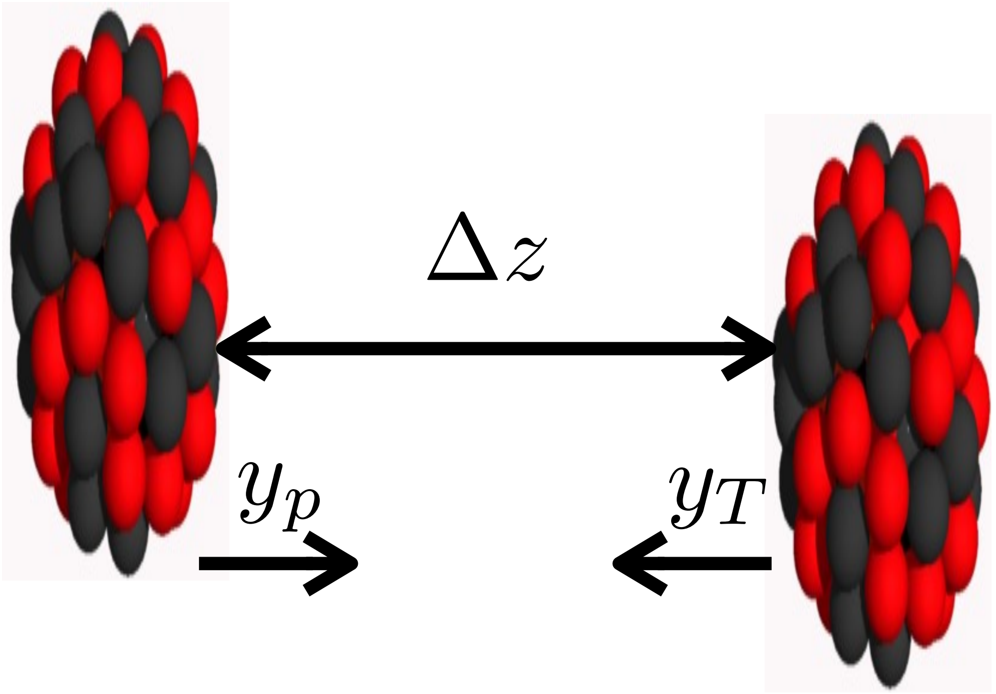

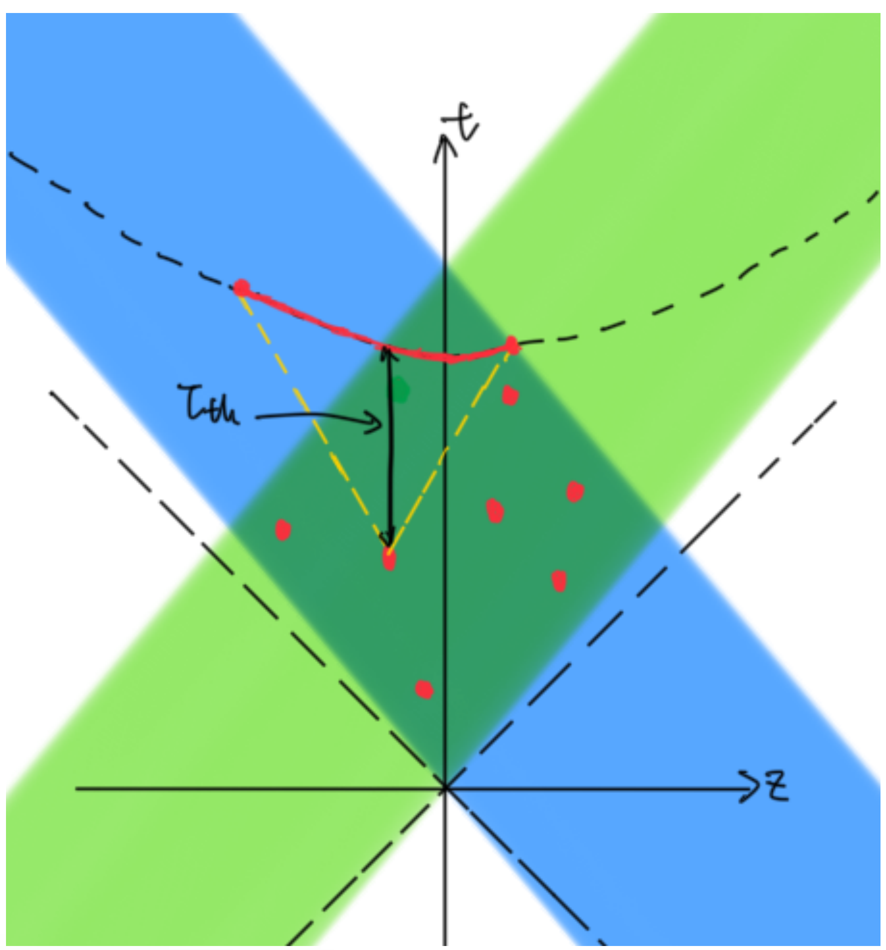

- Collision time and 3D spatial position are determined for every binary collision
- QCD strings are randomly produced from collision points

A. Bialas, A. Bzdak and V. Koch, arXiv:1608.07041 [hep-ph]

- These strings are decelerated with a constant string tension $\sigma = 1 GeV/fm$ before thermalized to medium

The 3D MCGlauber-LEXUS model

C. Shen, B. Schenke, in preparation

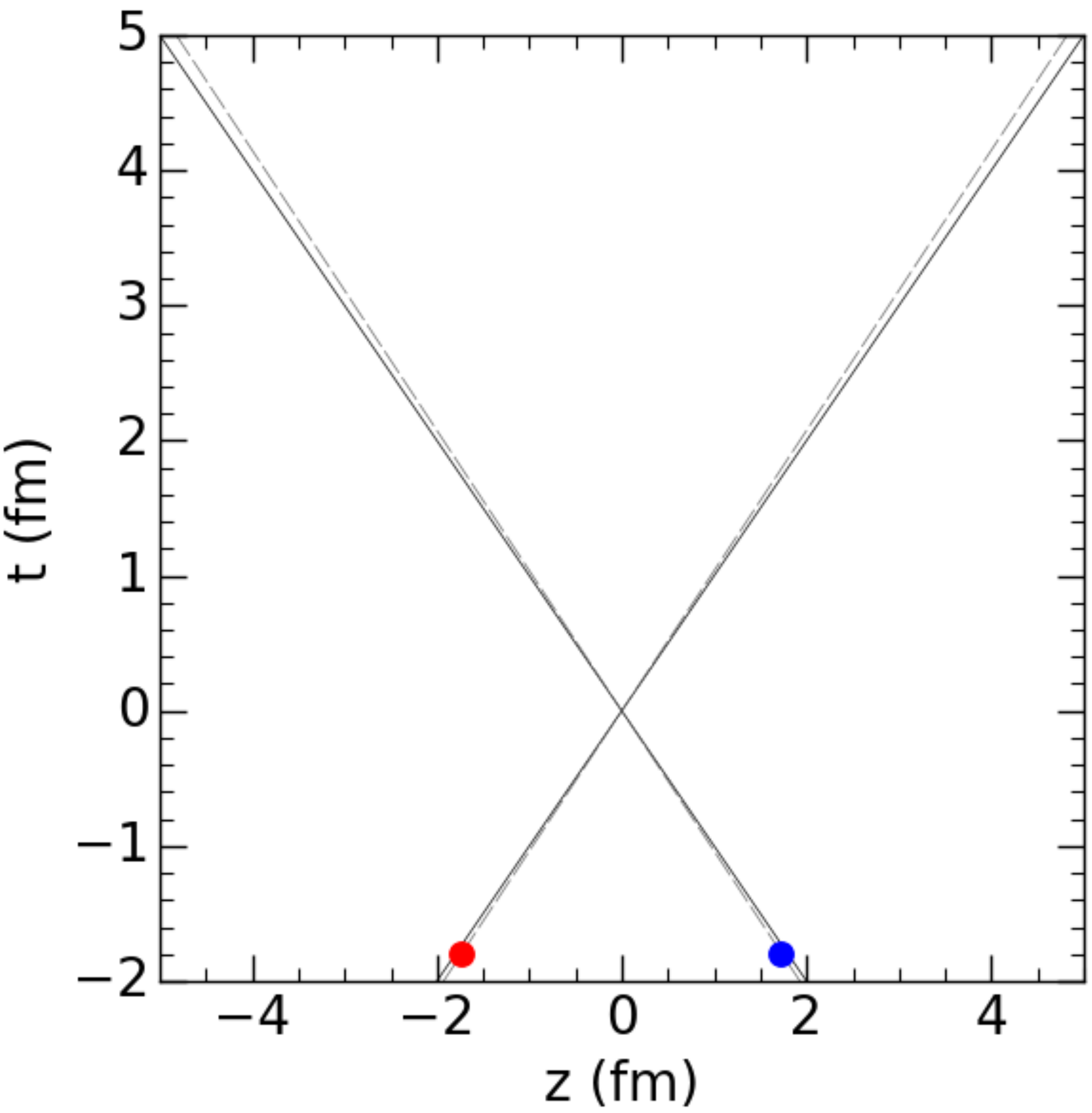

- Collision time and 3D spatial position are determined for every binary collision
- QCD strings are randomly produced from collision points

A. Bialas, A. Bzdak and V. Koch, arXiv:1608.07041 [hep-ph]

- These strings are decelerated with a constant string tension $\sigma = 1 GeV/fm$ before thermalized to medium

The 3D MCGlauber-LEXUS model

C. Shen, B. Schenke, in preparation

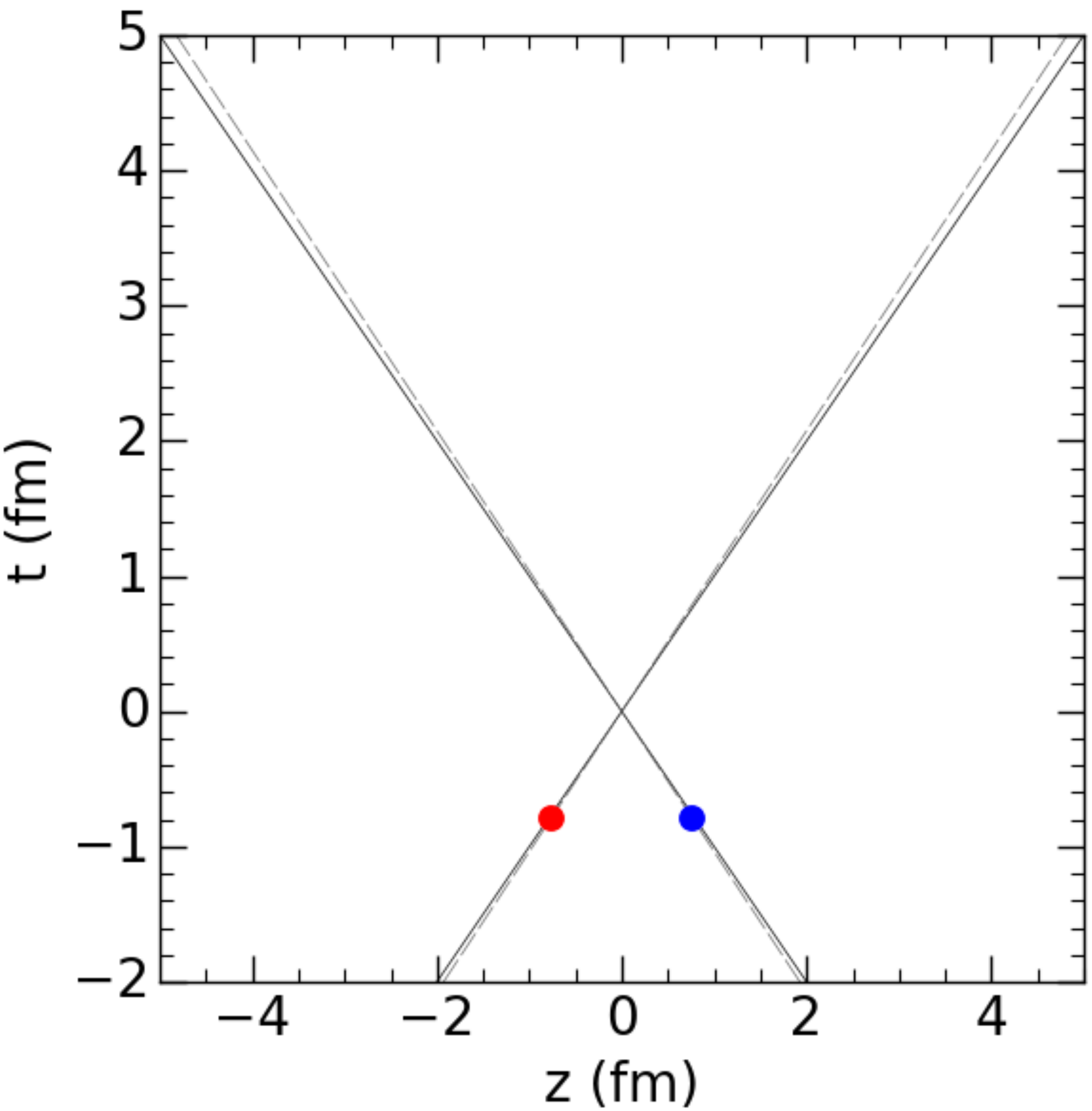

- Collision time and 3D spatial position are determined for every binary collision
- QCD strings are randomly produced from collision points

A. Bialas, A. Bzdak and V. Koch, arXiv:1608.07041 [hep-ph]

- These strings are decelerated with a constant string tension $\sigma = 1 GeV/fm$ before thermalized to medium

The 3D MCGlauber-LEXUS model

C. Shen, B. Schenke, in preparation

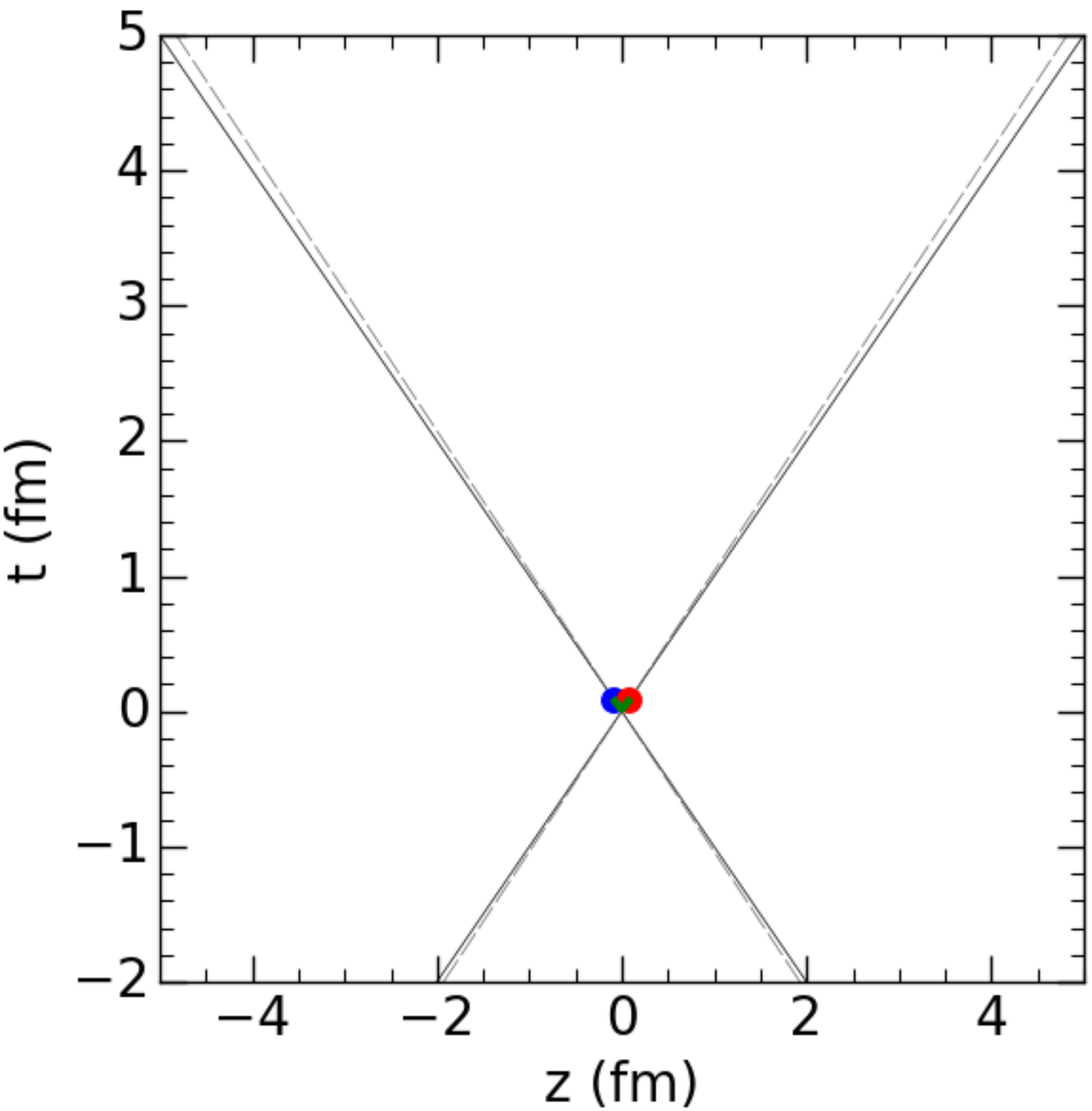

- Collision time and 3D spatial position are determined for every binary collision
- QCD strings are randomly produced from collision points

A. Bialas, A. Bzdak and V. Koch, arXiv:1608.07041 [hep-ph]

- These strings are decelerated with a constant string tension $\sigma = 1 GeV/fm$ before thermalized to medium

The 3D MCGlauber-LEXUS model

C. Shen, B. Schenke, in preparation

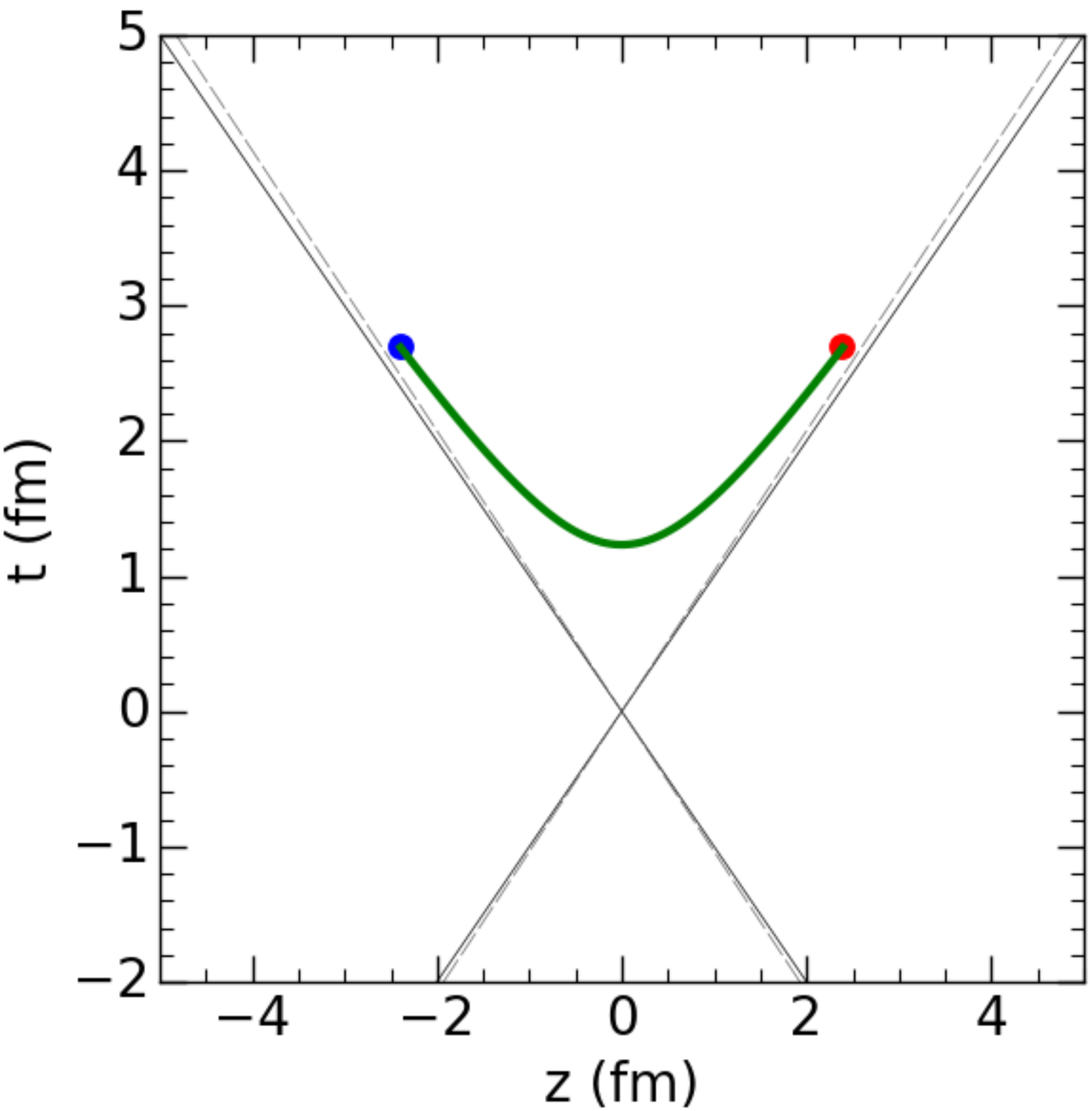

- Collision time and 3D spatial position are determined for every binary collision
- QCD strings are randomly produced from collision points

A. Bialas, A. Bzdak and V. Koch, arXiv:1608.07041 [hep-ph]

- These strings are decelerated with a constant string tension $\sigma = 1 GeV/fm$ before thermalized to medium

The 3D MCGlauber-LEXUS model

C. Shen, B. Schenke, in preparation

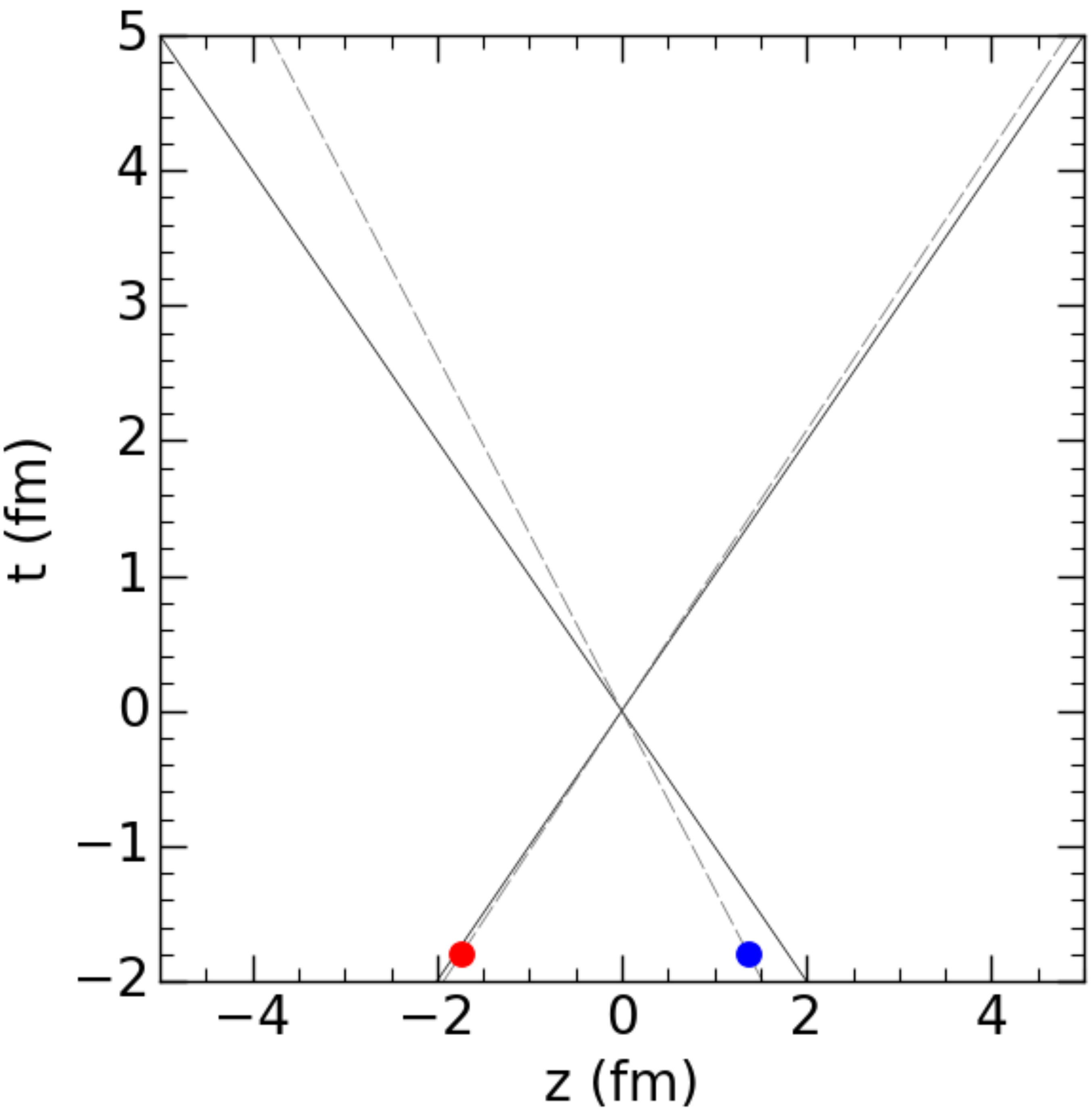

- Collision time and 3D spatial position are determined for every binary collision
- QCD strings are randomly produced from collision points

A. Bialas, A. Bzdak and V. Koch, arXiv:1608.07041 [hep-ph]

- These strings are decelerated with a constant string tension $\sigma = 1 GeV/fm$ before thermalized to medium

The 3D MCGlauber-LEXUS model

C. Shen, B. Schenke, in preparation

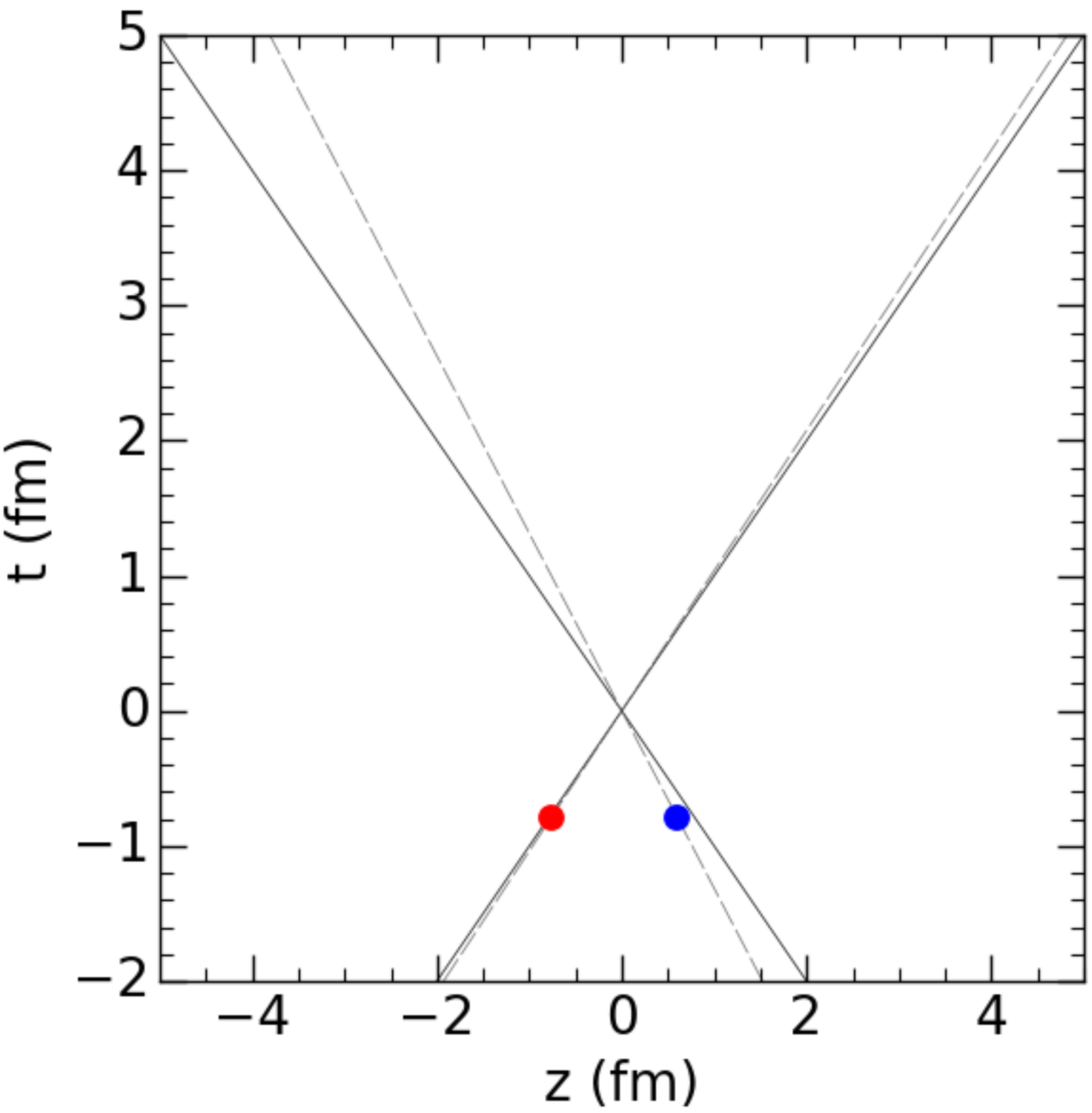

- Collision time and 3D spatial position are determined for every binary collision
- QCD strings are randomly produced from collision points

A. Bialas, A. Bzdak and V. Koch, arXiv:1608.07041 [hep-ph]

- These strings are decelerated with a constant string tension $\sigma = 1 GeV/fm$ before thermalized to medium

The 3D MCGlauber-LEXUS model

C. Shen, B. Schenke, in preparation

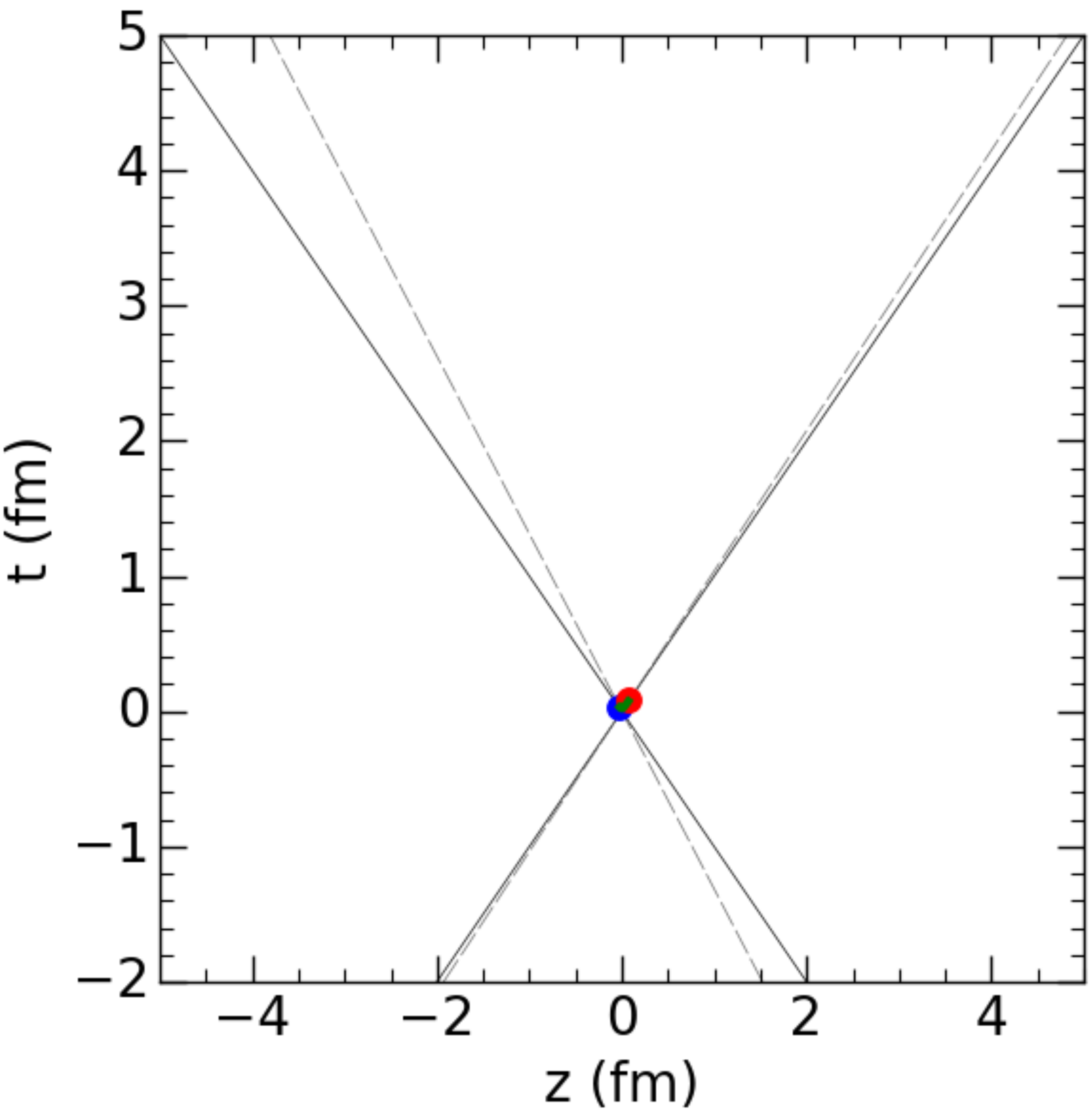

- Collision time and 3D spatial position are determined for every binary collision
- QCD strings are randomly produced from collision points

A. Bialas, A. Bzdak and V. Koch, arXiv:1608.07041 [hep-ph]

- These strings are decelerated with a constant string tension $\sigma = 1 GeV/fm$ before thermalized to medium

The 3D MCGlauber-LEXUS model

C. Shen, B. Schenke, in preparation

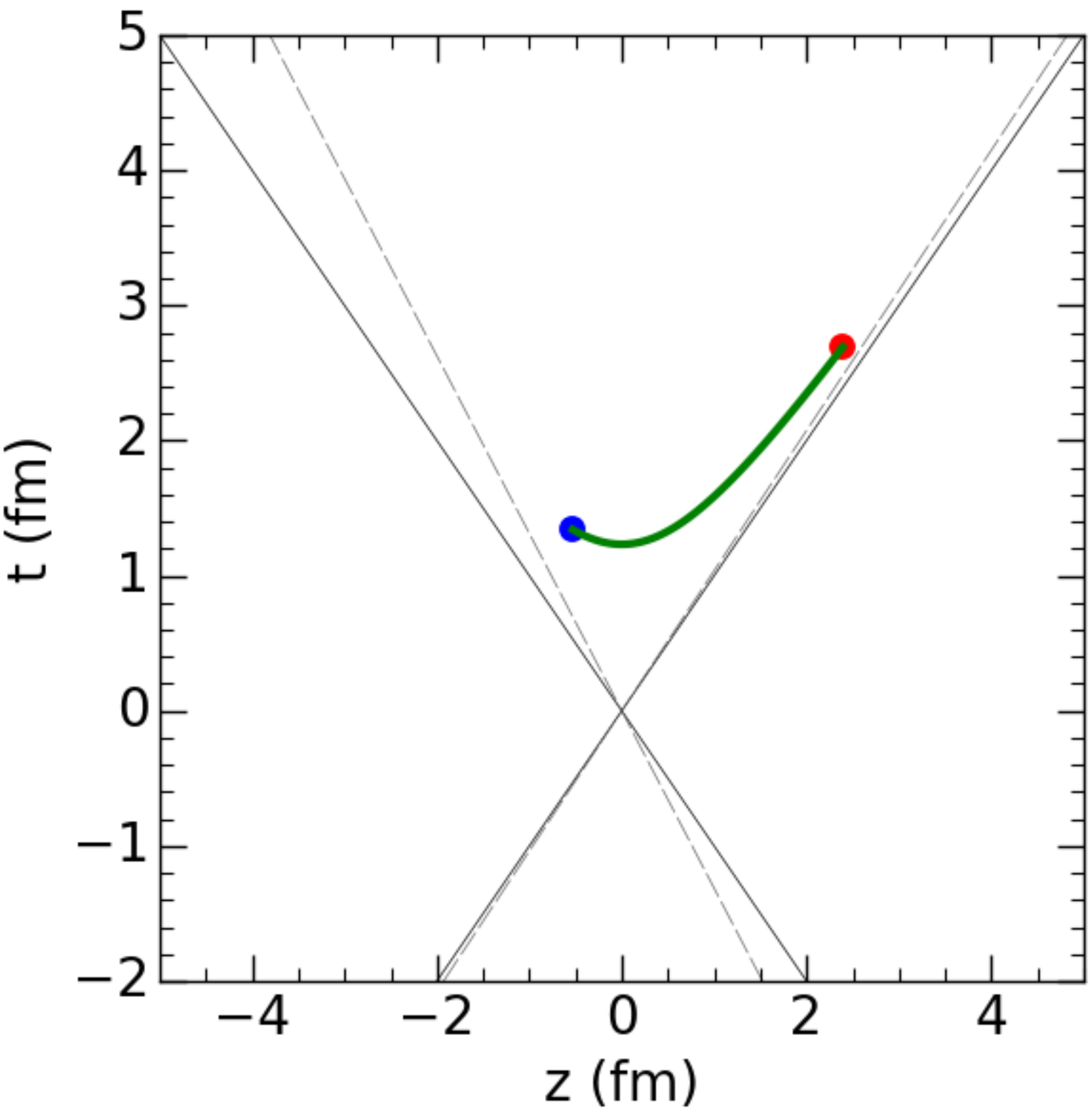

- Collision time and 3D spatial position are determined for every binary collision
- QCD strings are randomly produced from collision points

A. Bialas, A. Bzdak and V. Koch, arXiv:1608.07041 [hep-ph]

- These strings are decelerated with a constant string tension $\sigma = 1 GeV/fm$ before thermalized to medium

The 3D MCGlauber-LEXUS model

C. Shen, B. Schenke, in preparation

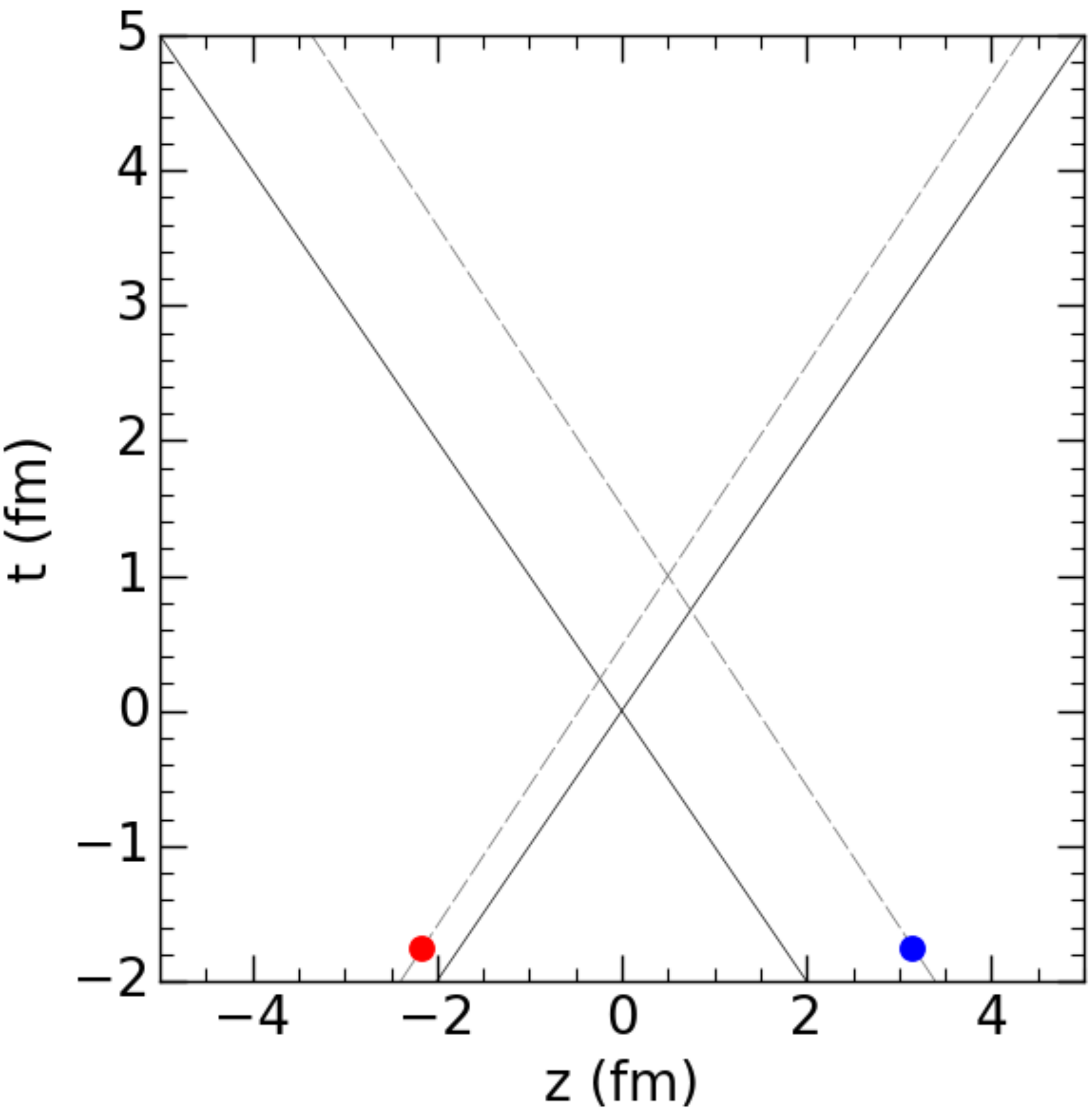

- Collision time and 3D spatial position are determined for every binary collision
- QCD strings are randomly produced from collision points

A. Bialas, A. Bzdak and V. Koch, arXiv:1608.07041 [hep-ph]

- These strings are decelerated with a constant string tension $\sigma = 1 GeV/fm$ before thermalized to medium

The 3D MCGlauber-LEXUS model

C. Shen, B. Schenke, in preparation

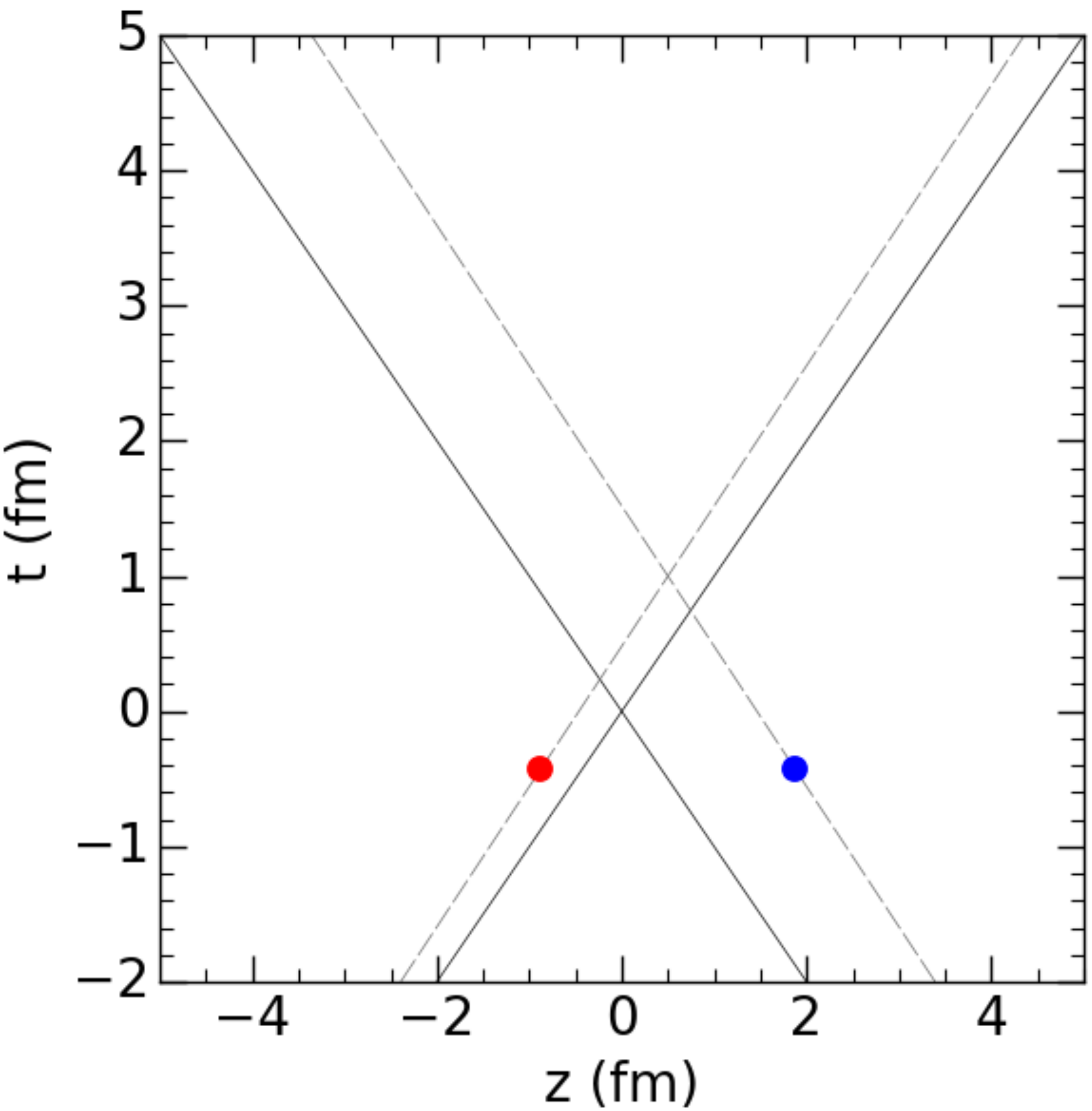

- Collision time and 3D spatial position are determined for every binary collision
- QCD strings are randomly produced from collision points

A. Bialas, A. Bzdak and V. Koch, arXiv:1608.07041 [hep-ph]

- These strings are decelerated with a constant string tension $\sigma = 1 GeV/fm$ before thermalized to medium

The 3D MCGlauber-LEXUS model

C. Shen, B. Schenke, in preparation

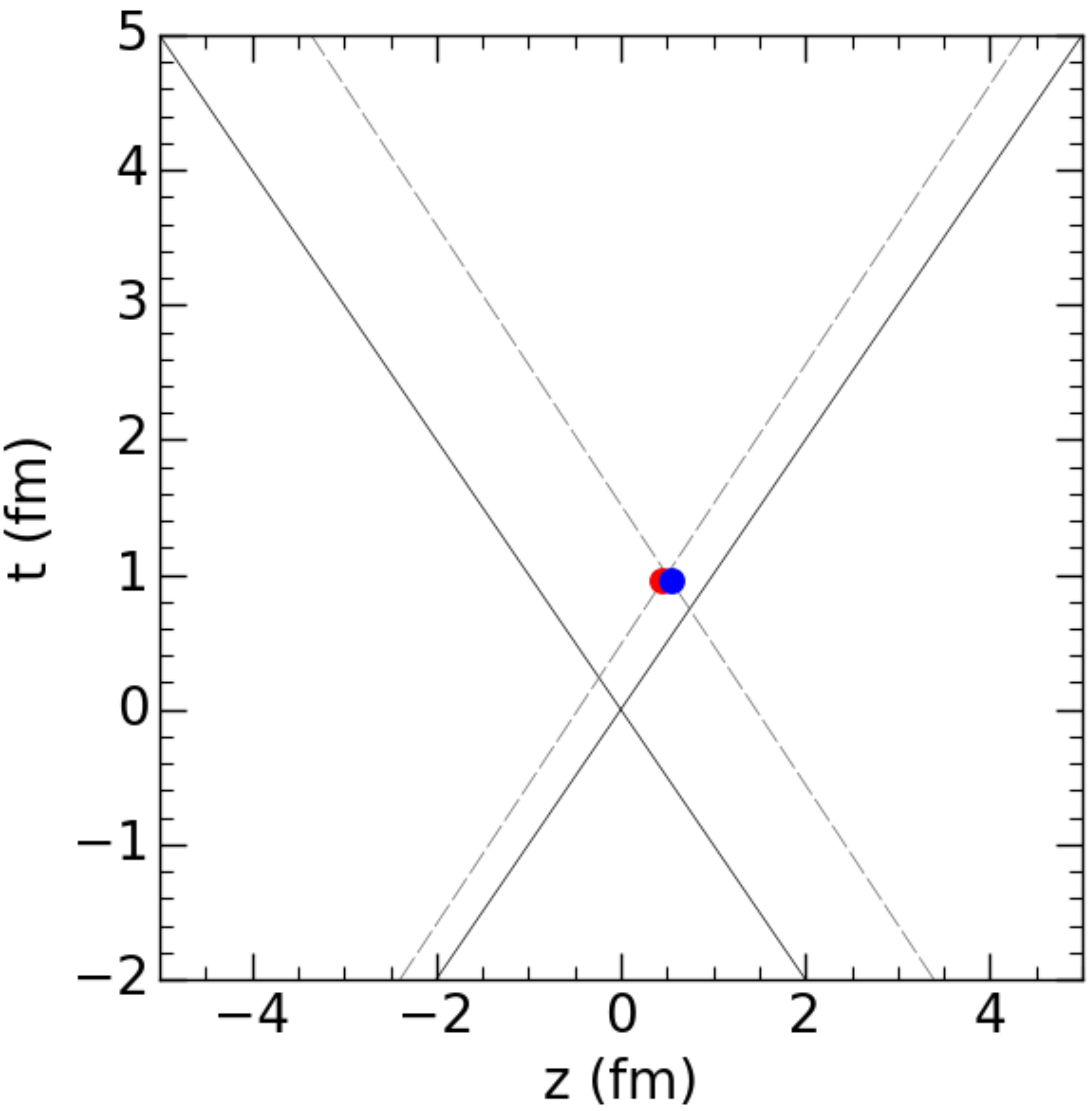

- Collision time and 3D spatial position are determined for every binary collision
- QCD strings are randomly produced from collision points

A. Bialas, A. Bzdak and V. Koch, arXiv:1608.07041 [hep-ph]

- These strings are decelerated with a constant string tension $\sigma = 1 GeV/fm$ before thermalized to medium

The 3D MCGlauber-LEXUS model

C. Shen, B. Schenke, in preparation

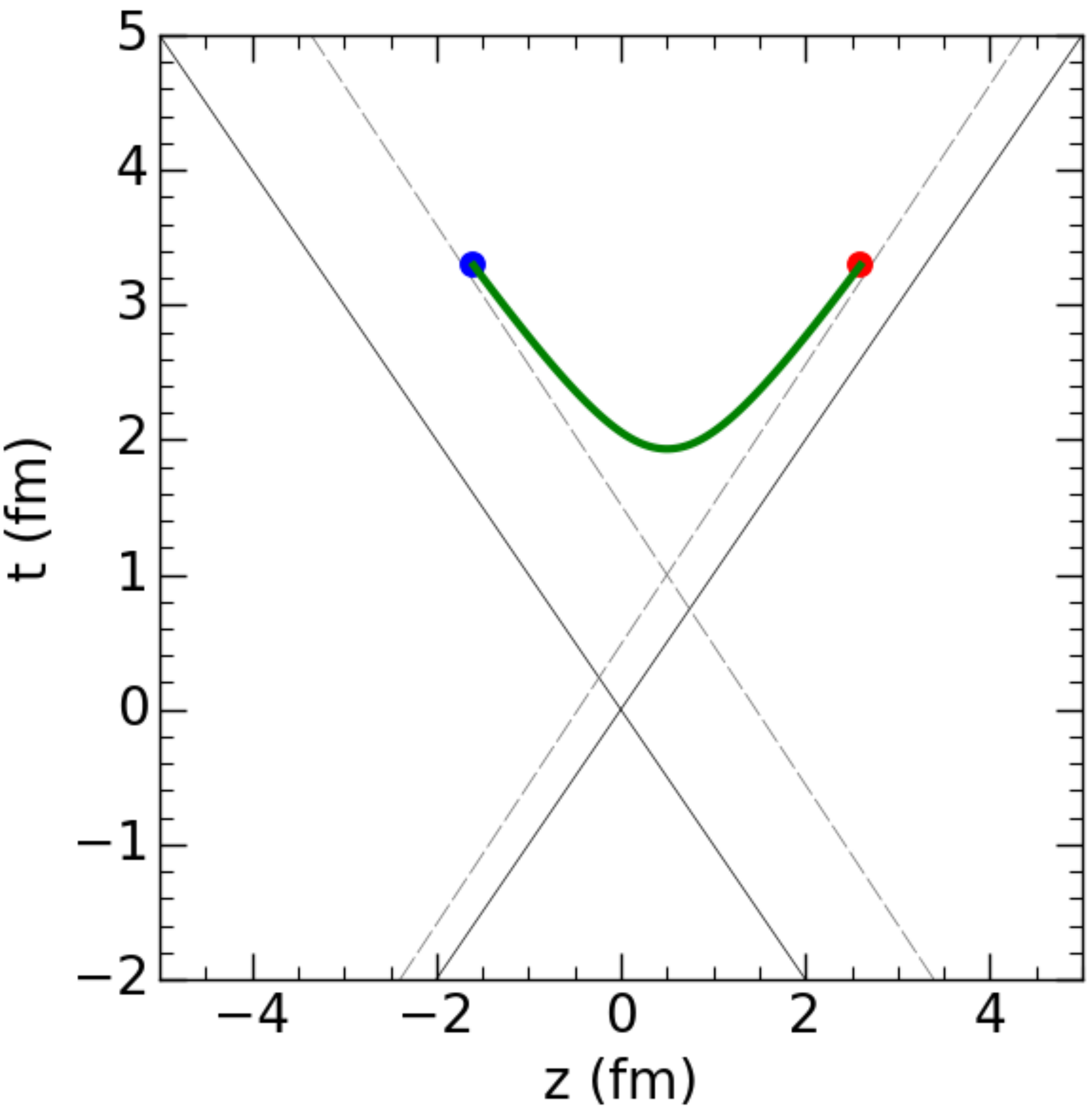

- Collision time and 3D spatial position are determined for every binary collision
- QCD strings are randomly produced from collision points

A. Bialas, A. Bzdak and V. Koch, arXiv:1608.07041 [hep-ph]

- These strings are decelerated with a constant string tension $\sigma = 1 GeV/fm$ before thermalized to medium

A 3D MCGlauber model

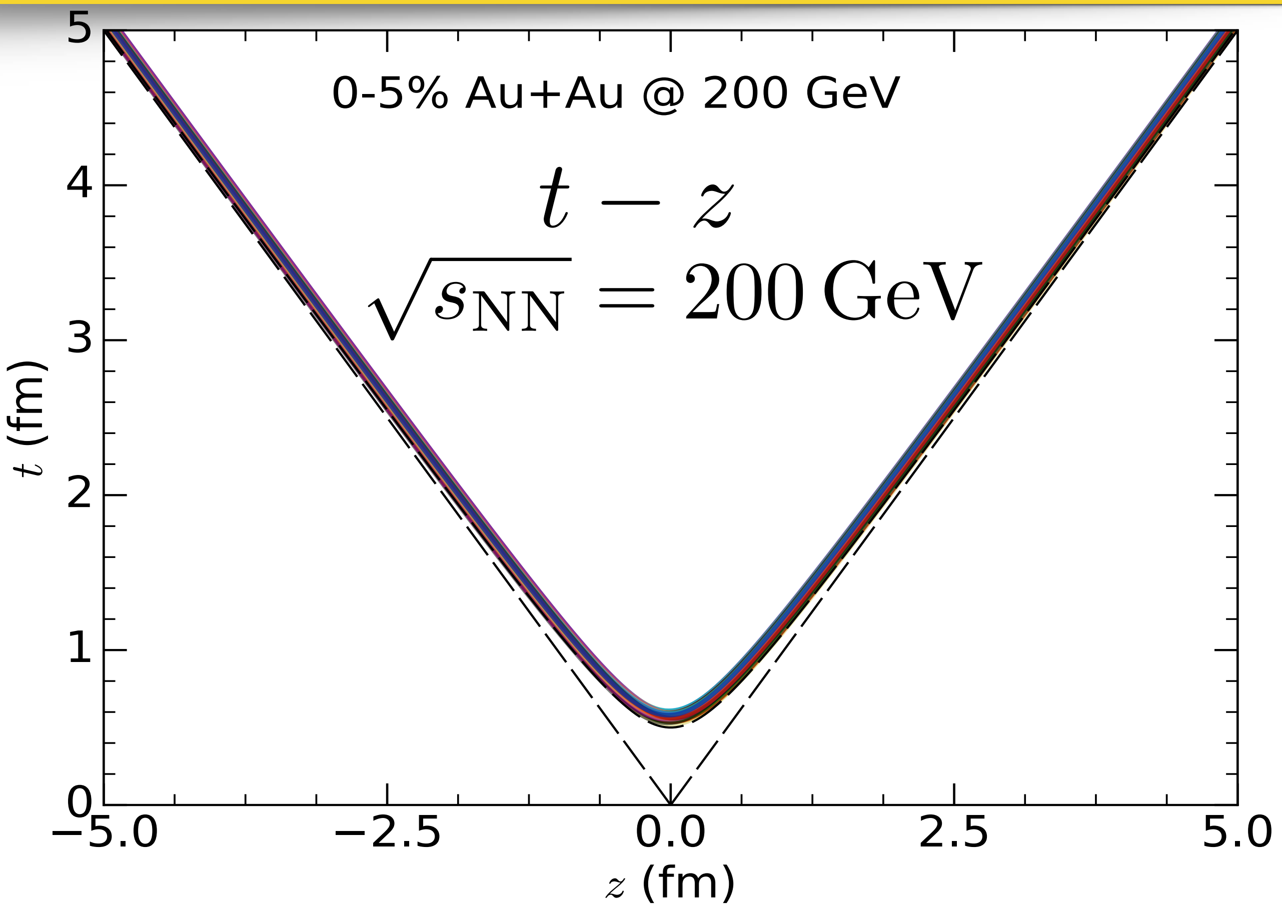

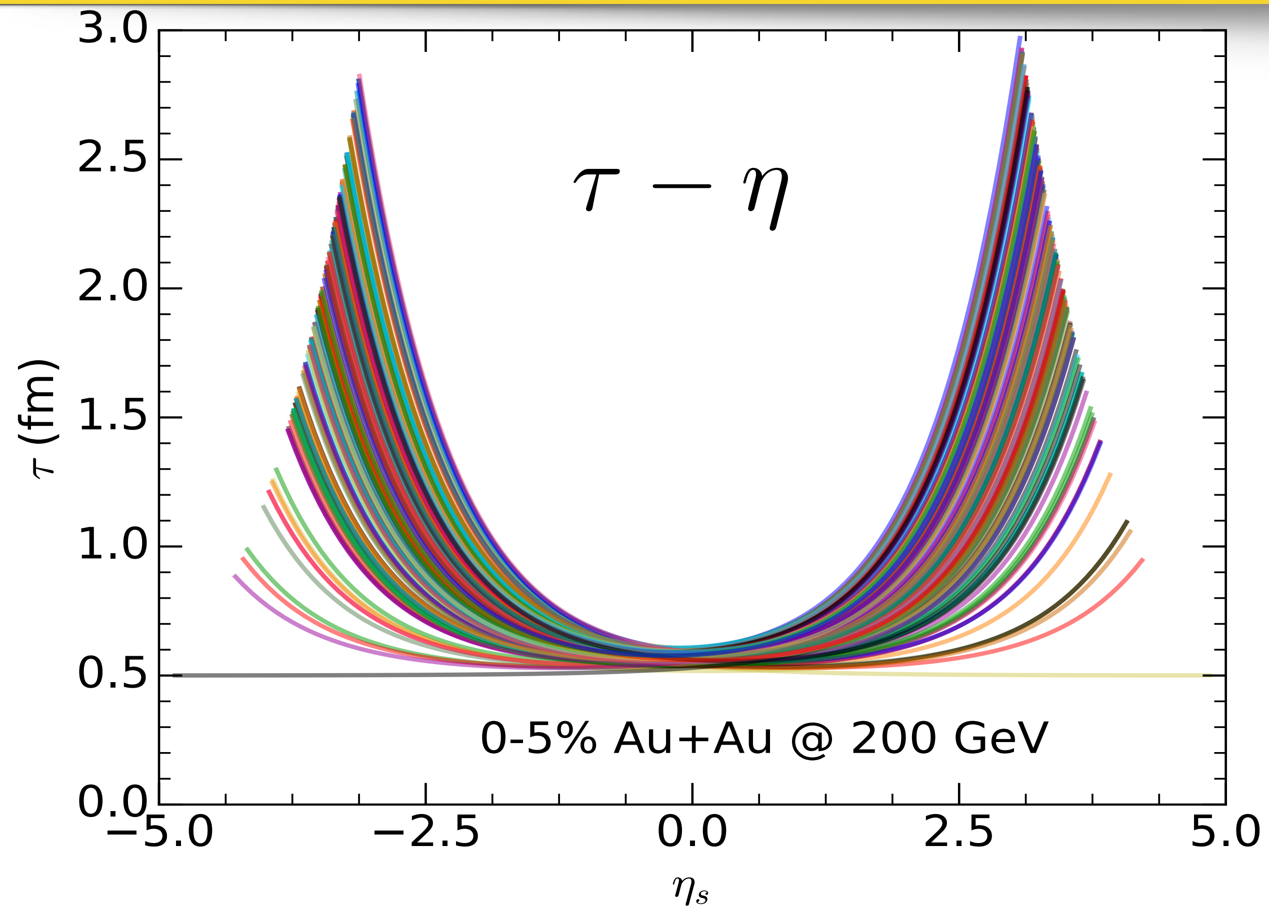

A 3D MCGlauber model

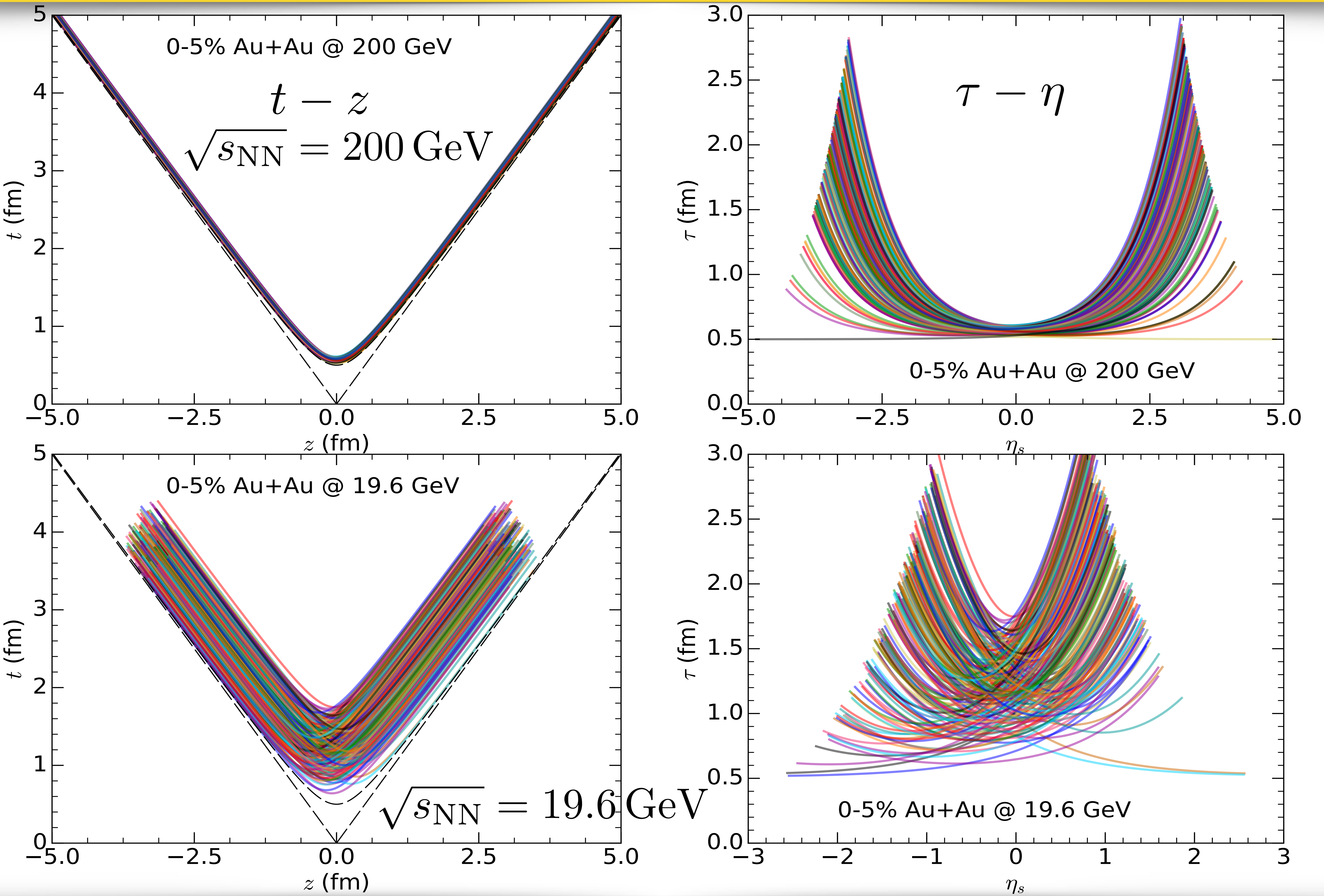

A 3D MCGlauber model

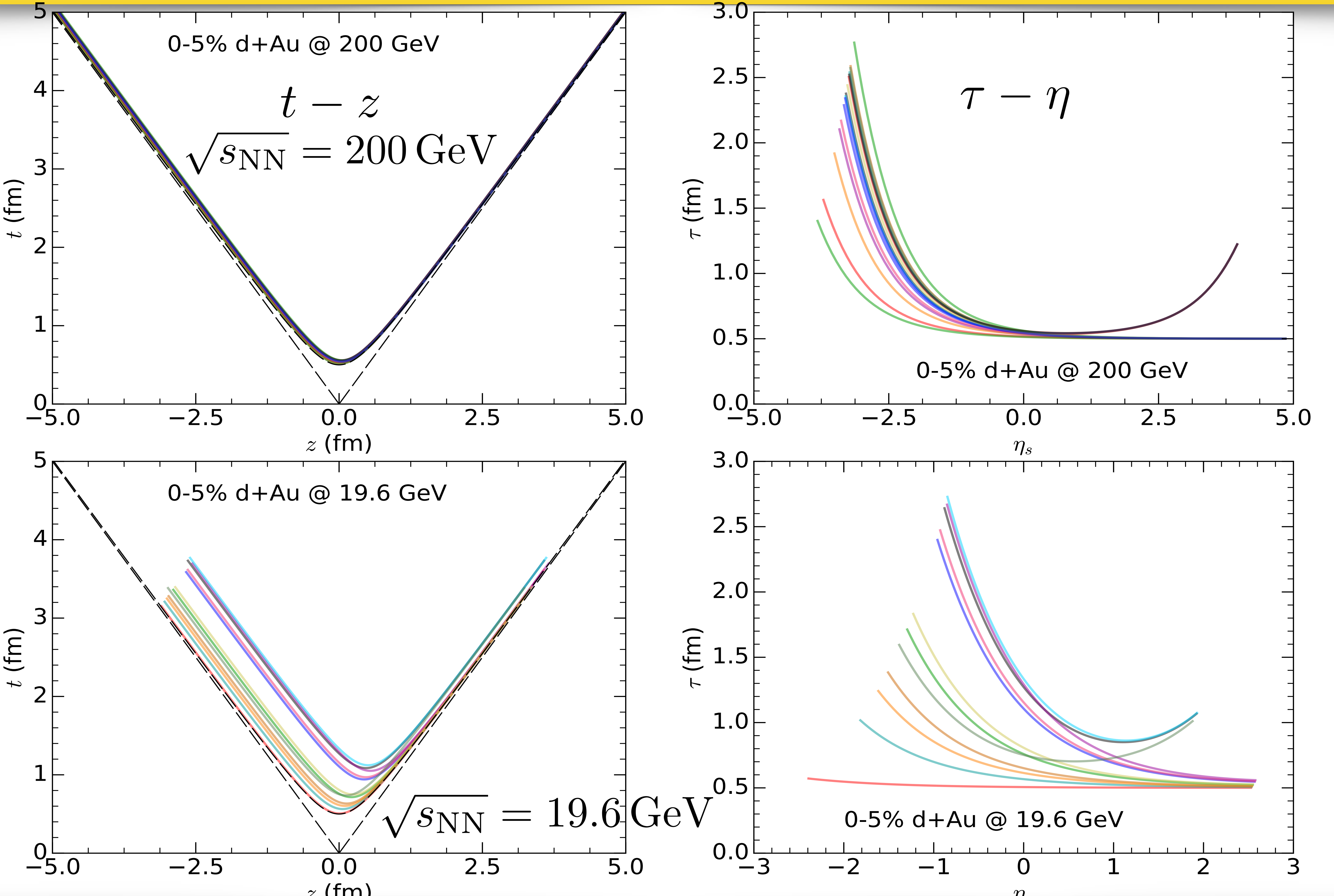

Introducing longitudinal fluctuations

- Sample valence quarks from the incoming participants

$$y_q = \mathrm{arcsinh}\left(x_q\sqrt{\frac{s}{4m_q^2} - 1}\right)$$

$$y_q = \log\left(\frac{x\sqrt{s}}{2m_q}\right)$$

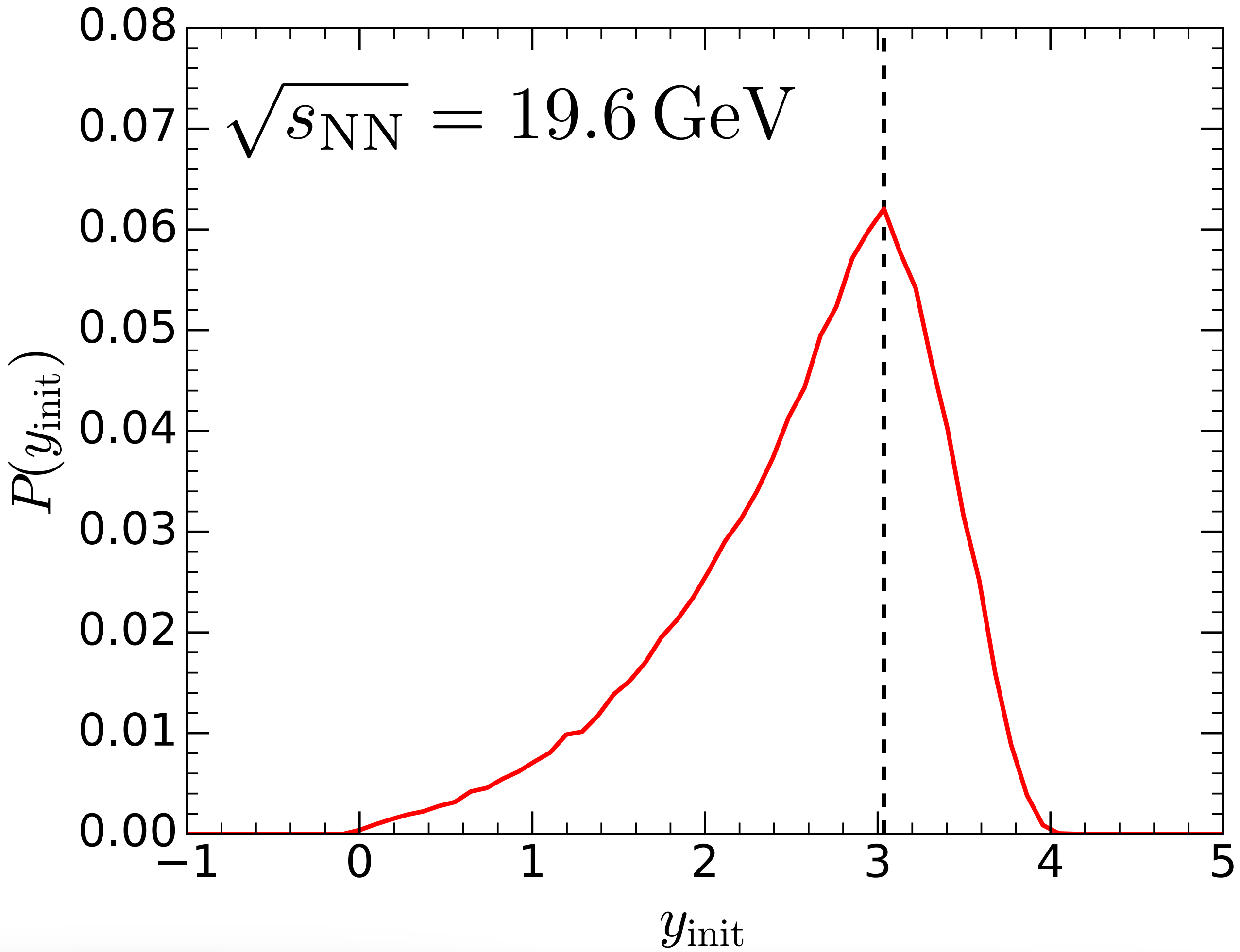

Introducing longitudinal fluctuations

- Sample valence quarks from the incoming participants

$$y_q = \text{arcsinh}\left(x_q\sqrt{\frac{s}{4m_q^2} - 1}\right) \qquad y_q = \log\left(\frac{x\sqrt{s}}{2m_q}\right)$$

- Sample the rapidity loss according to the LEXUS model

$$P(y_{\text{loss}}) = \frac{\cosh(2y_{\text{init}} - y_{\text{loss}})}{\sinh(2y_{\text{init}}) - \sinh(y_{\text{init}})} \qquad y_{\text{loss}} \in [0, y_{\text{init}}]$$

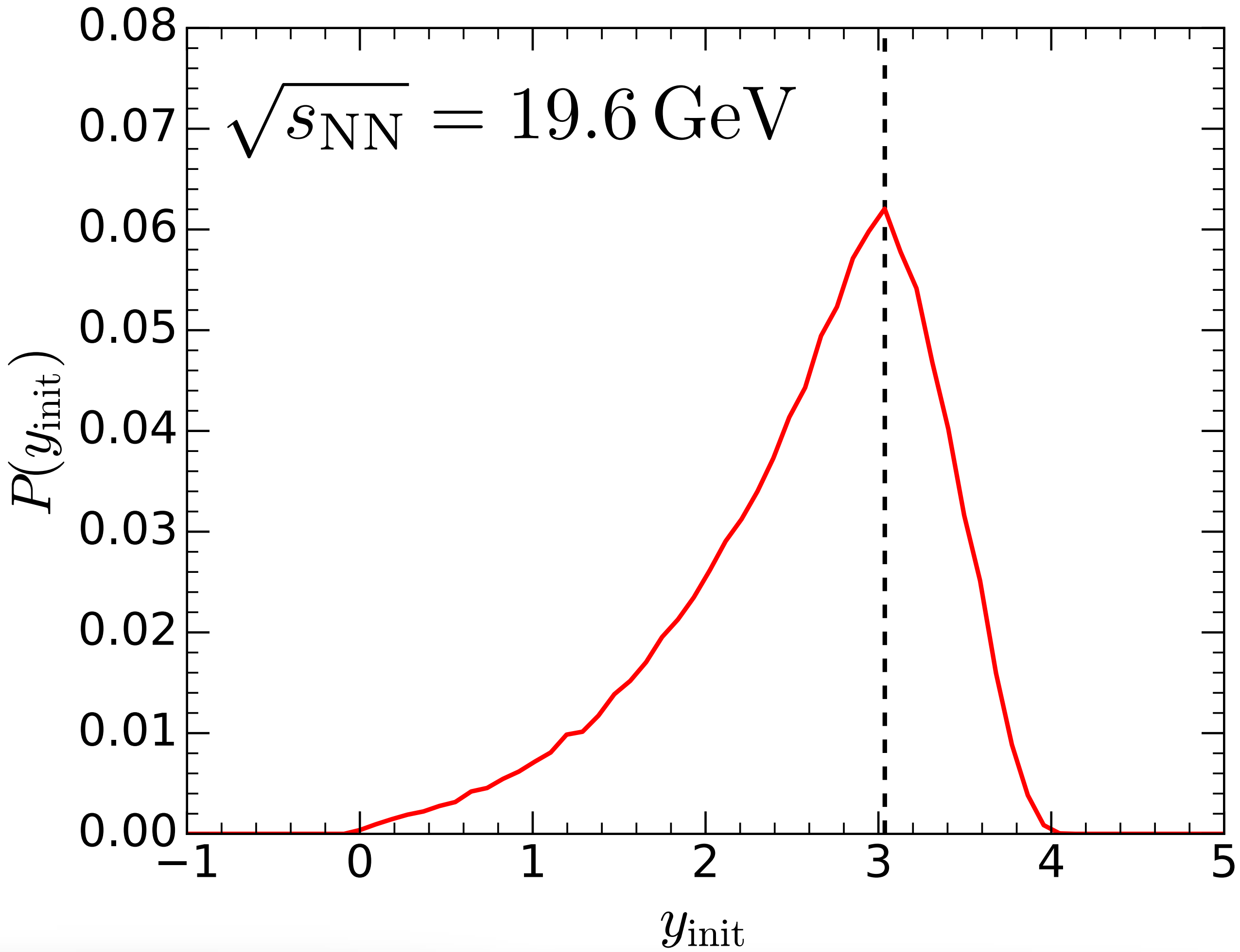

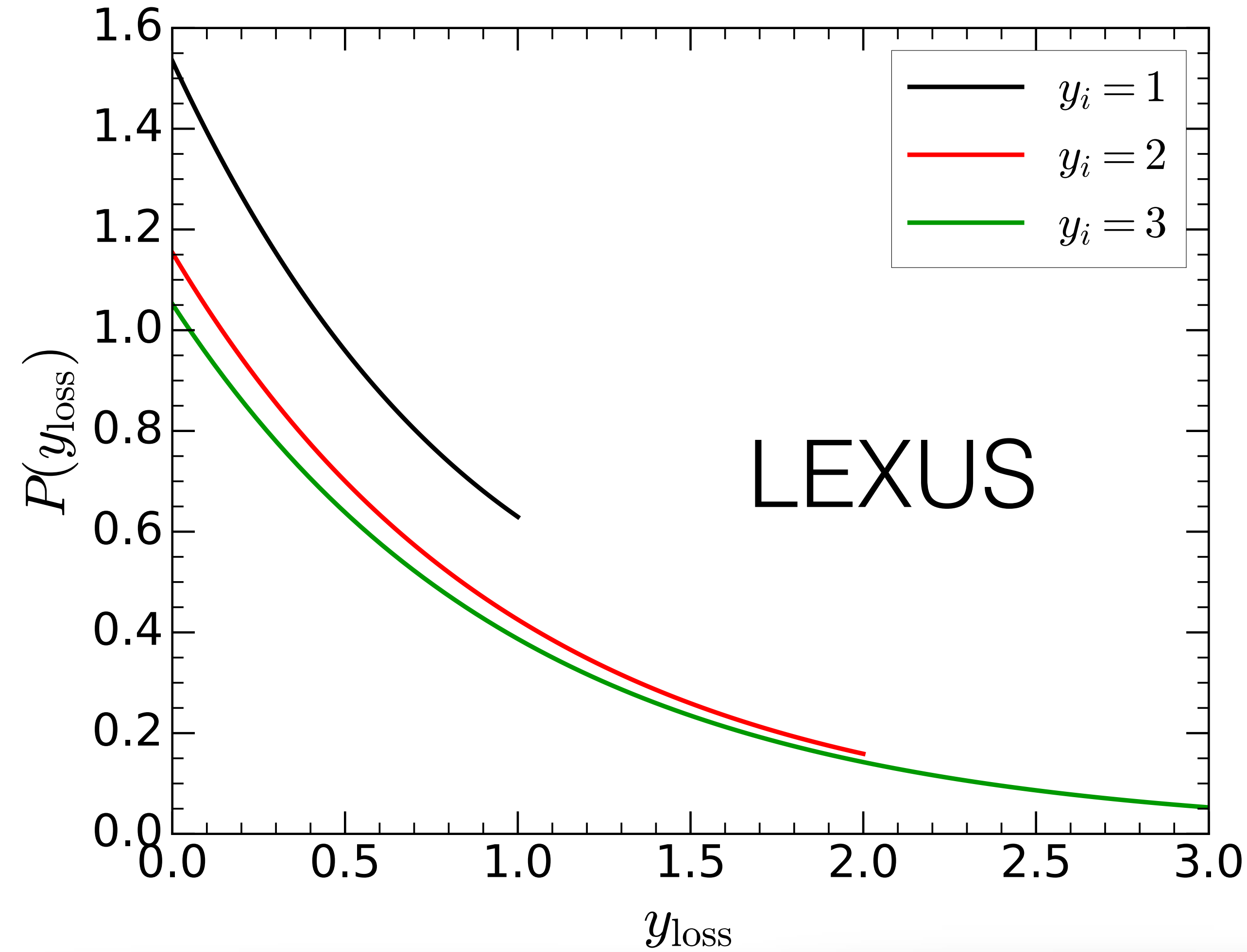

Net baryon rapidity distribution

C. Shen, B. Schenke, in preparation

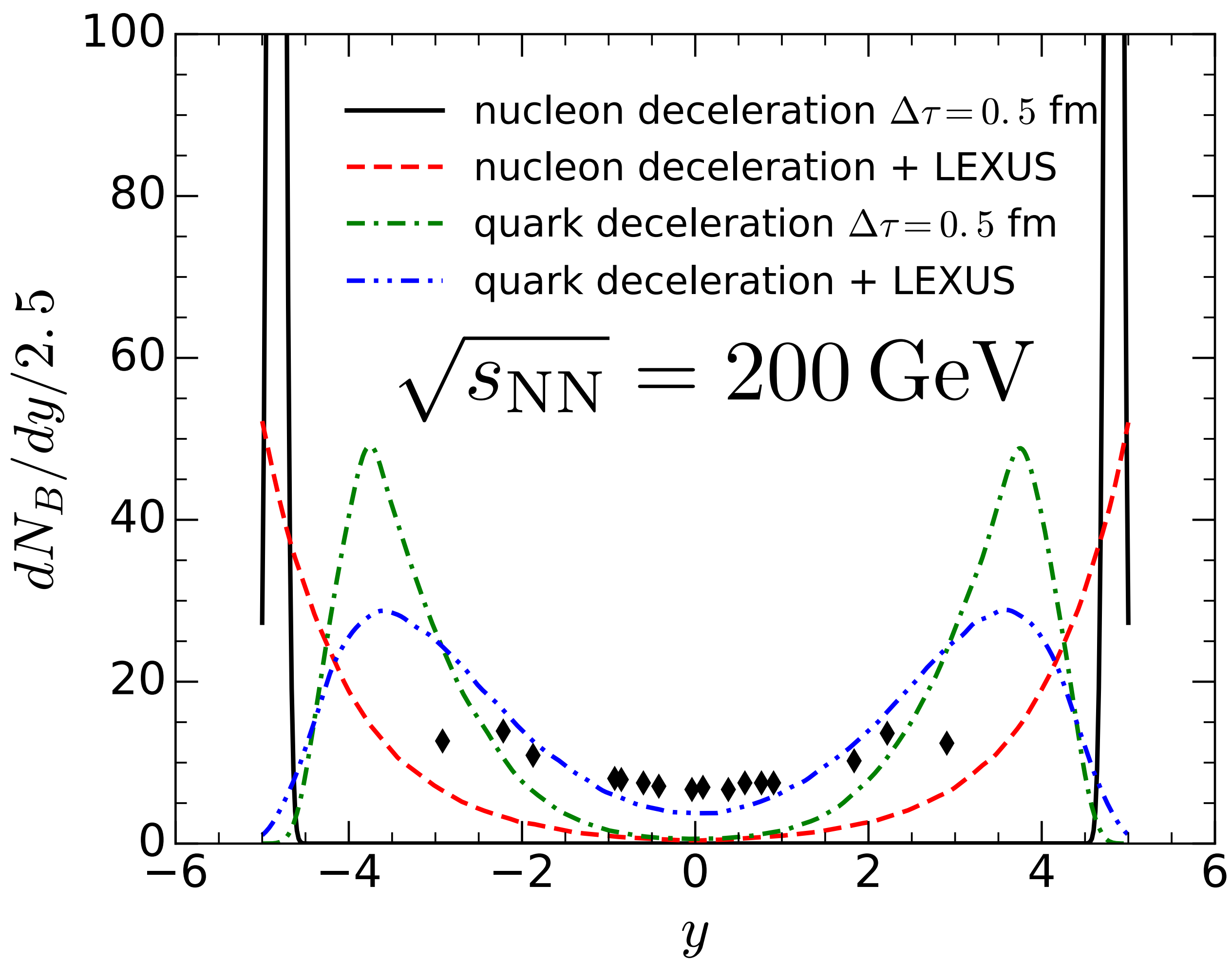

- Different rapidity fluctuation results different net baryon rapidity distribution

Net baryon rapidity distribution

C. Shen, B. Schenke, in preparation

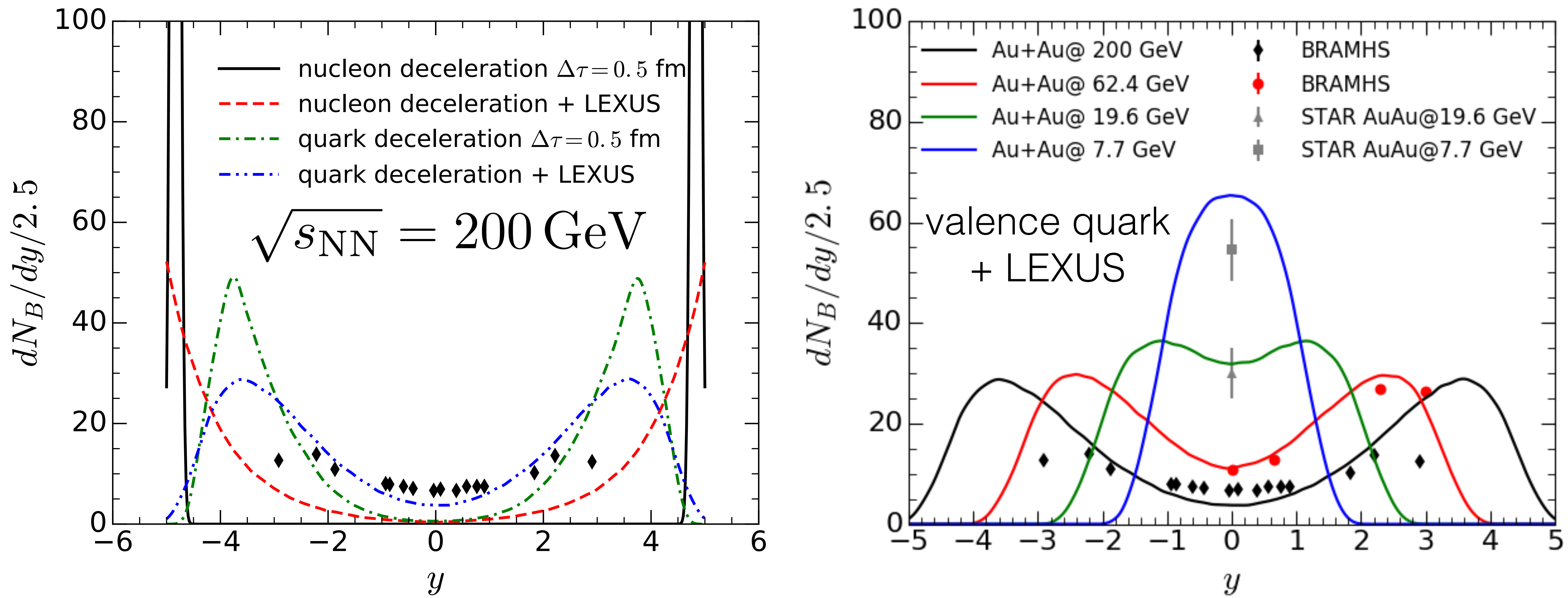

- Different rapidity fluctuation results different net baryon rapidity distribution
- The valence quark + LEXUS model provides a reasonable net baryon rapidity distribution compared to the RHIC BES data

Quantify rapidity fluctuation

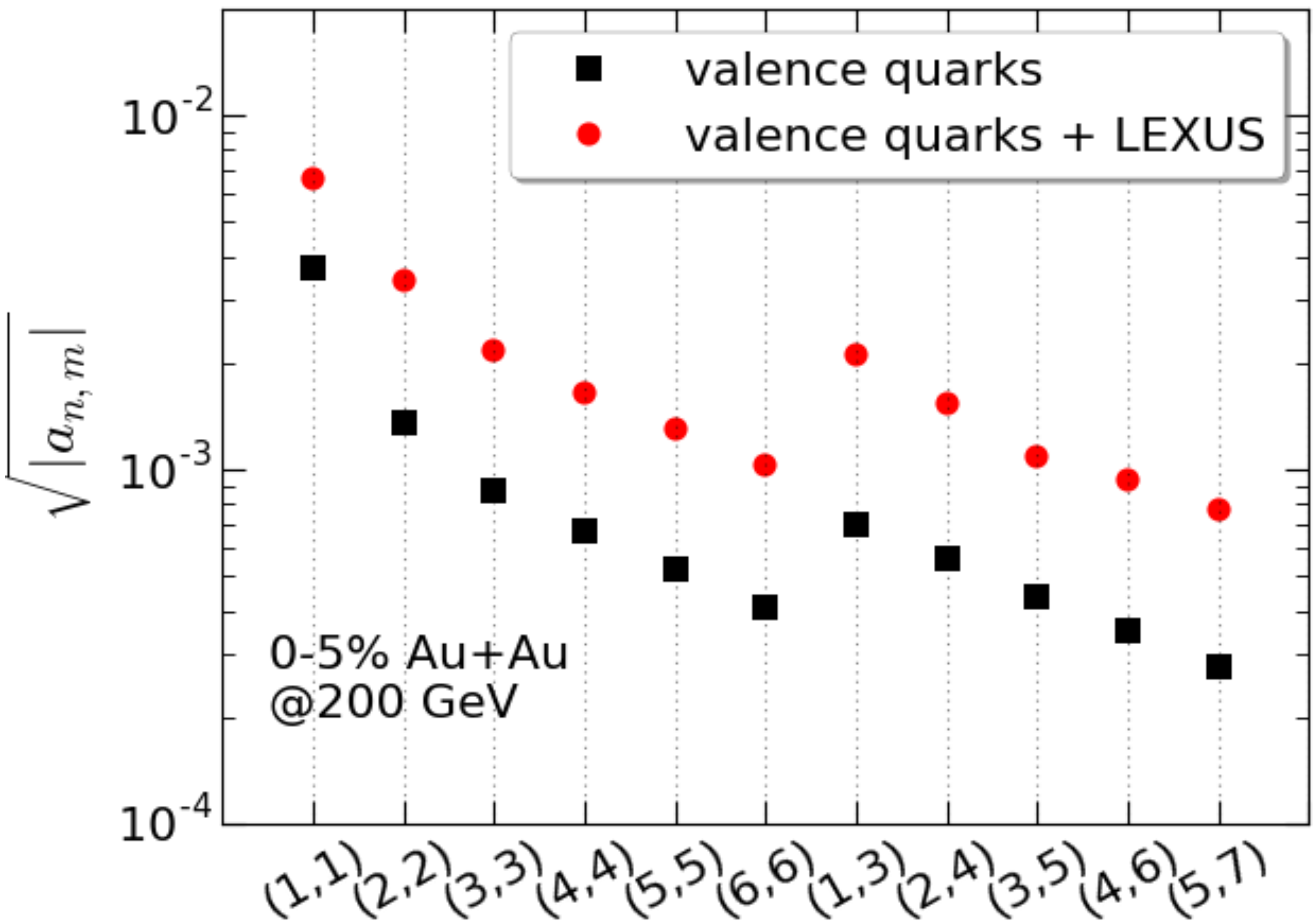

$$C(\eta_1, \eta_2) = \frac{\langle \frac{dN}{d\eta}(\eta_1) \frac{dN}{d\eta}(\eta_2) \rangle}{\langle \frac{dN}{d\eta}(\eta_1) \rangle \langle \frac{dN}{d\eta}(\eta_2) \rangle},$$

$$C_N(\eta_1, \eta_2) = \frac{C(\eta_1, \eta_2)}{C_p(\eta_1) C_p(\eta_2)},$$

$$C_p(\eta_1) = \frac{1}{2Y} \int_{-Y}^{Y} C(\eta_1, \eta_2) d\eta_2$$

$$a_{n,m} = \int \frac{d\eta_1}{Y} \frac{d\eta_2}{Y} C_N(\eta_1, \eta_2) \frac{T_n(\eta_1) T_m(\eta_2) + T_n(\eta_2) T_m(\eta_1)}{2}$$

$$T_n(\eta) = \sqrt{n + \tfrac{1}{2}} P_n(\tfrac{\eta}{Y})$$

- The size of the $a_{n,m}$ coefficient can quantify the mount of longitudinal fluctuations

Quantify rapidity fluctuation

C. Shen, B. Schenke, in preparation

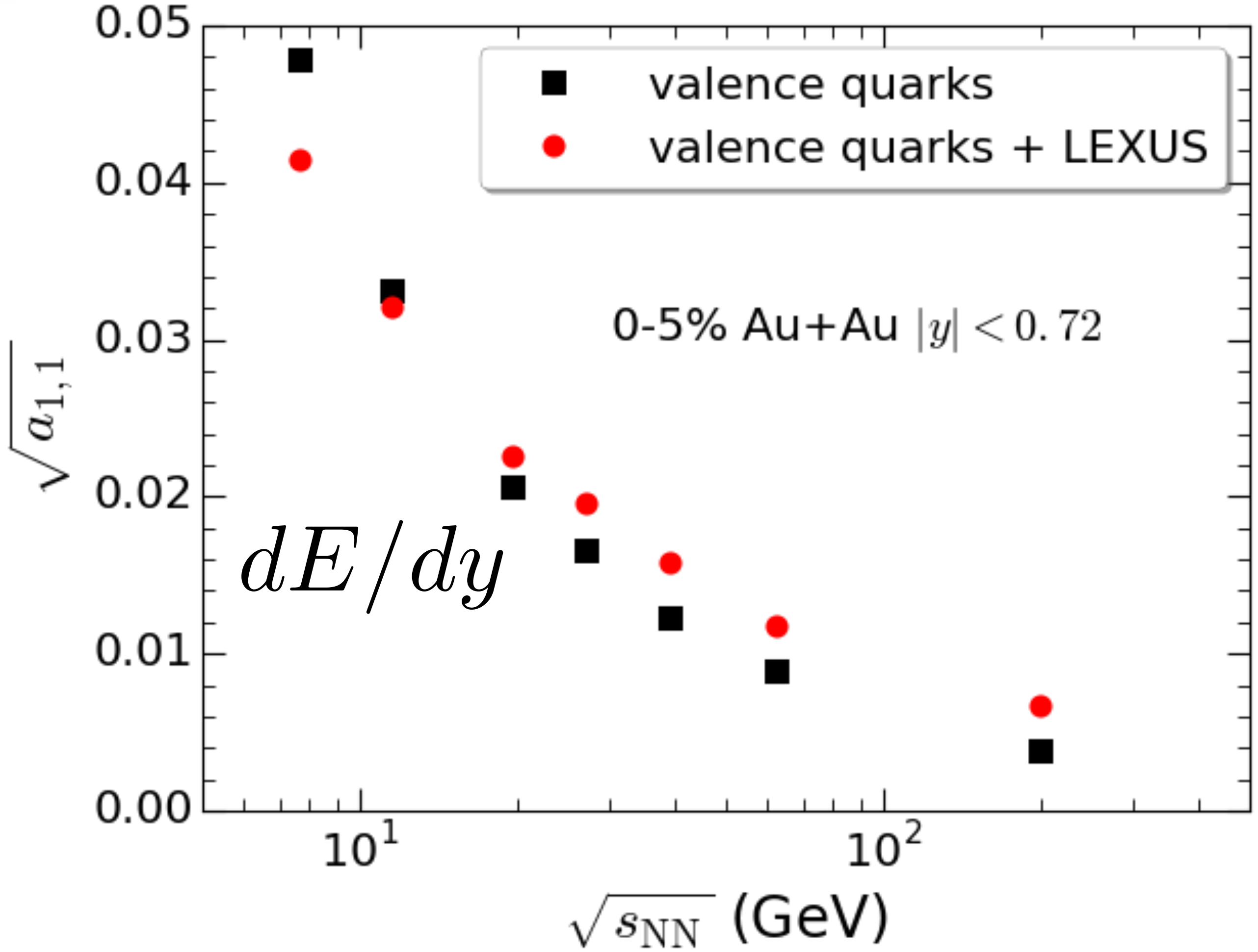

- The a_{11} coefficient for dE/dy decreases at high collision energy because the system becomes more boost-invariant

Quantify rapidity fluctuation

C. Shen, B. Schenke, in preparation

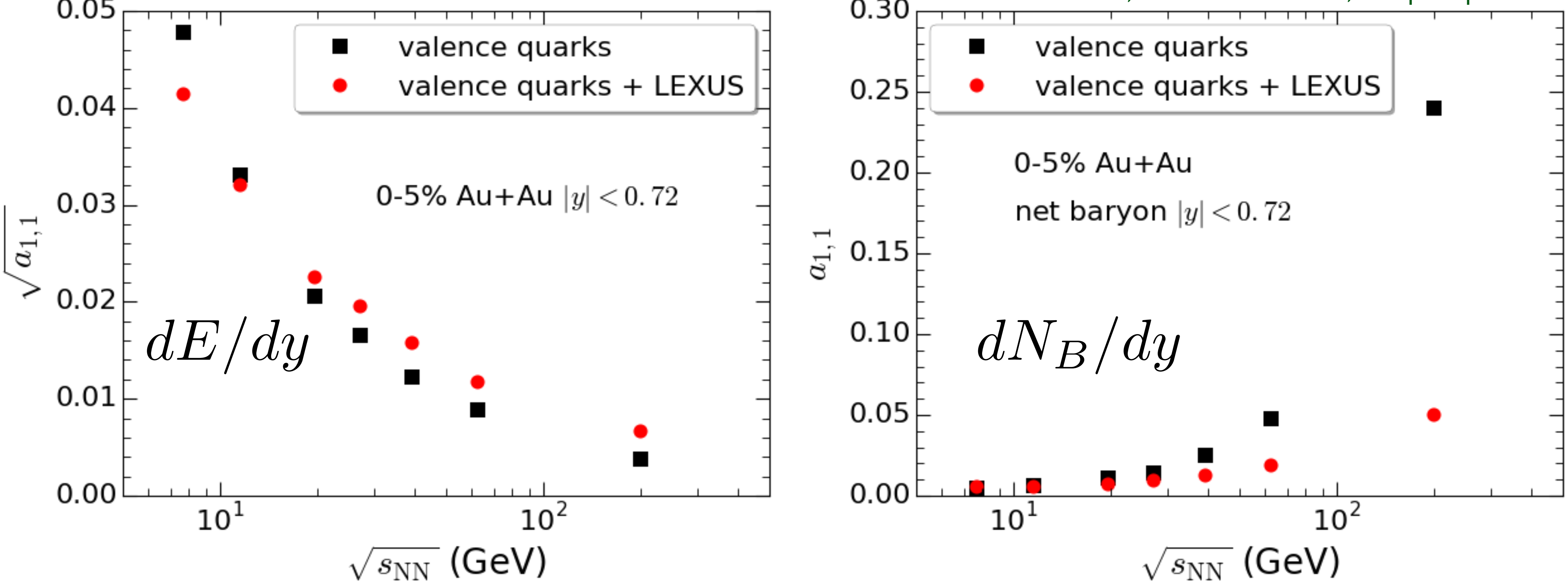

- The a_{11} coefficient for dE/dy decreases at high collision energy because the system becomes more boost-invariant
- The a_{11} coefficient for dN_B/dy increases at high collision energy because less net baryon number at mid-rapidity

Quantify rapidity fluctuation

C. Shen, B. Schenke, in preparation

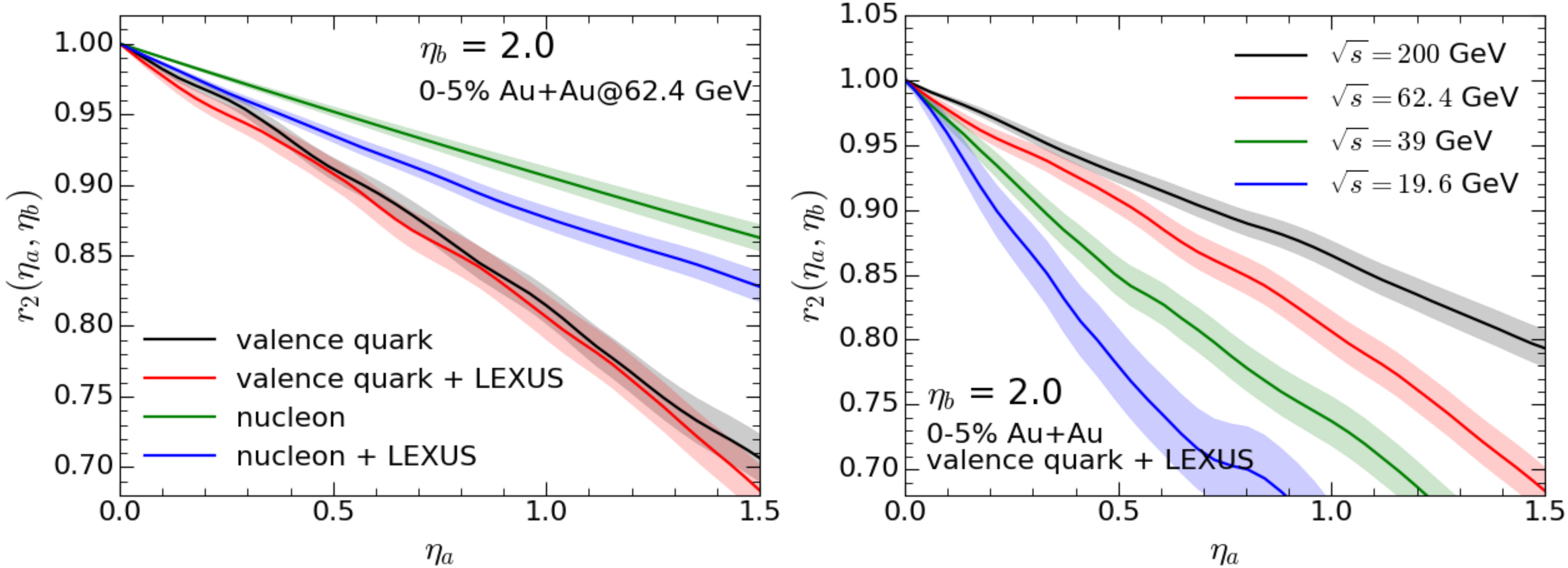

$$r_n(\eta_a, \eta_b) = \frac{\langle \Re\{\mathcal{E}_n(-\eta_a)\cdot\mathcal{E}_n^*(\eta_b)\}\rangle_{\mathrm{ev}}}{\langle \Re\{\mathcal{E}_n(\eta_a)\cdot\mathcal{E}_n^*(\eta_b)\}\rangle_{\mathrm{ev}}}.$$

$$\mathcal{E}_n(\eta) = -\frac{\int r dr d\phi r^n e(r,\phi,\eta) e^{in\phi}}{\int r dr d\phi r^n e(r,\phi,\eta)}$$

- The initial eccentricities decorrelate along η direction faster with more longitudinal fluctuation and at lower collision energy

Hydrodynamics with sources

Energy-momentum current and net baryon density are feed into hydrodynamic simulation as source terms

$$\partial_\mu T^{\mu\nu} = J^\nu_{\mathrm{source}}$$

$$\partial_\mu J^\mu = \rho_{\mathrm{source}}$$

where

$$J^\nu_{\mathrm{source}} = \delta e u^\nu + (e + P)\delta u^\nu$$

$$\delta u^\nu = \frac{\Delta^\nu_\mu J^\mu_{\mathrm{source}}}{e + P}$$

heats up the system   accelerates the flow velocity

ρ_{source} dopes baryon charges into the system

- Source terms are smeared with Gaussians in space and time

Hydrodynamical evolution with sources

energy density

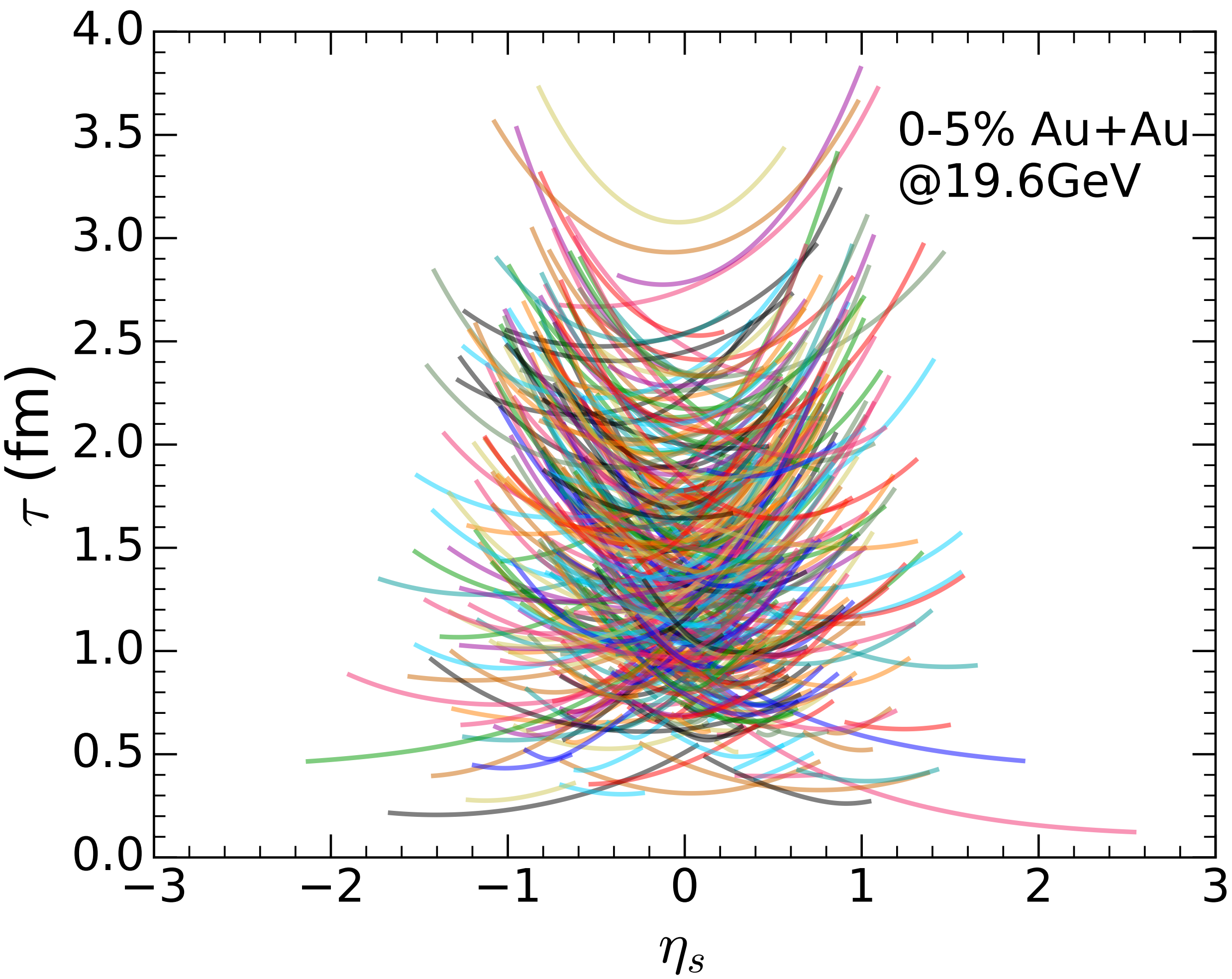

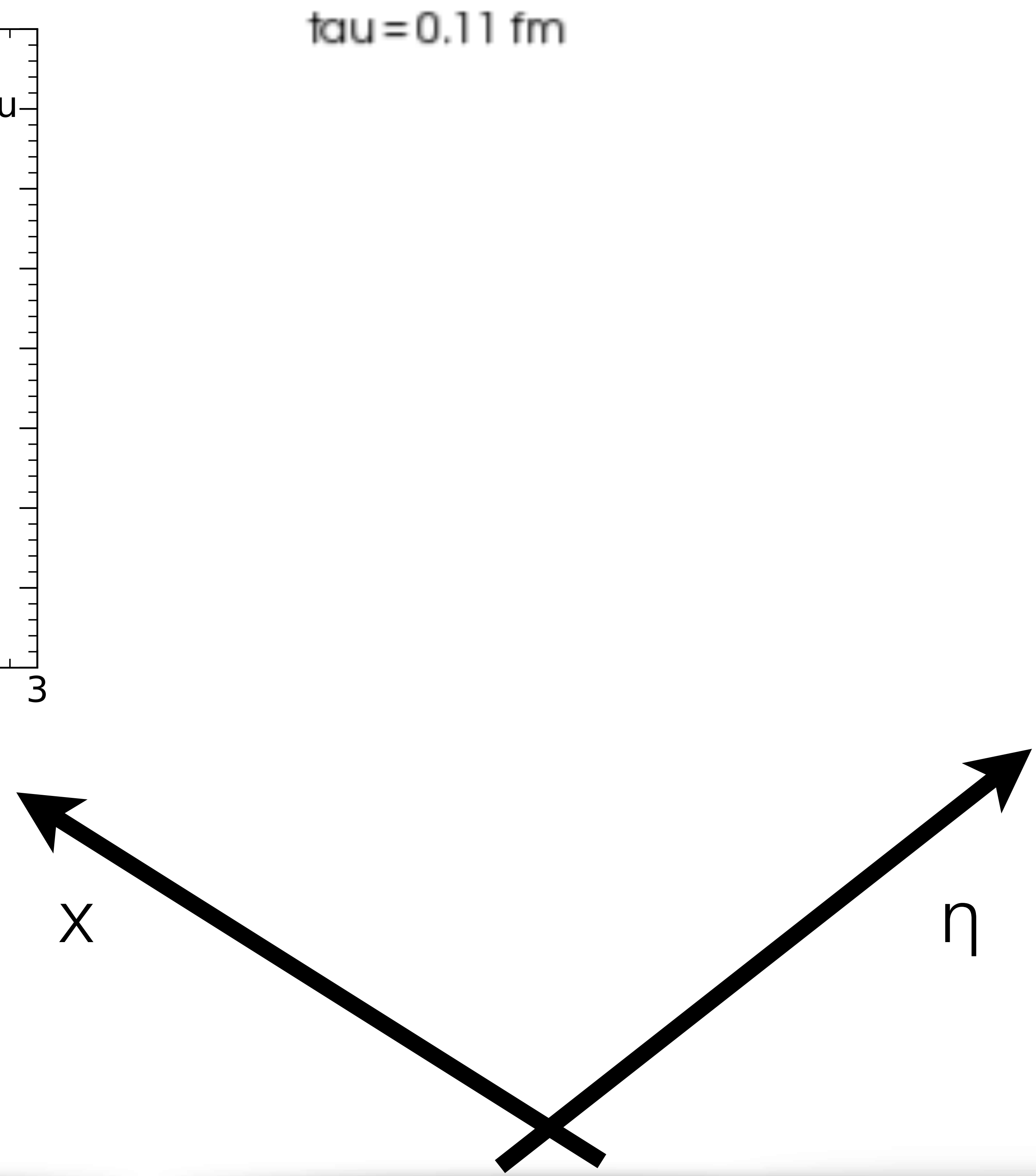

$$\sqrt{s_{\rm NN}} = 19.6\,\mathrm{GeV}$$

valence quark + LEXUS

Hydrodynamical evolution with sources

energy density

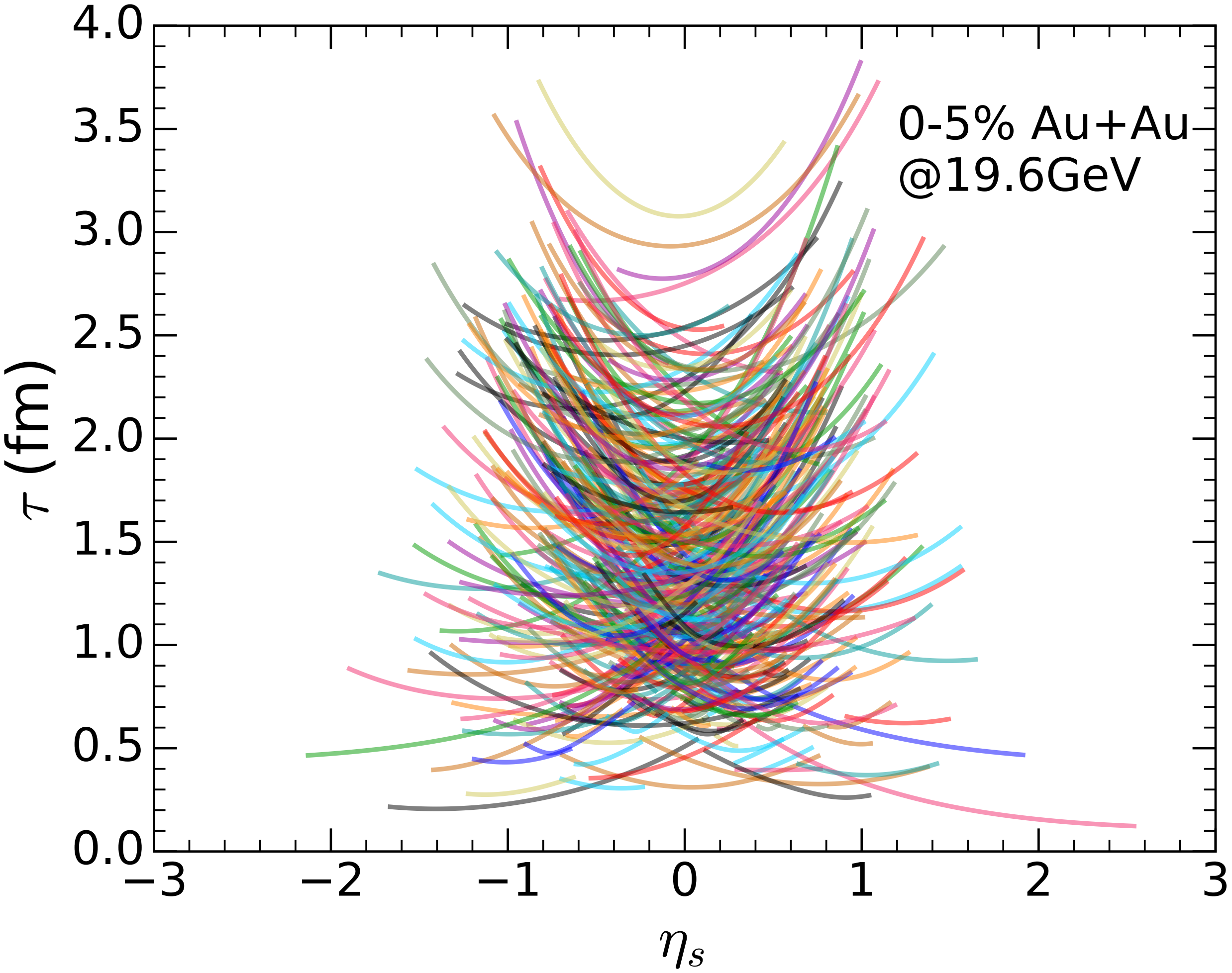

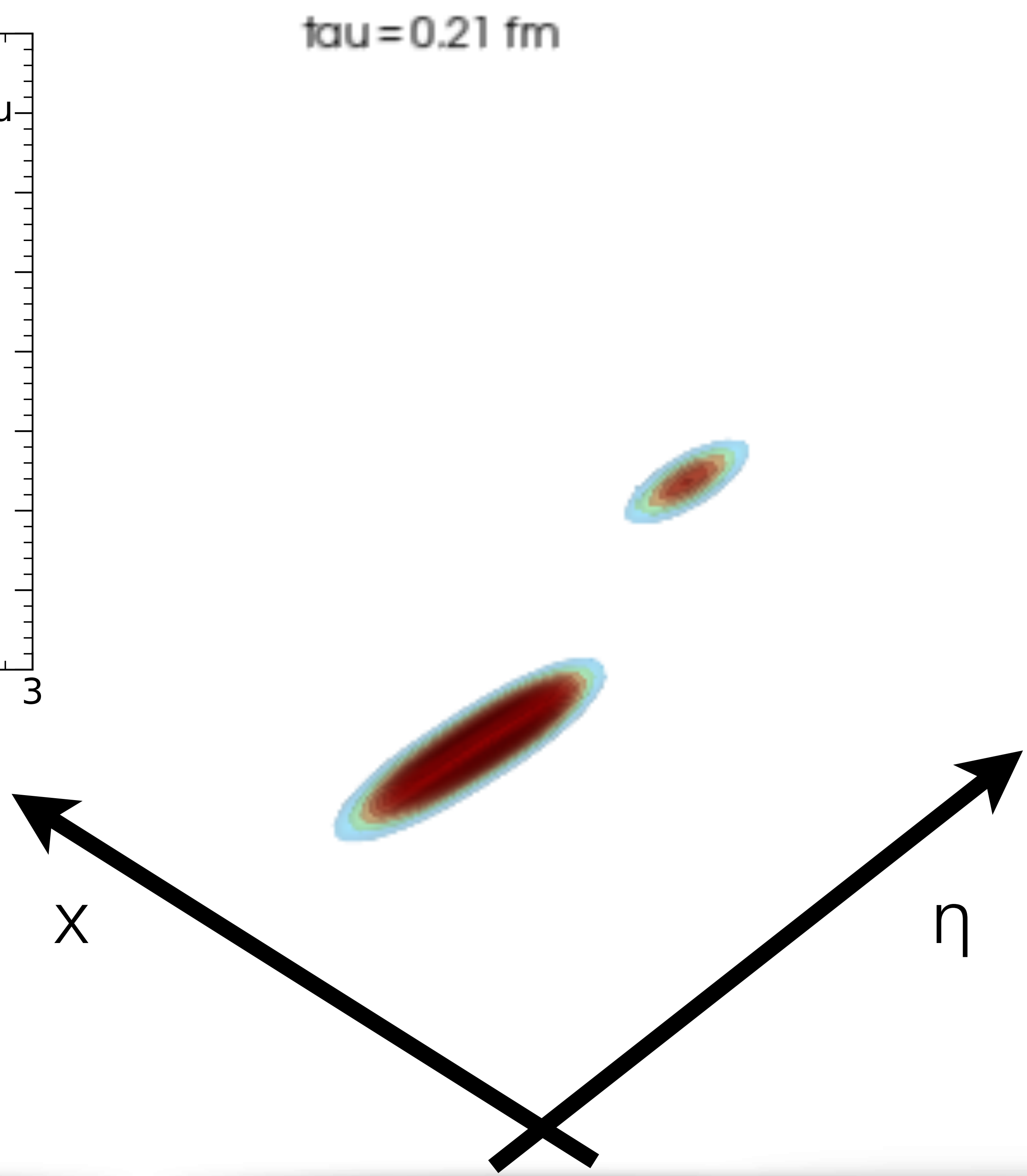

$$\sqrt{s_{\rm NN}} = 19.6\,\rm GeV$$

valence quark + LEXUS

Hydrodynamical evolution with sources

energy density

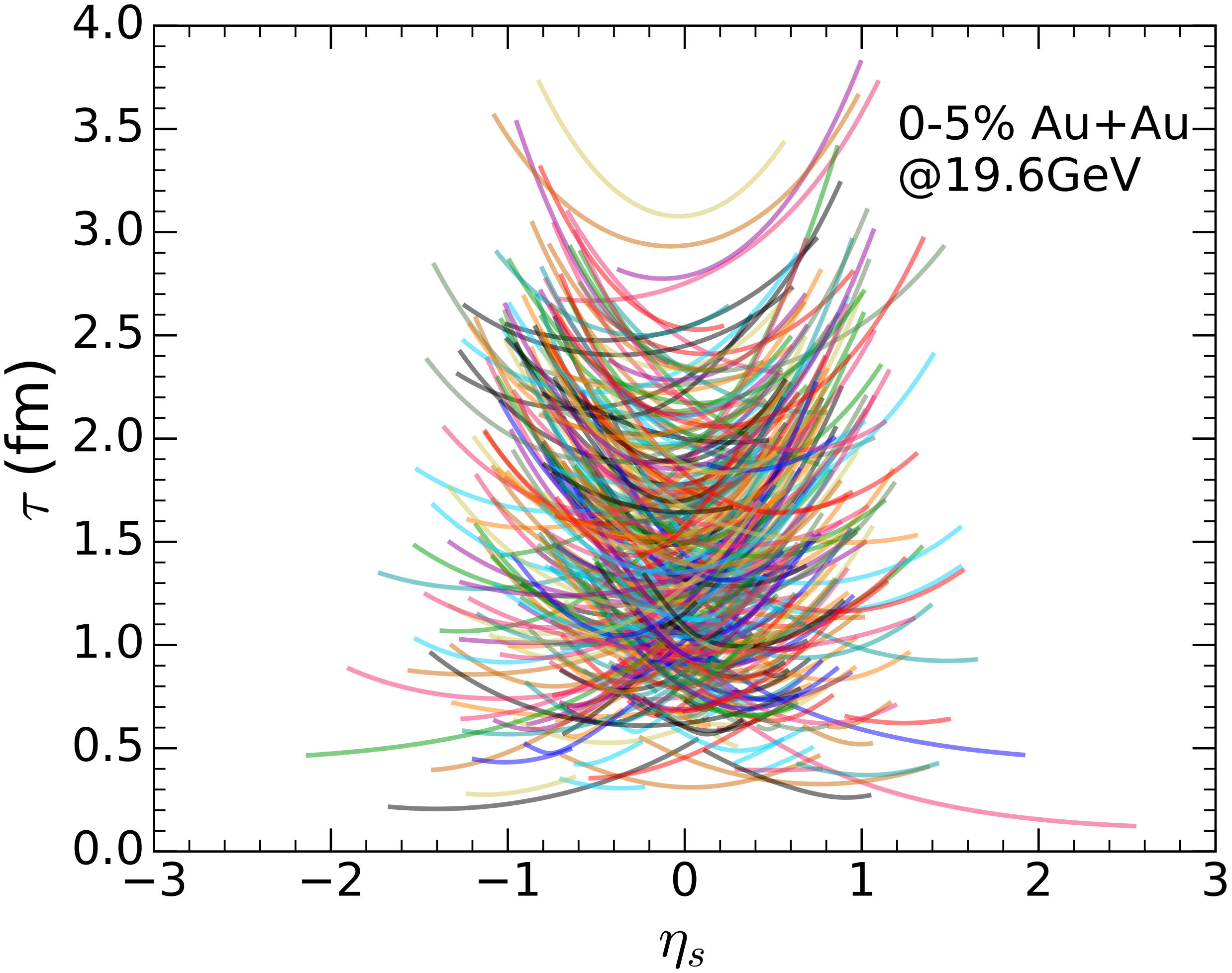

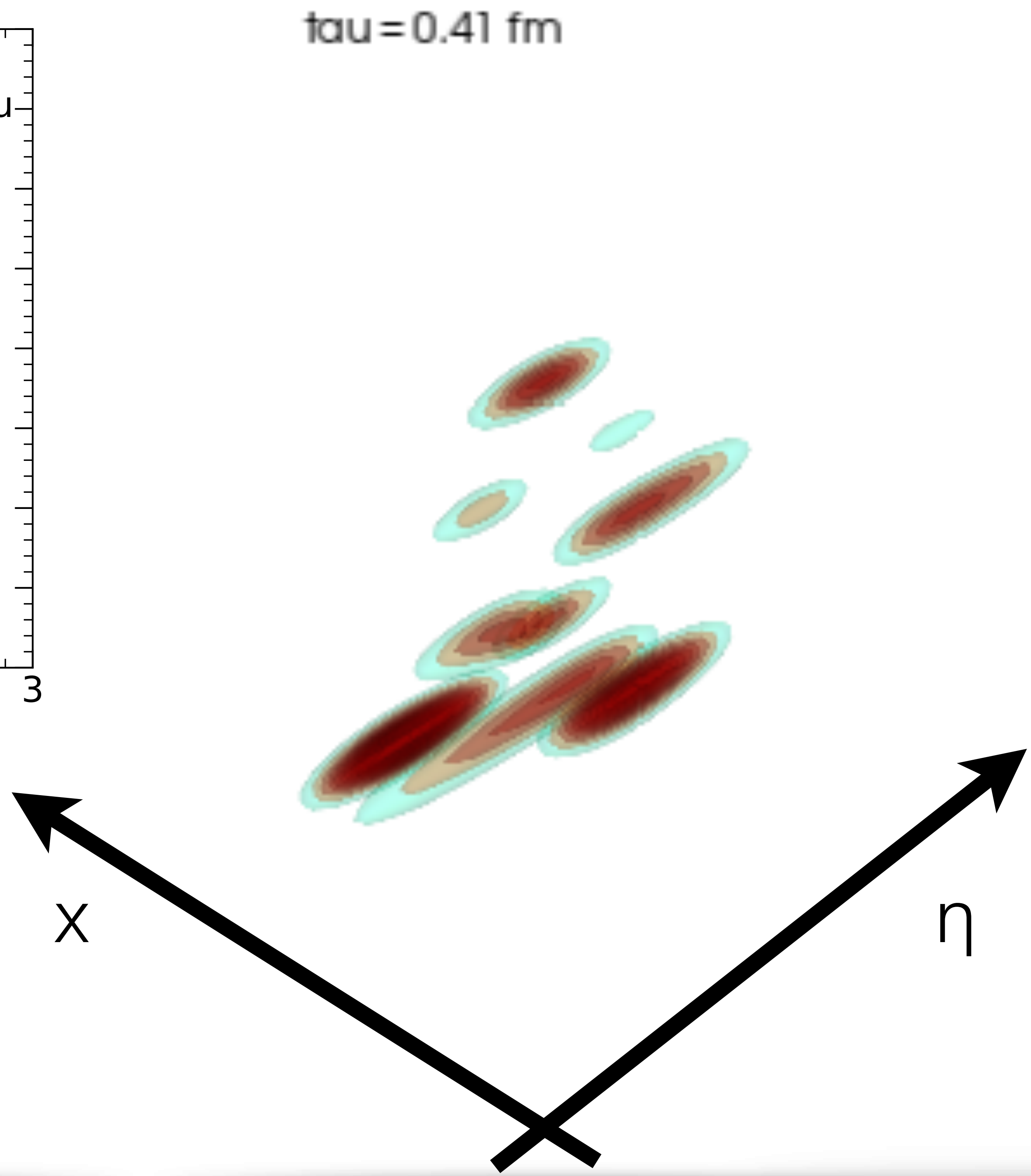

$$\sqrt{s_{\rm NN}} = 19.6\,\mathrm{GeV}$$

valence quark + LEXUS

Hydrodynamical evolution with sources

energy density

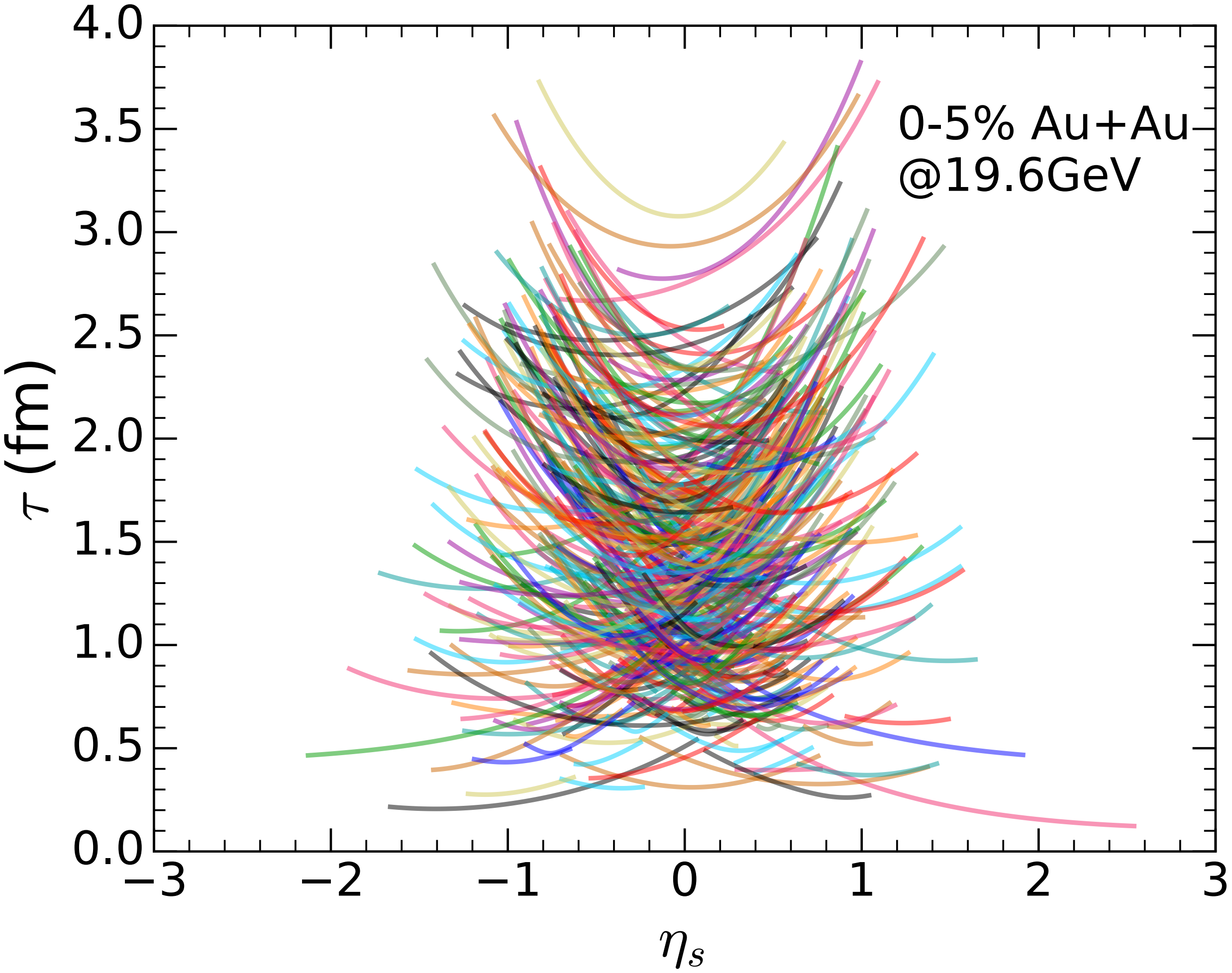

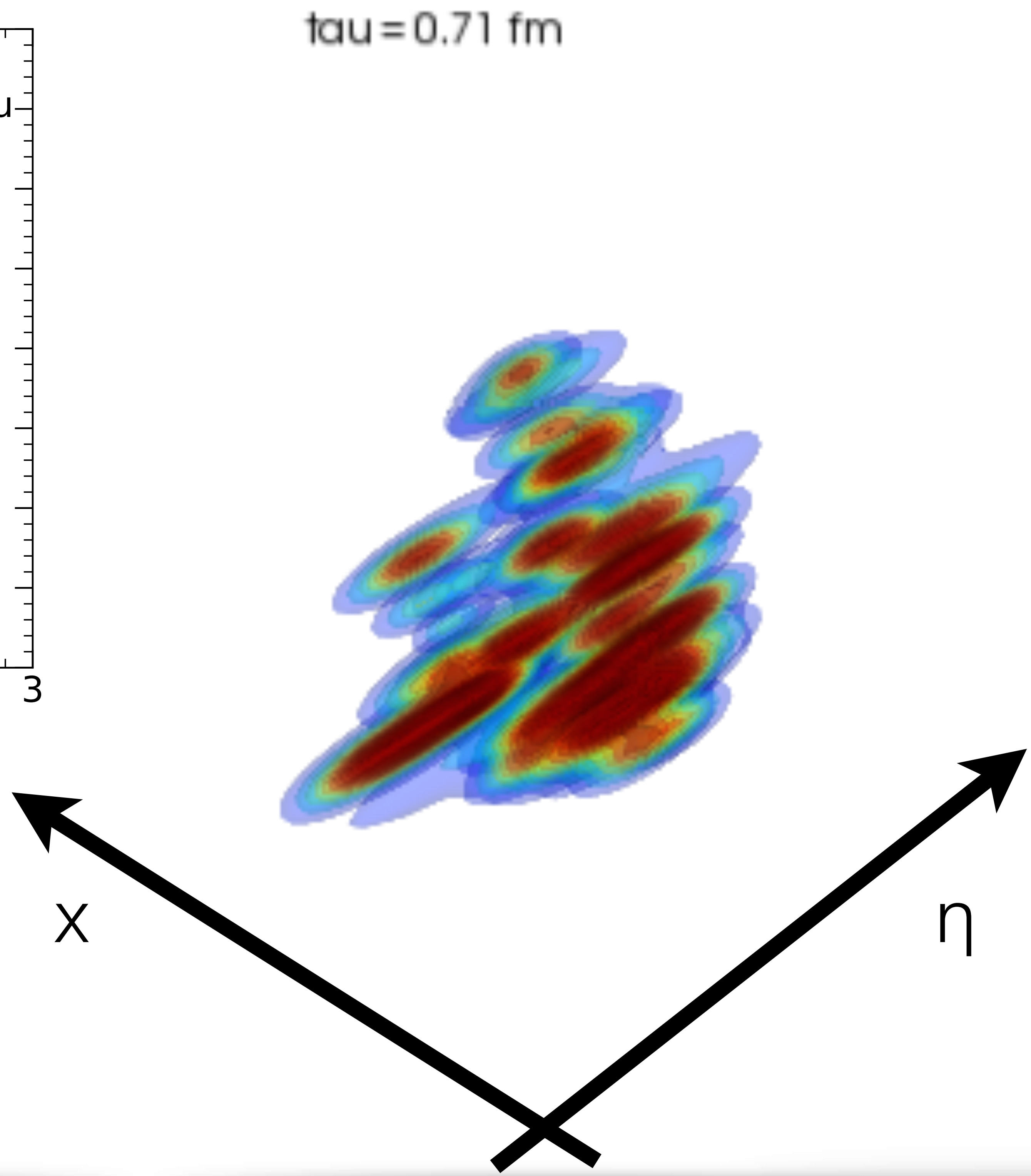

$$\sqrt{s_{\rm NN}} = 19.6\,{\rm GeV}$$

valence quark + LEXUS

Hydrodynamical evolution with sources

energy density

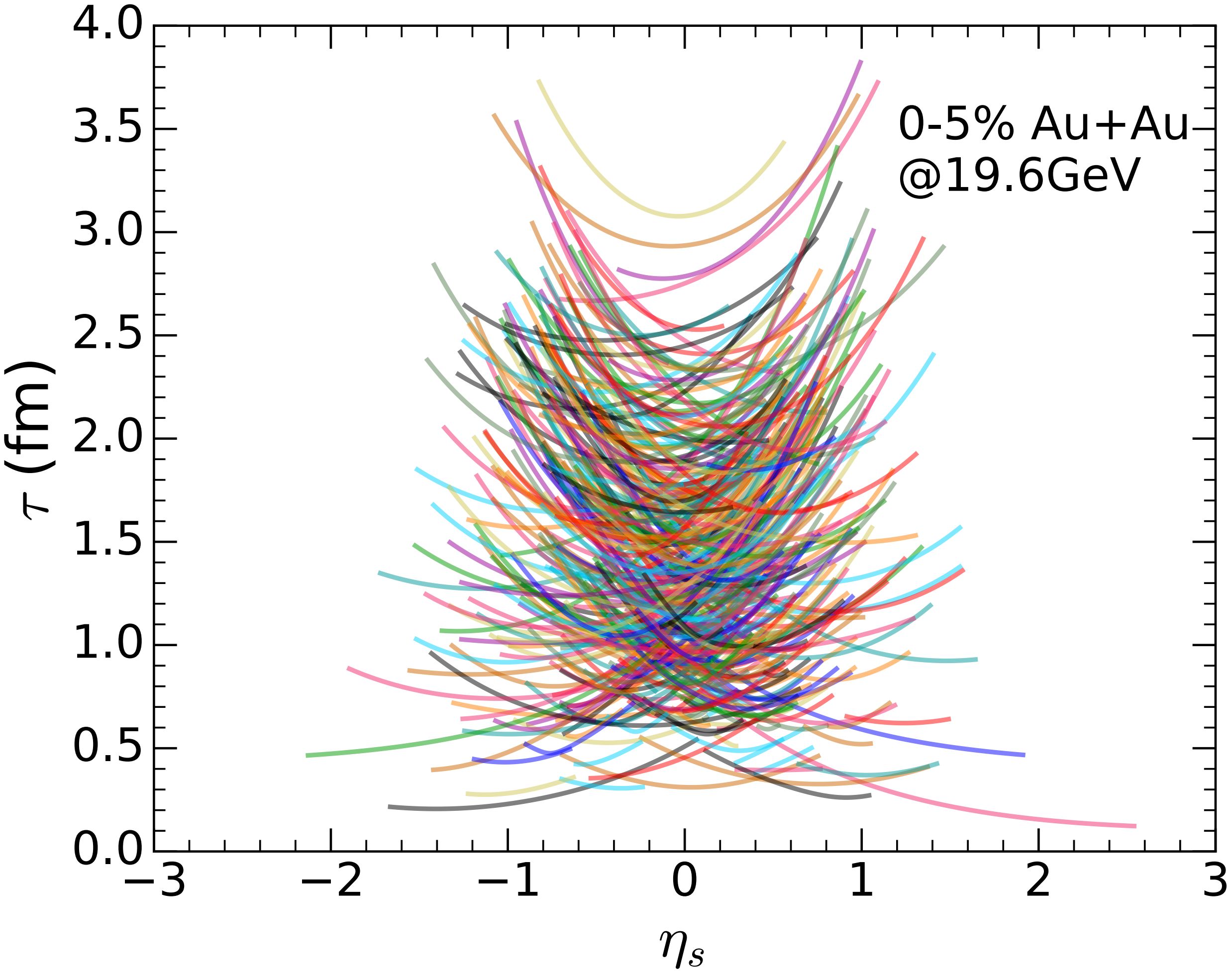

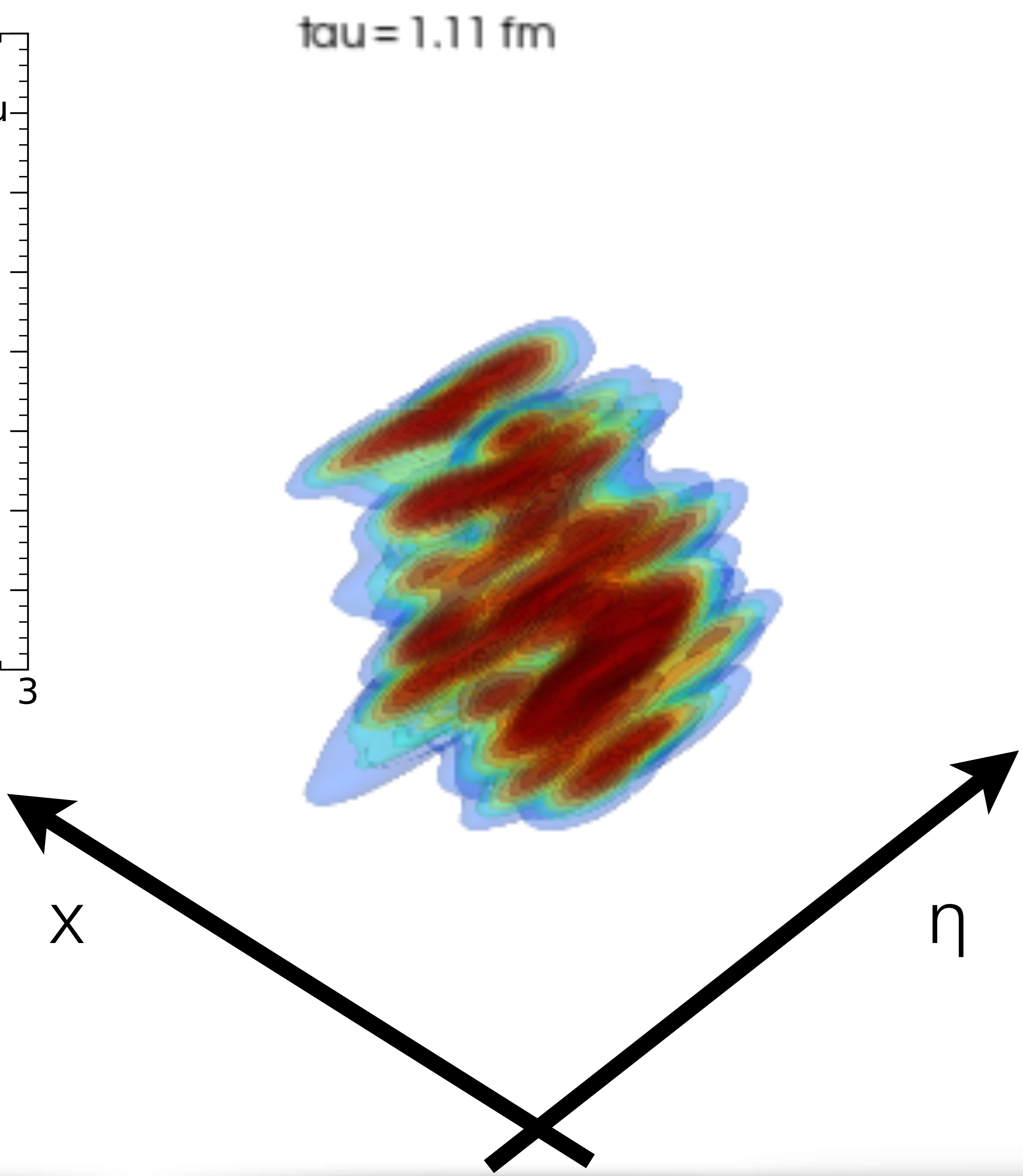

$$\sqrt{s_{\mathrm{NN}}} = 19.6\,\mathrm{GeV}$$

valence quark + LEXUS

Hydrodynamical evolution with sources

energy density

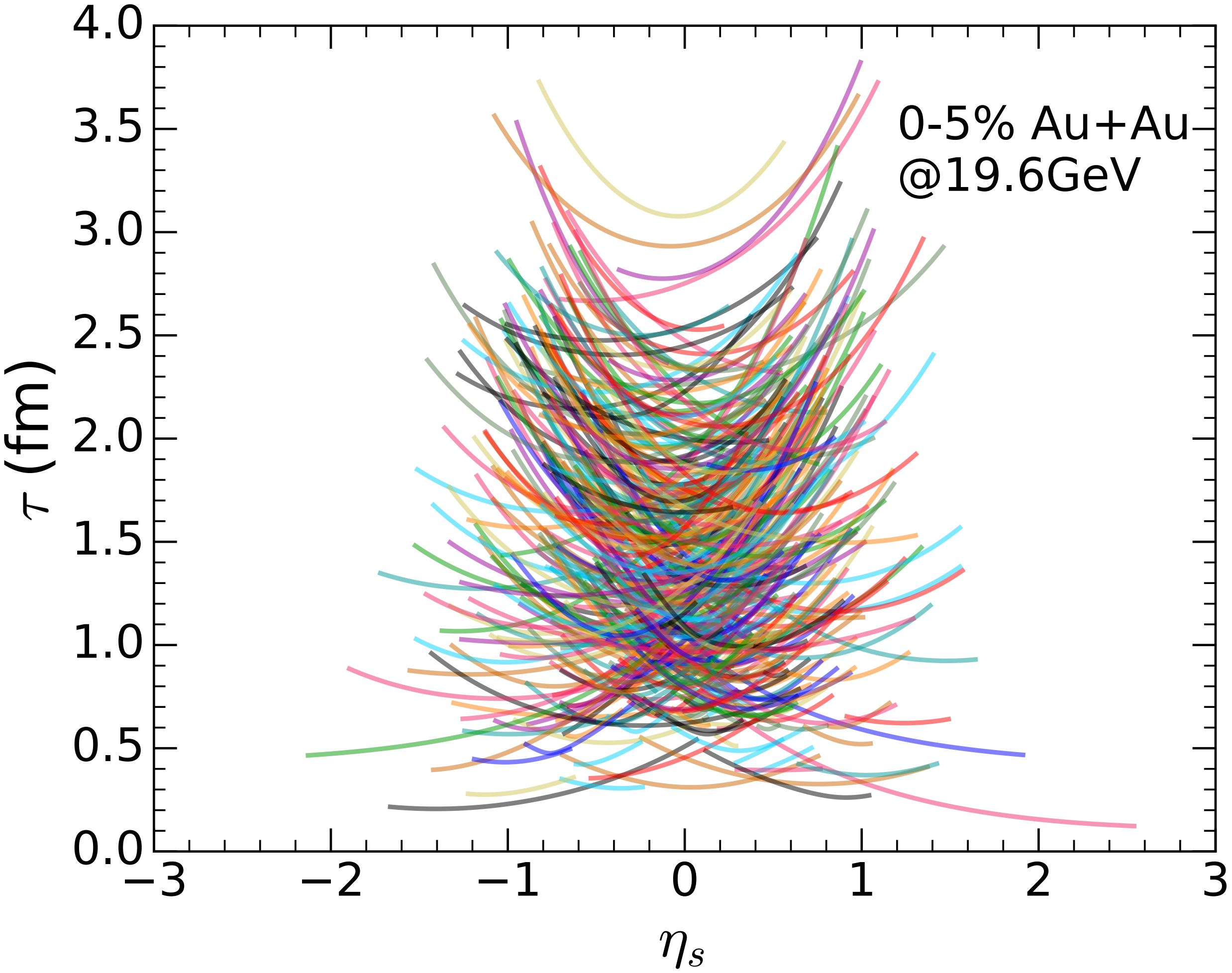

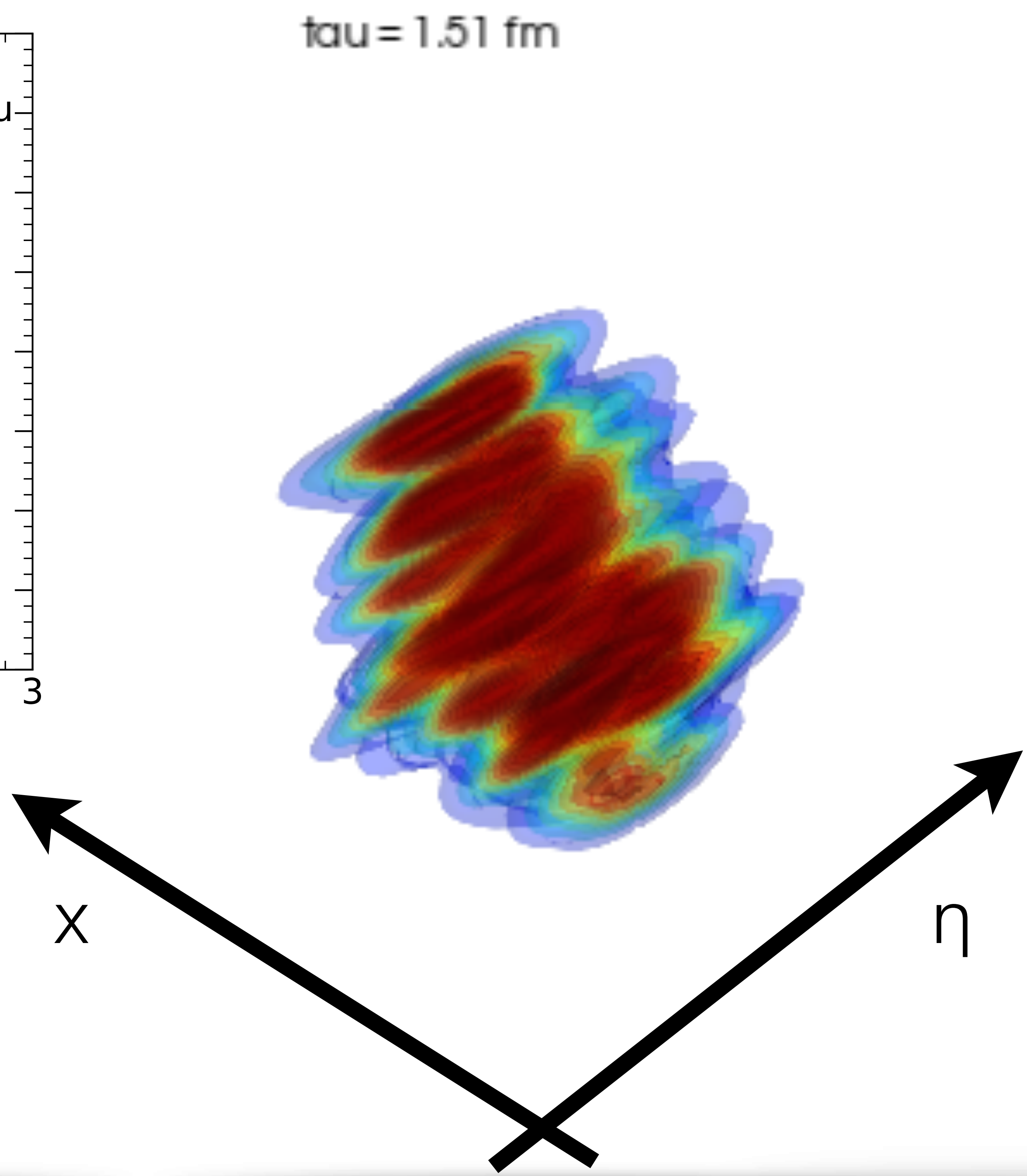

$$\sqrt{s_{\mathrm{NN}}} = 19.6\,\mathrm{GeV}$$

valence quark + LEXUS

Hydrodynamical evolution with sources

energy density

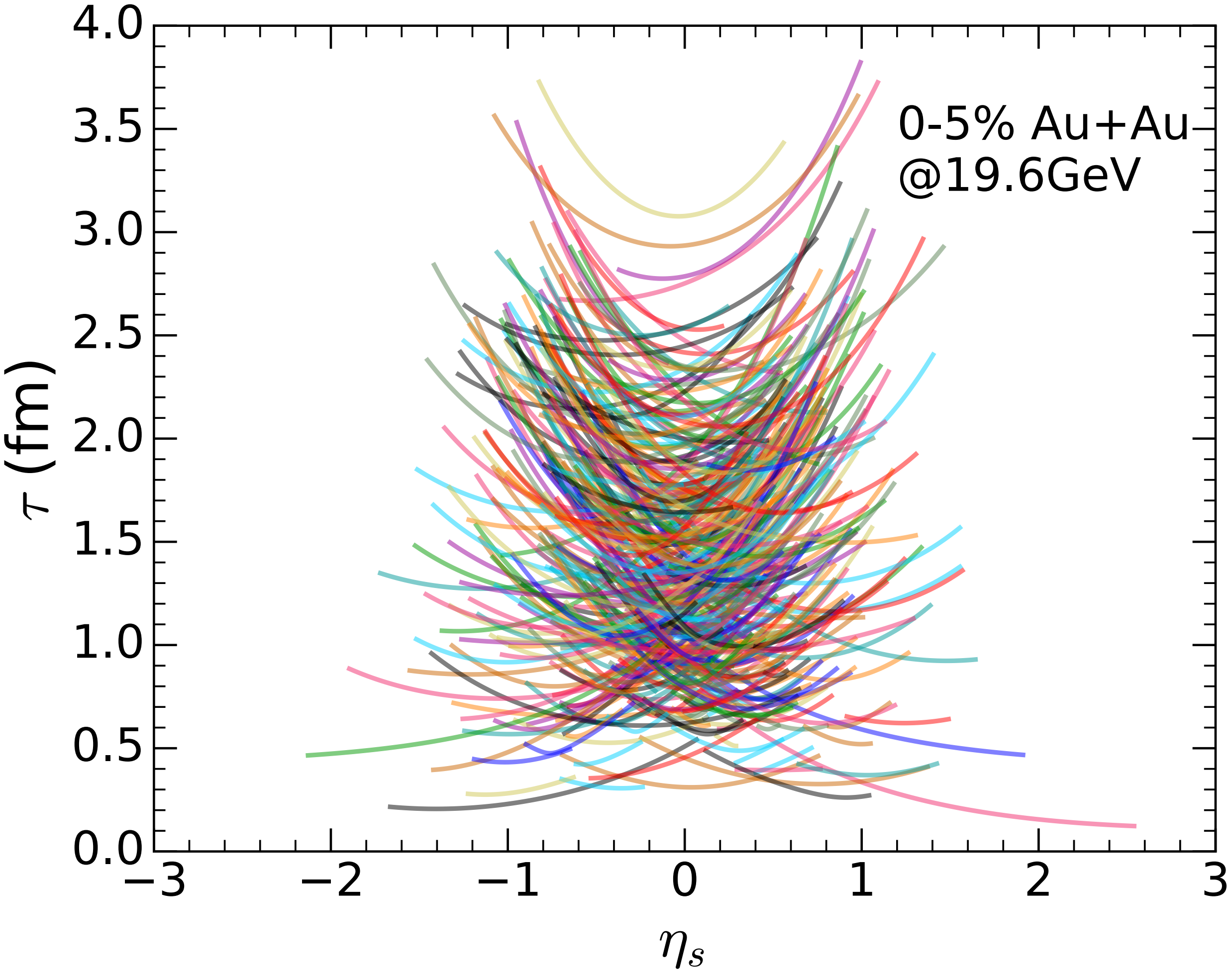

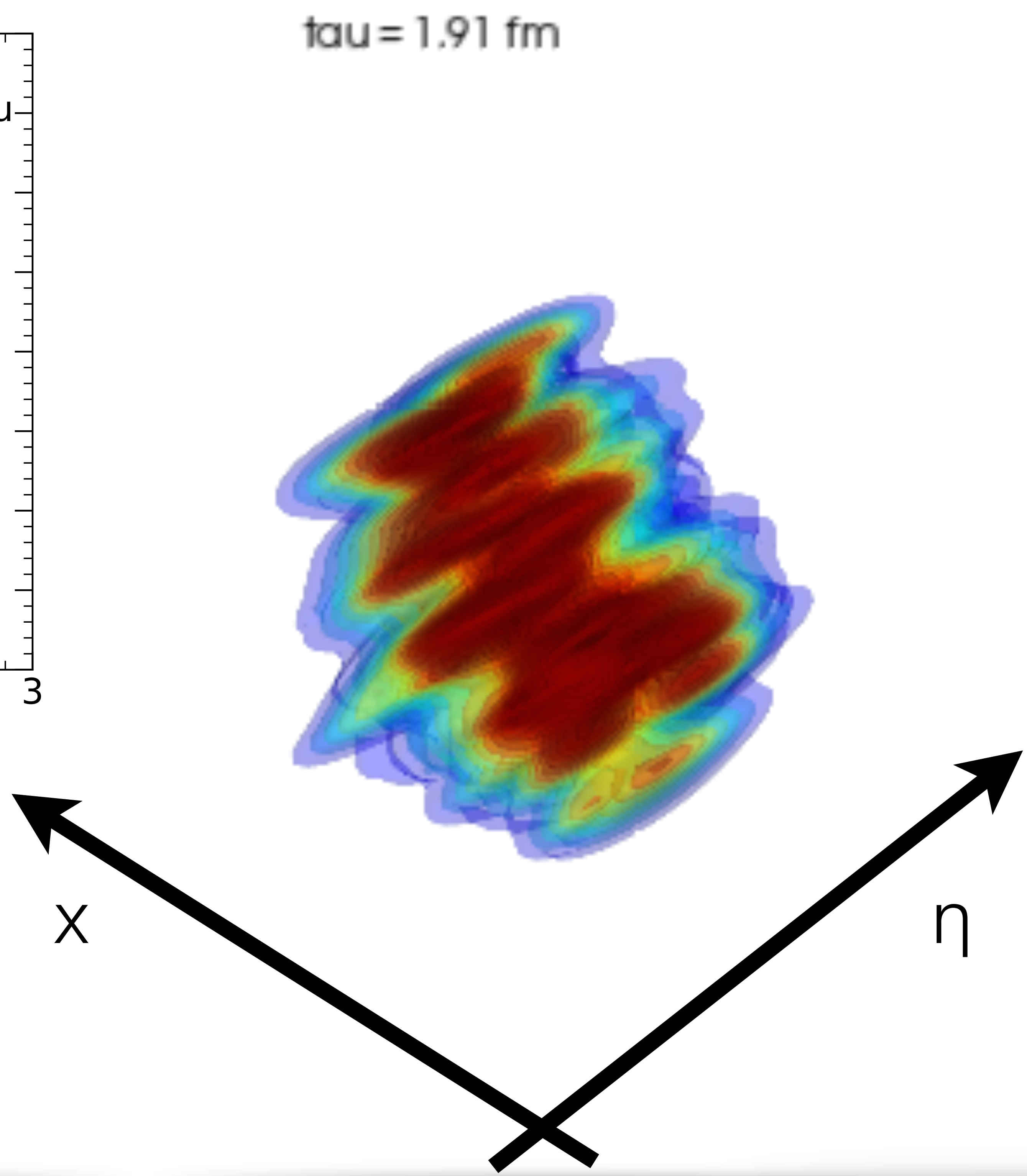

$$\sqrt{s_{\rm NN}} = 19.6\,{\rm GeV}$$

valence quark + LEXUS

Hydrodynamical evolution with sources

energy density

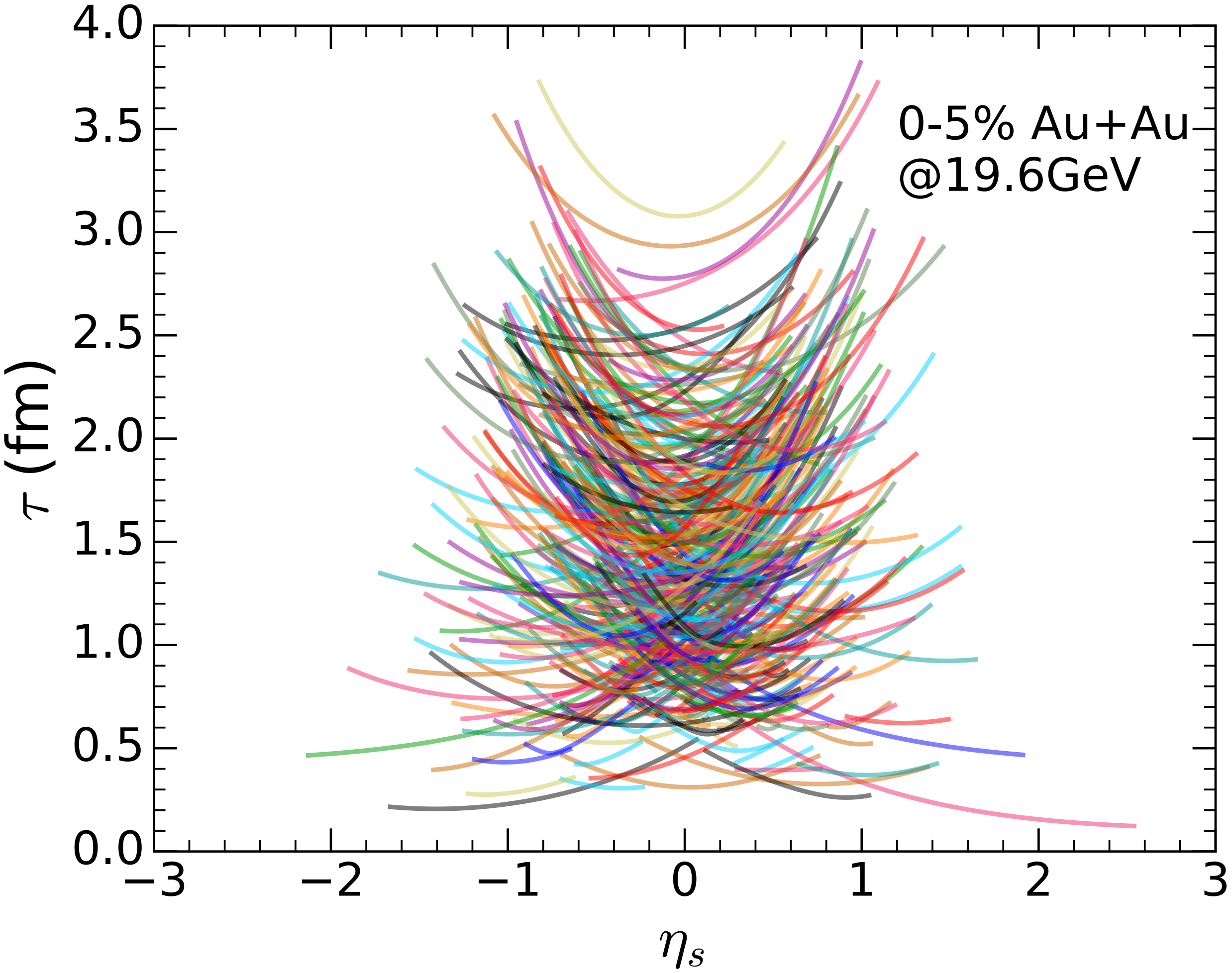

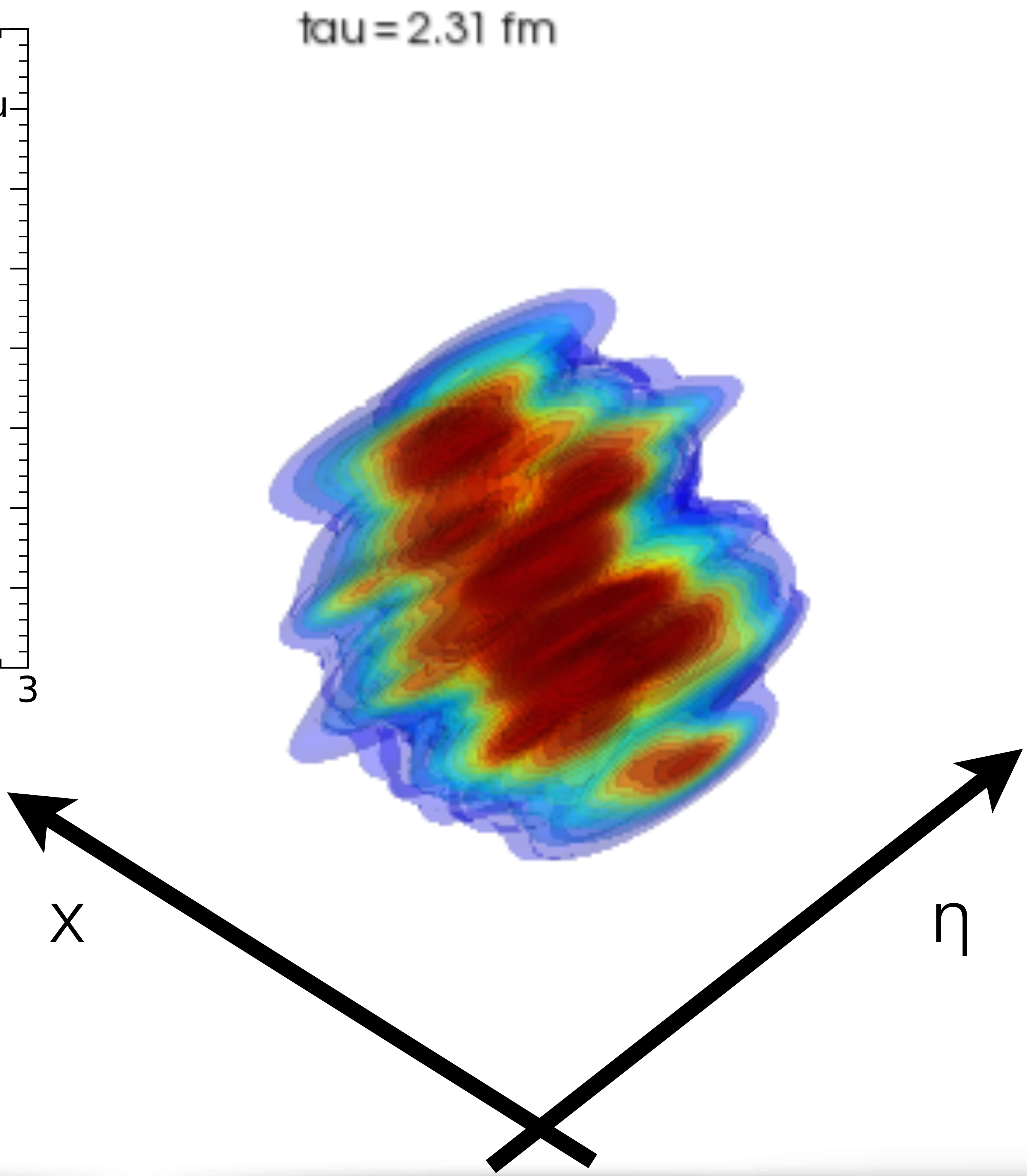

$$\sqrt{s_{\rm NN}} = 19.6\,{\rm GeV}$$

valence quark + LEXUS

Hydrodynamical evolution with sources

energy density

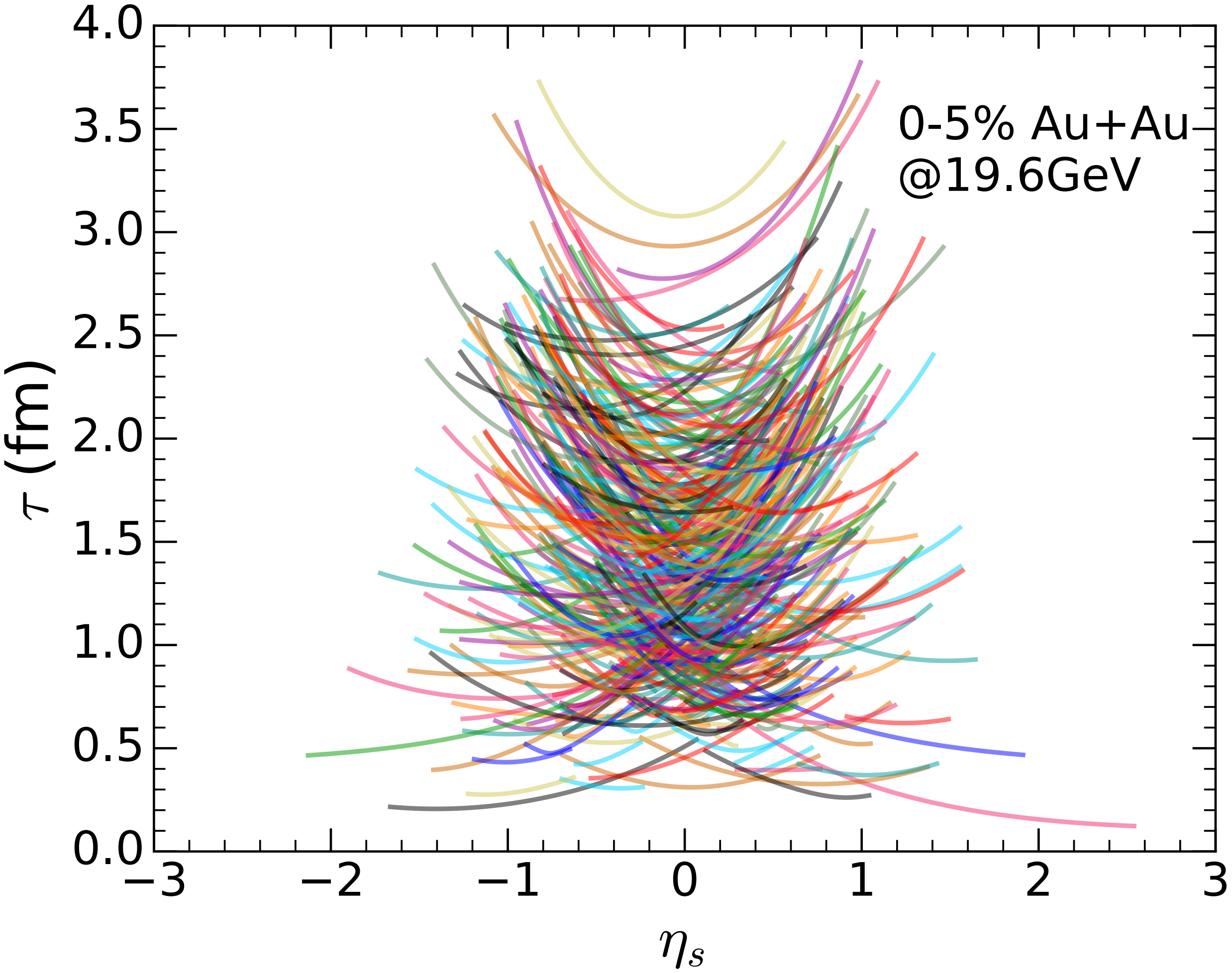

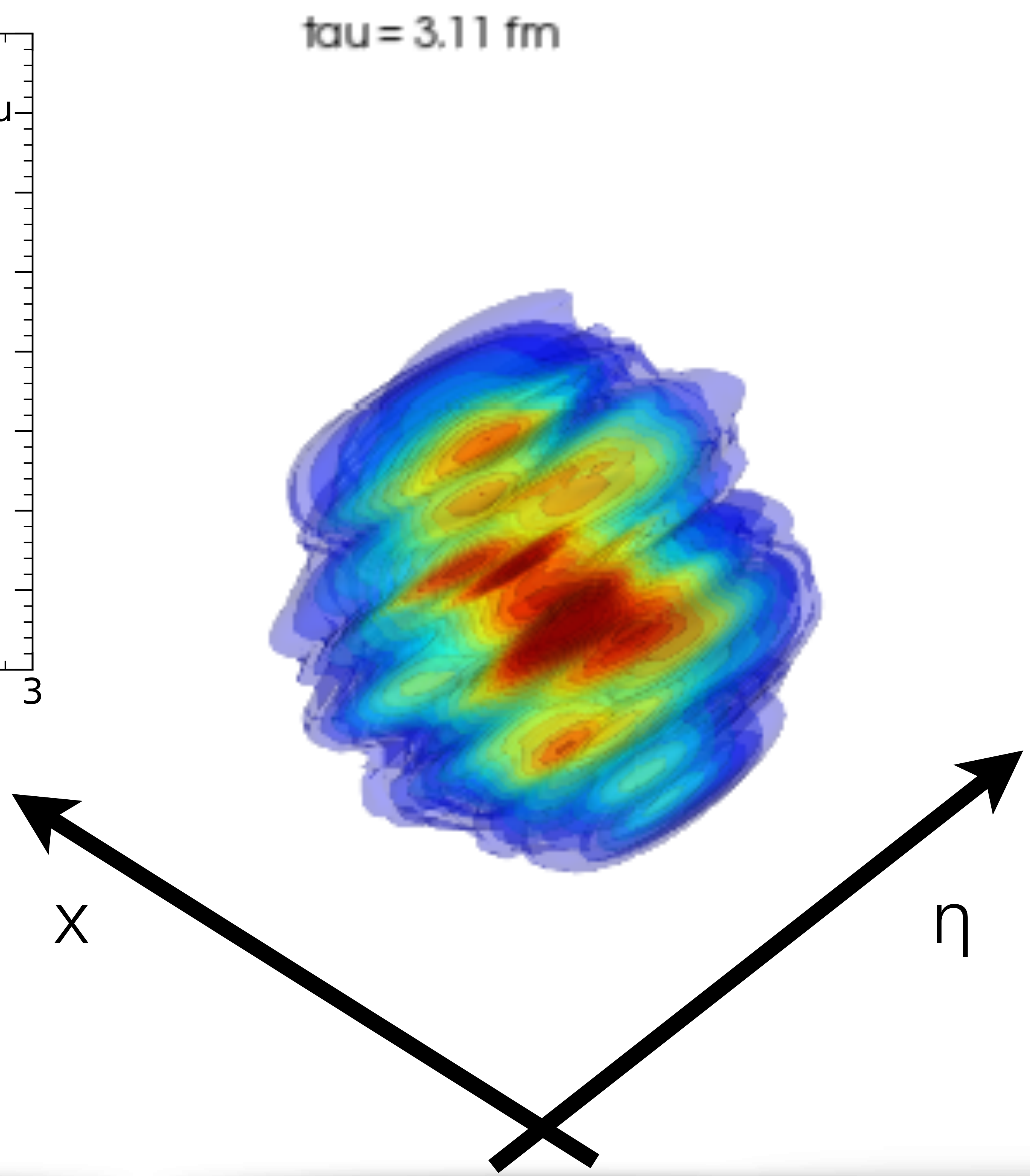

$$\sqrt{s_{\mathrm{NN}}} = 19.6\,\mathrm{GeV}$$

valence quark + LEXUS

Hydrodynamical evolution with sources

energy density

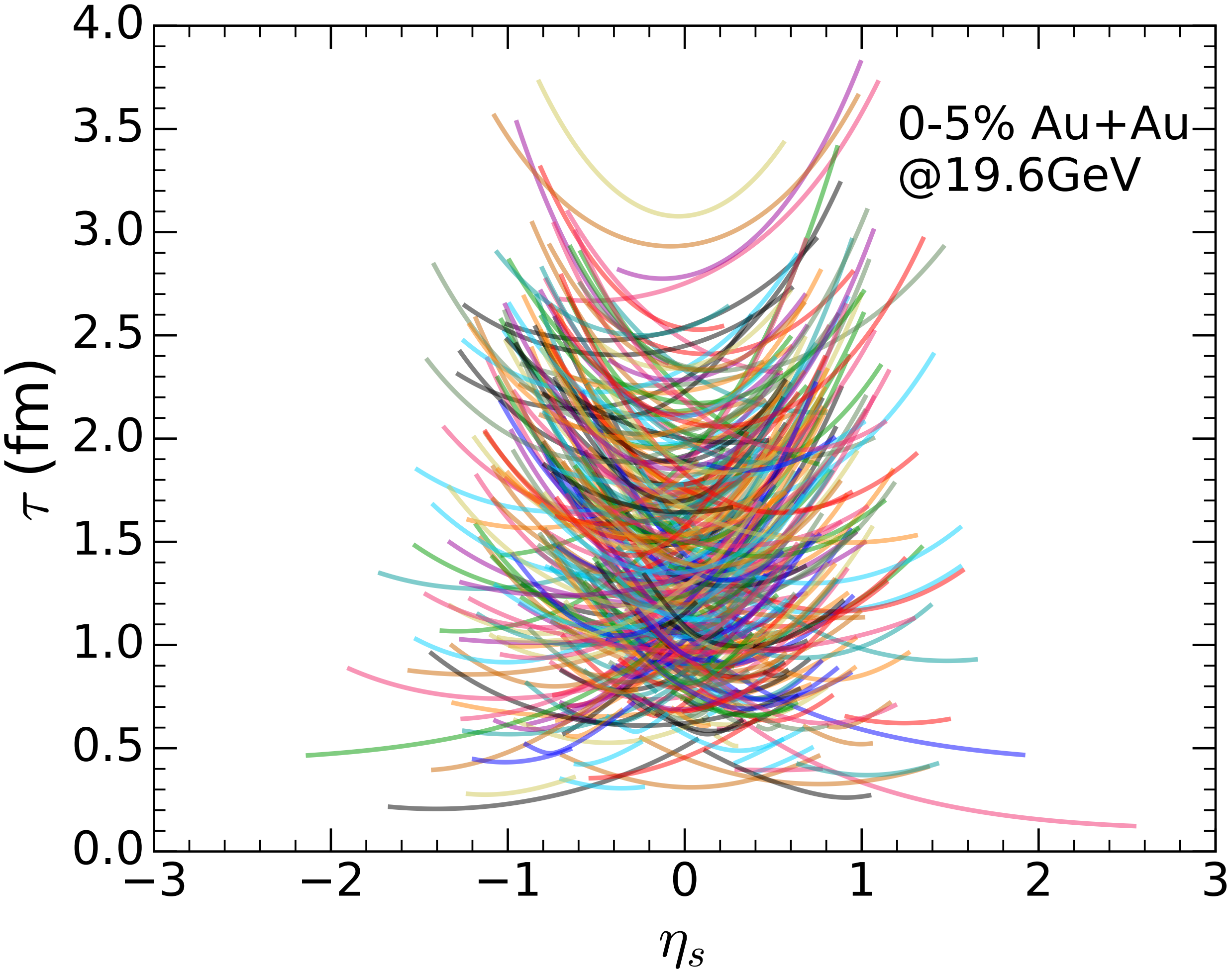

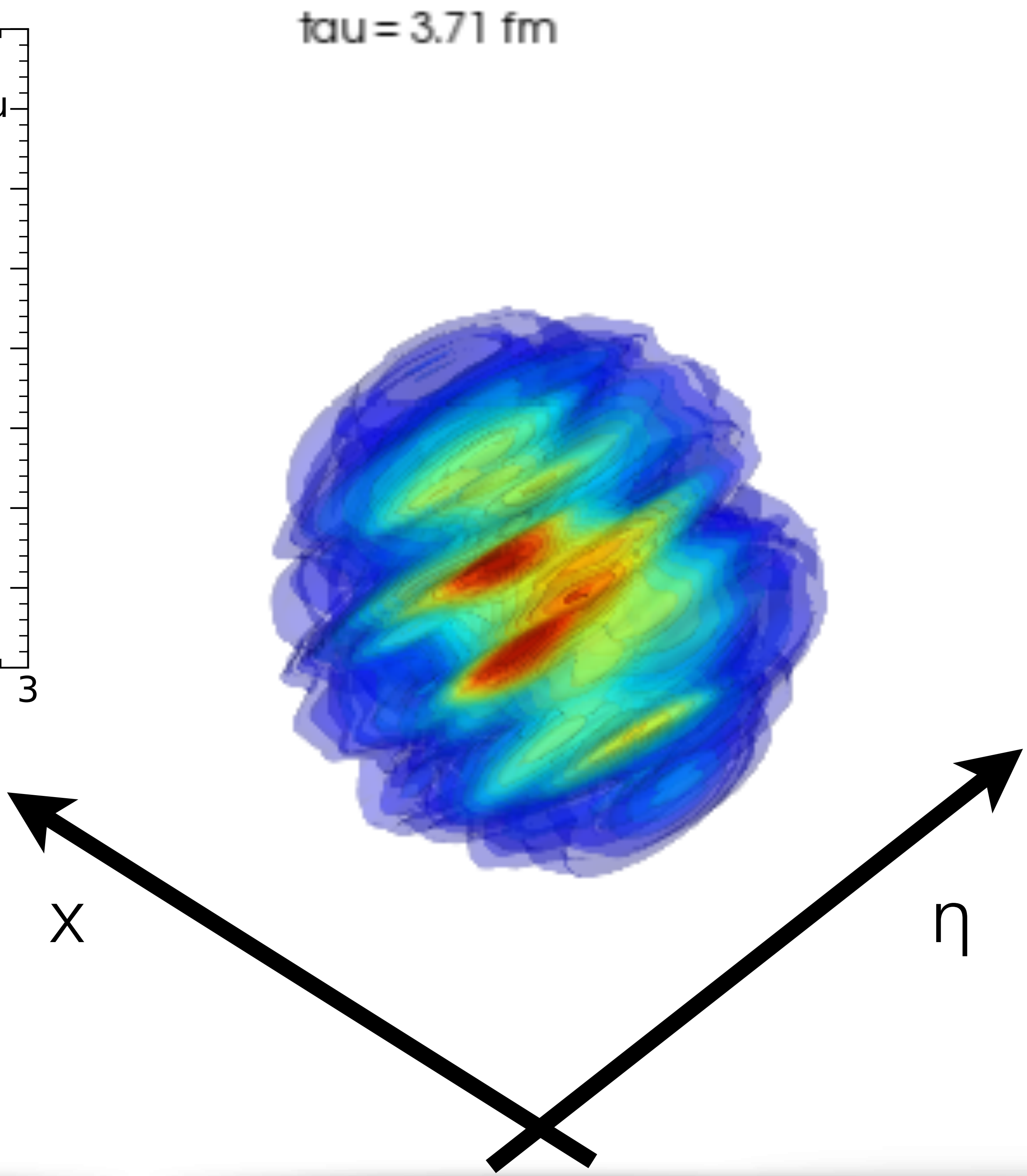

$$\sqrt{s_{\mathrm{NN}}} = 19.6\,\mathrm{GeV}$$

valence quark + LEXUS

Hydrodynamical evolution with sources

energy density

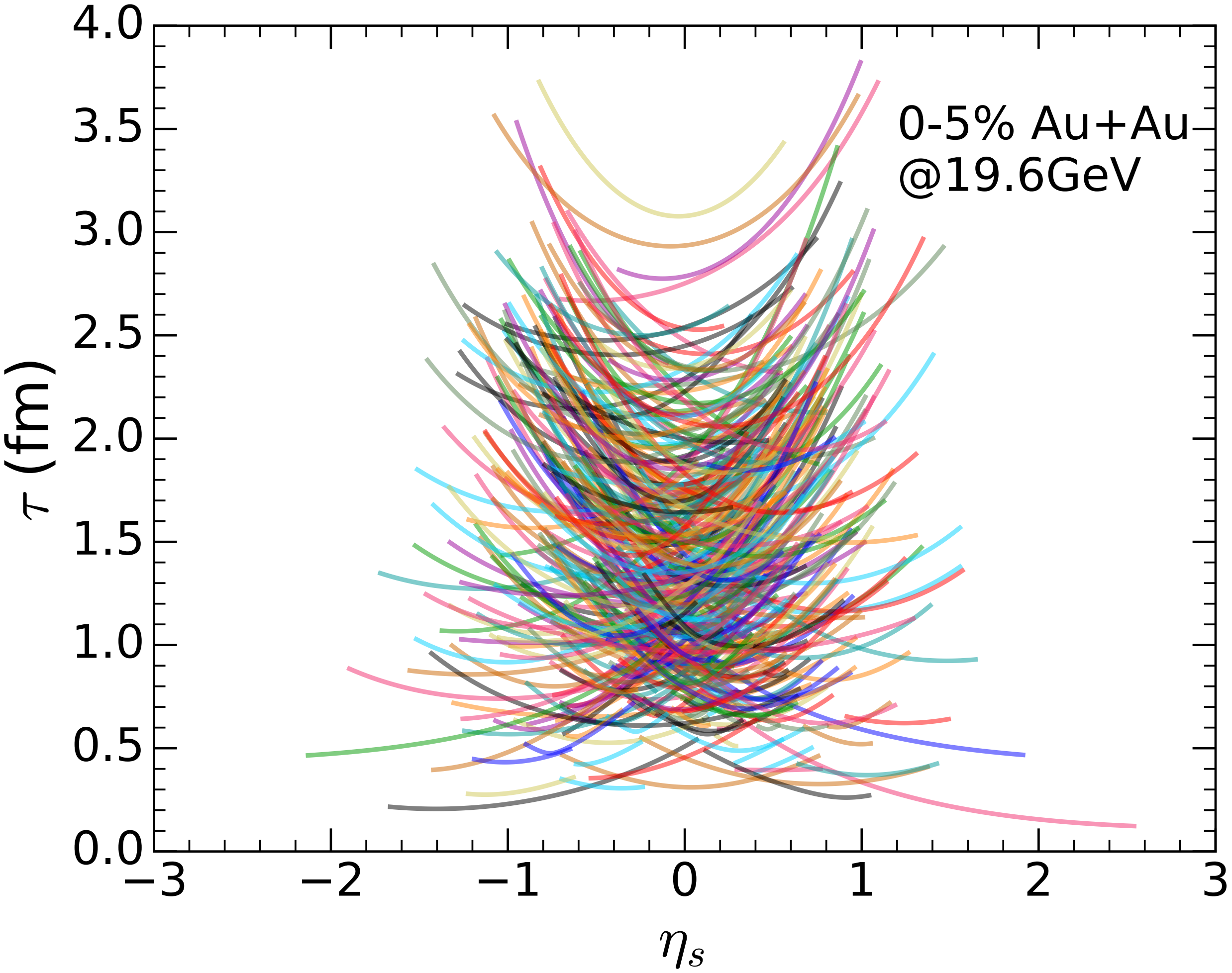

$$\sqrt{s_{\rm NN}} = 19.6\,\mathrm{GeV}$$

valence quark + LEXUS

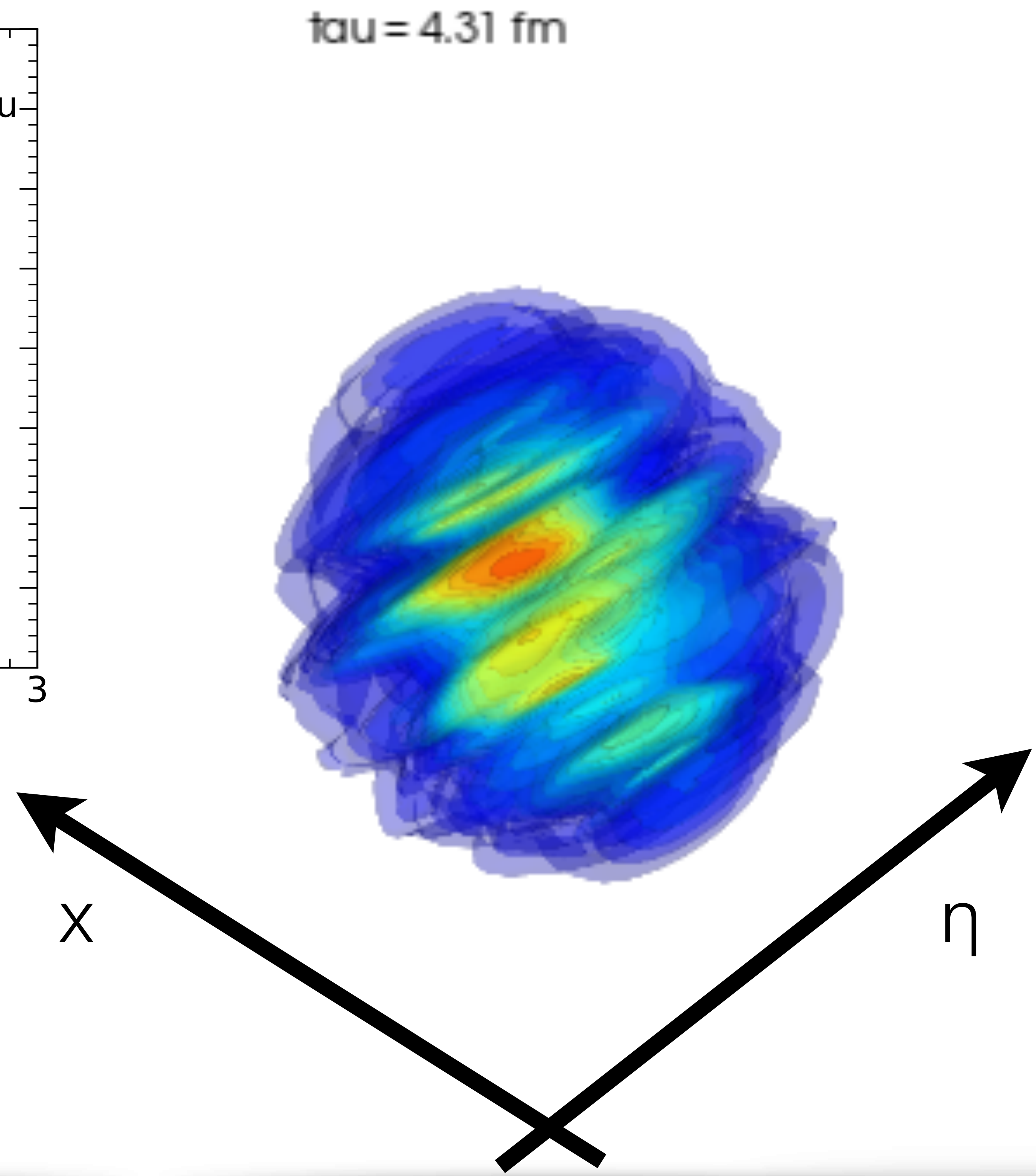

energy density

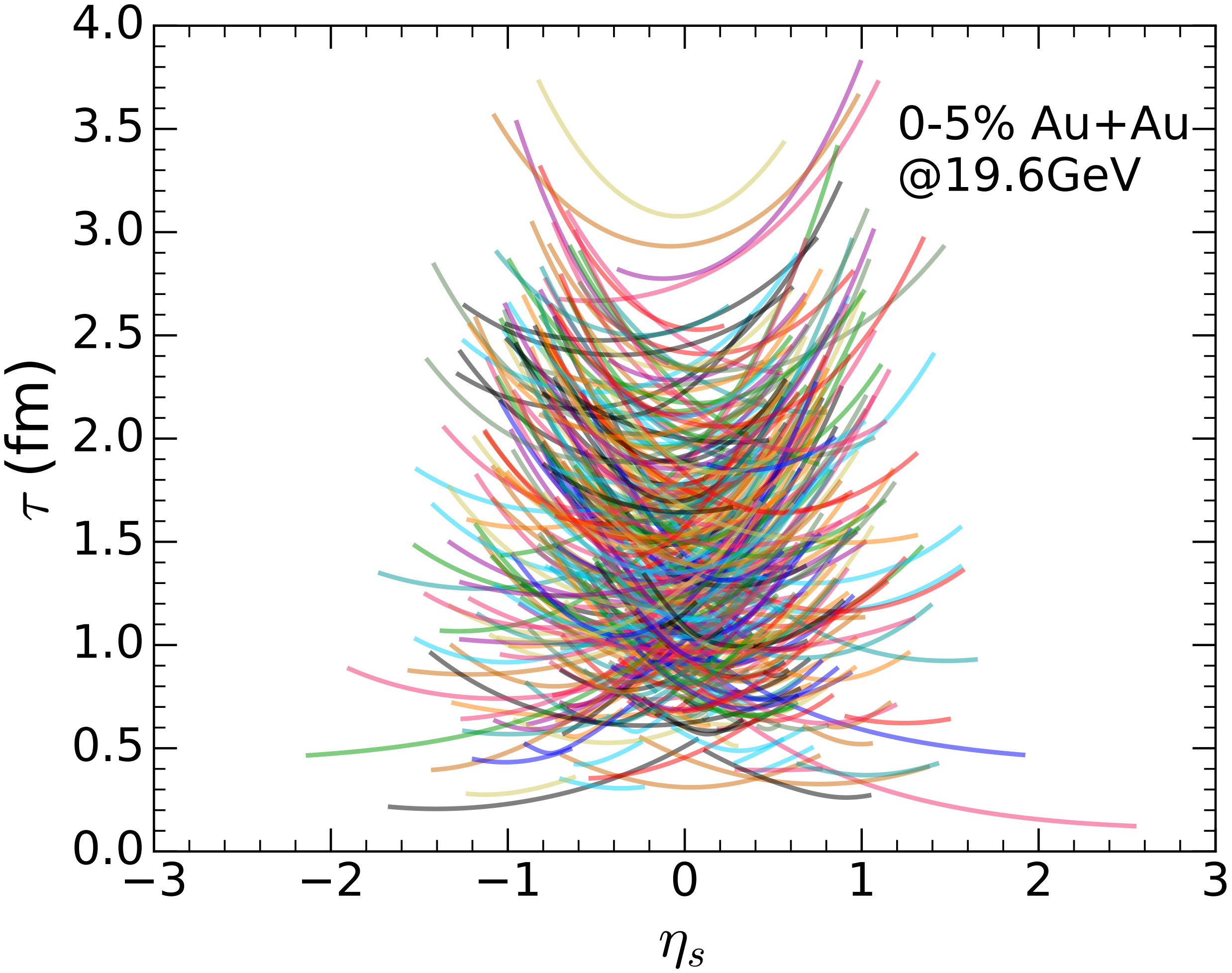

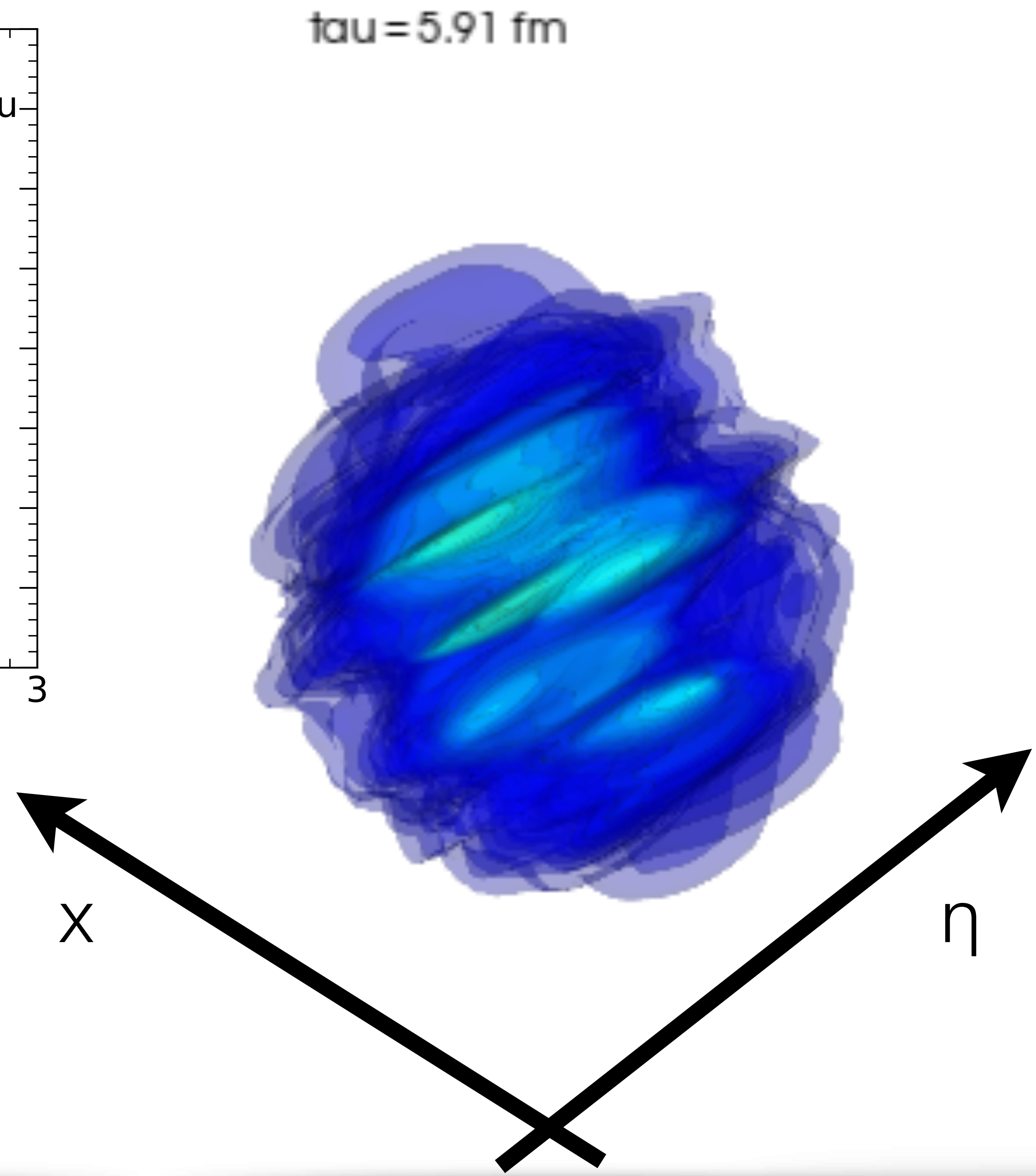

$$\sqrt{s_{\mathrm{NN}}} = 19.6\,\mathrm{GeV}$$

valence quark + LEXUS

Hydrodynamical evolution with sources

energy density

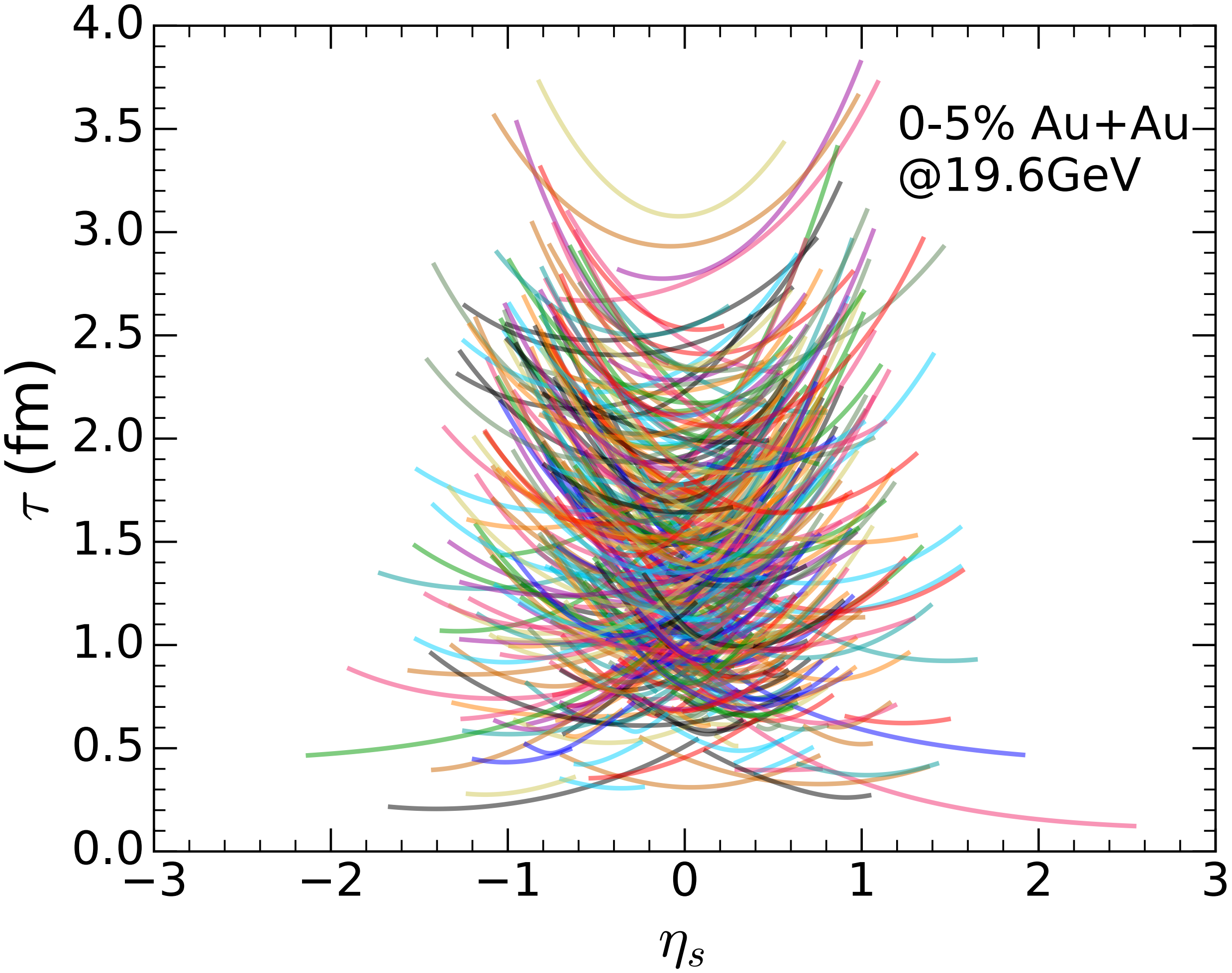

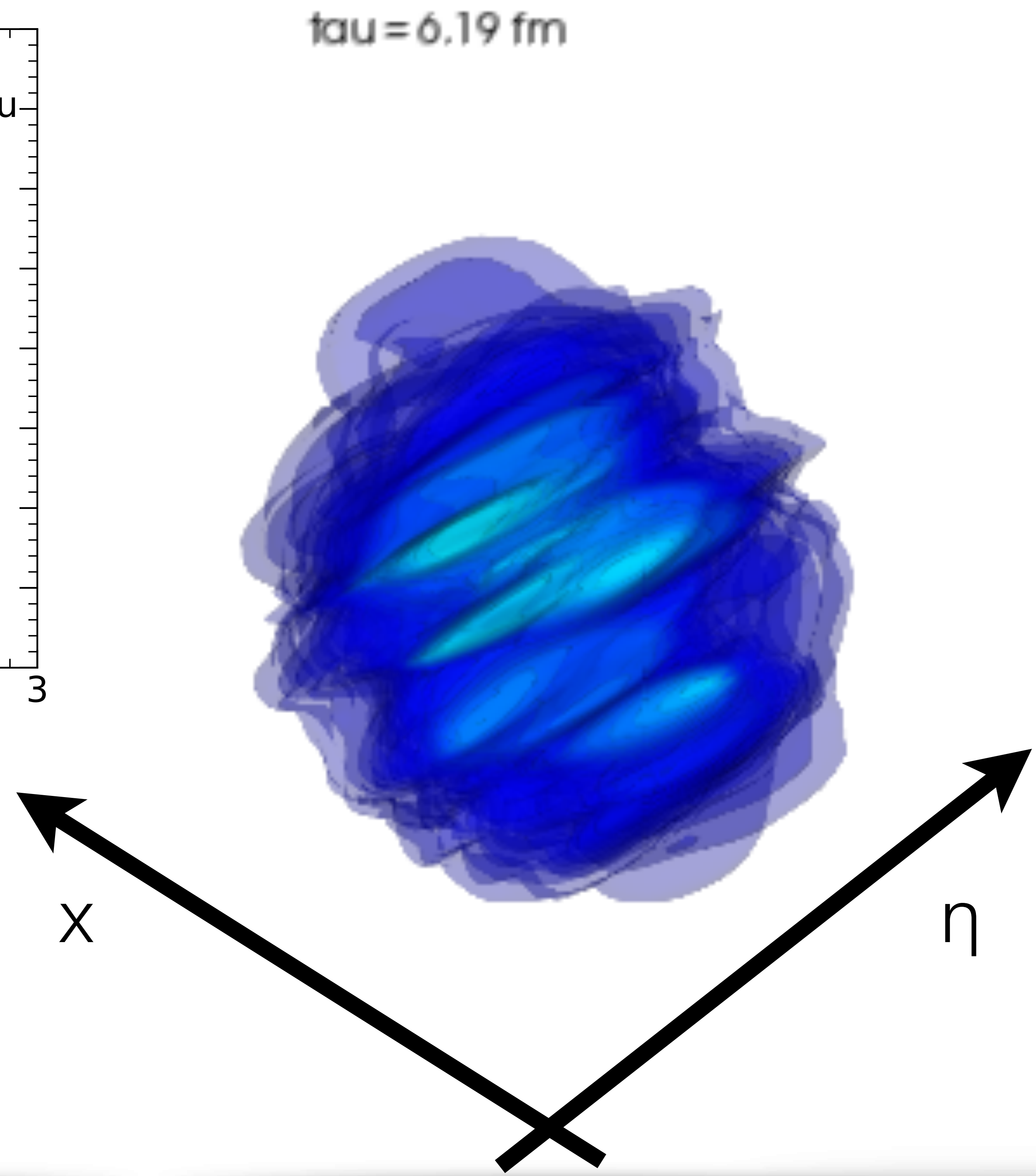

$$\sqrt{s_{\rm NN}} = 19.6\,\mathrm{GeV}$$

valence quark + LEXUS

net baryon density

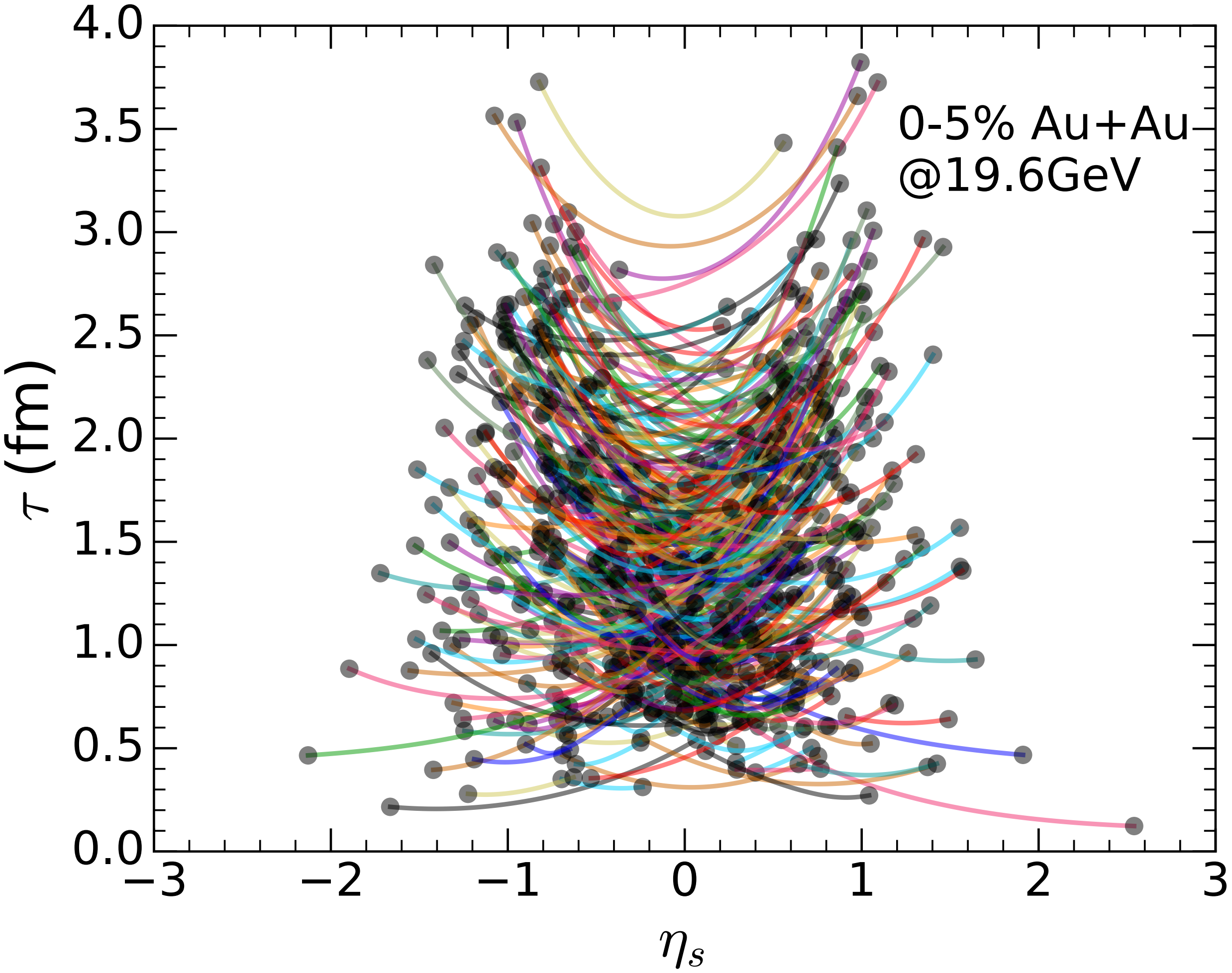

$$\sqrt{s_{\mathrm{NN}}} = 19.6\,\mathrm{GeV}$$

valence quark + LEXUS

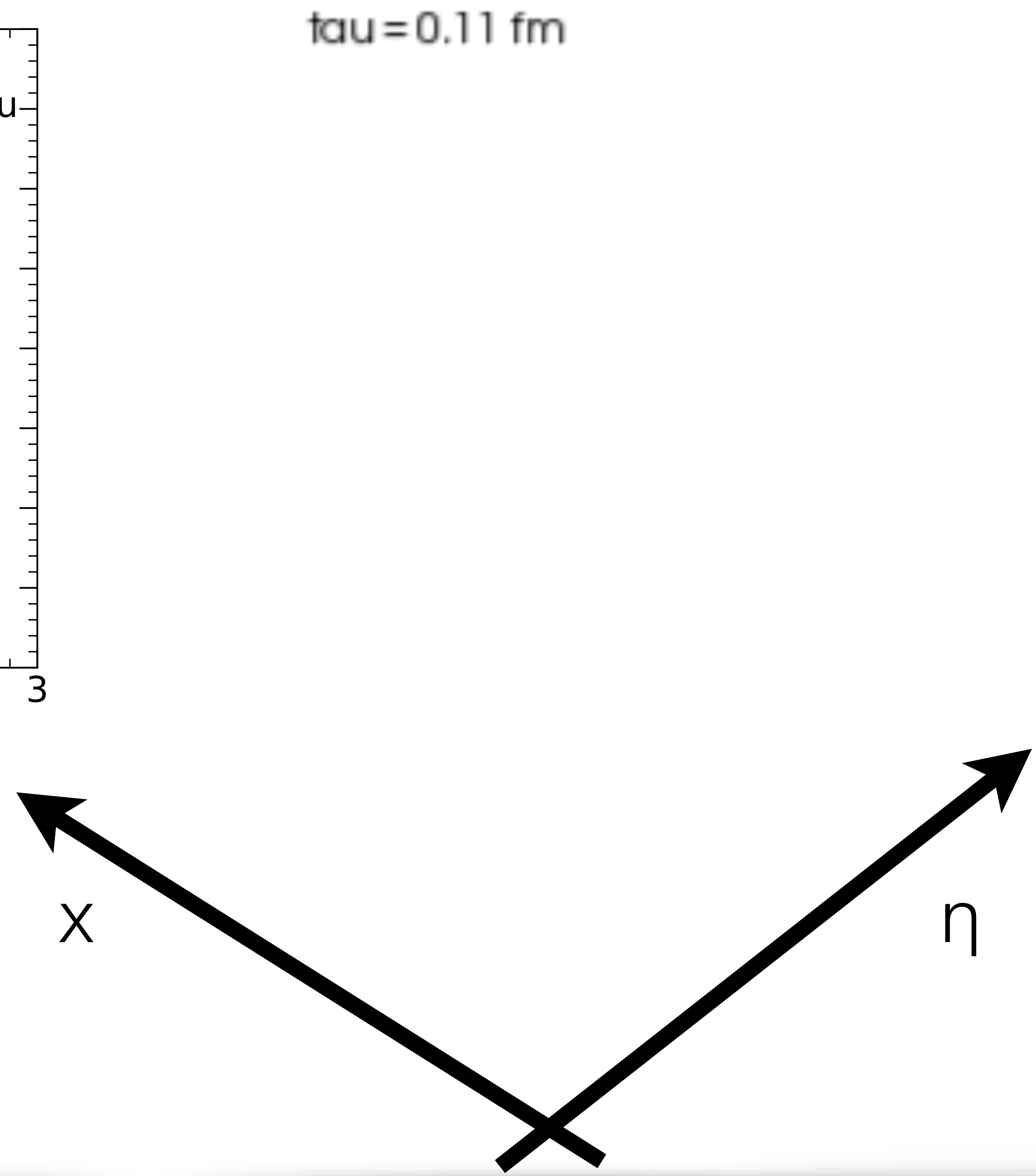

Hydrodynamical evolution with sources

net baryon density

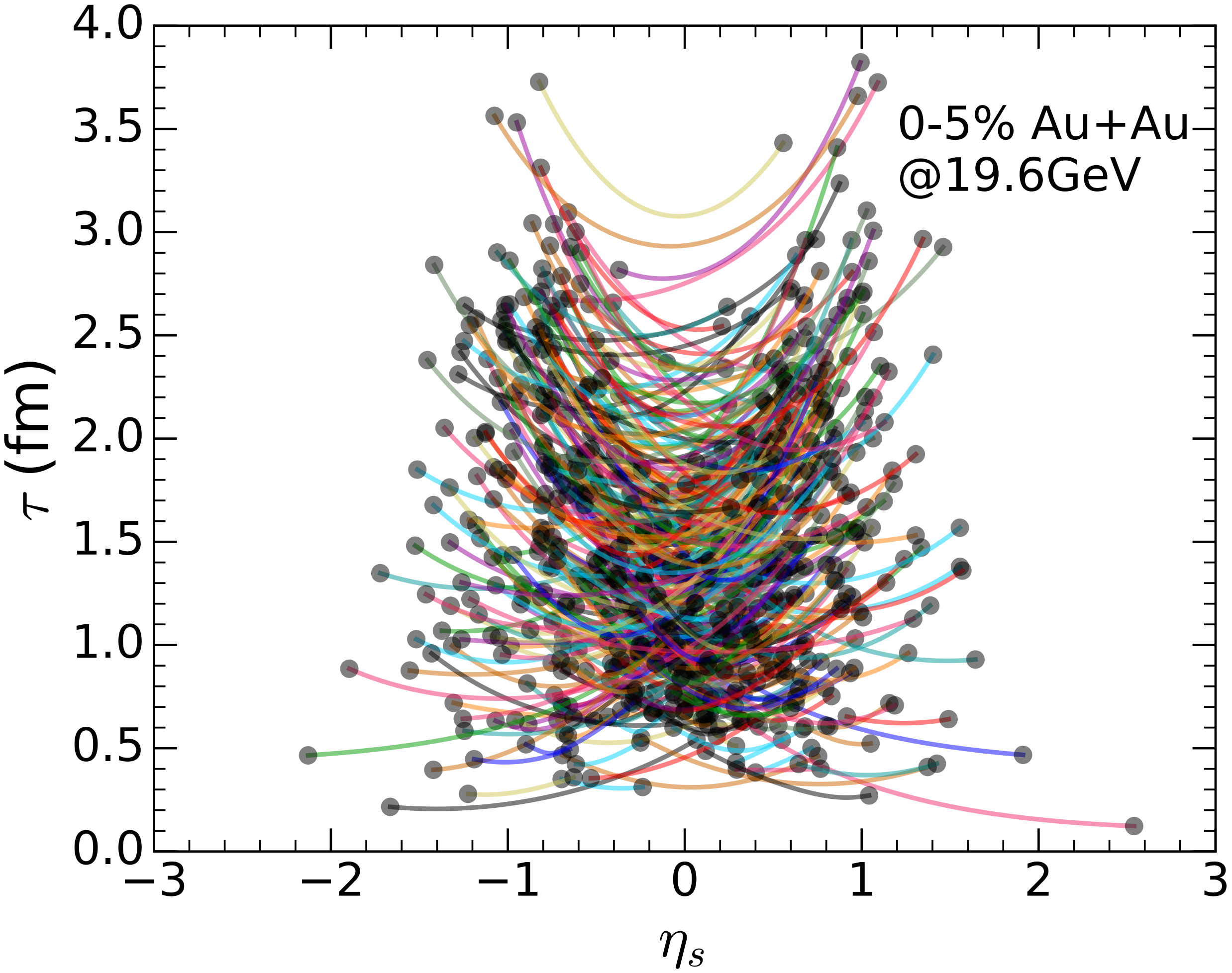

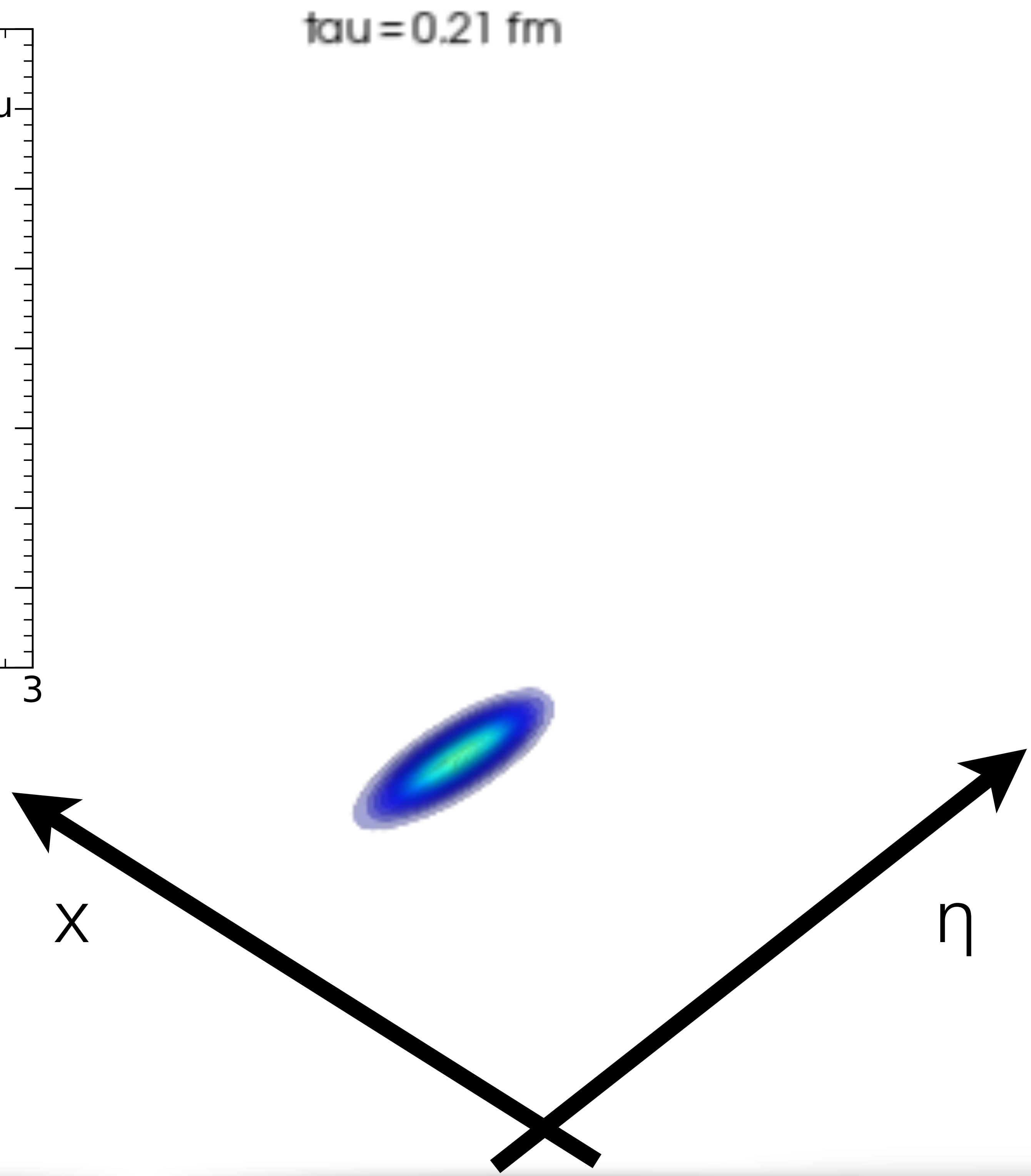

$$\sqrt{s_{\rm NN}} = 19.6\,{\rm GeV}$$

valence quark + LEXUS

Hydrodynamical evolution with sources

net baryon density

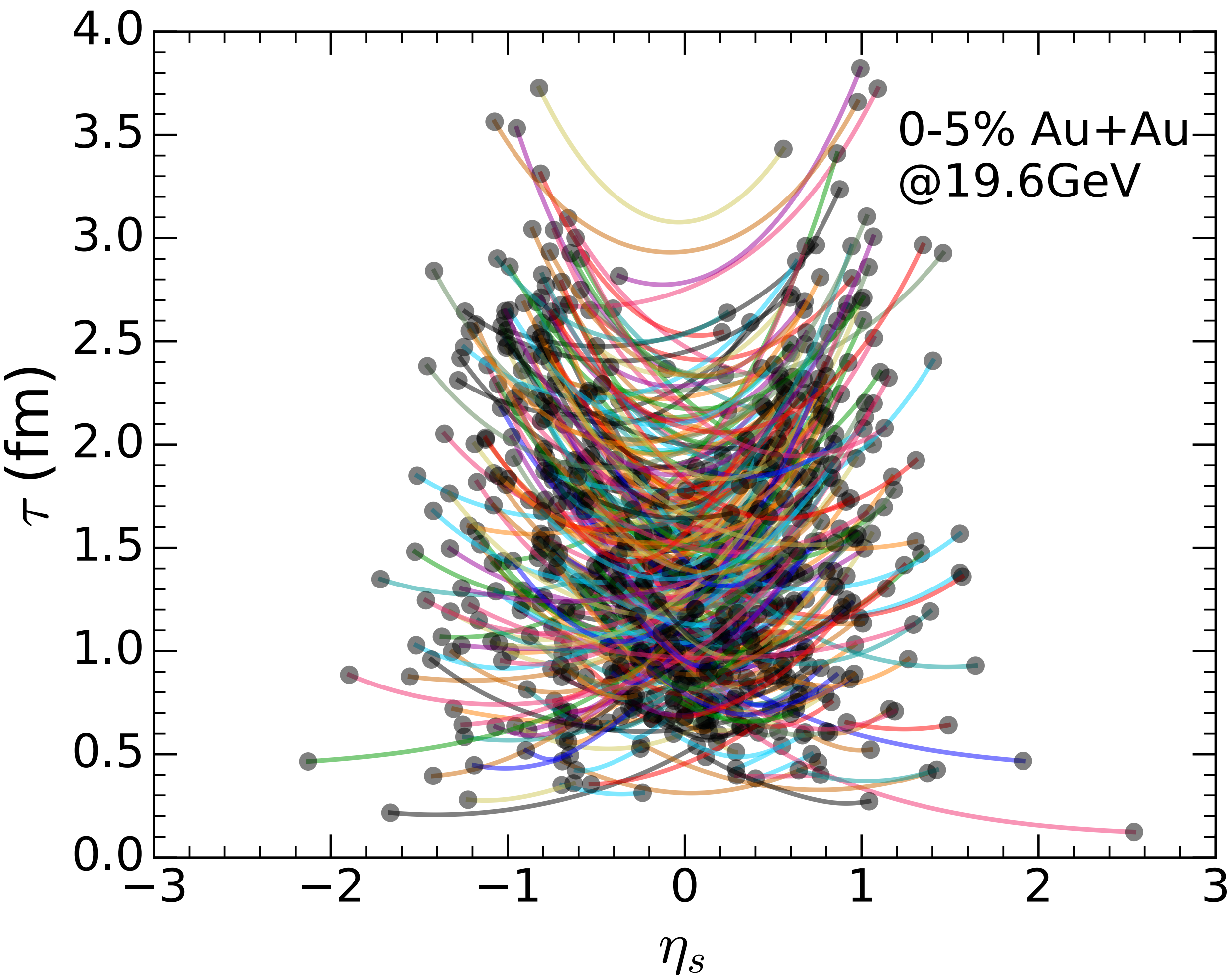

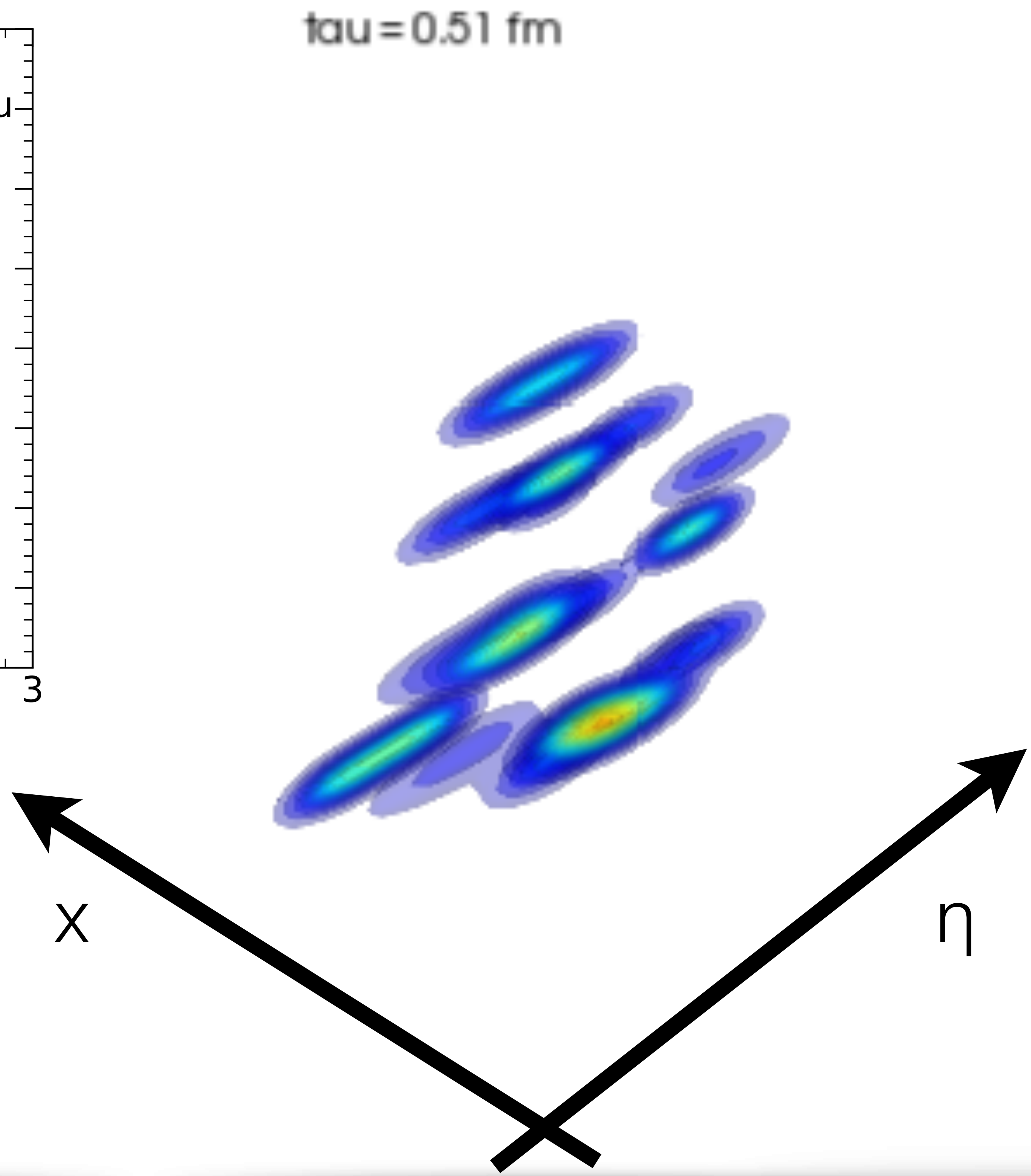

$$\sqrt{s_{\rm NN}} = 19.6\,{\rm GeV}$$

valence quark + LEXUS

Hydrodynamical evolution with sources

net baryon density

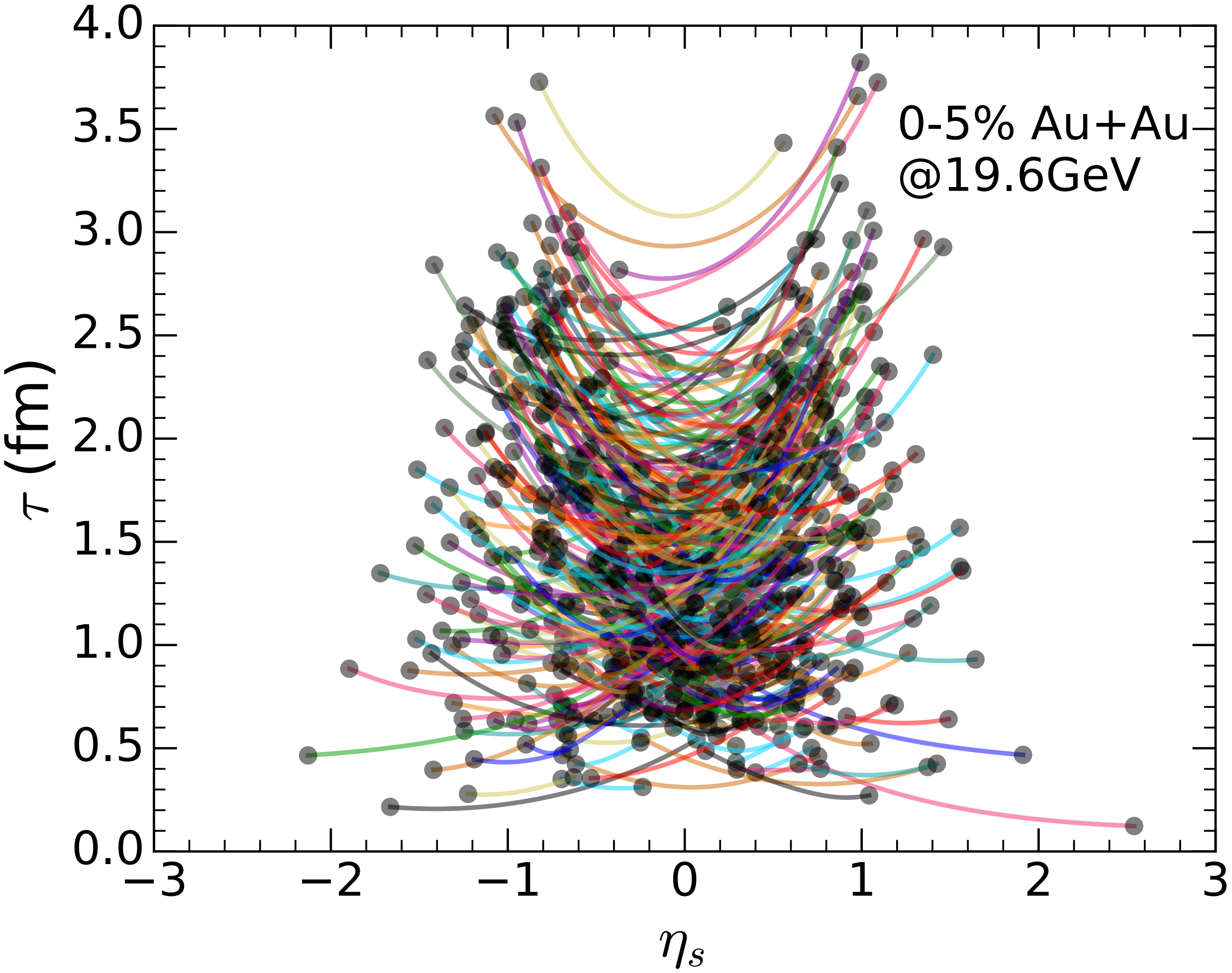

$$\sqrt{s_{\mathrm{NN}}} = 19.6\,\mathrm{GeV}$$

valence quark + LEXUS

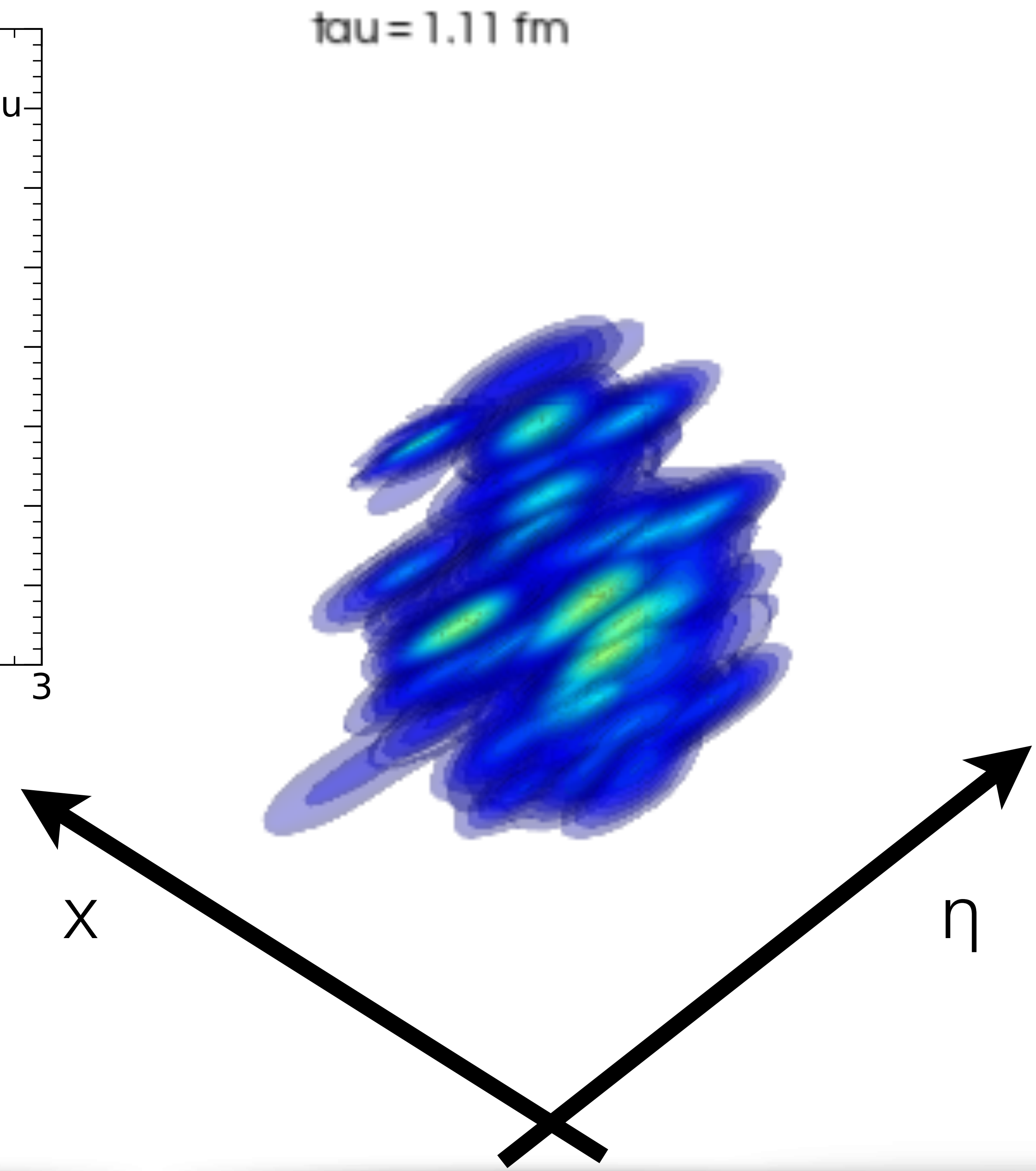

Hydrodynamical evolution with sources

net baryon density

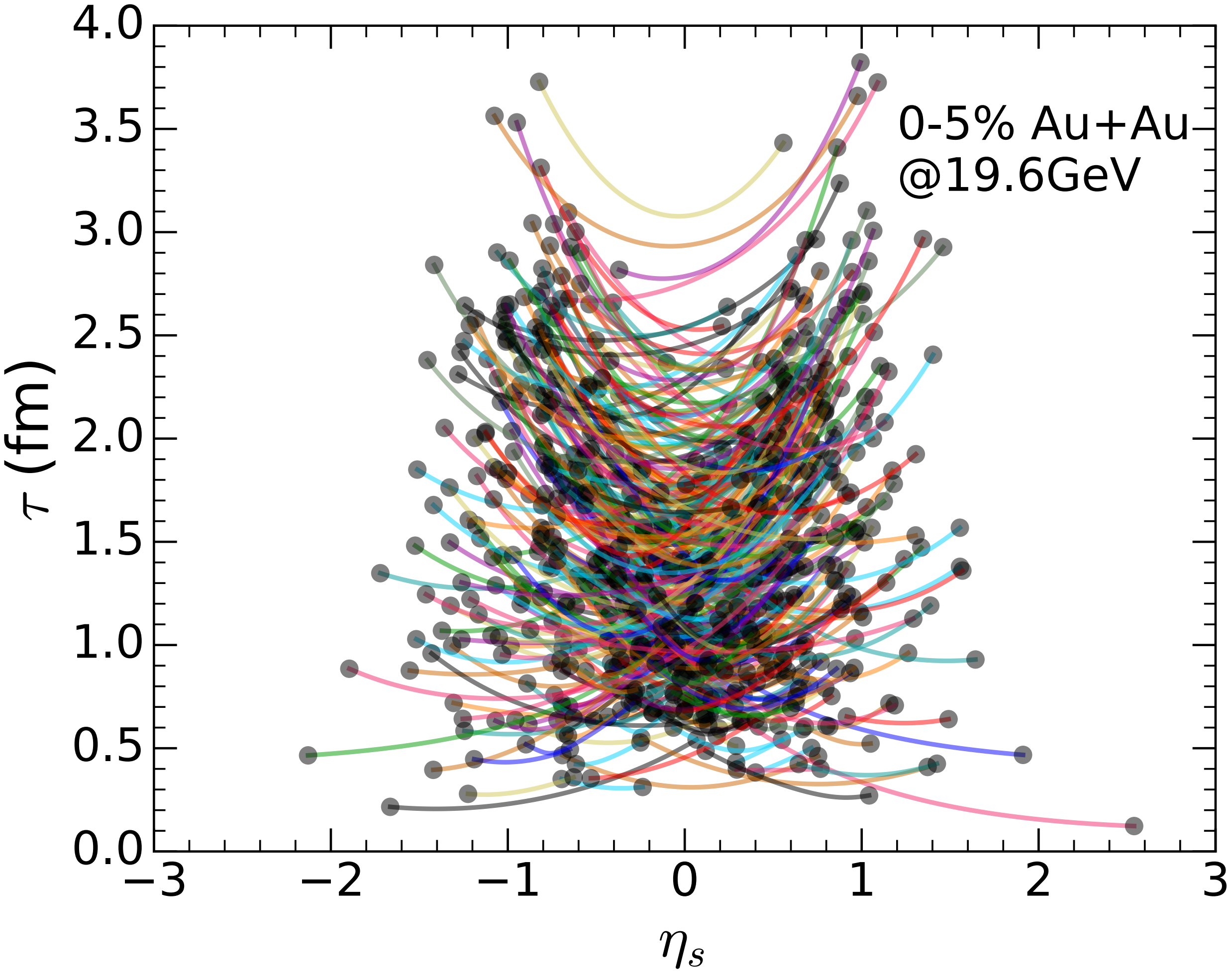

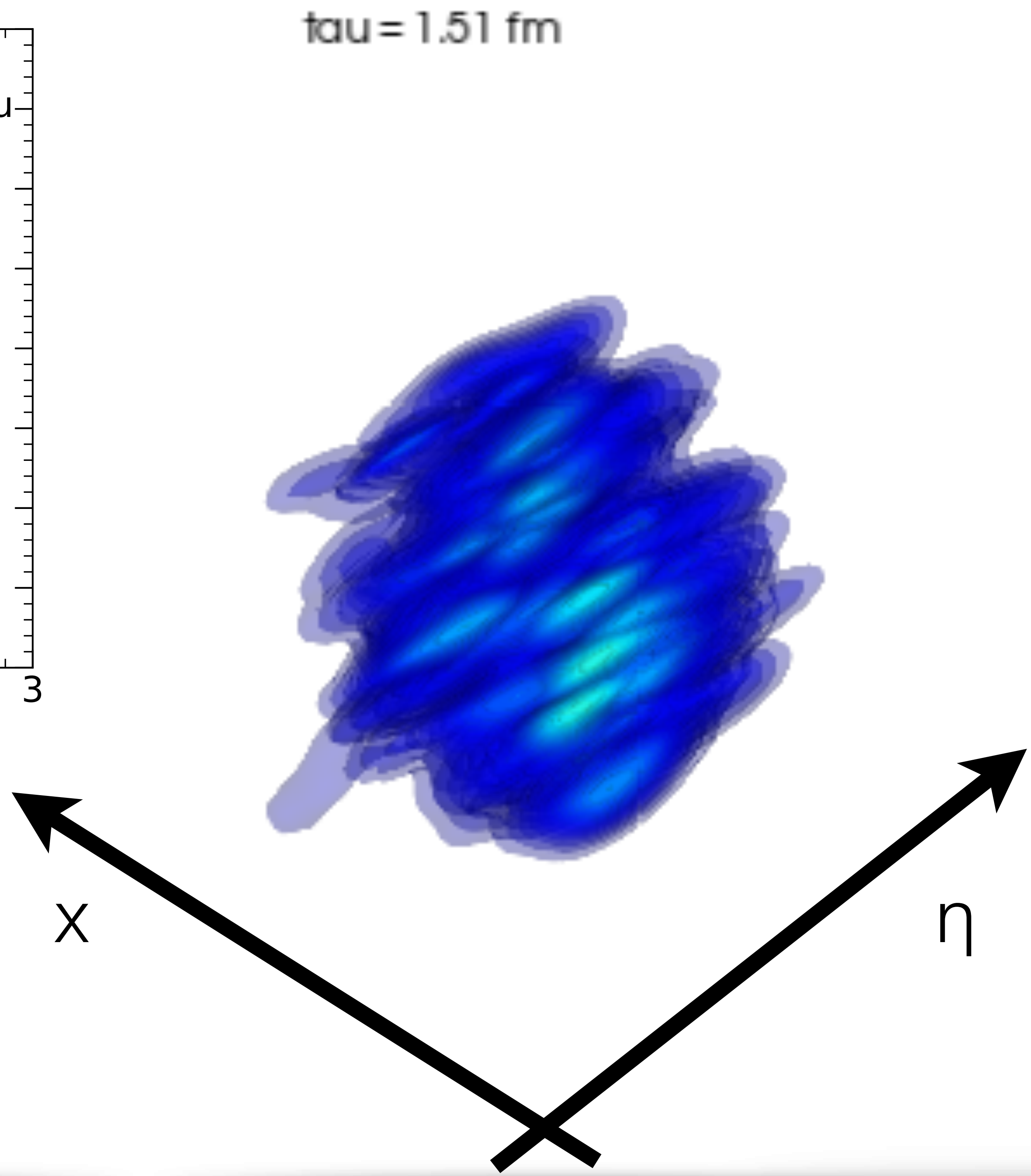

$$\sqrt{s_{\mathrm{NN}}} = 19.6\,\mathrm{GeV}$$

valence quark + LEXUS

Hydrodynamical evolution with sources

net baryon density

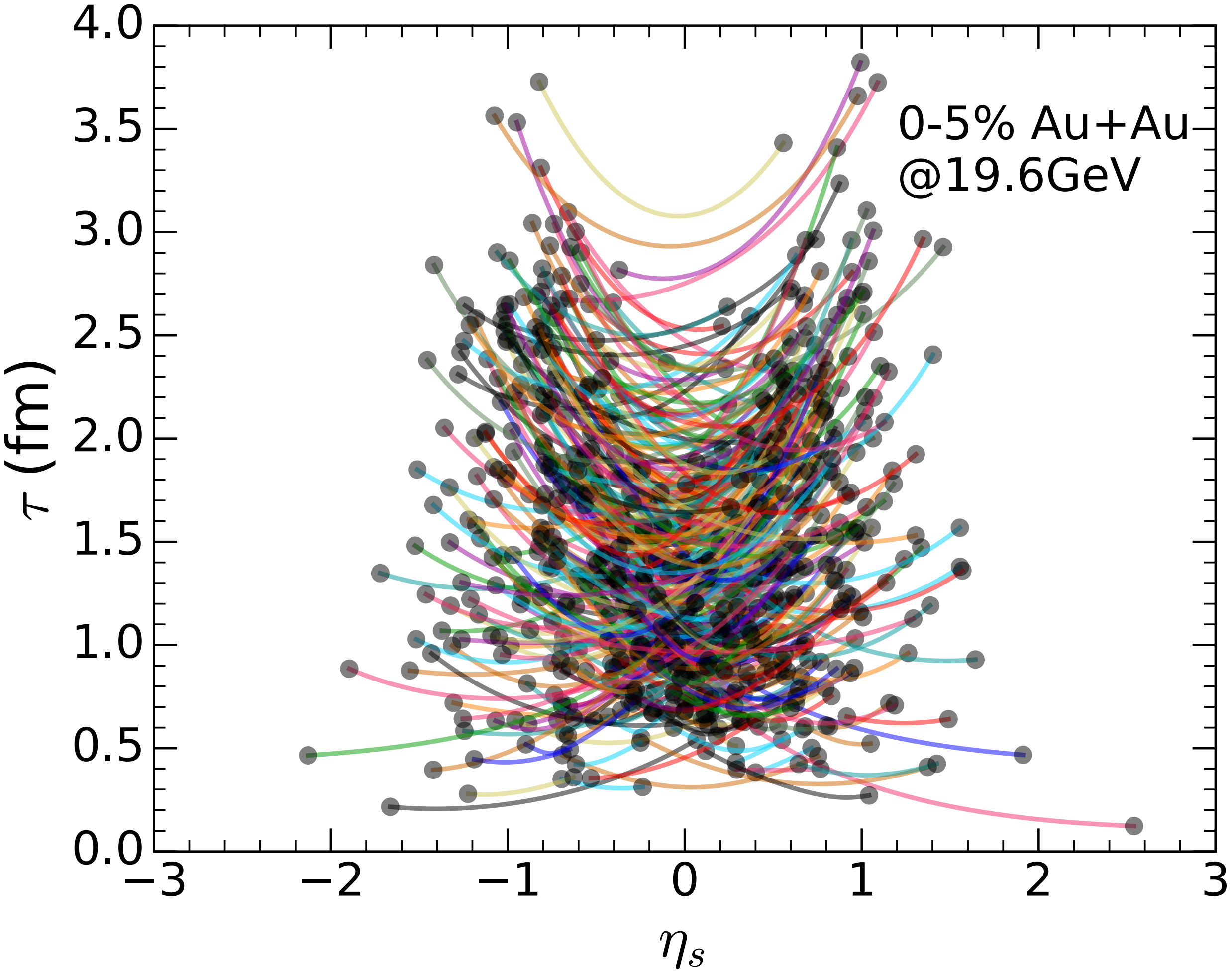

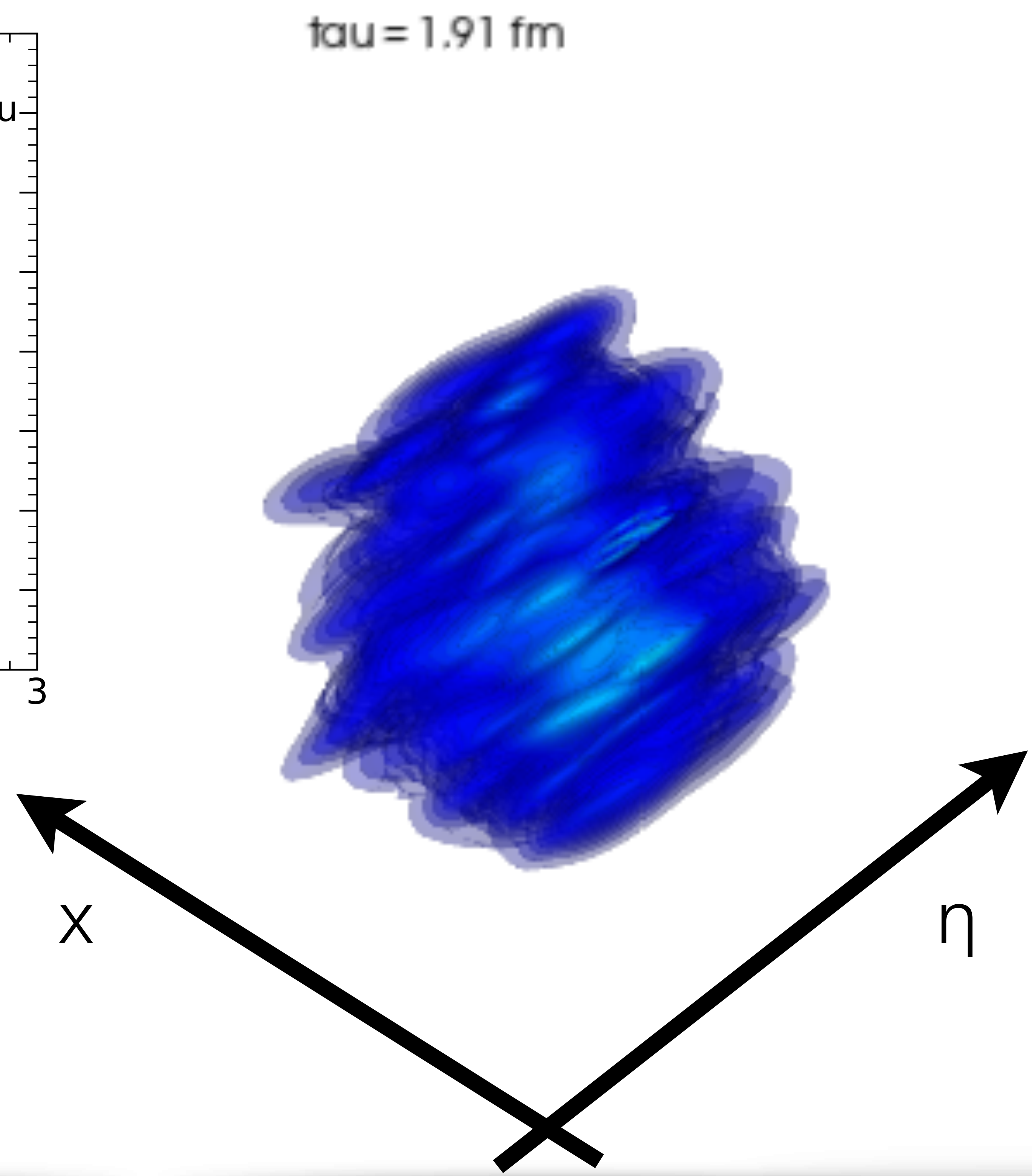

$$\sqrt{s_{\rm NN}} = 19.6\,\text{GeV}$$

valence quark + LEXUS

Hydrodynamical evolution with sources

net baryon density

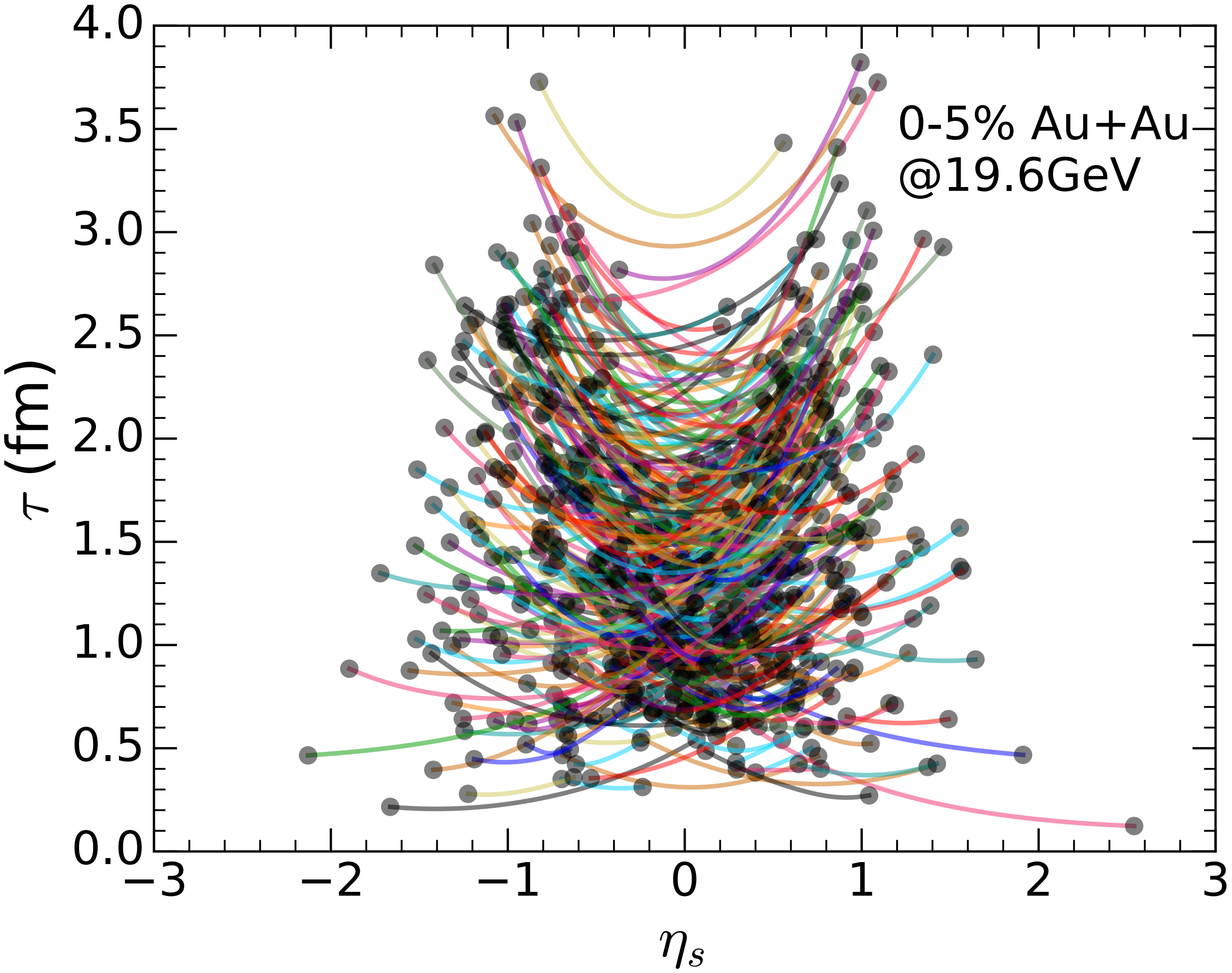

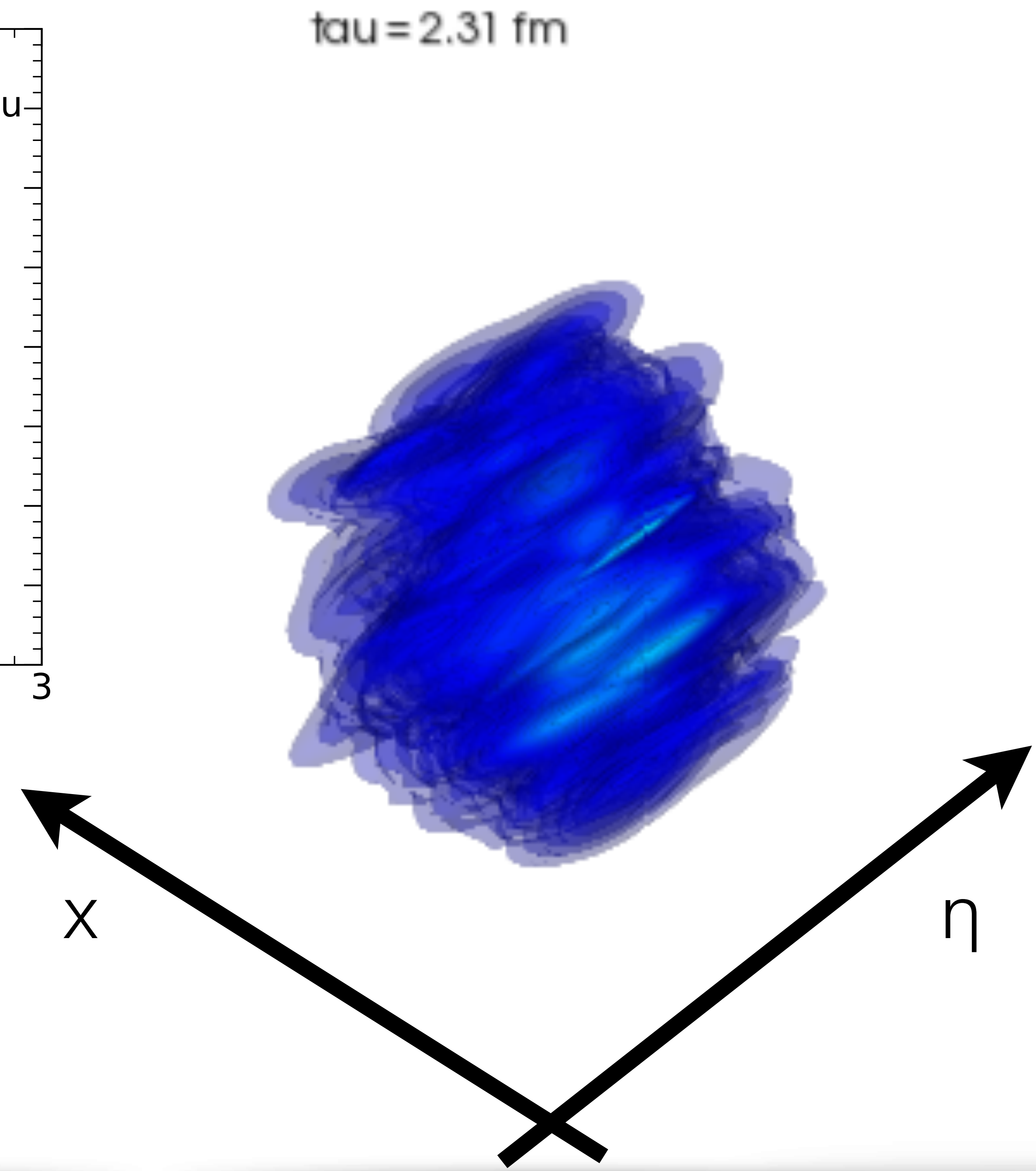

$$\sqrt{s_{\mathrm{NN}}} = 19.6\,\mathrm{GeV}$$

valence quark + LEXUS

Hydrodynamical evolution with sources

net baryon density

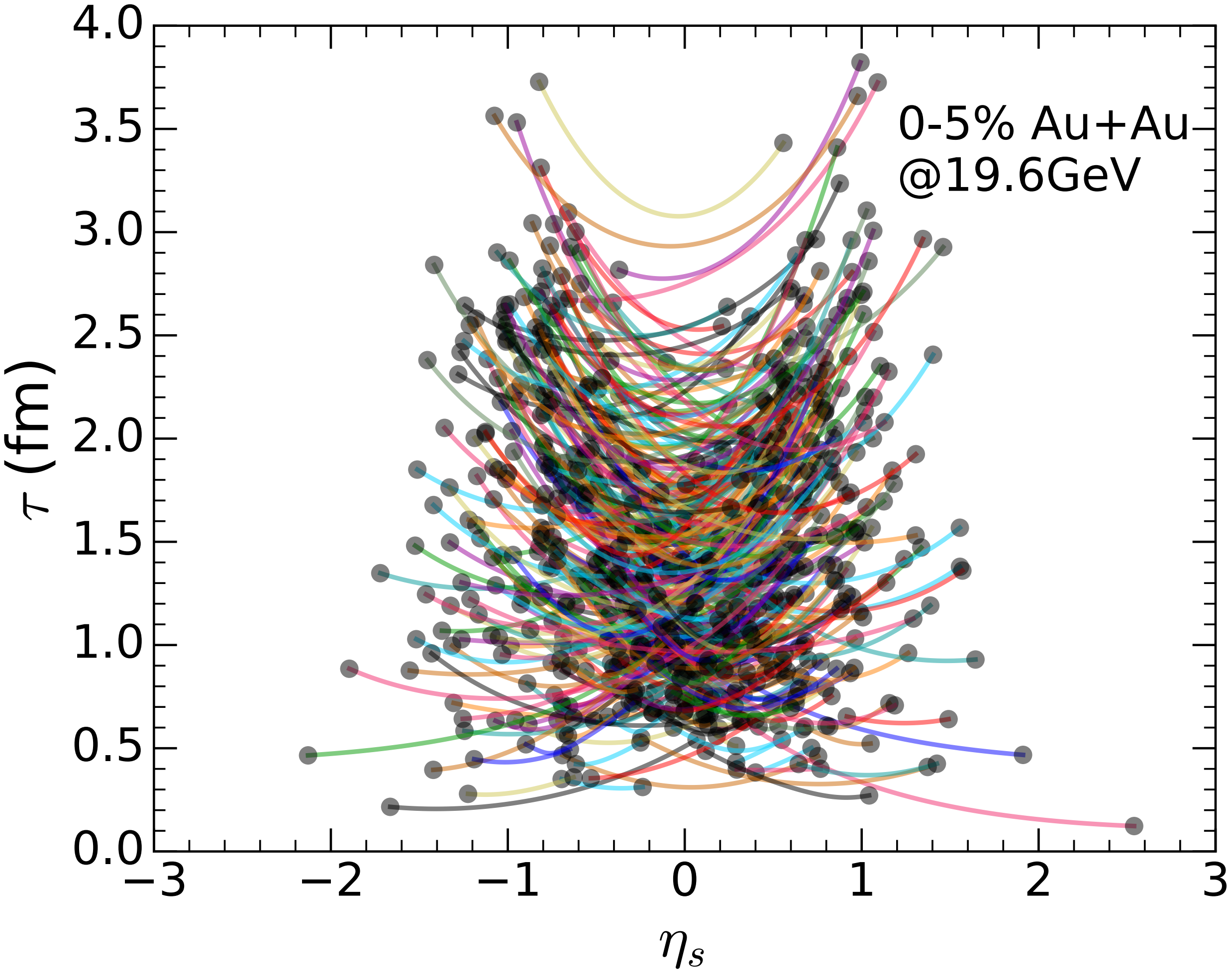

$$\sqrt{s_{\rm NN}} = 19.6\,\mathrm{GeV}$$

valence quark + LEXUS

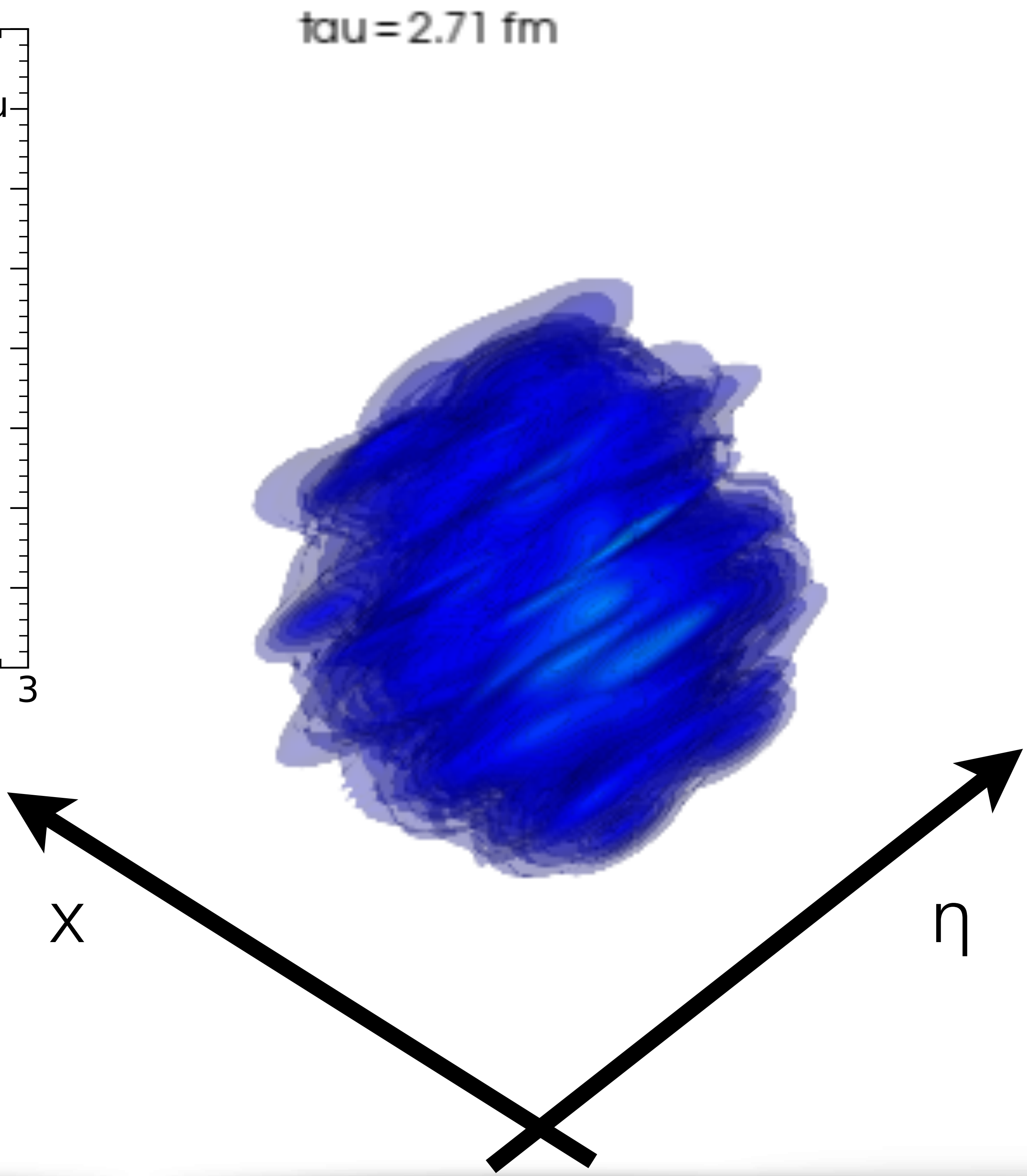

Hydrodynamical evolution with sources

net baryon density

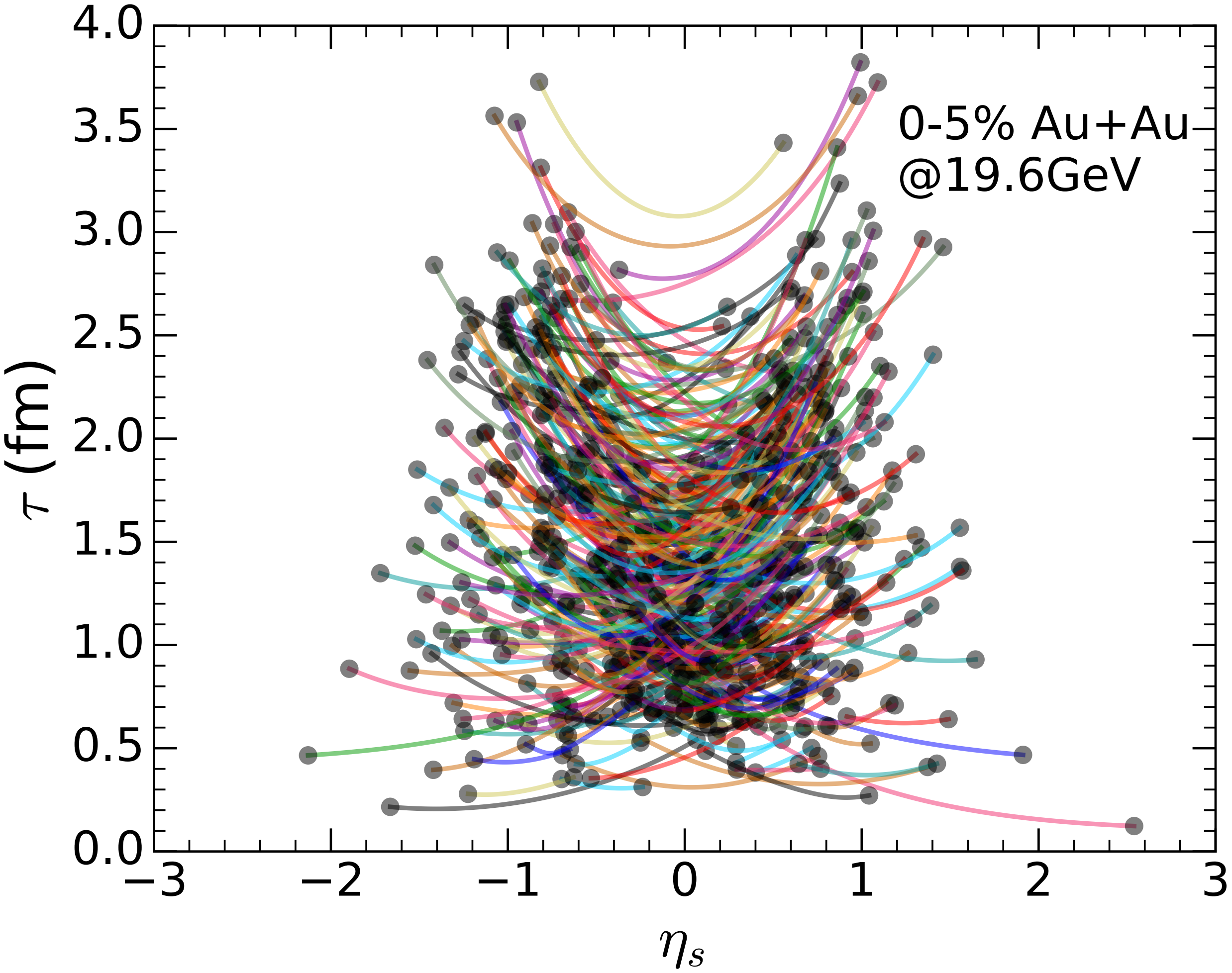

$$\sqrt{s_{\rm NN}} = 19.6\,\mathrm{GeV}$$

valence quark + LEXUS

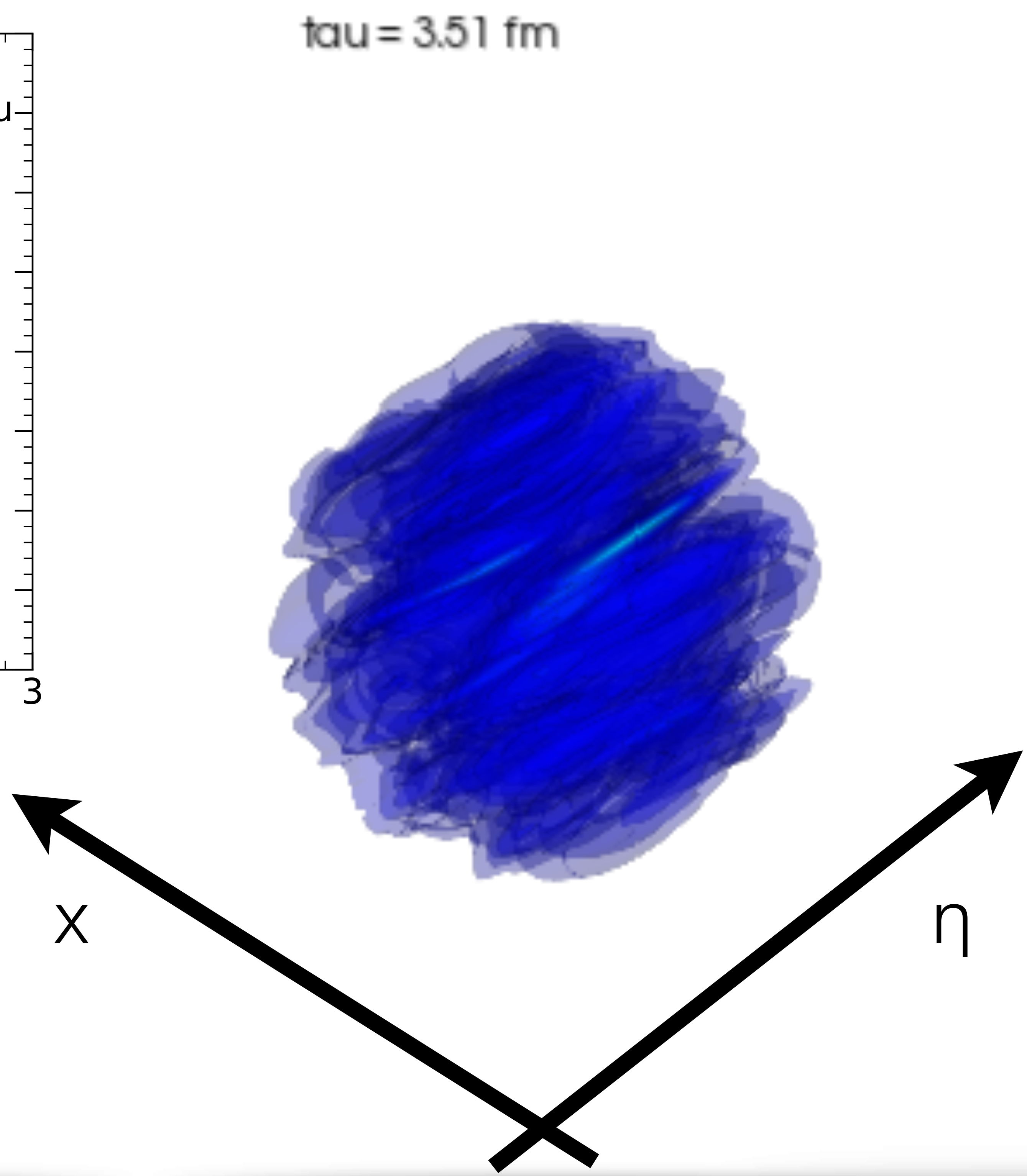

Hydrodynamical evolution with sources

net baryon density

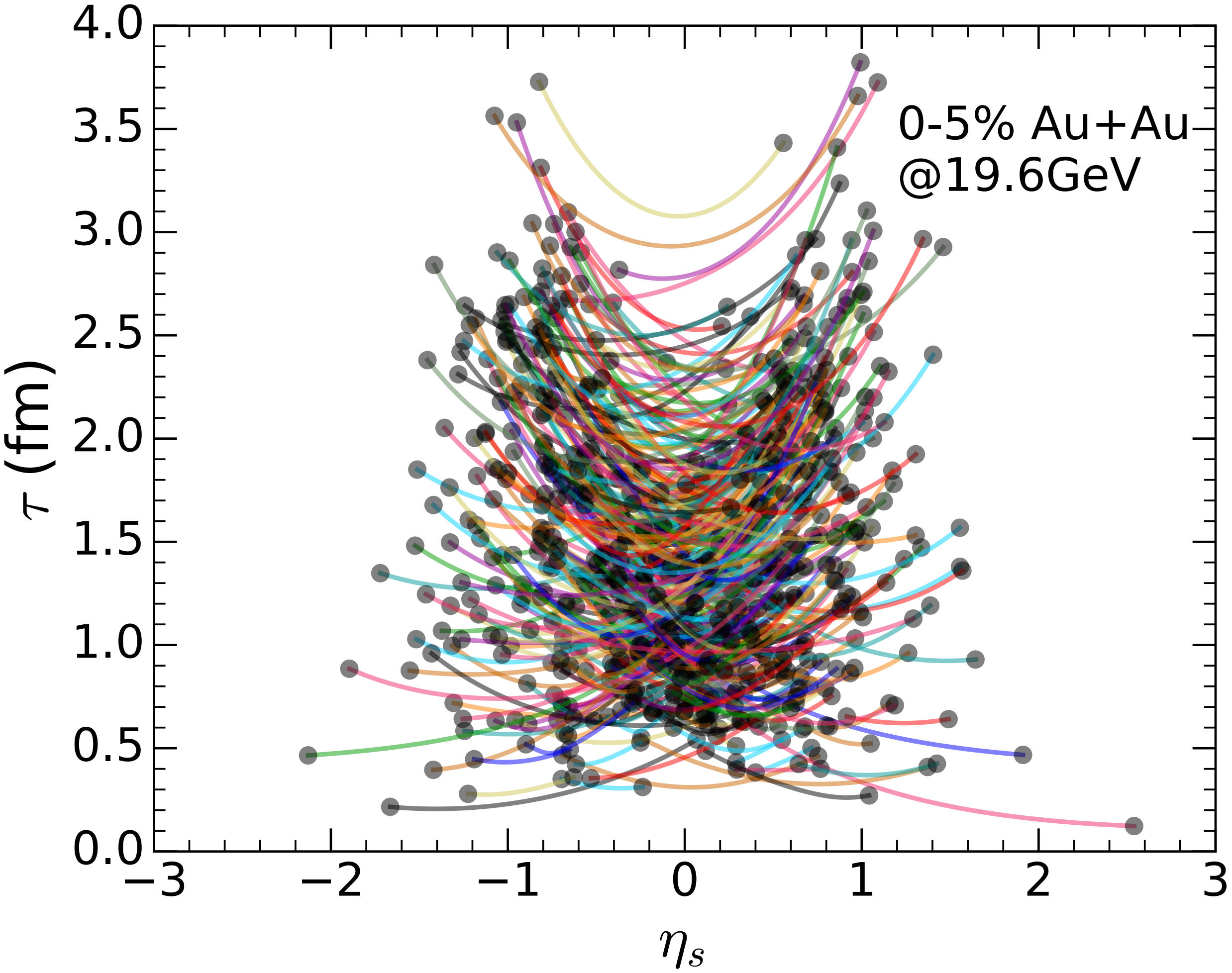

$$\sqrt{s_{\rm NN}} = 19.6\,\mathrm{GeV}$$

valence quark + LEXUS

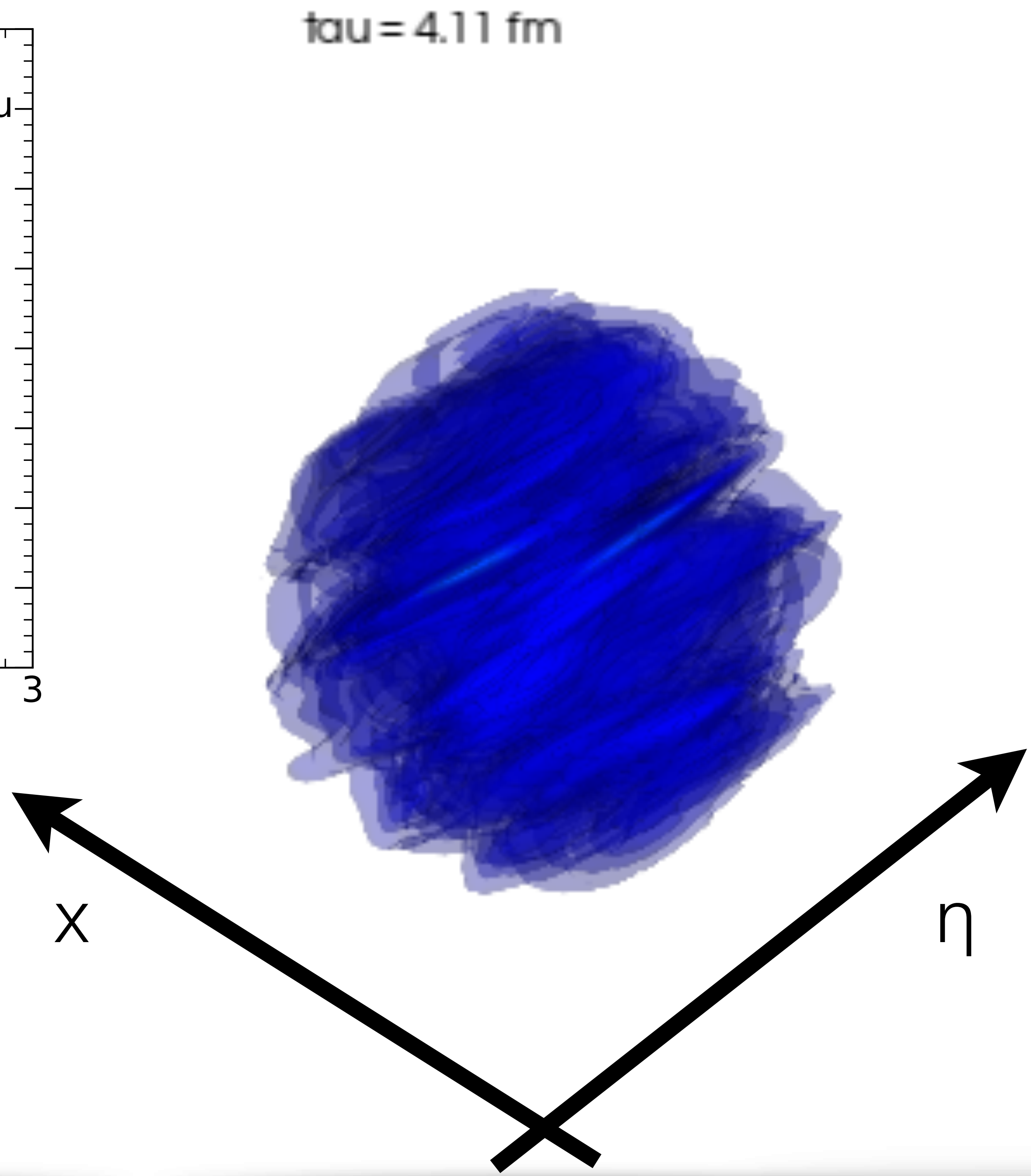

Hydrodynamical evolution with sources

net baryon density

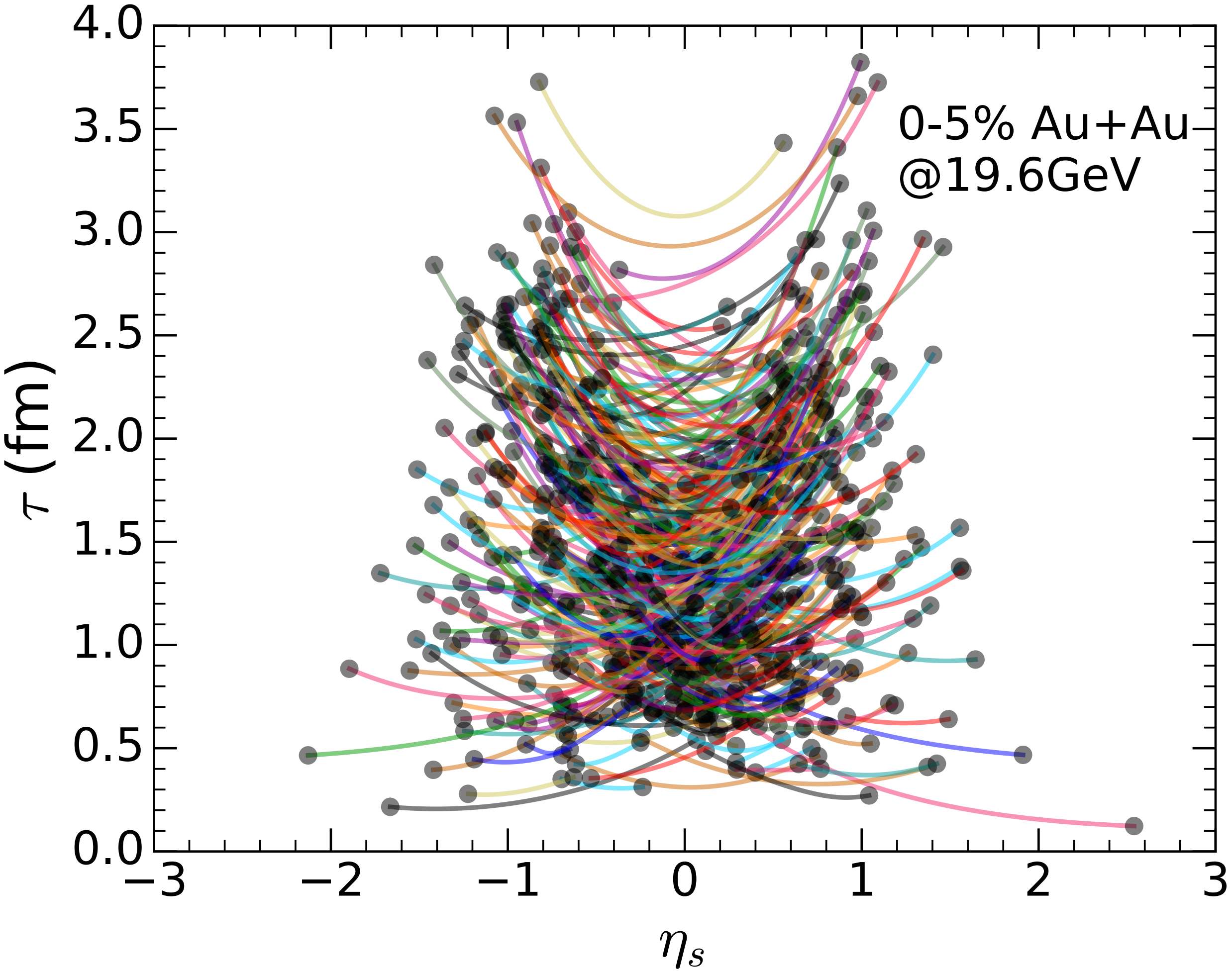

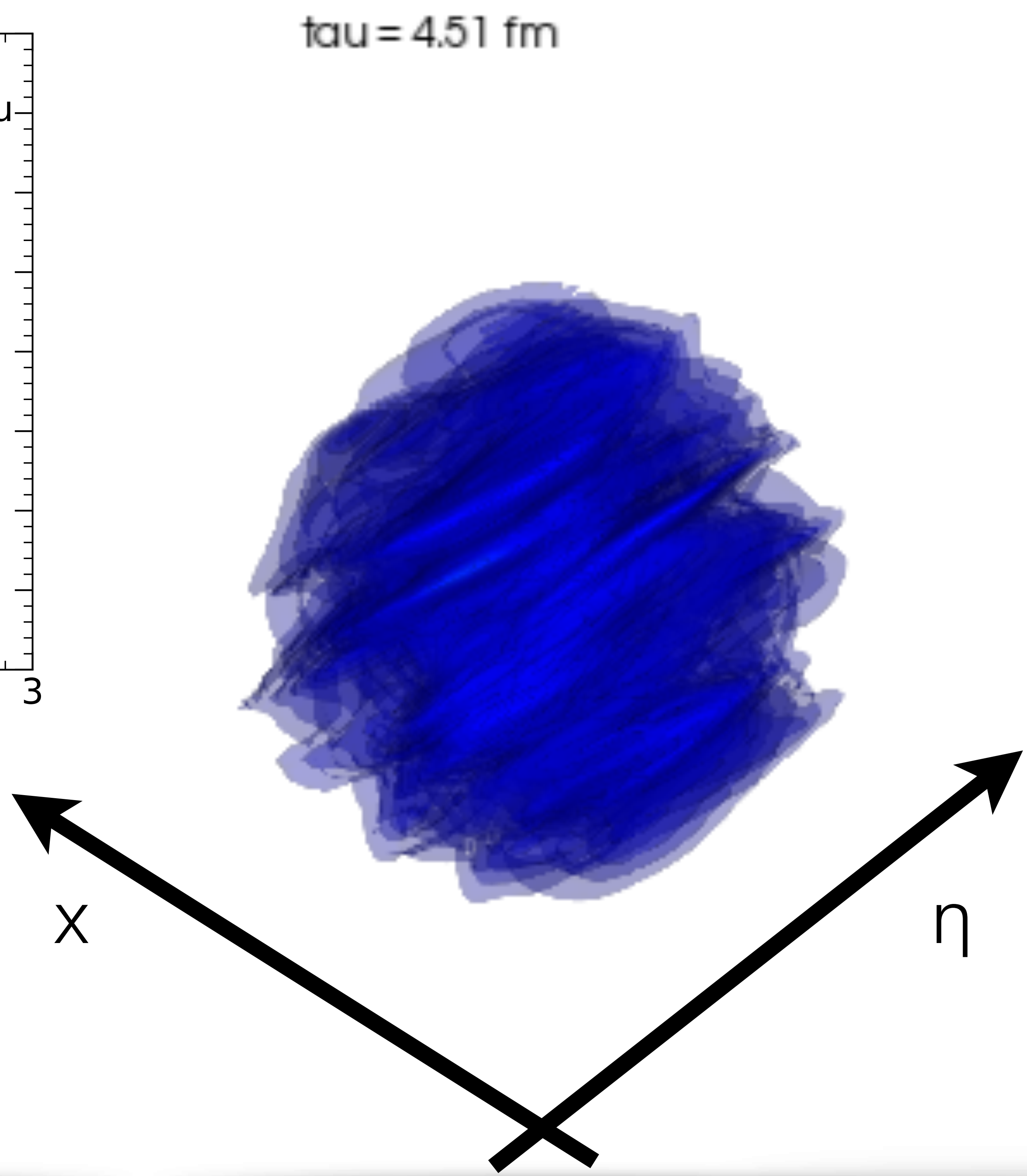

$$\sqrt{s_{\mathrm{NN}}} = 19.6\,\mathrm{GeV}$$

valence quark + LEXUS

Hydrodynamical evolution with sources

net baryon density

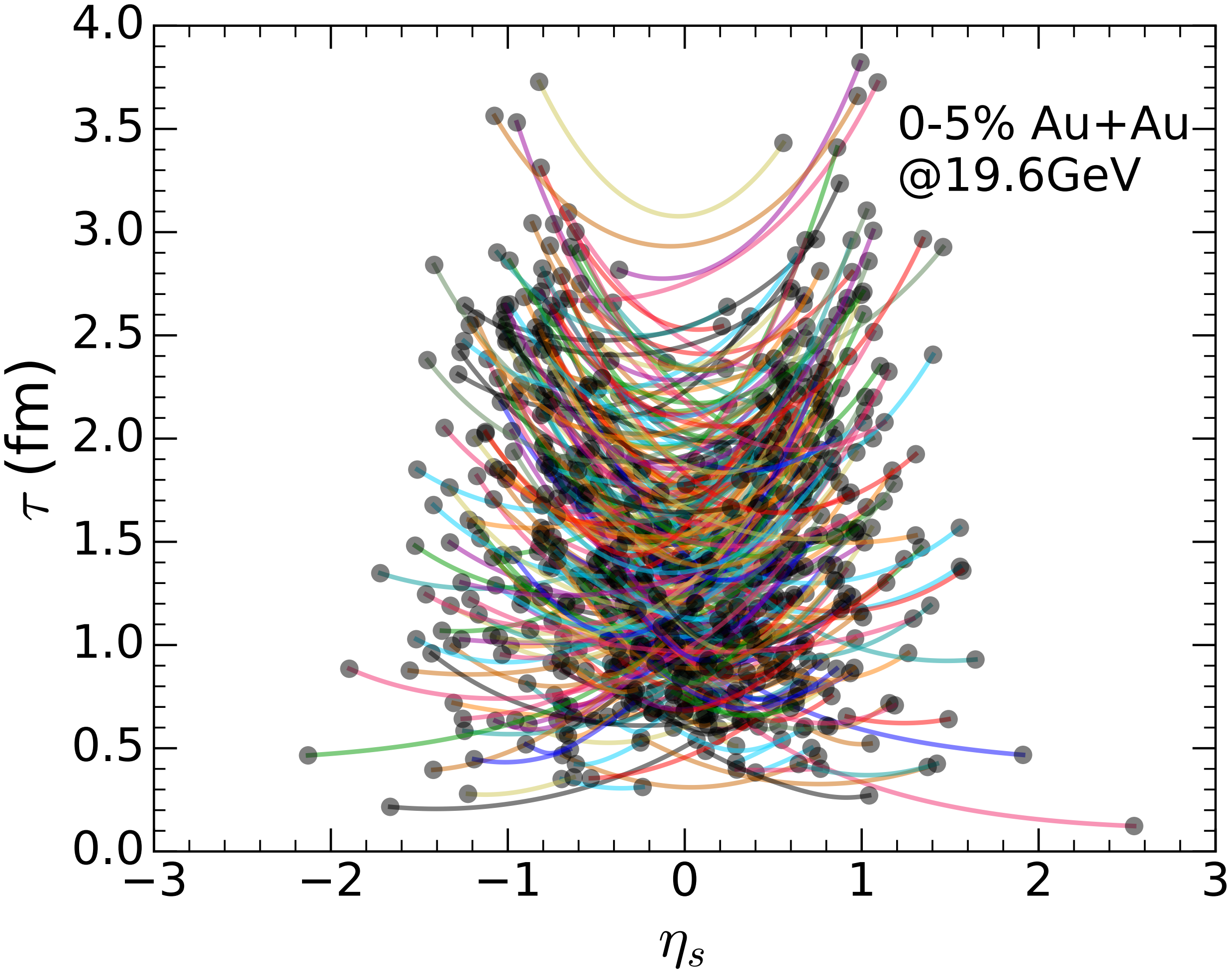

$$\sqrt{s_{\mathrm{NN}}} = 19.6\,\mathrm{GeV}$$

valence quark + LEXUS

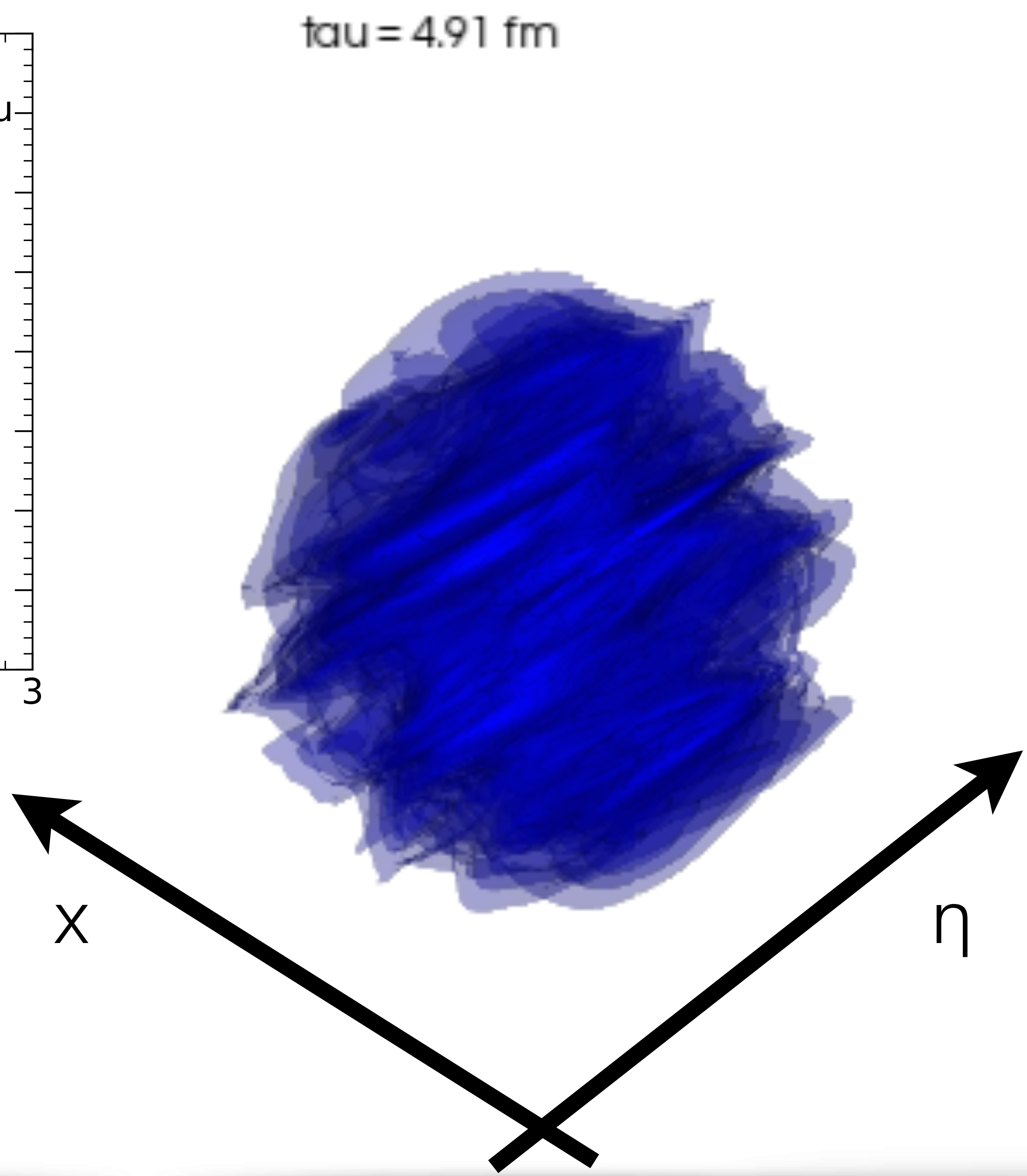

Hydrodynamical evolution with sources

net baryon density

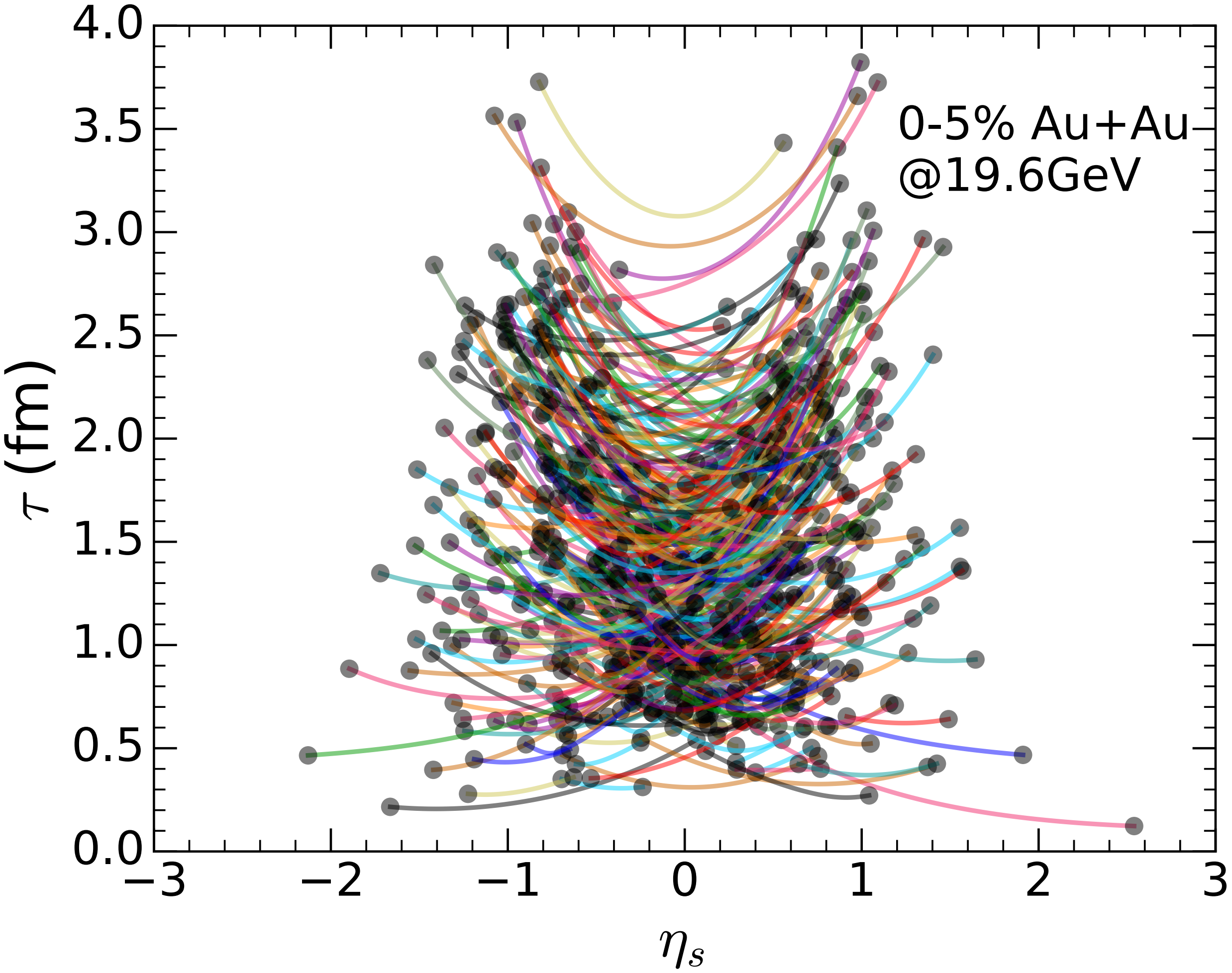

$$\sqrt{s_{\rm NN}} = 19.6\,\text{GeV}$$

valence quark + LEXUS

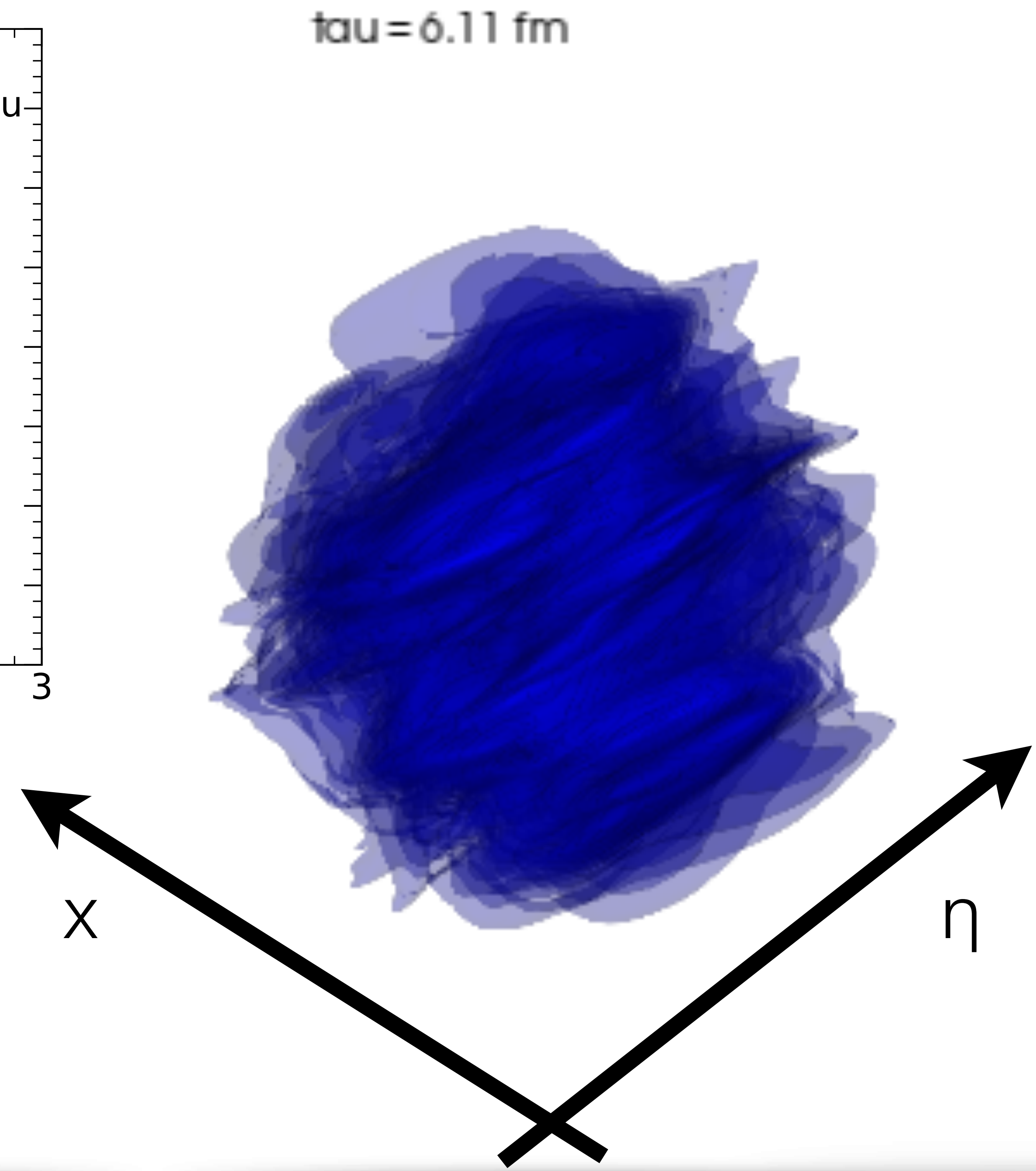

Progress in hydrodynamics

Dissipative hydrodynamics

Energy momentum tensor

$$T^{\mu\nu} = e u^\mu u^\nu - (P + \Pi)\Delta^{\mu\nu} + \pi^{\mu\nu} \qquad \Delta^{\mu\nu} = g^{\mu\nu} - u^\mu u^\nu$$

Conserved currents

$$J^\mu = n u^\mu + q^\mu$$

Equations of motion

$$\partial_\mu T^{\mu\nu} = 0 \qquad \partial_\mu J^\mu = 0 \qquad + \quad P(e, n)$$

Dissipative quantities are evolved with 2nd order Israel-Stewart type of equations

At Navier-Stokes limit,

$$\pi^{\mu\nu} \sim 2\eta \nabla^{\langle\mu} u^{\nu\rangle} \quad \Pi \sim -\zeta \partial_\mu u^\mu \quad q^\mu \sim \kappa \nabla^\mu \frac{\mu}{T}$$

$$\nabla^\mu = \Delta^{\mu\nu}\partial_\nu$$

EoS at finite μ_B

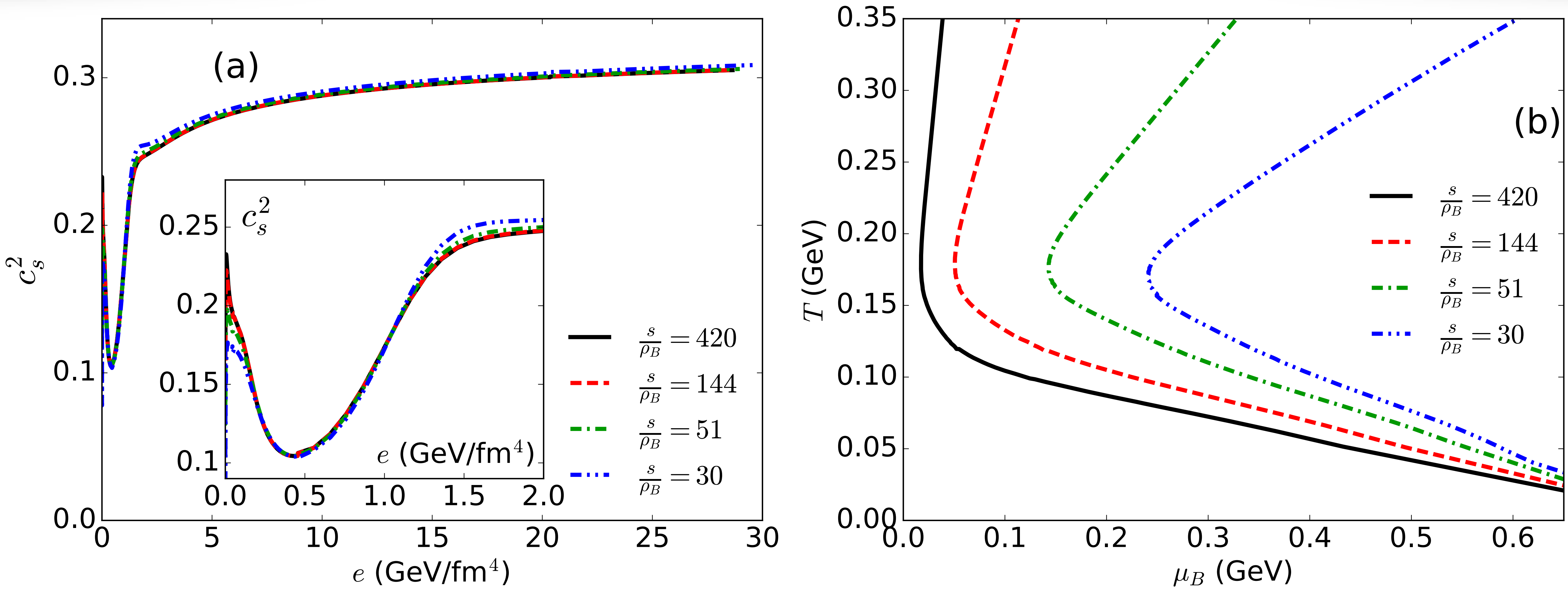

High temperature:

- Lattice QCD EoS up to $\mathcal{O}(\mu_B^4)$

Low temperature:

- Glued with hadron resonance gas EoS

Transport coefficients

Dissipative part: (relaxation time approximation)

$$\Delta^{\mu\nu}_{\alpha\beta} D\pi^{\alpha\beta} = -\frac{1}{\tau_\pi}(\pi^{\mu\nu} - 2\eta\sigma^{\mu\nu}) - \frac{\delta_{\pi\pi}}{\tau_\pi}\pi^{\mu\nu}\theta - \frac{\tau_{\pi\pi}}{\tau_\pi}\pi^{\lambda\langle\mu}\sigma^{\nu\rangle}{}_\lambda + \frac{\phi_7}{\tau_\pi}\pi_\alpha^{\langle\mu}\pi^{\nu\rangle\alpha}$$

$$\Delta^{\mu\nu} Dq_\nu = -\frac{1}{\tau_q}(q^\mu - \kappa\nabla^\mu \frac{\mu_B}{T}) - \frac{\delta_{qq}}{\tau_q}q^\mu\theta - \frac{\lambda_{qq}}{\tau_q}q_\nu\sigma^{\mu\nu}$$

With non-zero μ, we choose $\tau_\pi = \tau_q = \frac{0.4}{T}$ $\quad \frac{\eta T}{e + \mathcal{P}} = 0.08$

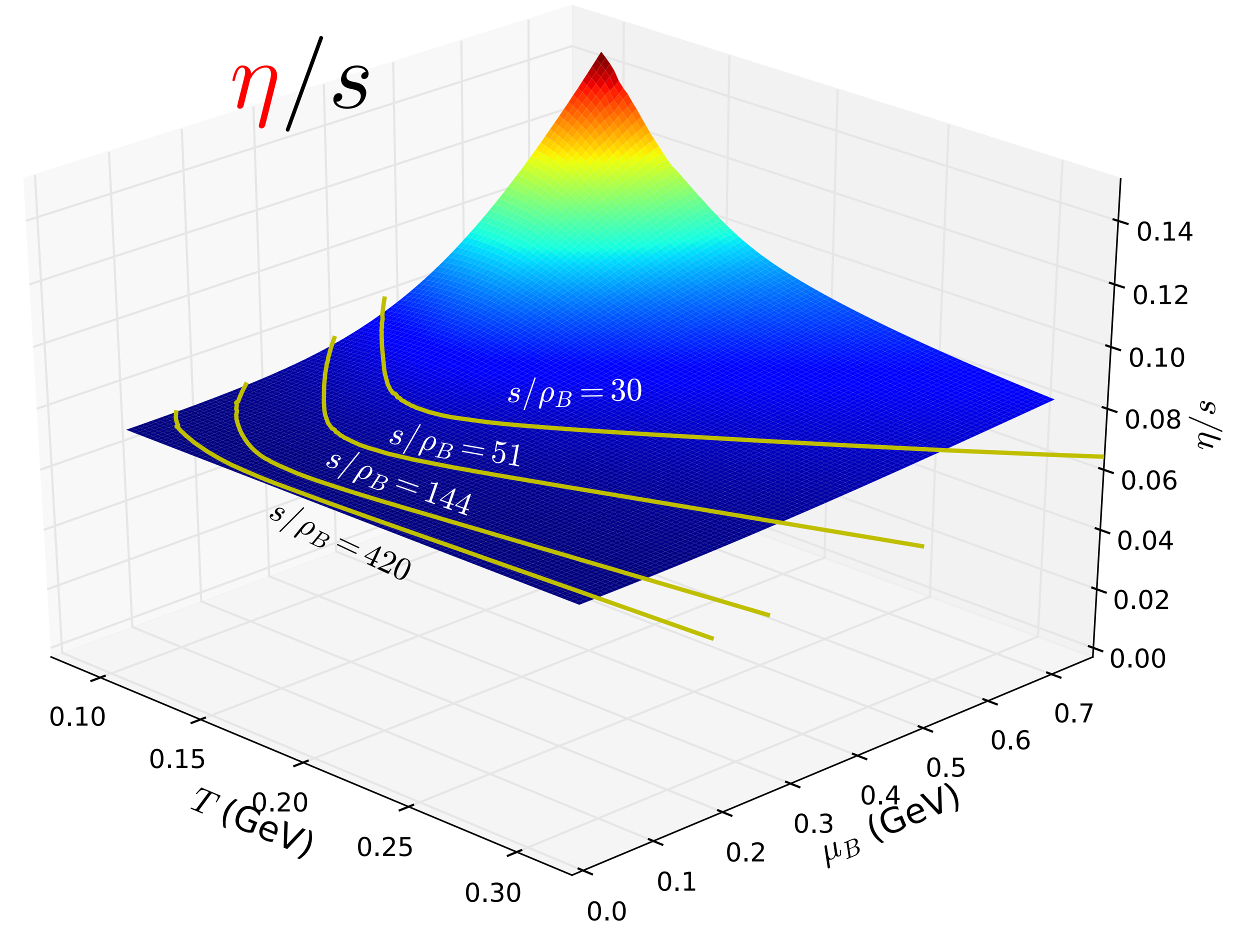

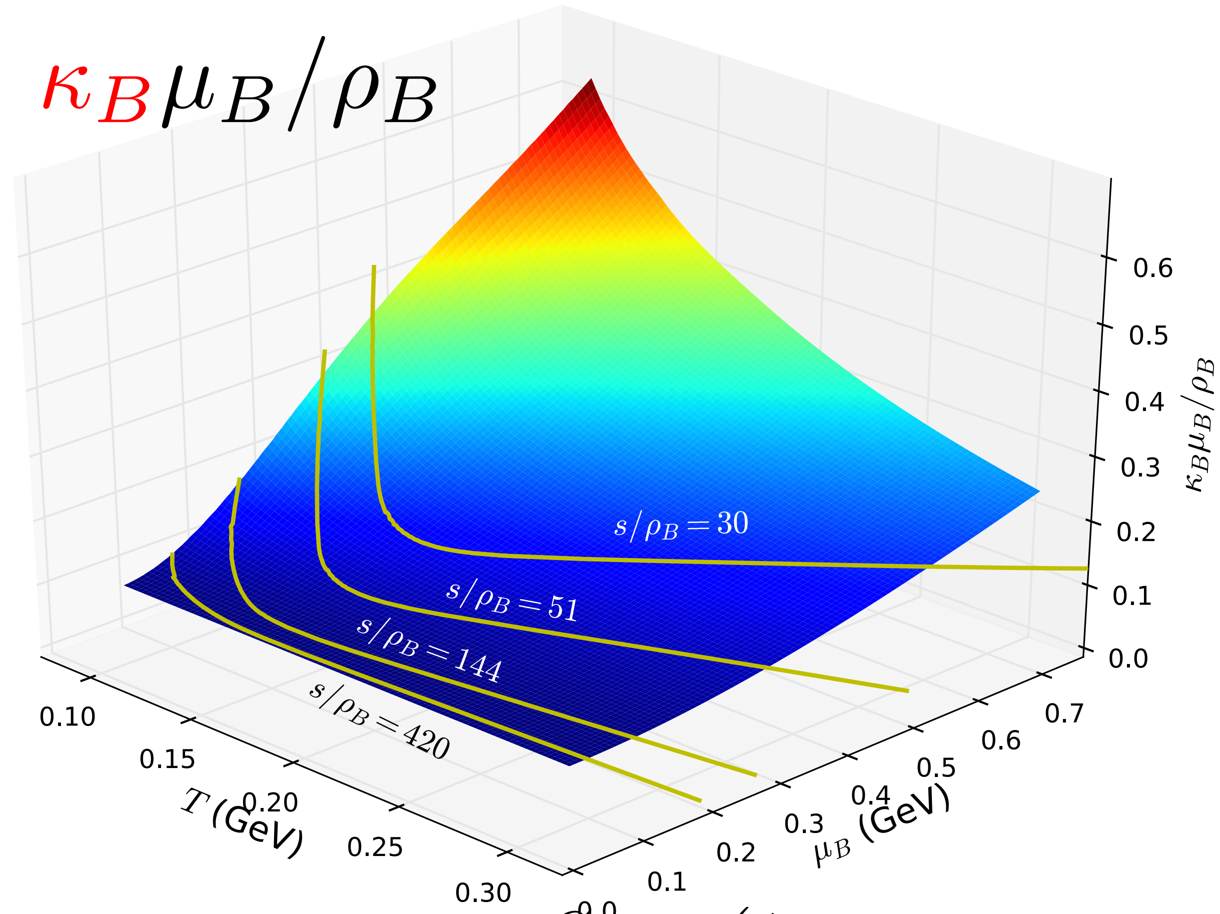

$$\kappa_B = \frac{C_B}{T}\rho_B\left(\frac{1}{3}\coth\left(\frac{\mu_B}{T}\right) - \frac{\rho_B T}{e + P}\right)$$

Effects of net baryon diffusion on particle yields

C. Shen, G. Denicol, C. Gale, S. Jeon, A. Monnai, B. Schenke, in preparation

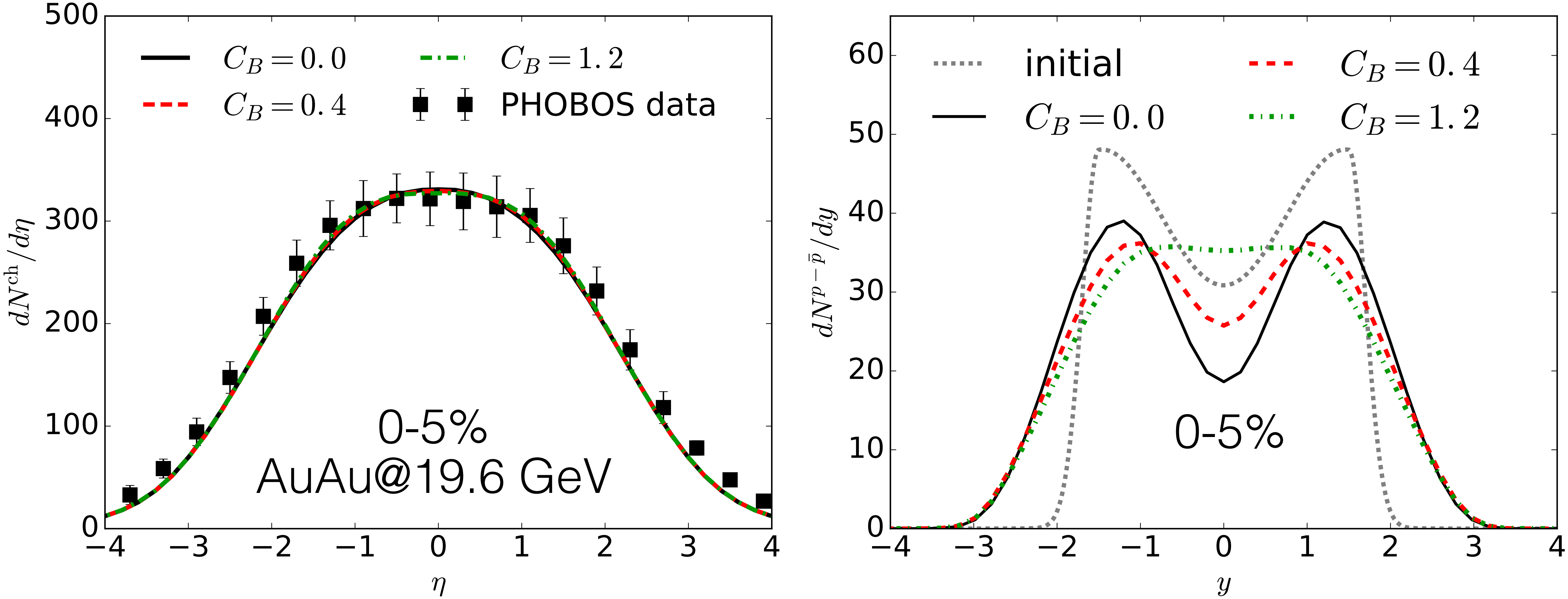

$$\kappa_B = \frac{C_B}{T}\rho_B\left(\frac{1}{3}\coth\left(\frac{\mu_B}{T}\right) - \frac{\rho_B T}{e+P}\right)$$

- More net baryon numbers are transported to mid-rapidity with a larger diffusion constant

Constraints on net baryon diffusion and initial condition

Effects of net baryon diffusion on particle yields

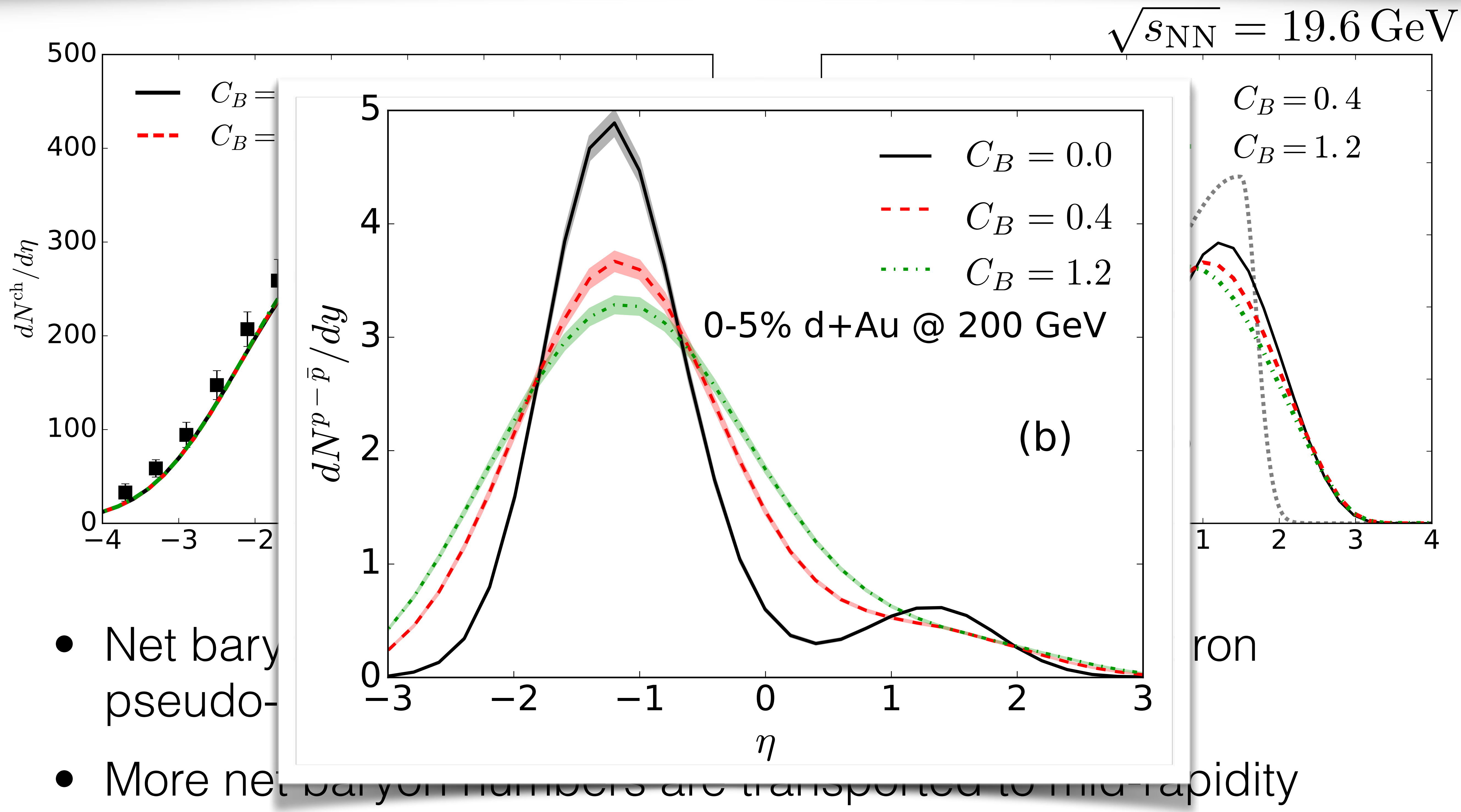

- Net bary… ron pseudo-…
- More net baryon numbers are transported to mid-rapidity with a larger diffusion constant

Constraints on net baryon diffusion and initial condition

Effects of net baryon diffusion on pid spectra

C. Shen, G. Denicol, C. Gale, S. Jeon, A. Monnai, B. Schenke, in preparation

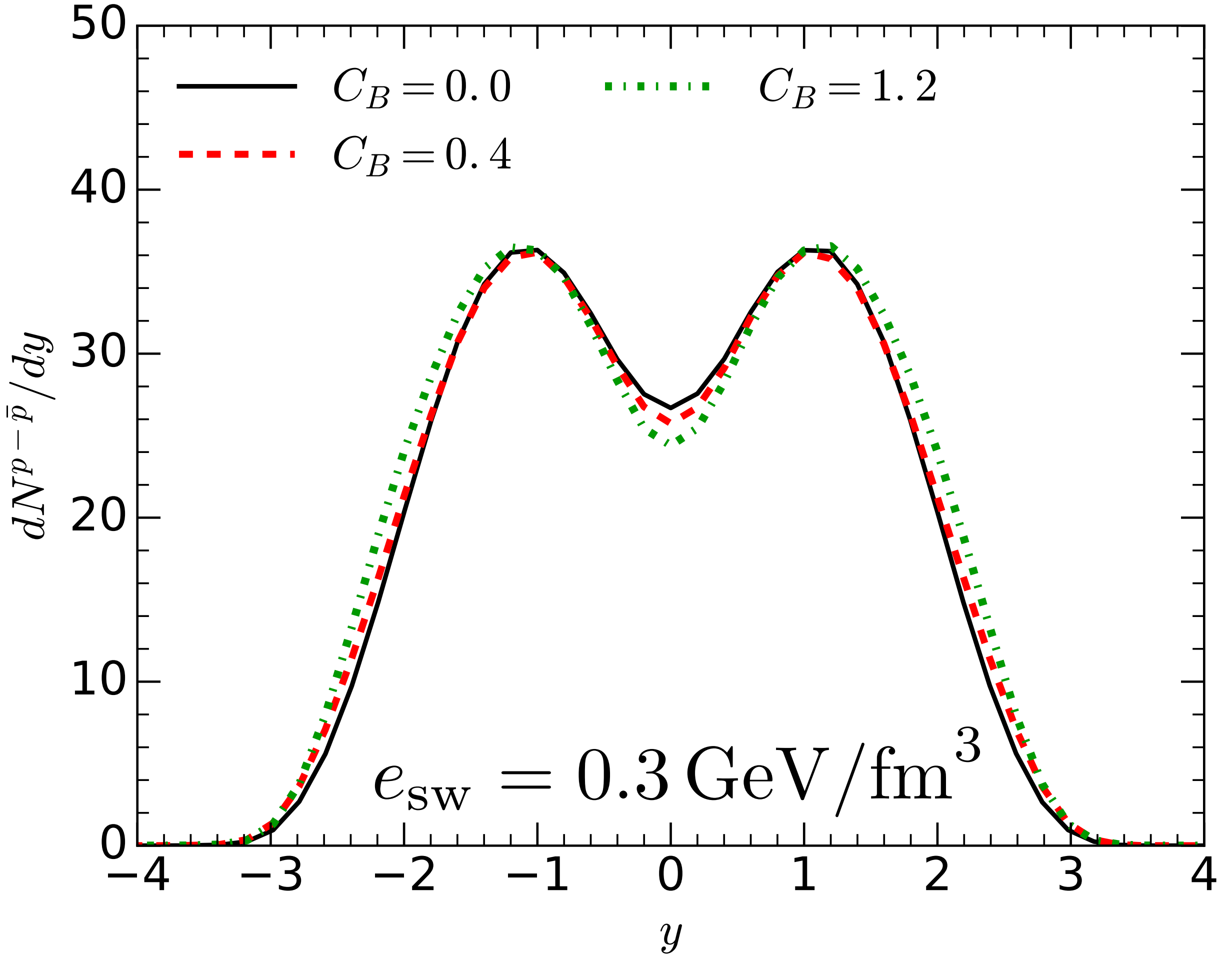

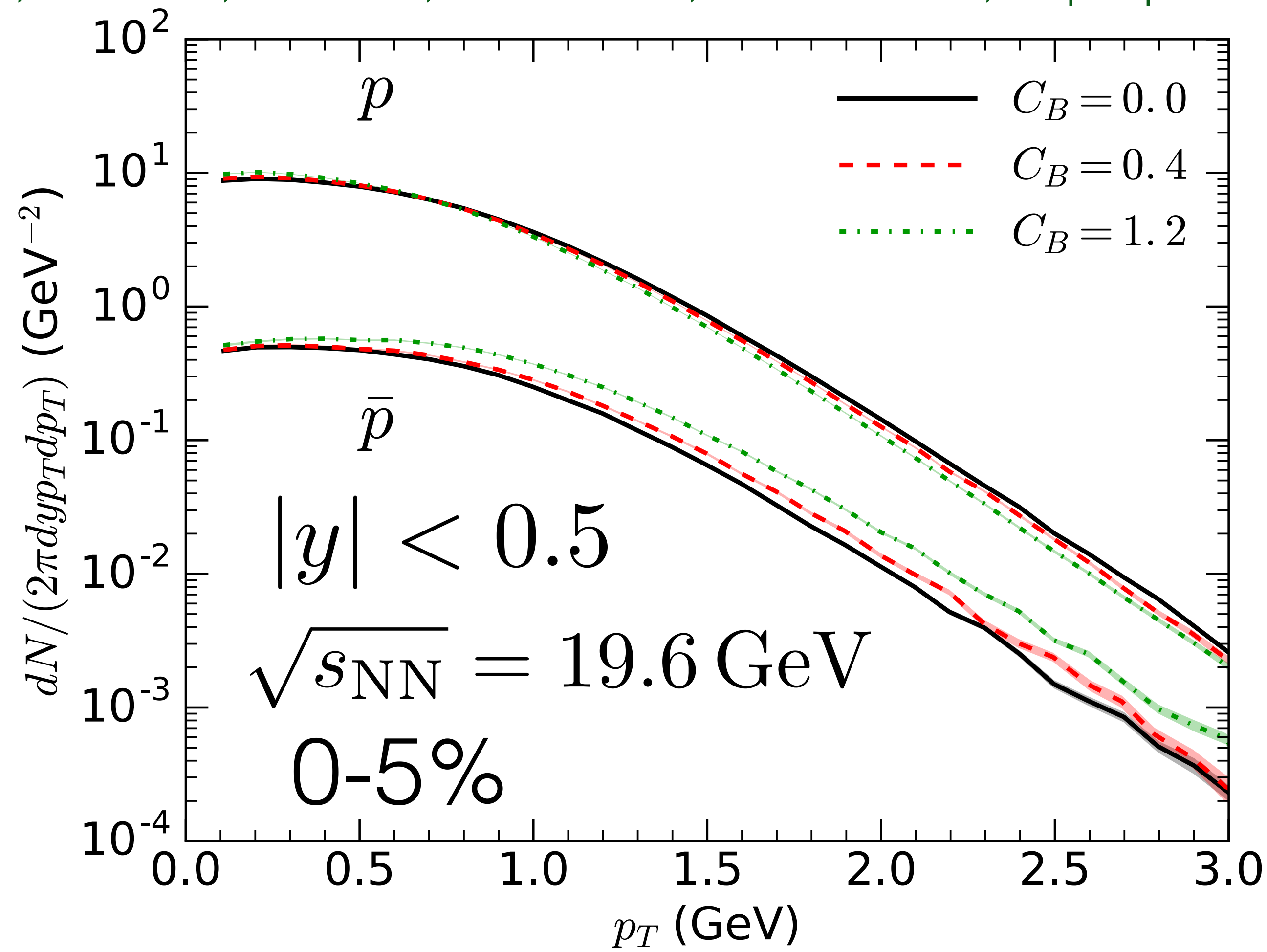

- Net baryon diffusion results a flatter spectra for anti-proton compared to proton's

	$C_B = 0.0$	$C_B = 0.4$	$C_B = 1.2$
$\langle p_\perp \rangle^{\bar{p}} - \langle p_\perp \rangle^{p}$ (GeV)	0.046	0.091	0.158

Effects of hadronic afterburner on pid spectra

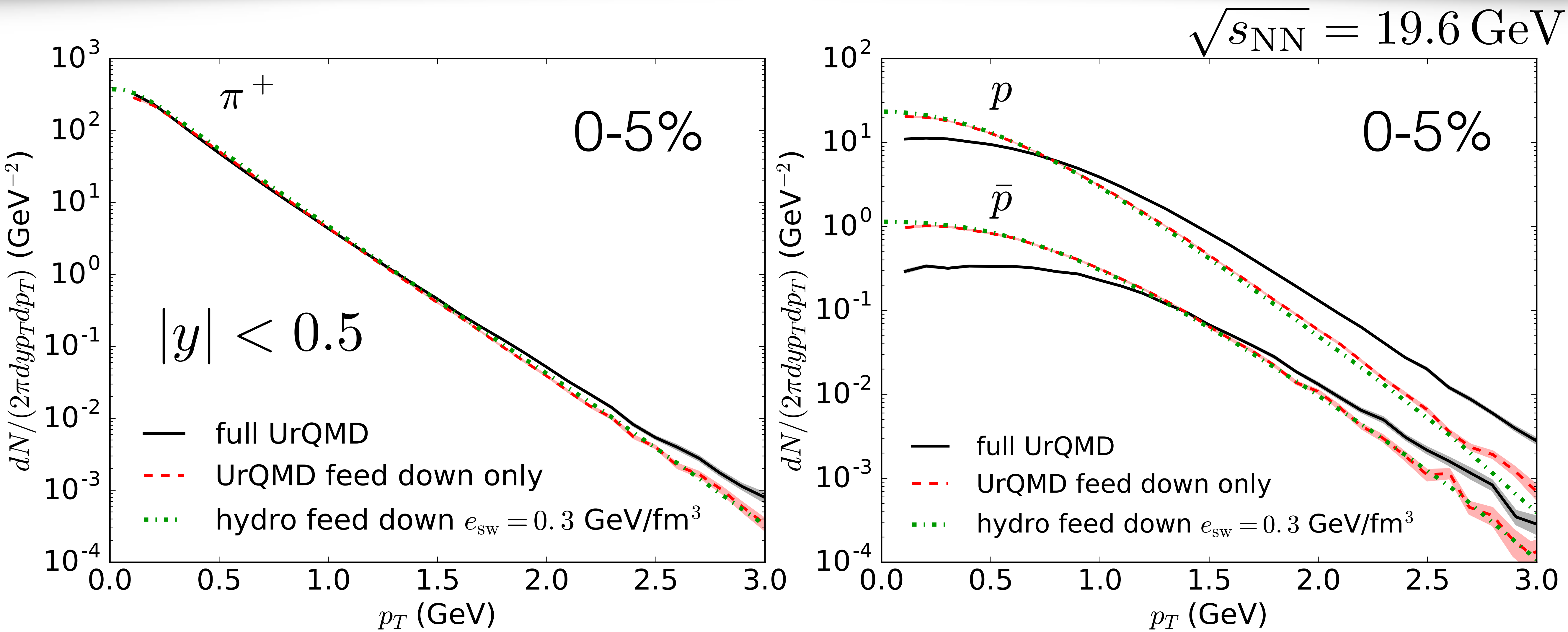

- Hadronic afterburner harden pion spectra at high p_T
- Heavy baryon spectra are largely affected

hadronic afterburner is essential for baryon spectra

Effects of hadronic afterburner on pid spectra

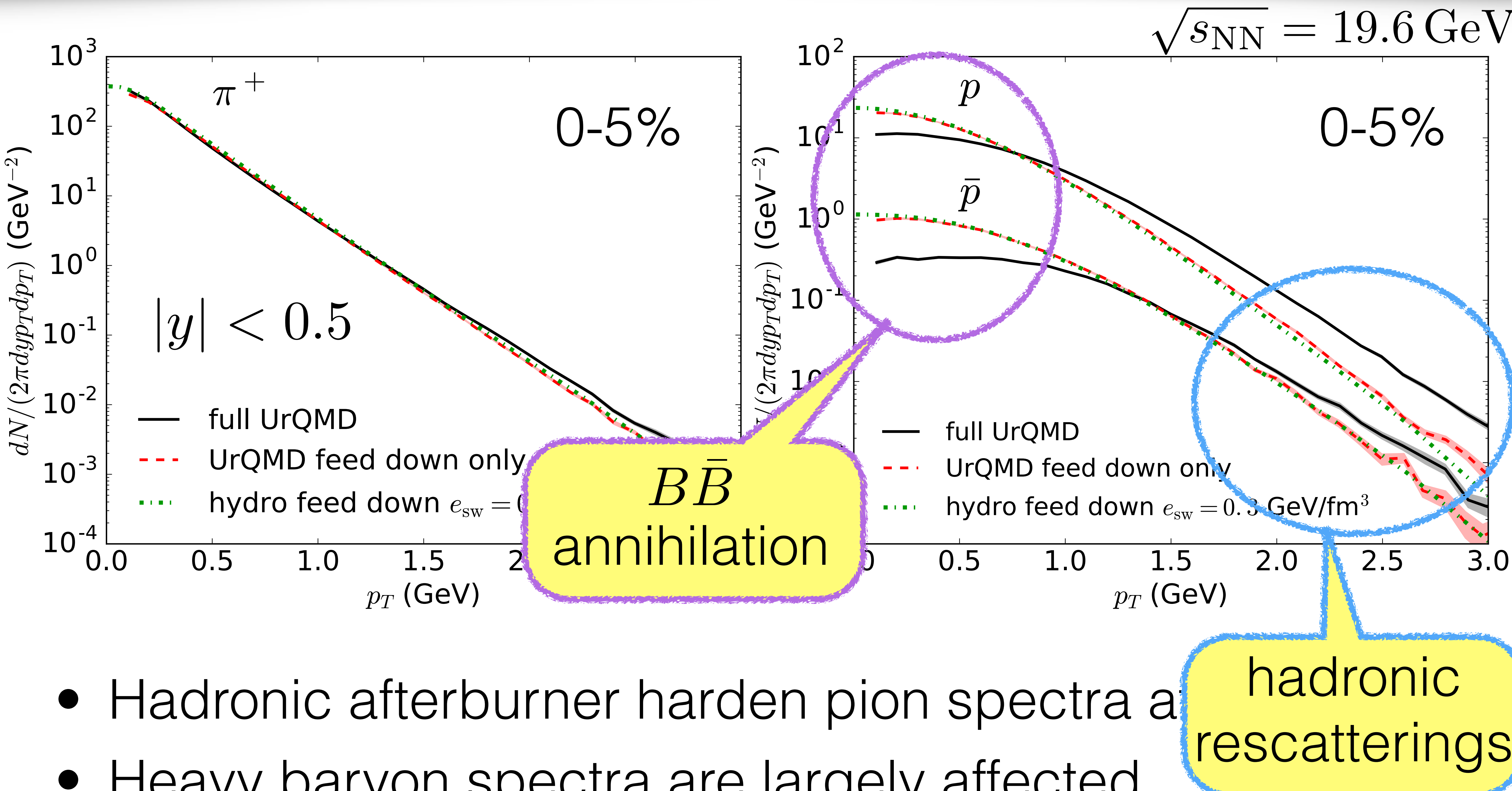

- Hadronic afterburner harden pion spectra a
- Heavy baryon spectra are largely affected

hadronic afterburner is essential for baryon spectra

Conclusion

- We develop a dynamical initialization model to study the early time evolution of heavy-ion collisions at the BES energies

  full **(3+1)-d** event-by-event with net baryon current

- With a hybrid approach, we identified a few experiment observables that could constrain the net baryon diffusion

$$dN^{p-\bar{p}}/dy \qquad \langle p_\perp \rangle^{\bar{p}} - \langle p_\perp \rangle^{p}$$

- Future combining with the Bayesian analysis will help us to constrain the initial state and transport coefficients of the QGP in a baryon-rich environment


BACKUP

Transport coefficients

R. Rougemont, R. Critelli, J. Noronha-Hostler, J. Noronha and C. Ratti, Phys. Rev. D 96, 014032 (2017)

The holographic Einstein-Maxwell-Dilation (EMD) model is fit to the lattice results on thermodynamic quantities at $\mu_B = 0$

Predictions are made for thermodynamic variables at finite μ_B and for the temperature and μ_B dependence of various transport coefficients

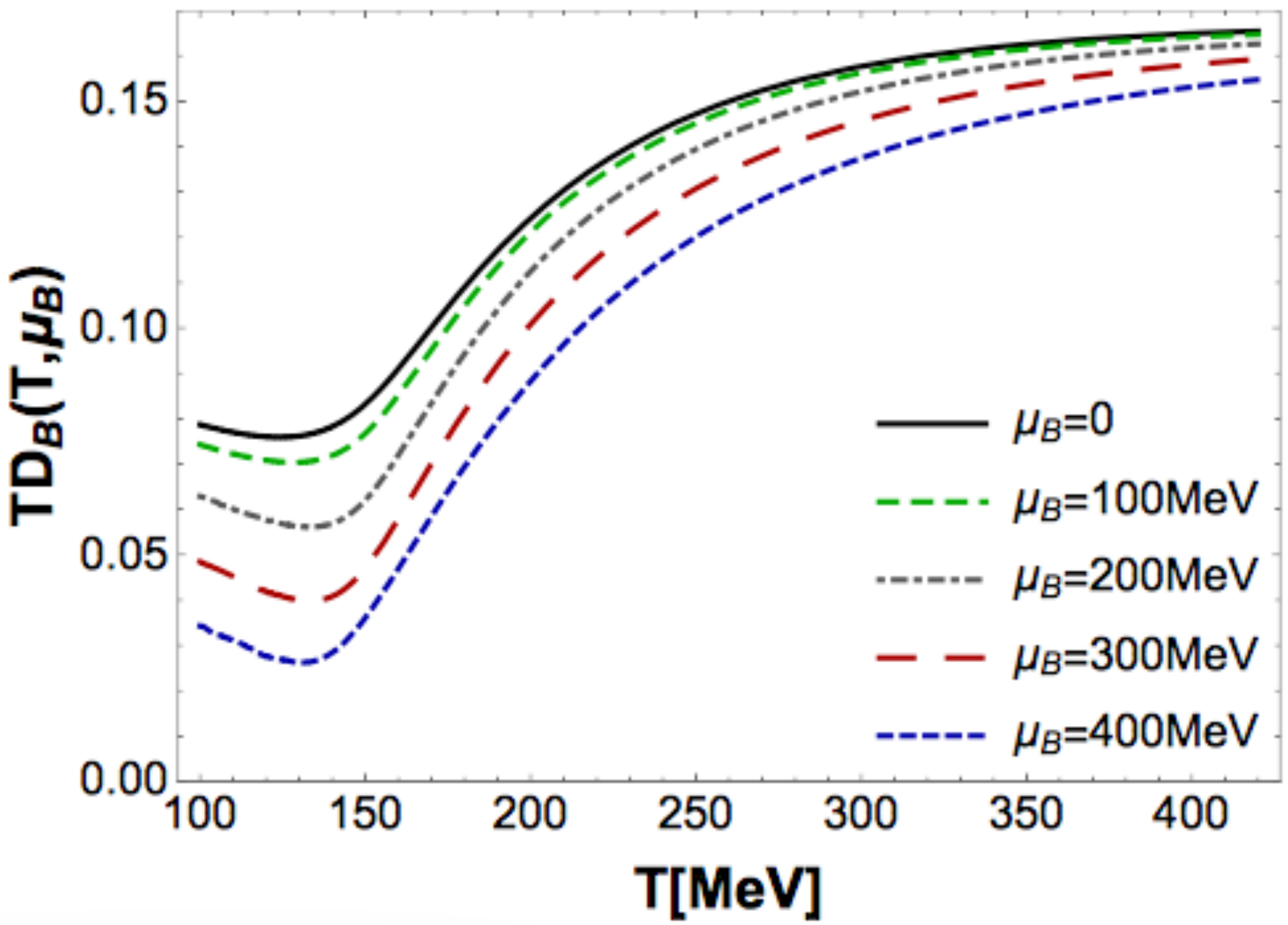

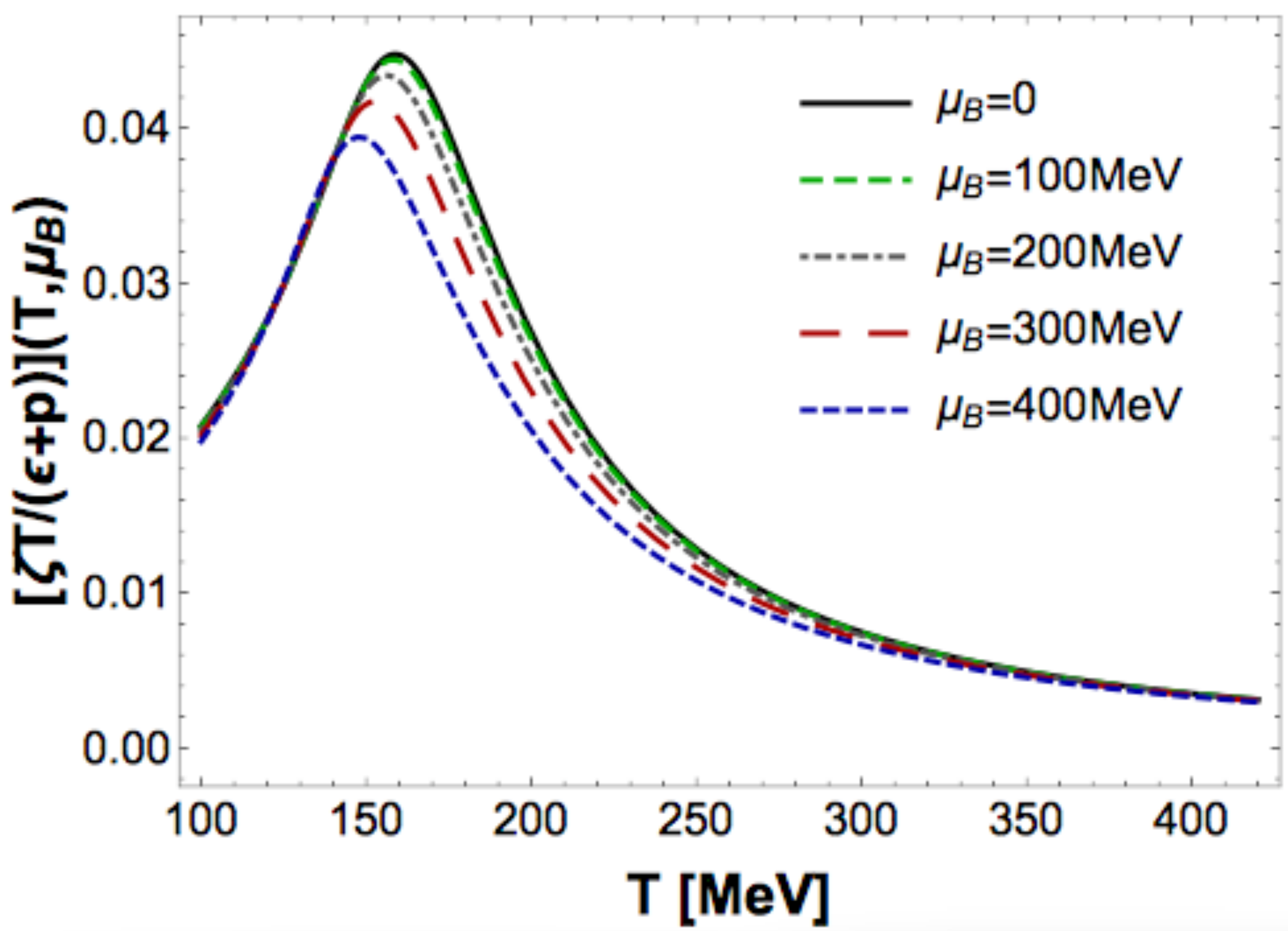

Net baryon number distribution

space-time rapidity

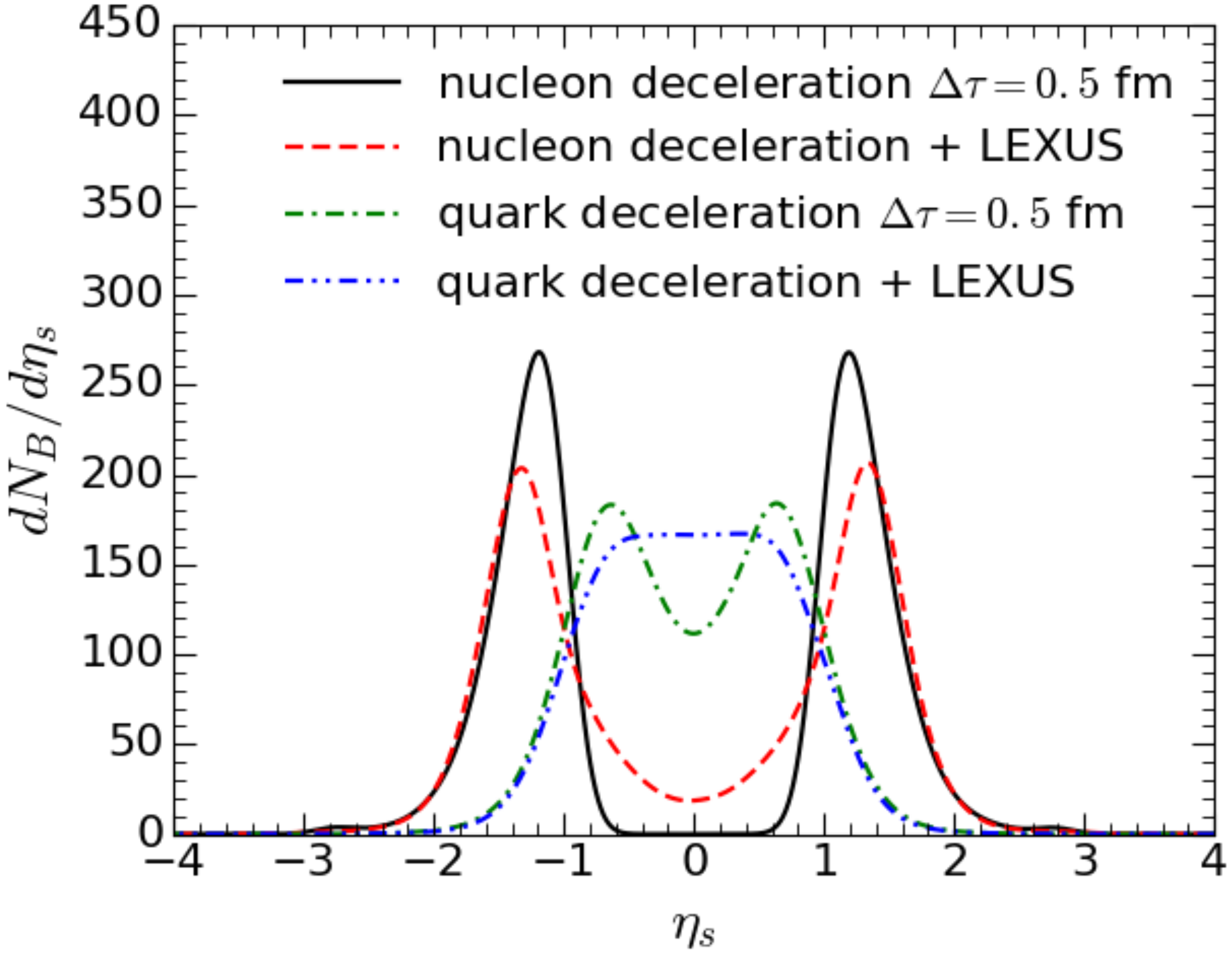

momentum rapidity

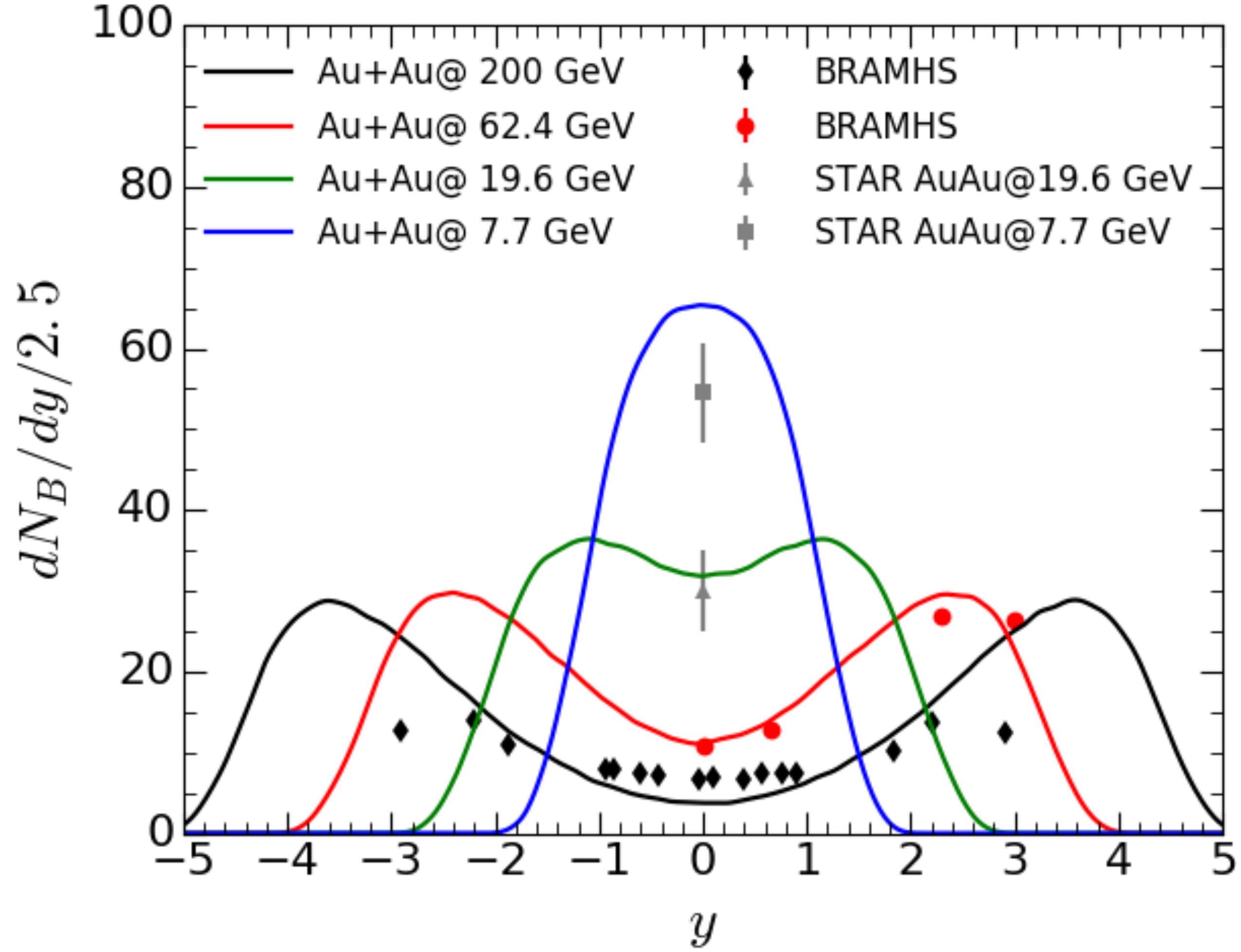

Convert to particles

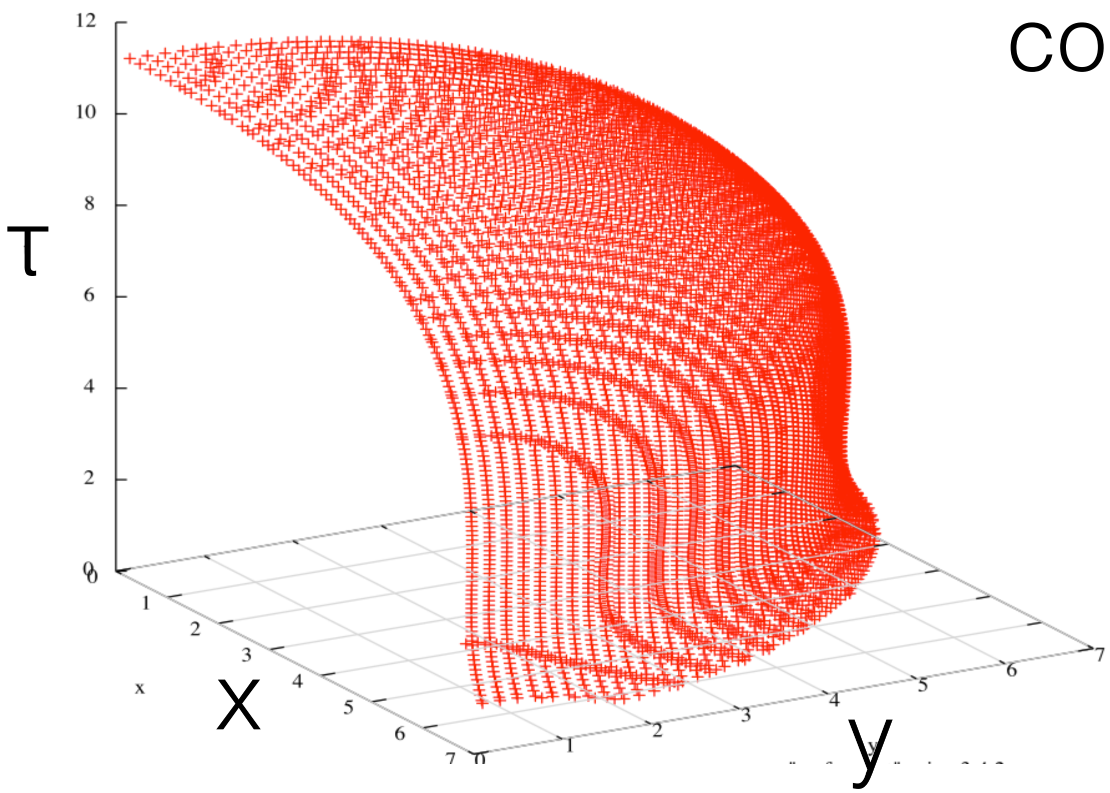

Conversion surface is determined at a constant energy density

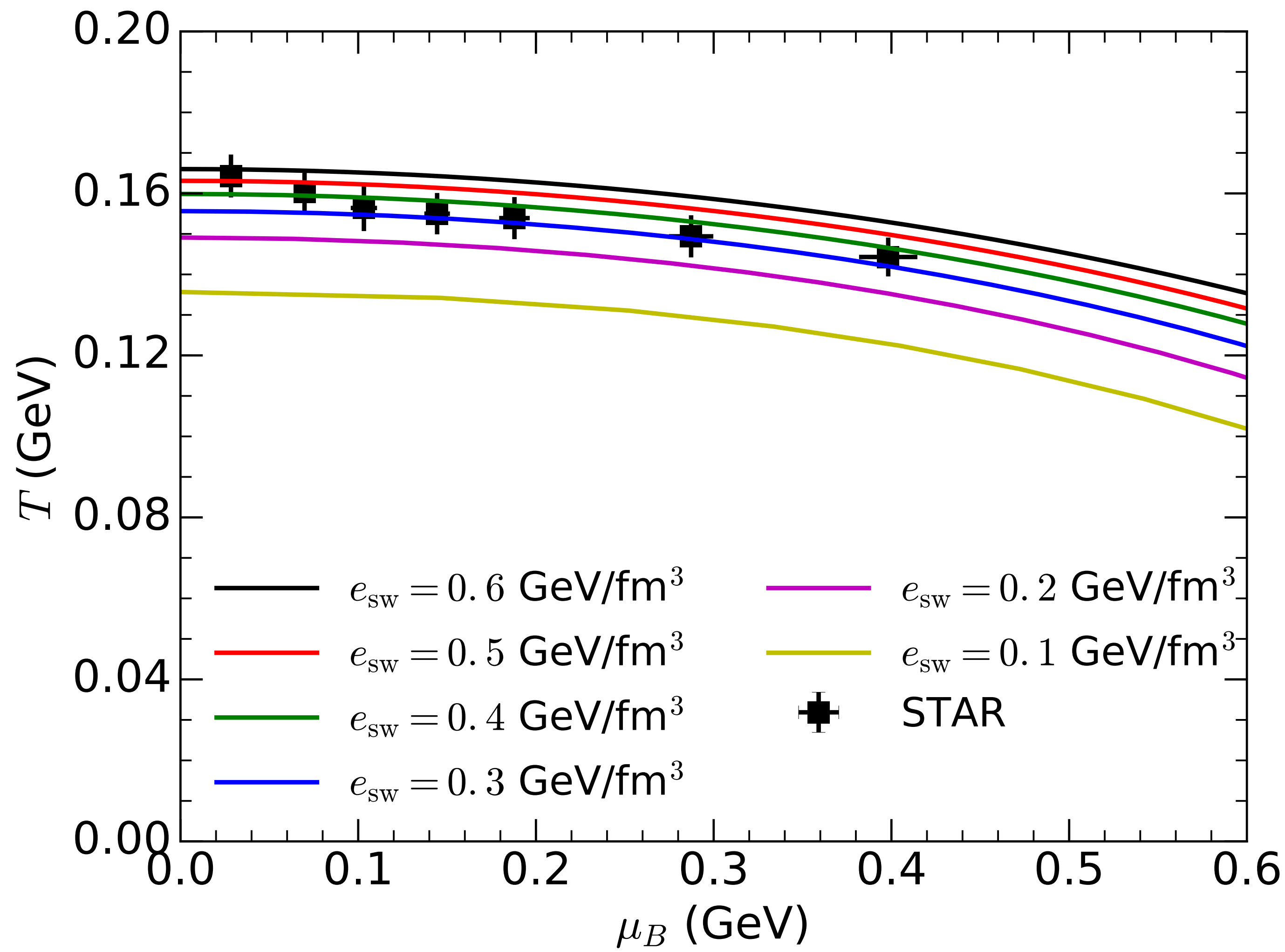

Cooper-Frye conversion:

$$E\frac{dN_i}{d^3p} = \frac{g_i}{(2\pi)^3}\int p^\mu d^3\sigma_\mu(x)\left(f_0(x,p) + \delta f(x,p)\right)$$

$$f_0^i(x,p) = \frac{1}{e^{(E - b_i \mu_B(x))/T(x)} \pm 1}$$

Heavy-ion collisions at BES energies…

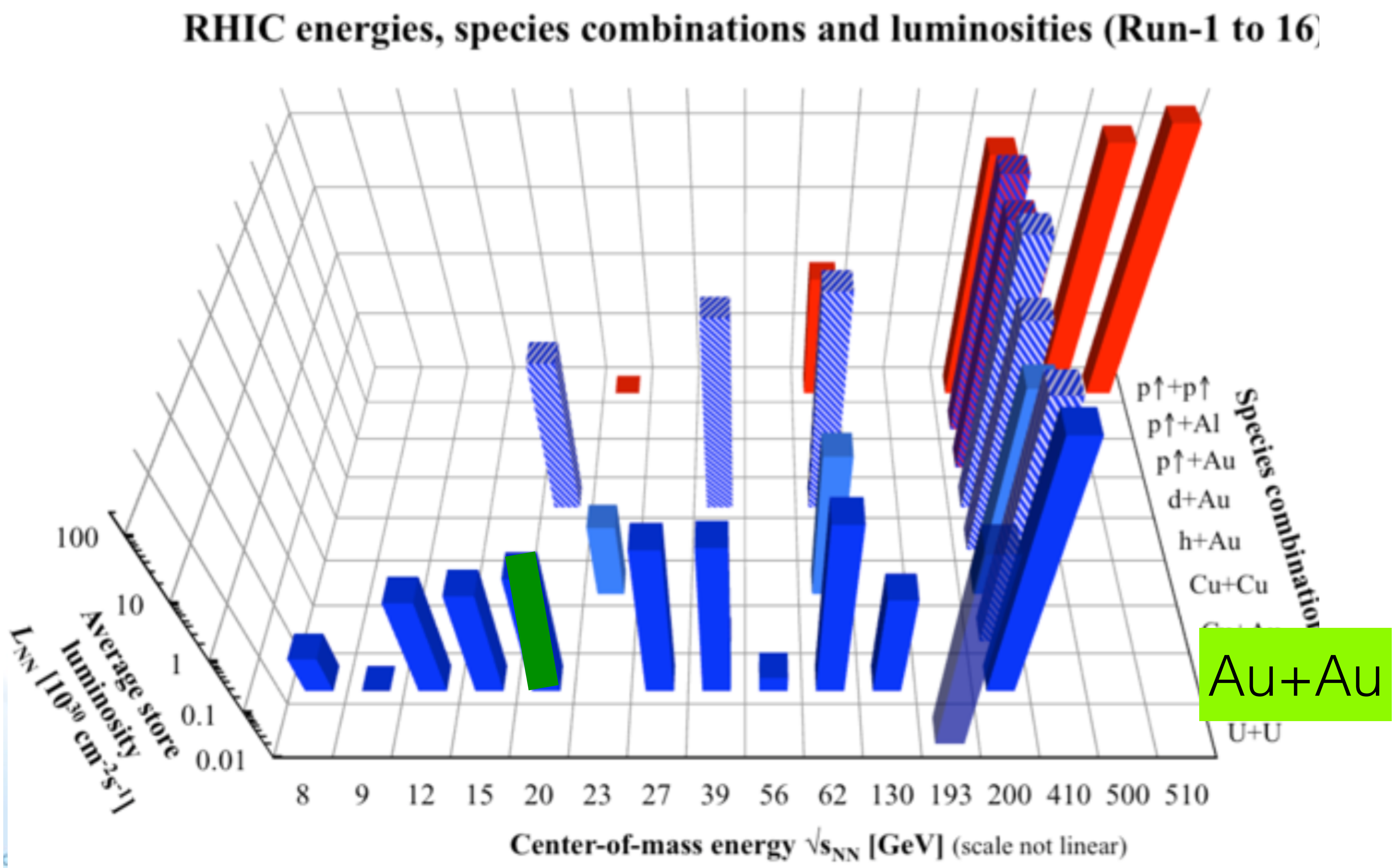

picture taken from http://www.agsrhichome.bnl.gov/RHIC/Runs/

Effects of hadronic afterburner on particle yields

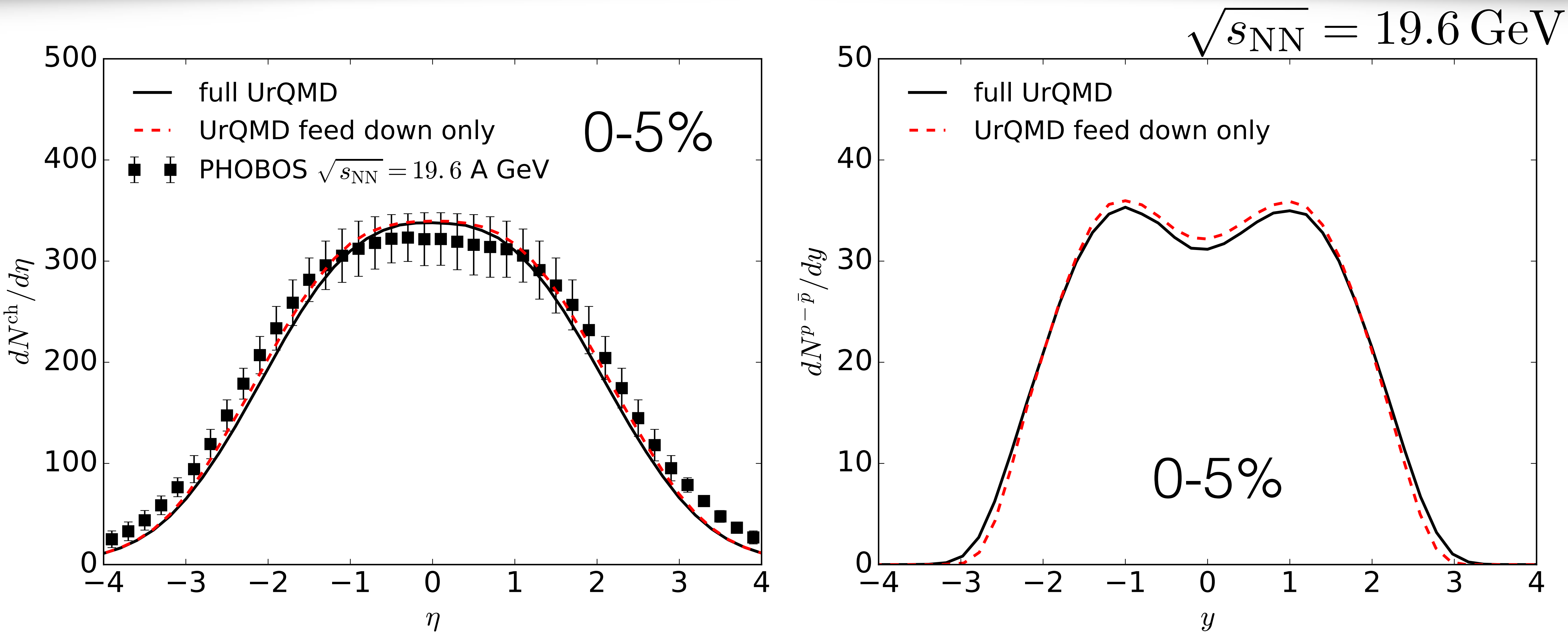

- Hadronic afterburner has little effect on charged hadron pseudo-rapidity distribution
- Net proton rapidity profile is slightly flatter after hadronic scatterings

more sensitive to early stage dynamics

Effects of net baryon diffusion on particle yields

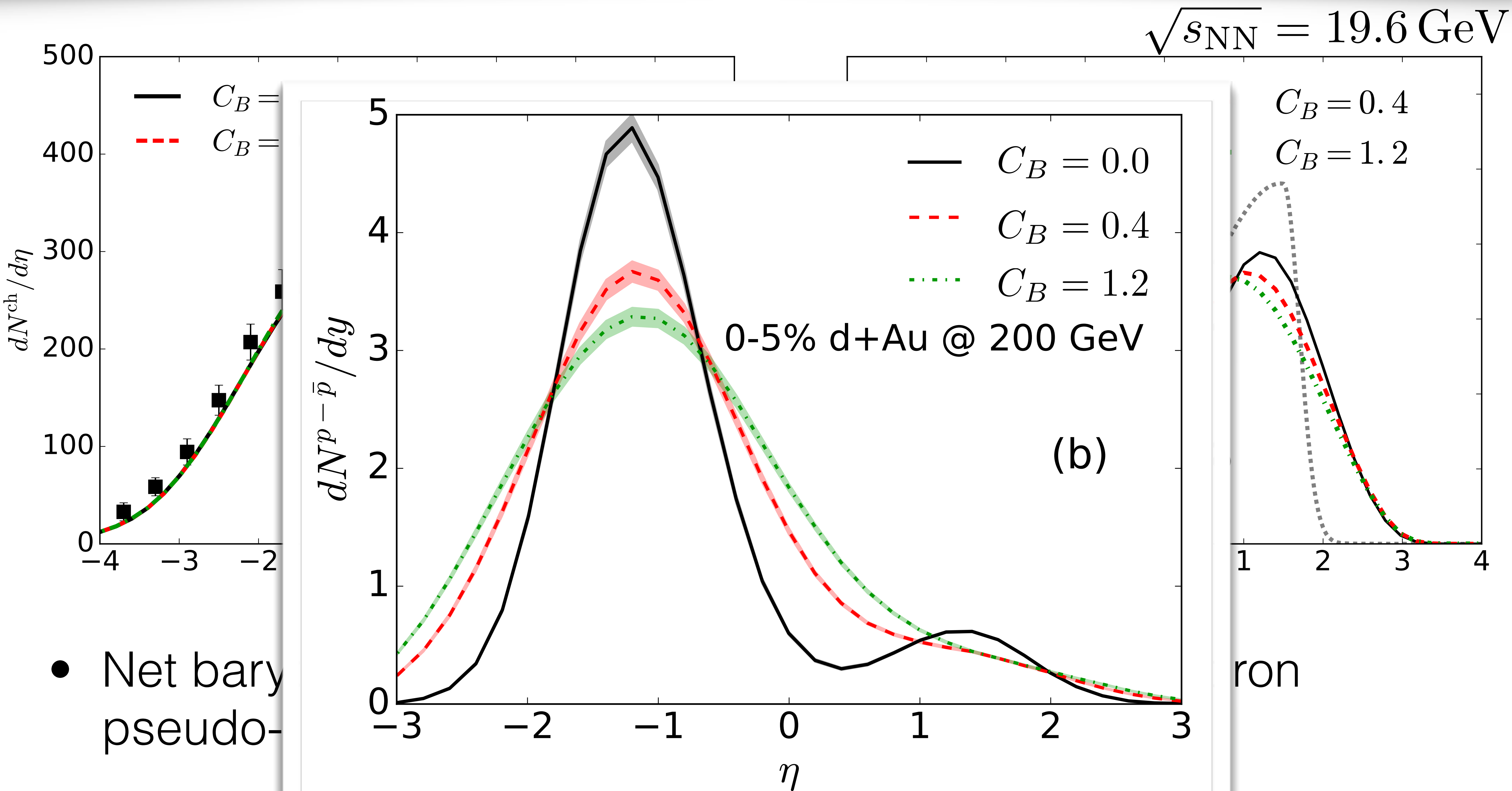

- Net bary… ron pseudo-…
- More net baryon numbers are transported to mid-rapidity with a larger diffusion constant

Constraints on net baryon diffusion and initial condition

Effects of hadronic afterburner on pid spectra

$\sqrt{s_{\rm NN}} = 19.6\,{\rm GeV}$

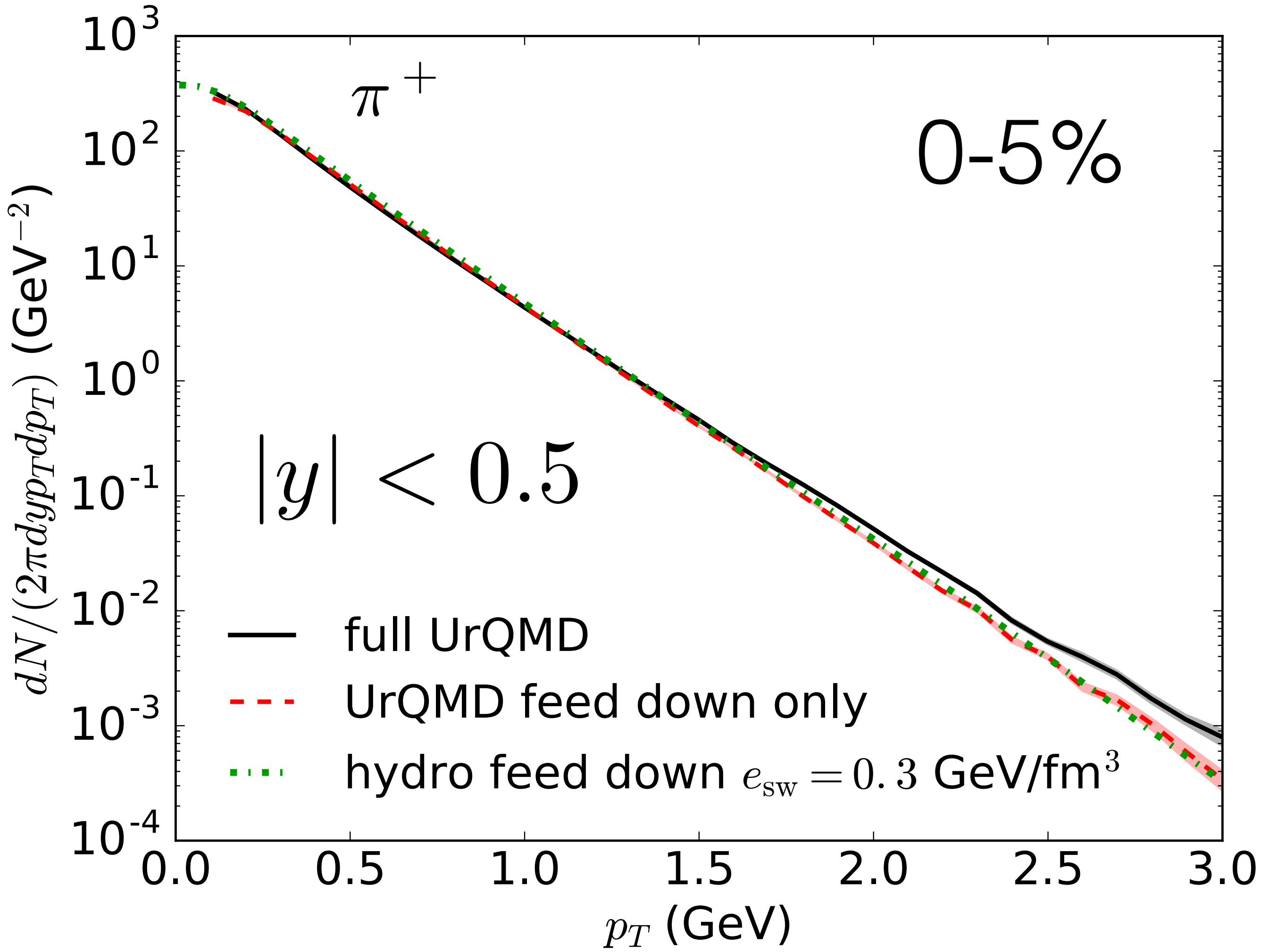

- Hadronic afterburner harden pion spectra at high p_T

Effects of hadronic afterburner on pid spectra

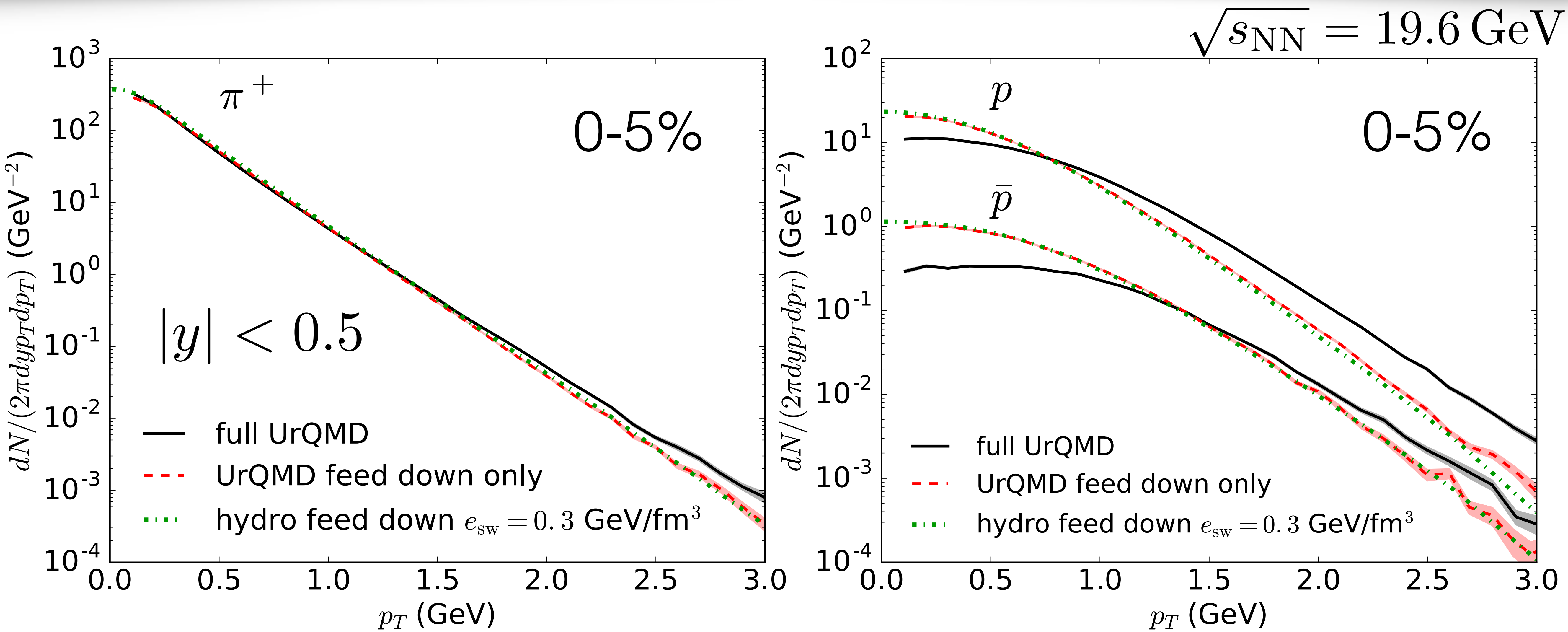

- Hadronic afterburner harden pion spectra at high p_T
- Heavy baryon spectra are largely affected

hadronic afterburner is essential for baryon spectra

Effects of hadronic afterburner on pid spectra

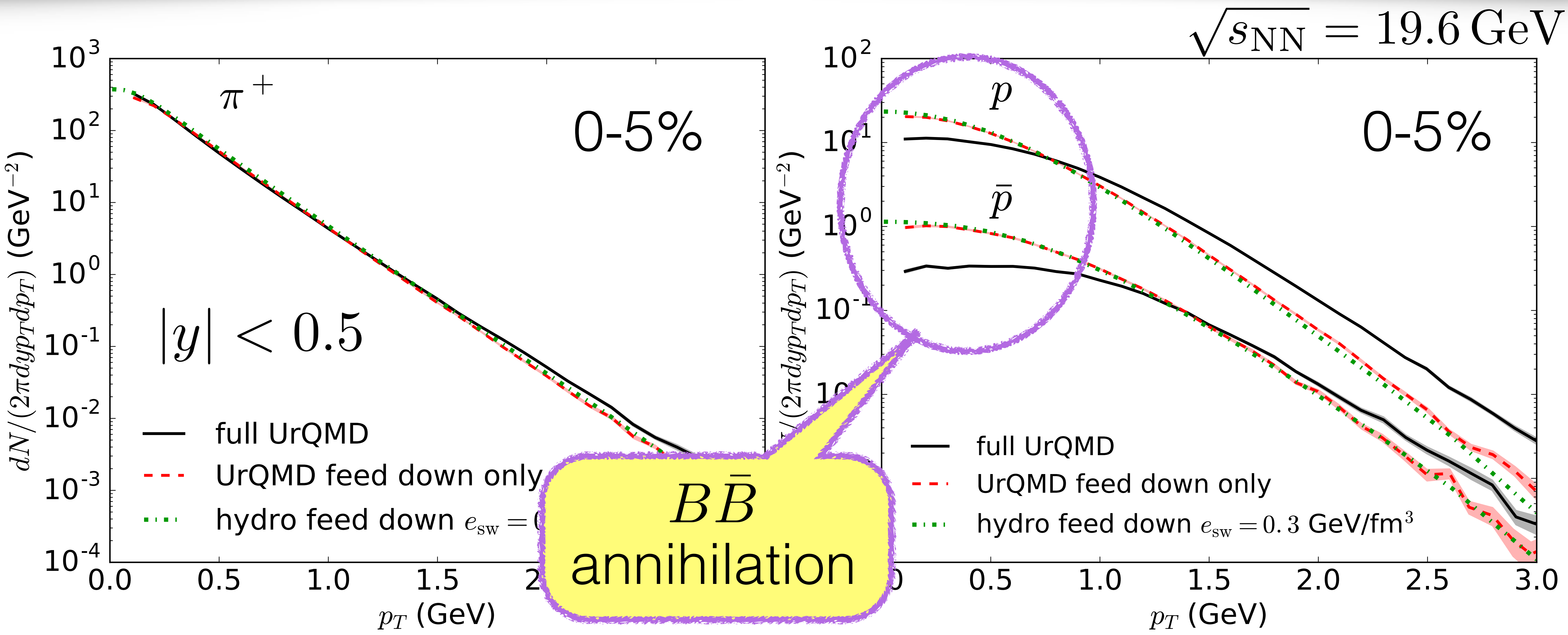

- Hadronic afterburner harden pion spectra at high p_T
- Heavy baryon spectra are largely affected

hadronic afterburner is essential for baryon spectra

Effects of hadronic afterburner on pid spectra

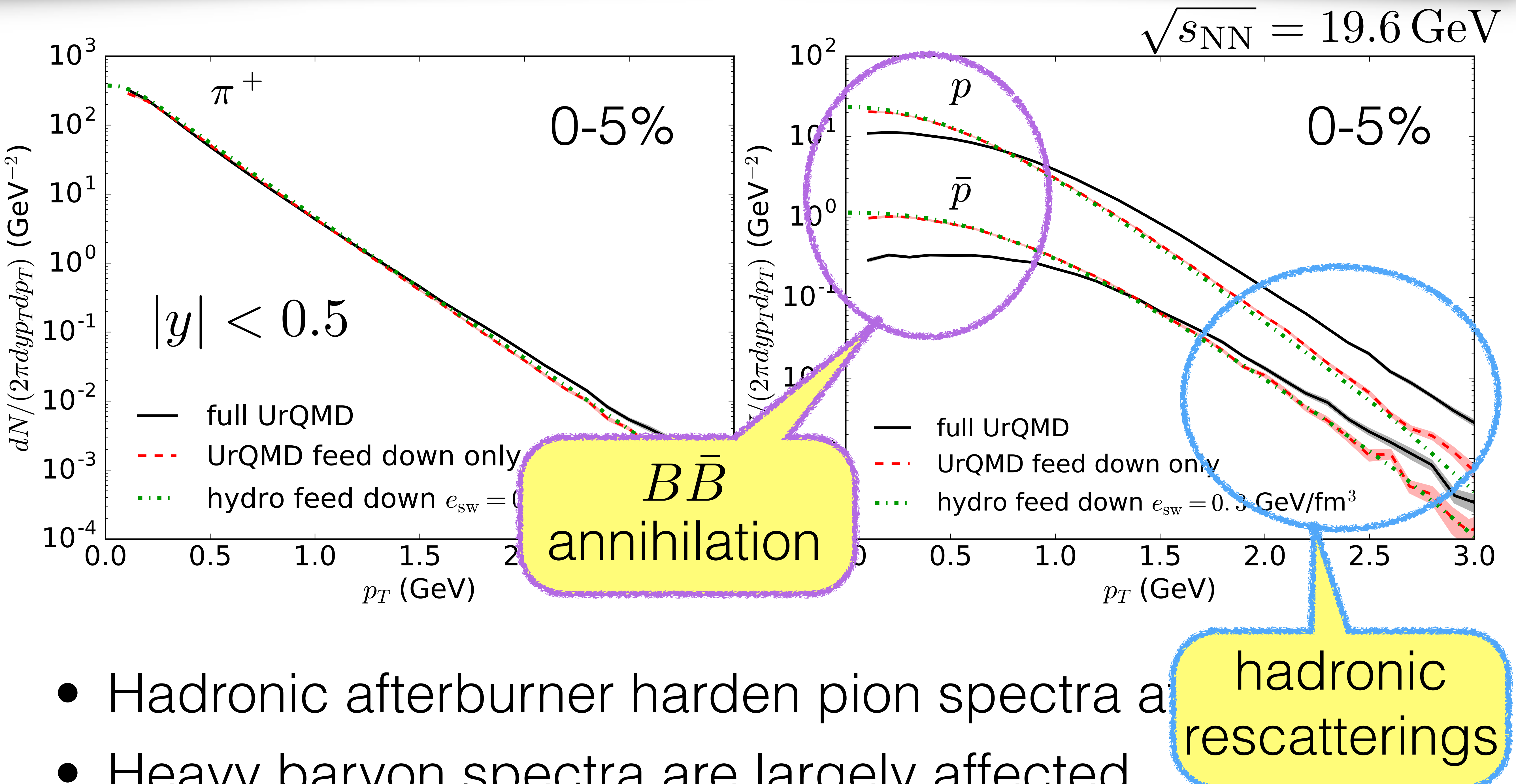

- Hadronic afterburner harden pion spectra a
- Heavy baryon spectra are largely affected

hadronic afterburner is essential for baryon spectra

Effects of net baryon diffusion on pid spectra

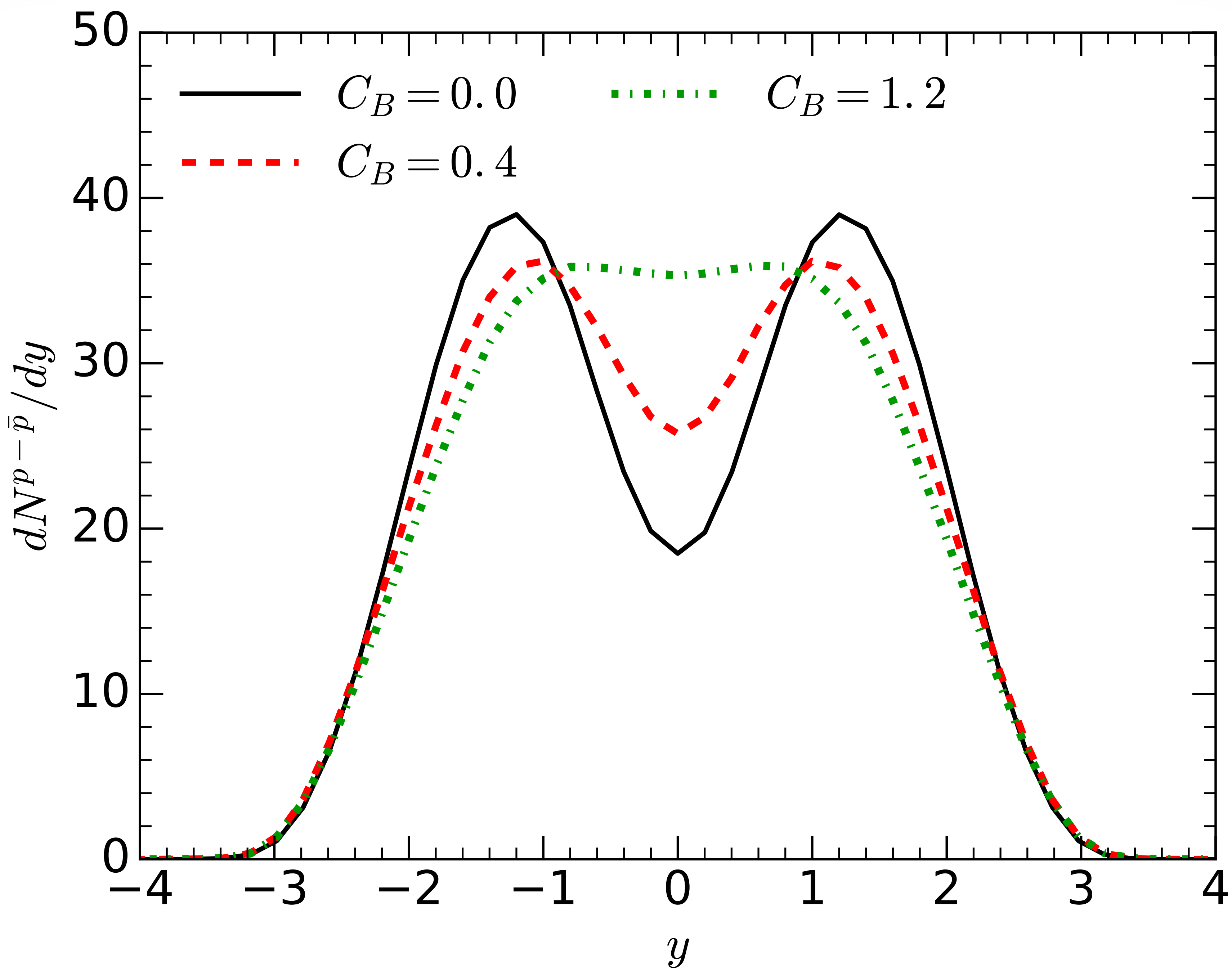

- To study the net baryon diffusion effects on transverse observables, we first tune the initial longitudinal profiles to product the same $dN^{p-\bar{p}}/dy$

Effects of net baryon diffusion on pid spectra

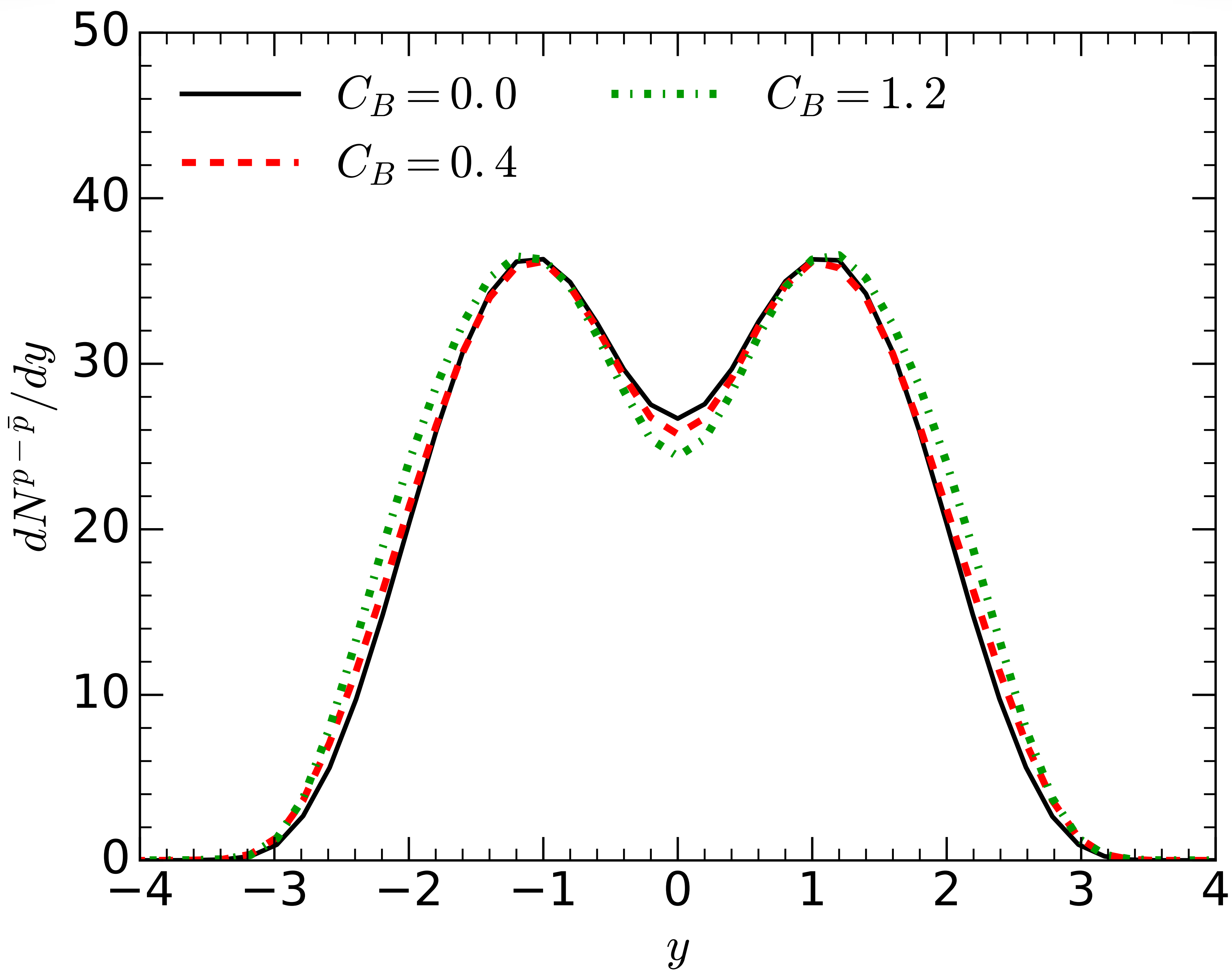

- To study the net baryon diffusion effects on transverse observables, we first tune the initial longitudinal profiles to product the same $dN^{p-\bar{p}}/dy$

Effects of net baryon diffusion on pid spectra

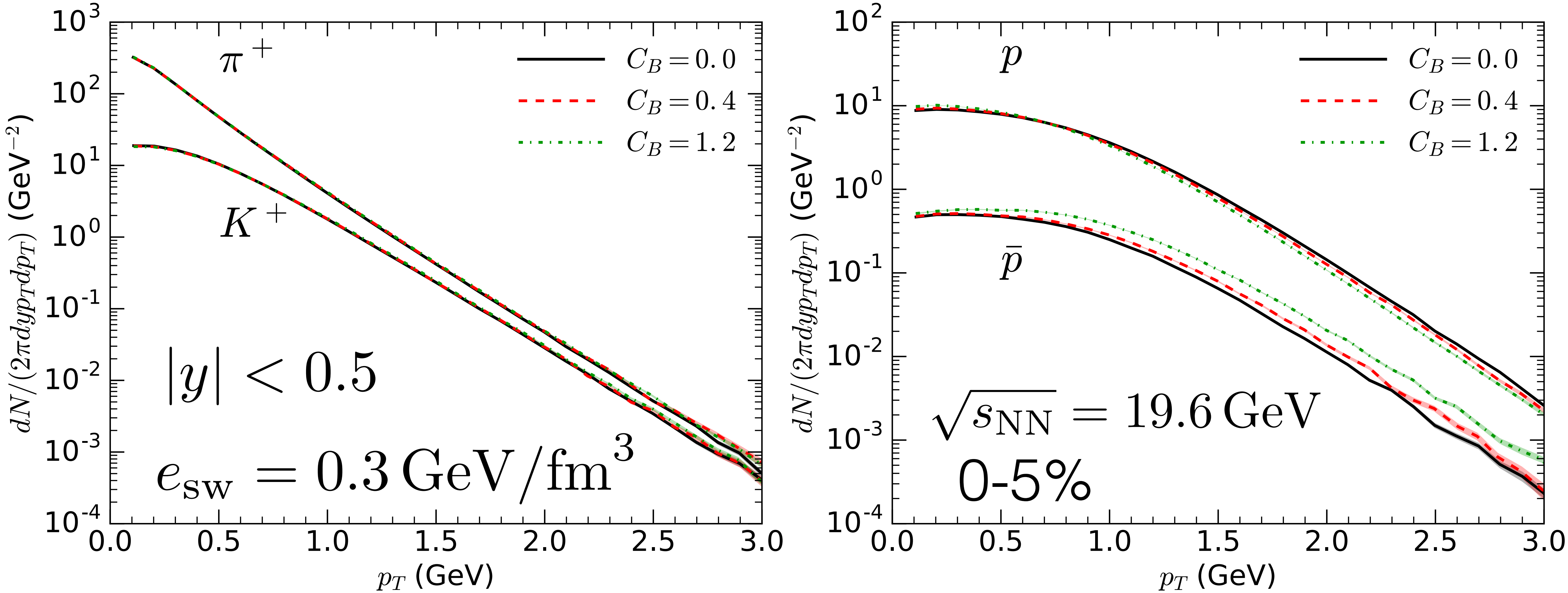

- Net baryon diffusion results a flatter spectra for anti-proton compared to proton's

Effects of hadronic afterburner on pid v_2

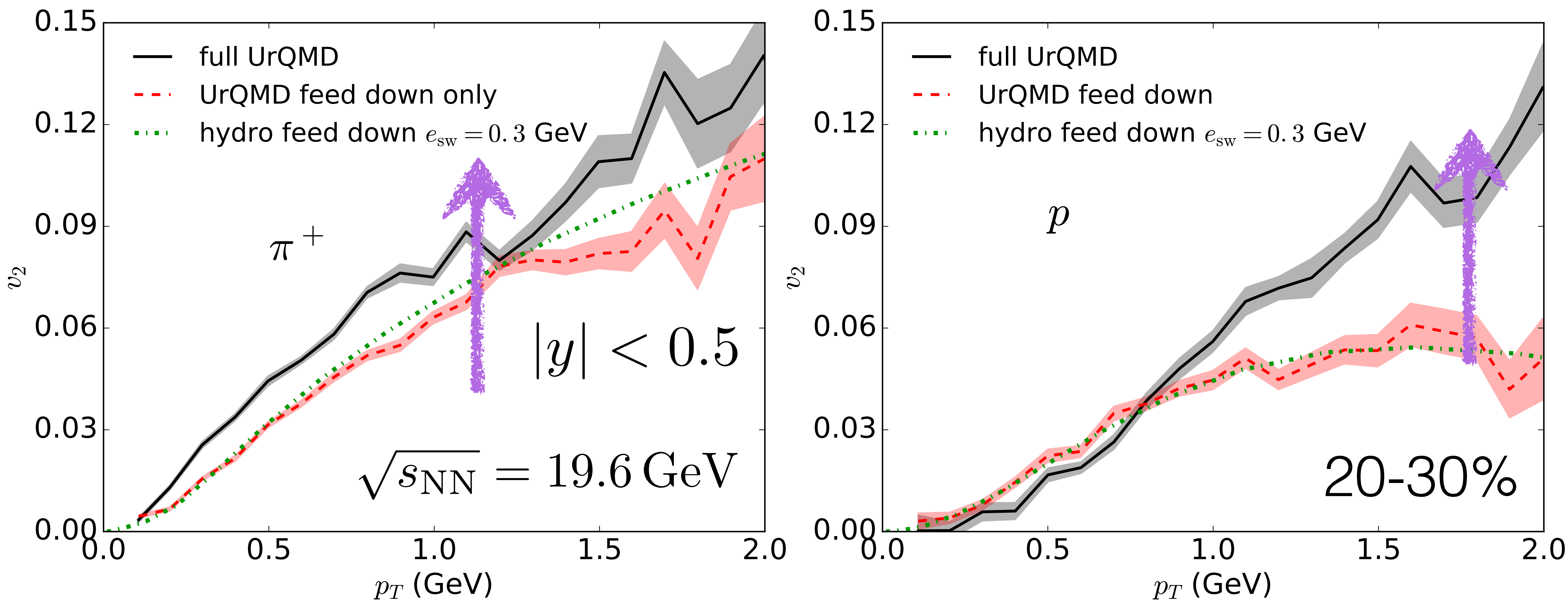

- Momentum anisotropy keeps developing in the UrQMD phase

hadronic afterburner is essential

Effects of hadronic afterburner on pid v_2

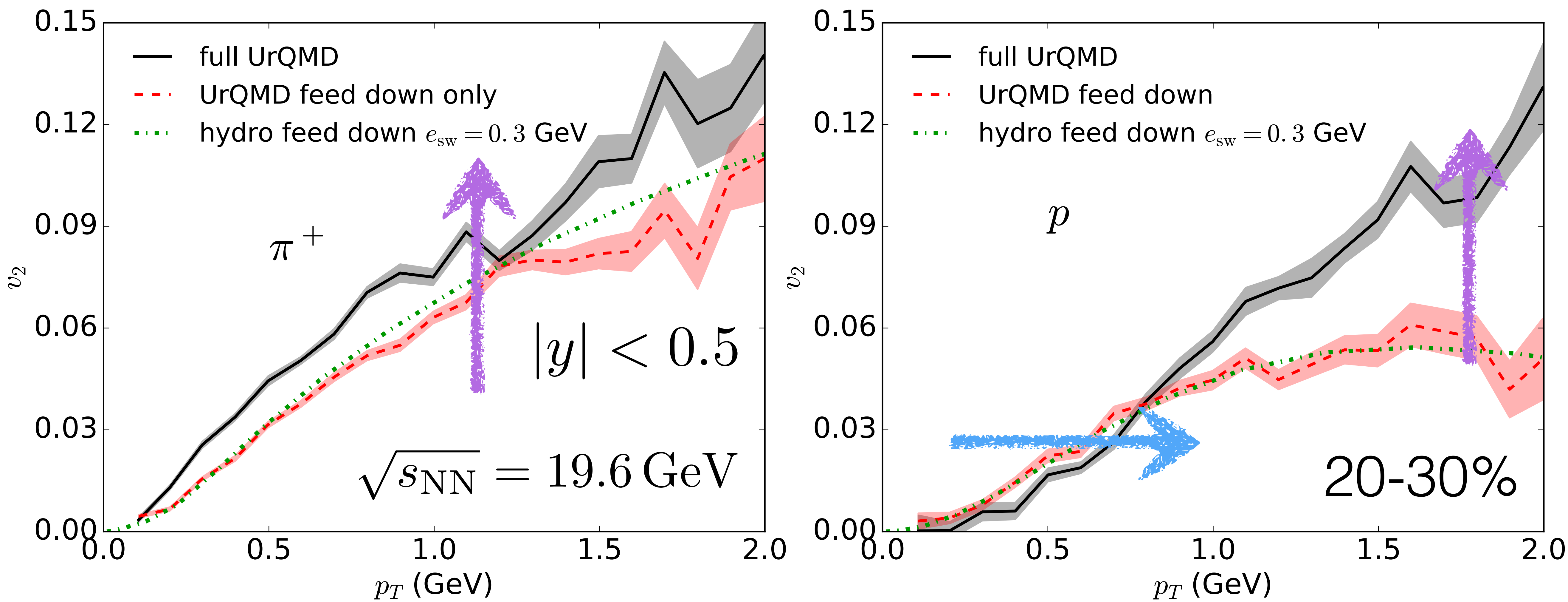

- Momentum anisotropy keeps developing in the UrQMD phase
- Low p_T proton v_2 is blue shifted because of the pion "wind"

hadronic afterburner is essential

Effects of net baryon diffusion on pid v_2

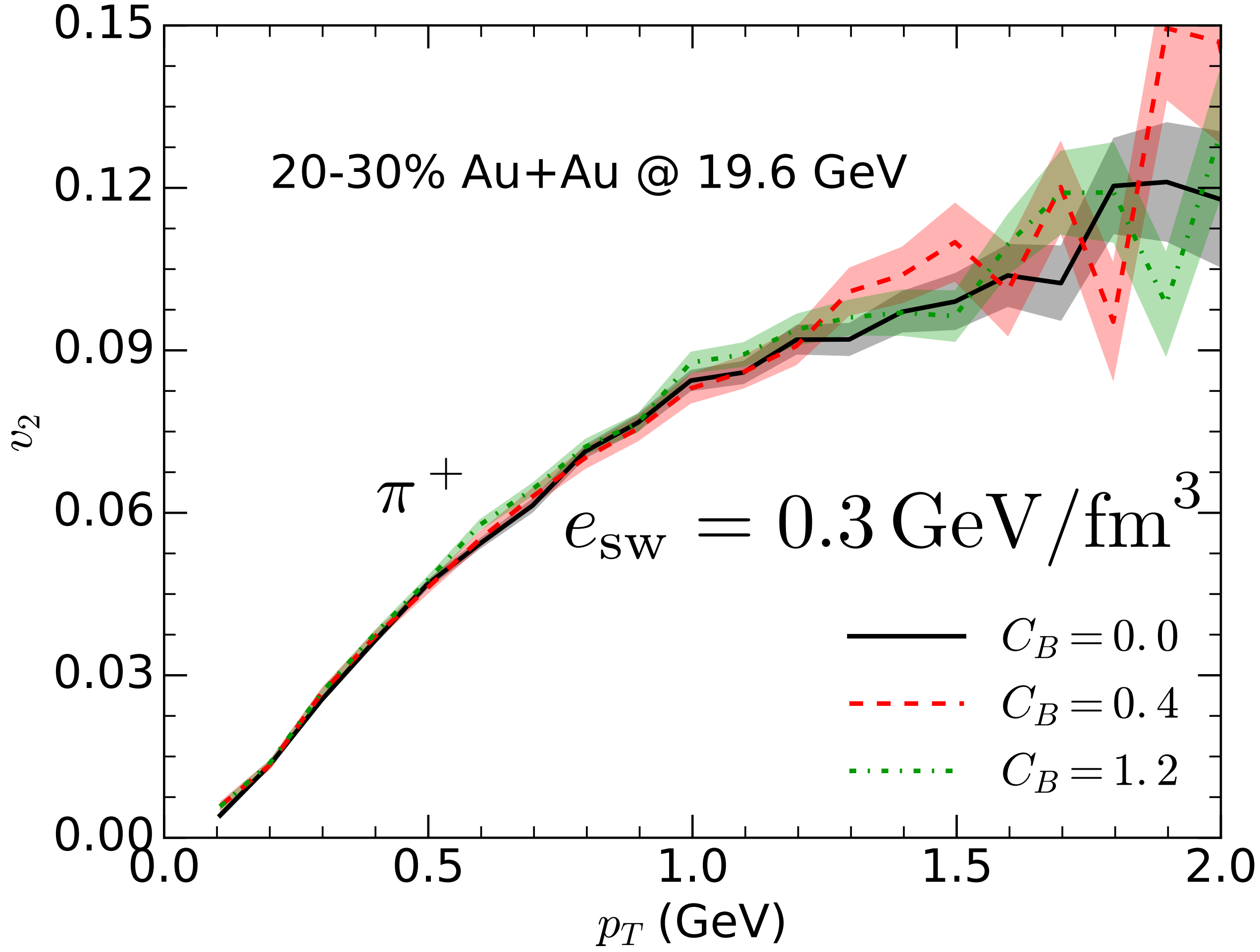

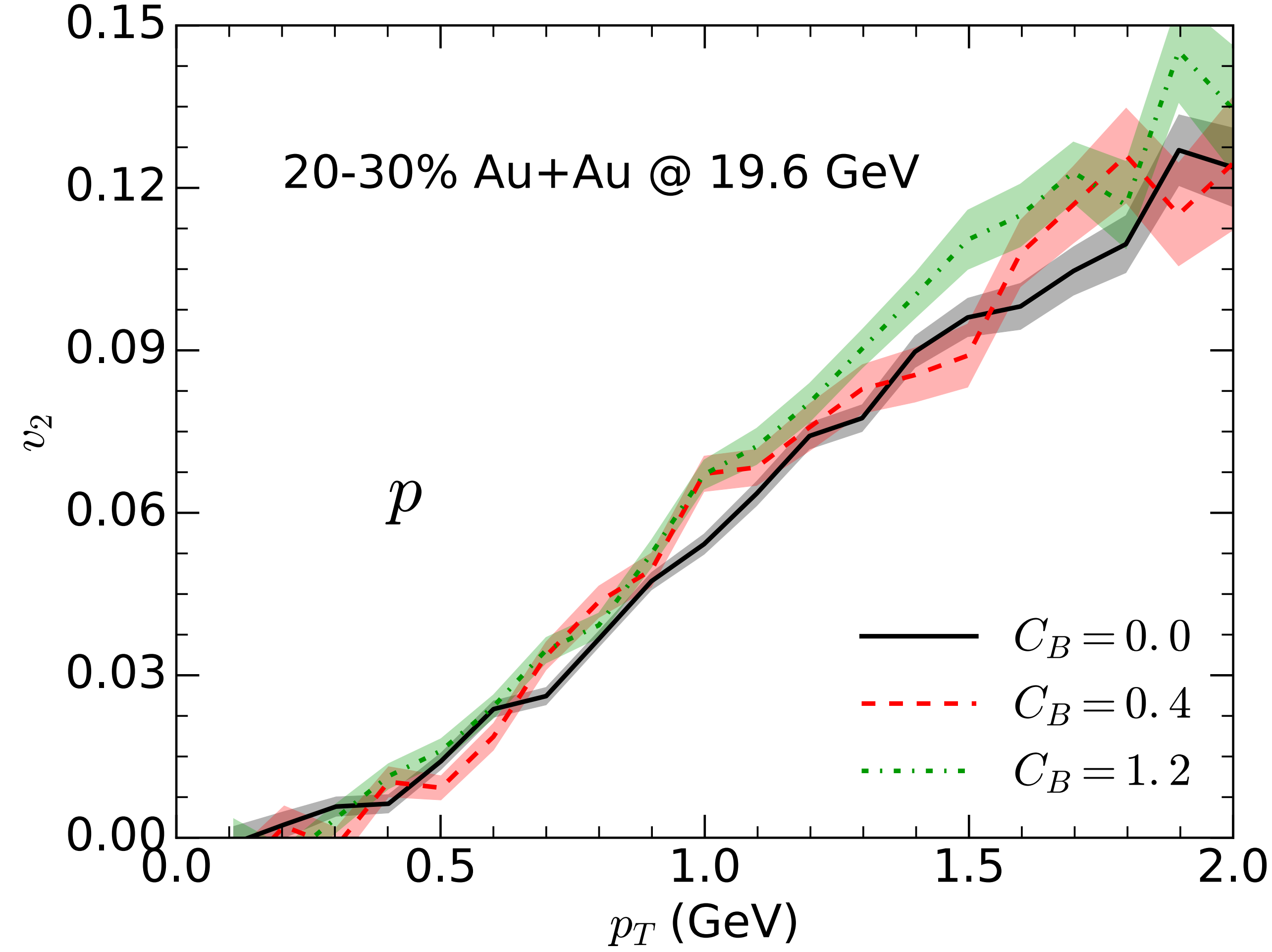

- Hadronic scatterings wash out most of the diffusion effects on pid v_2

$v_2(p)$ vs $v_2(\bar{p})$

STAR

Phys.Rev. C88 (2013) 014902

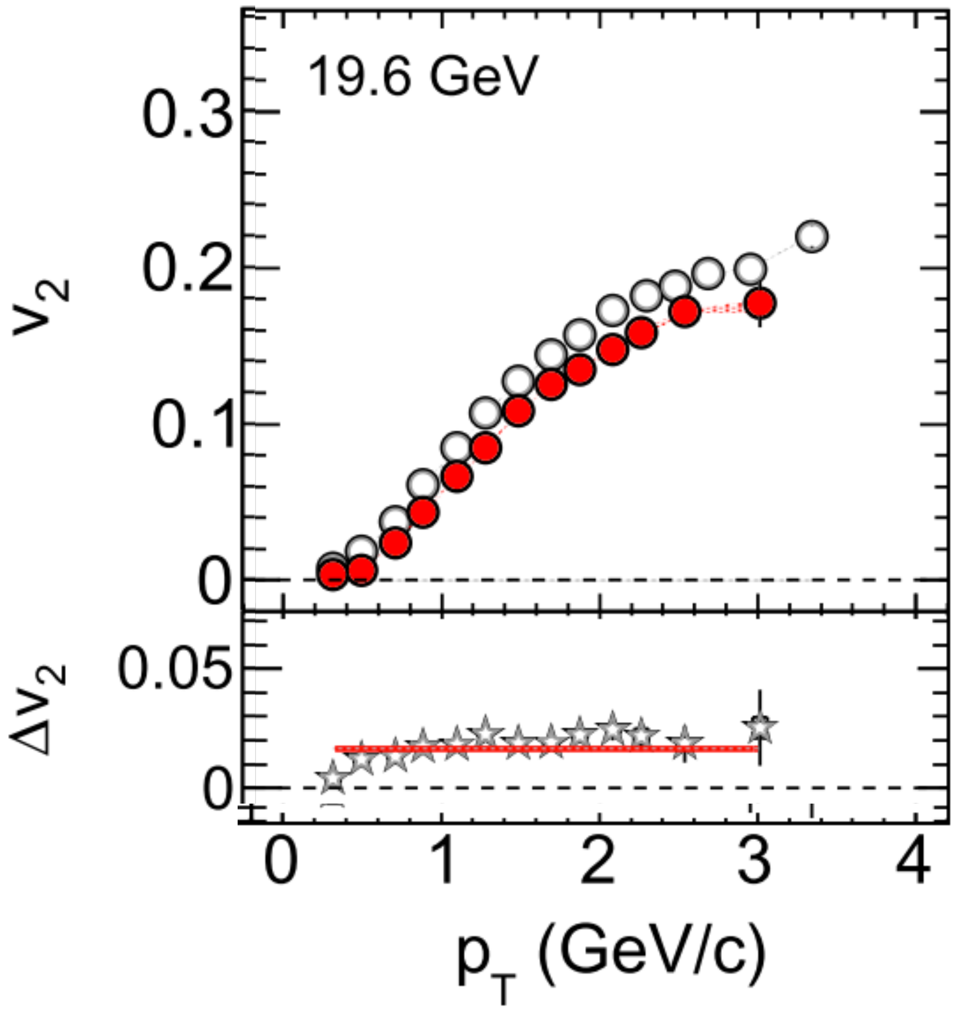

AMPT

Phys.Rev. C93 (2016) no.1, 014907

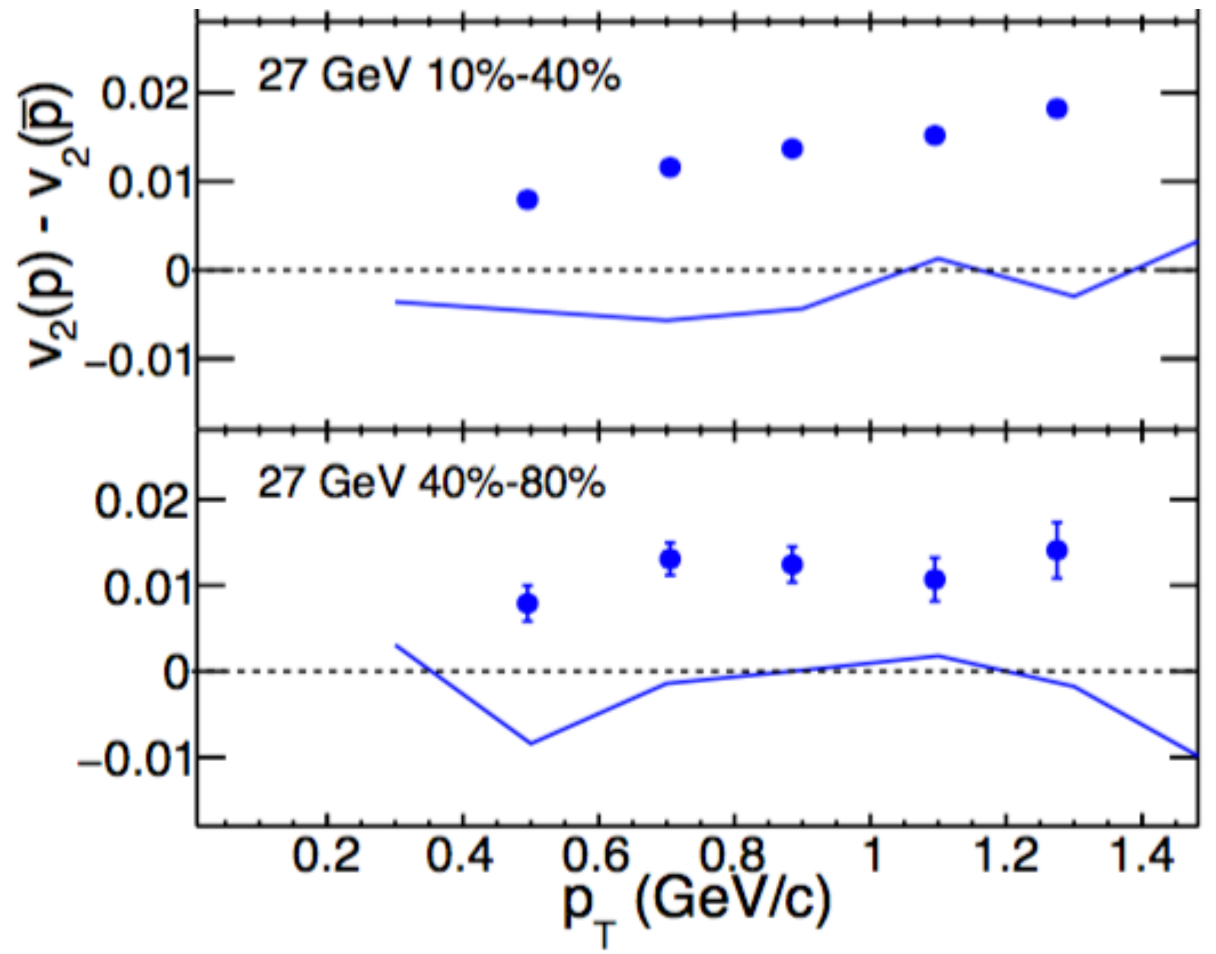

- Transport simulations give $v_2(\bar{p}) > v_2(p)$, which is opposite compared to the STAR data

mean field effects in the hadronic phase?

$v_2(p)$ vs $v_2(\bar{p})$

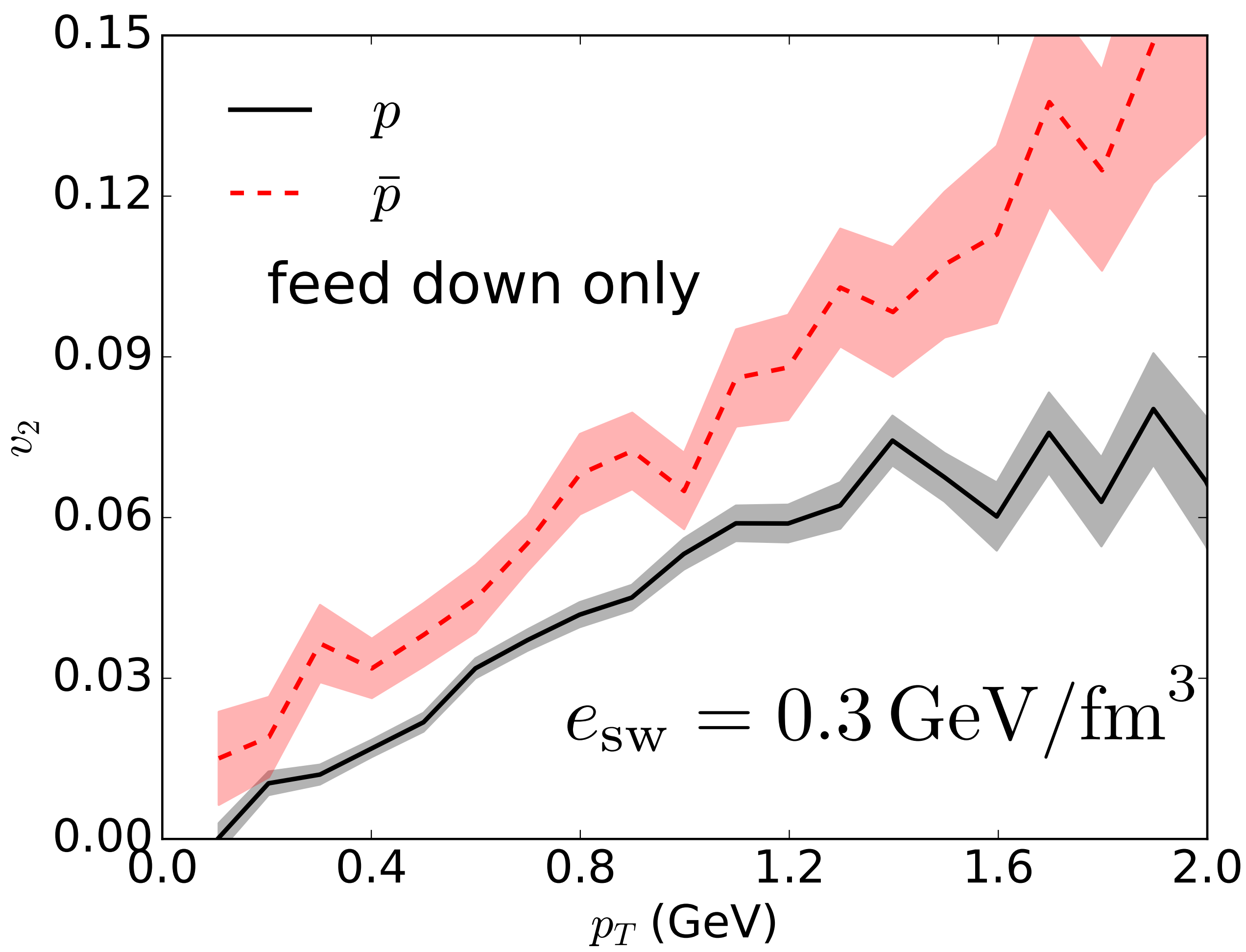

$v_2(p)$ vs $v_2(\bar{p})$

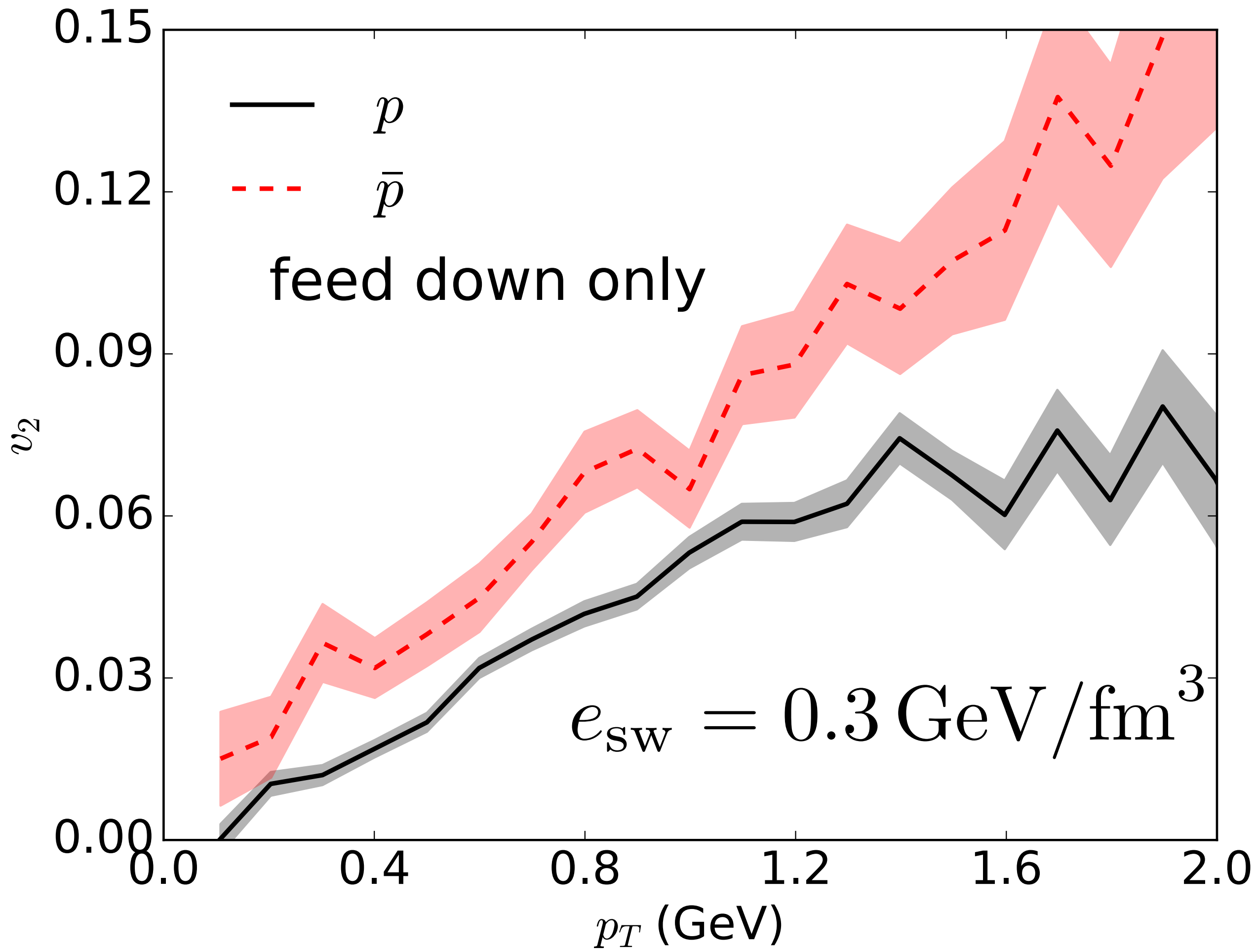

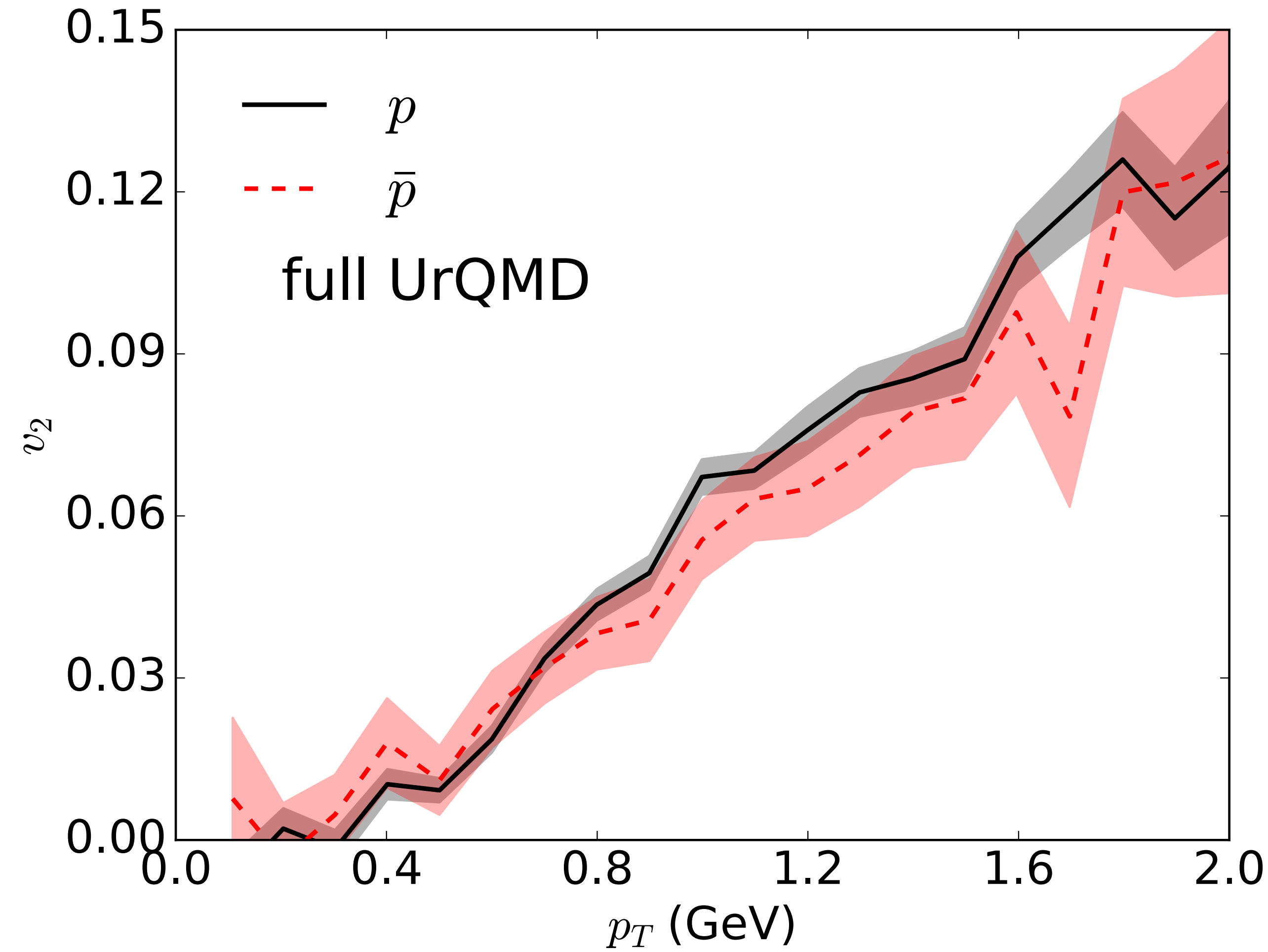

- Late stage hadronic scatterings correct the $v_2(p_T)$ ordering in our hybrid simulations

more statistics is needed

$v_2(p)$ vs $v_2(\bar{p})$

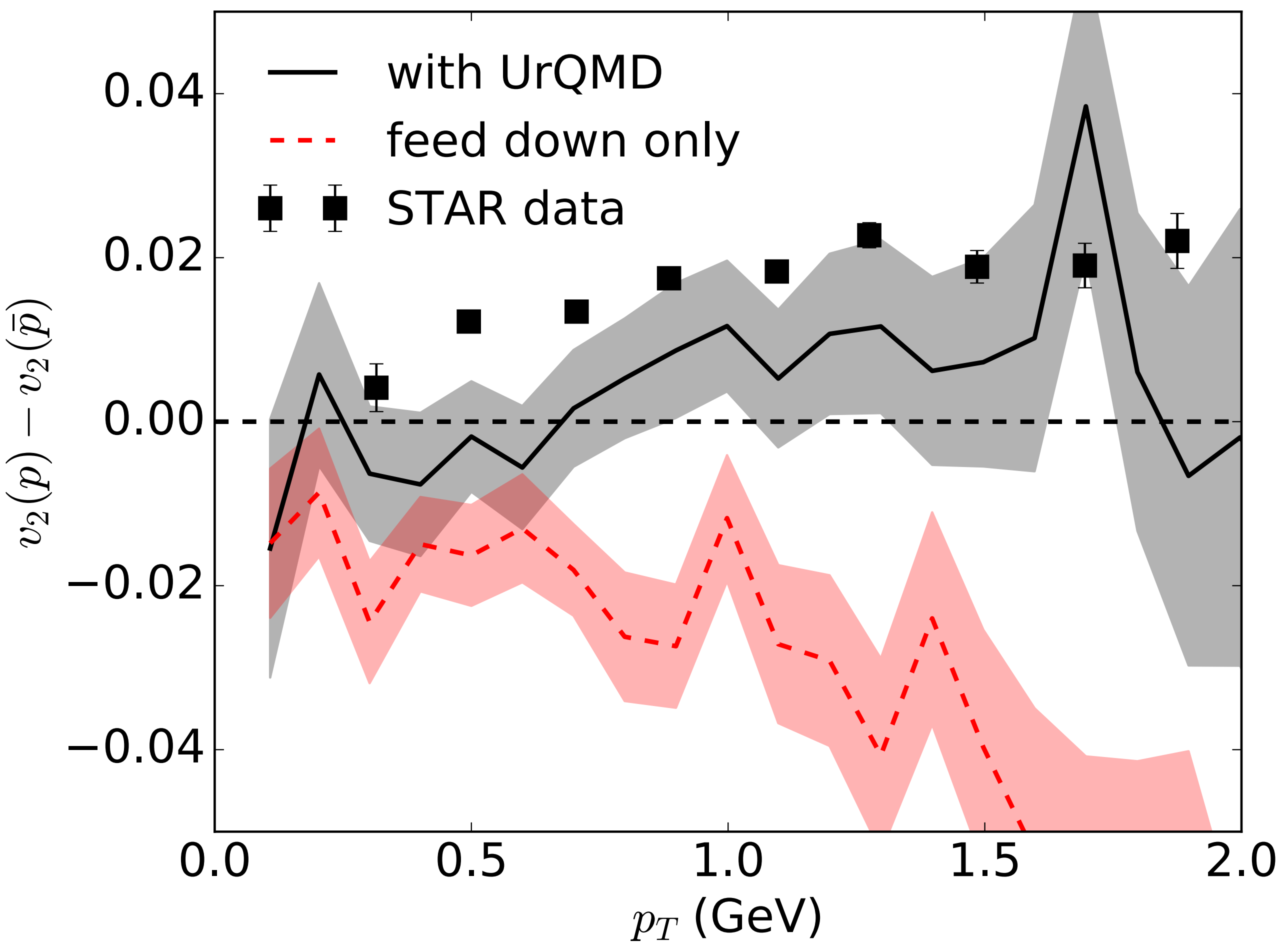

$$e_{\rm sw} = 0.3\,{\rm GeV/fm}^3$$

- Late stage hadronic scatterings correct the $v_2(p_T)$ ordering in our hybrid simulations

more statistics is needed

$v_2(p)$ vs $v_2(\bar{p})$

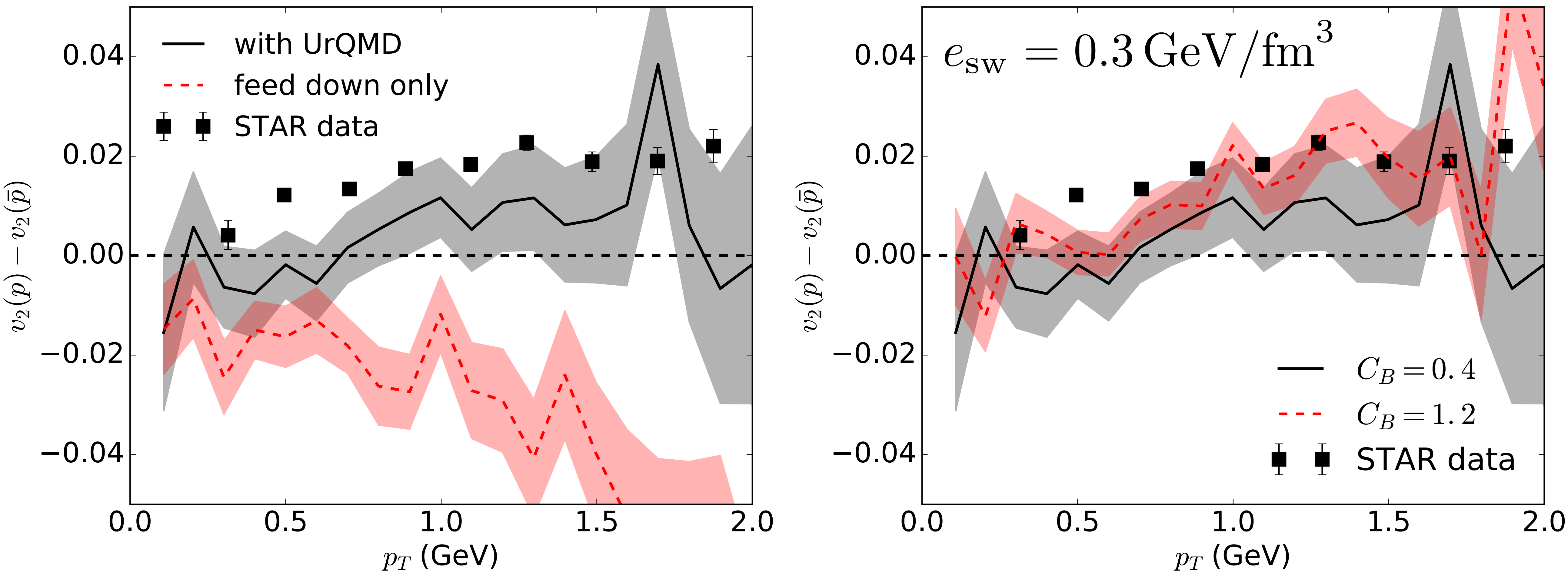

- Late stage hadronic scatterings correct the $v_2(p_T)$ ordering in our hybrid simulations
- A larger net baryon diffusion constant results a larger $v_2(p) - v_2(\bar{p})$

more statistics is needed

Fireball evolution in the QCD phase diagram

Fluctuating

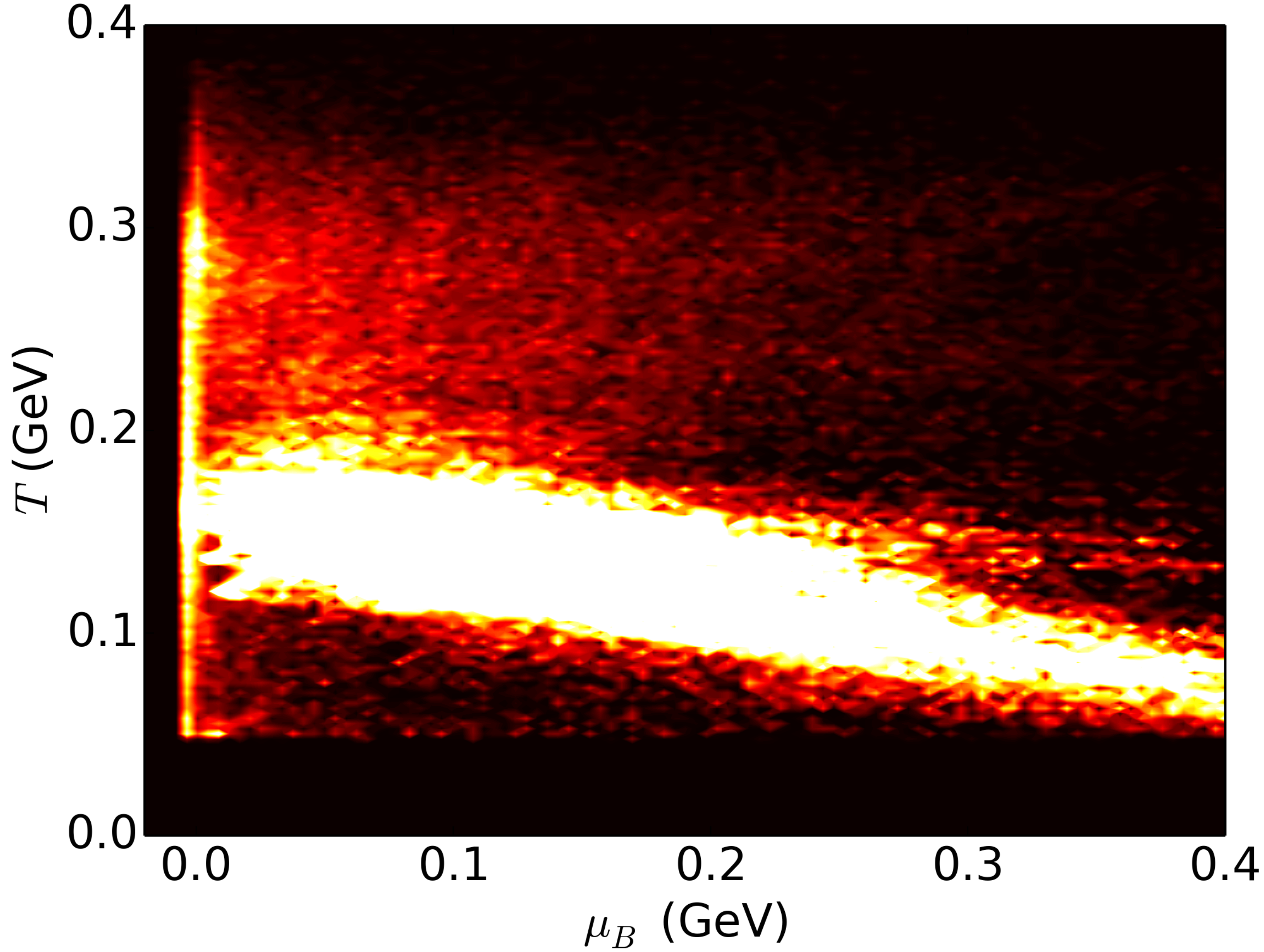

Smooth

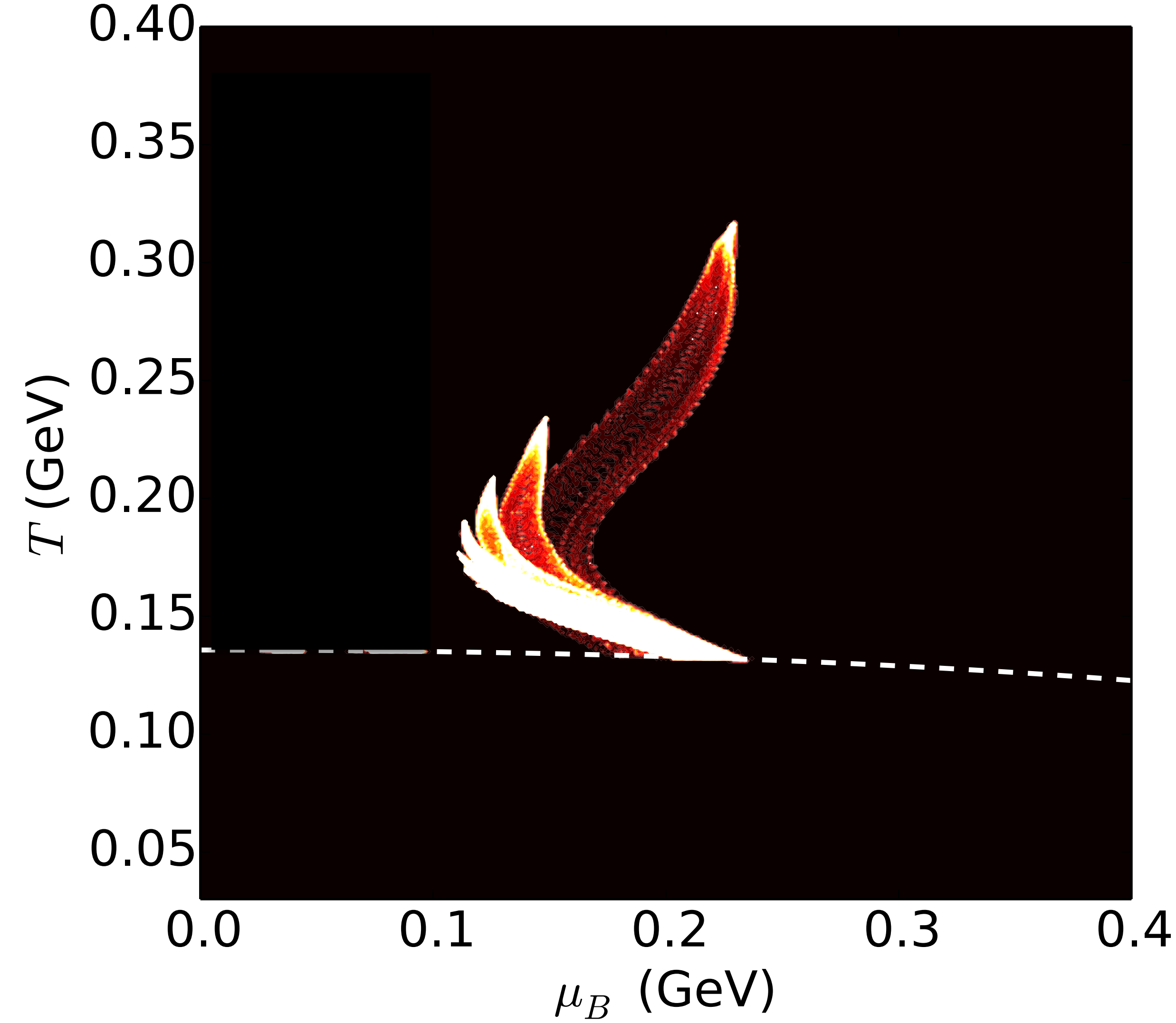

- In the fluctuating case, the hydrodynamic fluid cells are scattered on the phase diagram

A challenge to the search of critical point

Diffusion δf is essential

$$E\frac{dN_i}{d^3p} = \frac{g_i}{(2\pi)^3}\int p^\mu d^3\sigma_\mu(x)(f_0(x,p) + \delta f(x,p))$$

$$f_0^i(x,p) = \frac{1}{e^{(E - b_i \mu_B(x))/T(x)} \pm 1}$$

$$\delta f_0^i(x,p) = f_0^i(x,p)(1 \pm f_0^i(x,p))\left(\frac{n_B}{e+\mathcal{P}} - \frac{b_i}{E}\right)\frac{p\cdot q}{\hat{\kappa}}$$

$$N^B - N^{\bar{B}} = \int d^3\sigma_\mu \sum \frac{g_i}{(2\pi)^3}\int_p p^\mu \left[(f_0^B(x,p) - f_0^{\bar{B}}(x,p)) + (\delta f^B(x,p) - \delta f^{\bar{B}}(x,p))\right]$$

$$= \int d^3\sigma_\mu (n_B u^\mu + q^\mu)$$

$$\partial_\mu (n_B u^\mu + q^\mu) = 0$$

→ $N^B - N^{\bar{B}}$ is conserved

- With diffusion, δf is essential to ensure net baryon number conservation

Diffusion δf is essential

$$E\frac{dN_i}{d^3p} = \frac{g_i}{(2\pi)^3}\int p^\mu d^3\sigma_\mu(x)(f_0(x,p) + \delta f(x,p))$$

$$f_0^i(x,p) = \frac{1}{e^{(E-b_i\mu_B(x))/T(x)} \pm 1}$$

$$\delta f_0^i(x,p) = f_0^i(x,p)(1 \pm f_0^i(x,p))\left(\frac{n_B}{e+\mathcal{P}} - \frac{b_i}{E}\right)\frac{p\cdot q}{\hat{\kappa}}$$

$$N^B - N^{\bar{B}} = \int d^3\sigma_\mu \sum \frac{g_i}{(2\pi)^3}\int_p p^\mu \left[(f_0^B(x,p \quad \ldots \quad x,p))\right]$$

$$= \int d^3\sigma_\mu(n_B u^\mu + q^\mu)$$

$$\partial_\mu(n_B u^\mu + q^\mu) = 0$$

Conservation laws (net baryon number and total energy) are checked at every time step; the relative violation is below 1×10^{-5}

- With diffusion, δf is essential to e
  conservation

Baryon diffusion constant

$$N^\mu_Q = \sum_{i=1}^{N} g_i Q_i \int dK_i k_i^\mu f_k^i,$$

Relaxation time approximation

$$q^\mu_B = \sum_{i=1}^{N} g_i b_i \int dK_i k_i^{\langle\mu\rangle} \delta f_k^i$$

$$q^\mu_B = \kappa_B \nabla^\mu \alpha_B = \tau_R \hat{\kappa}_B \nabla^\mu \alpha_B$$

$$\hat{\kappa}_B = \frac{1}{3} \Delta_{\mu\nu} \sum_{i=1}^{N} g_i b_i \int dK_i k_i^\nu k_i^\alpha f_{ik}^{(0)} \tilde{f}_{ik}^{(0)} \left[\frac{n_B}{e+P} - \frac{b_i}{E_{ik}} \right]$$

$$\kappa_B = \frac{C_B}{T} n_B \left(\frac{1}{3} \coth(\alpha_B) - \frac{n_B T}{e + \mathcal{P}} \right).$$

Initialize MUSIC with 3D density profiles

MC-Glauber model:

$$s(x, y, \eta; \tau_0) = \frac{s_0}{\tau_0} \sum_{i=\pm} f_i^s(\eta) s_i(x, y), \quad \rho_B(x, y, \eta; \tau_0) = \frac{1}{\tau_0} \sum_{i=\pm} f_i^{\rho_B}(\eta) s_i(x, y).$$

$$s_i(r, \phi) = \sum_{j=1}^{N^i_{\rm part}} \frac{1}{2\pi\sigma^2} \exp\left(-\frac{(\mathbf{r} - \mathbf{r_j})^2}{2\sigma^2}\right)$$

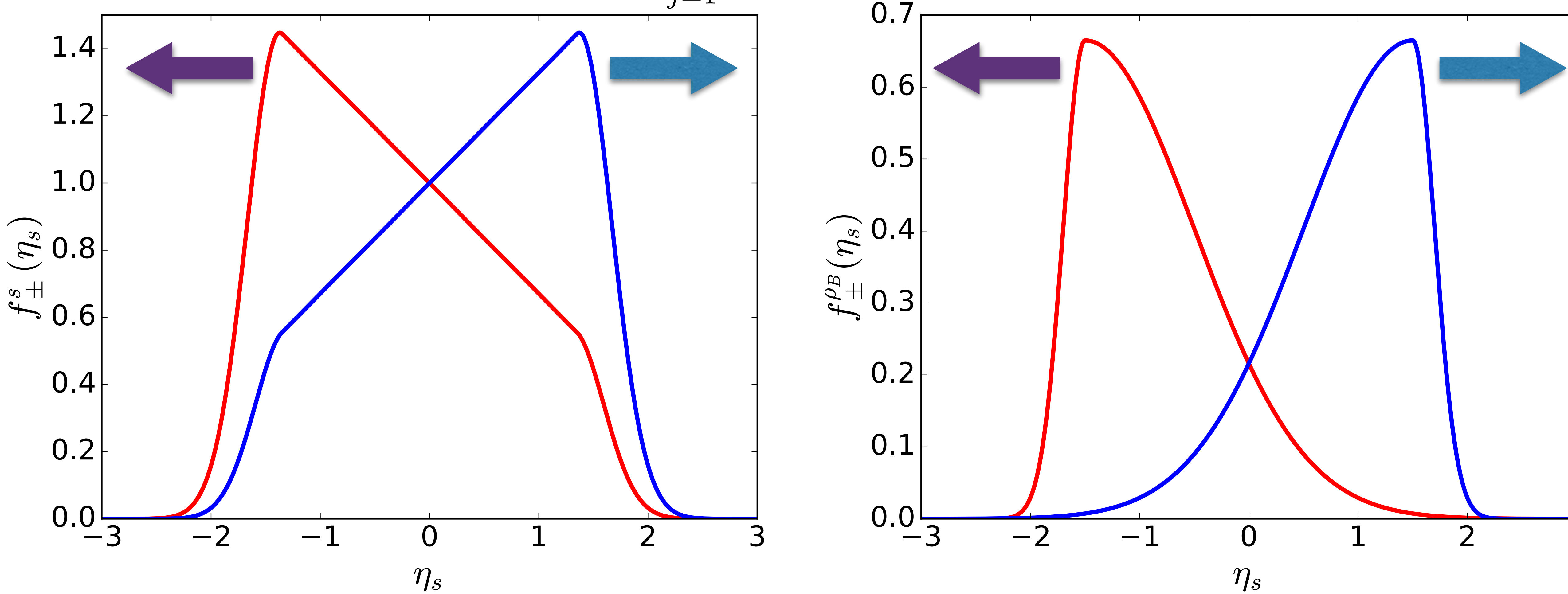

In every event, the net baryon number is

$$\int \tau_0 d\eta_s \int d^2\mathbf{x}_\perp \rho_B(\mathbf{x}_\perp, \eta_s) = N_{\rm part}.$$

Rapidity dependence of particle yield

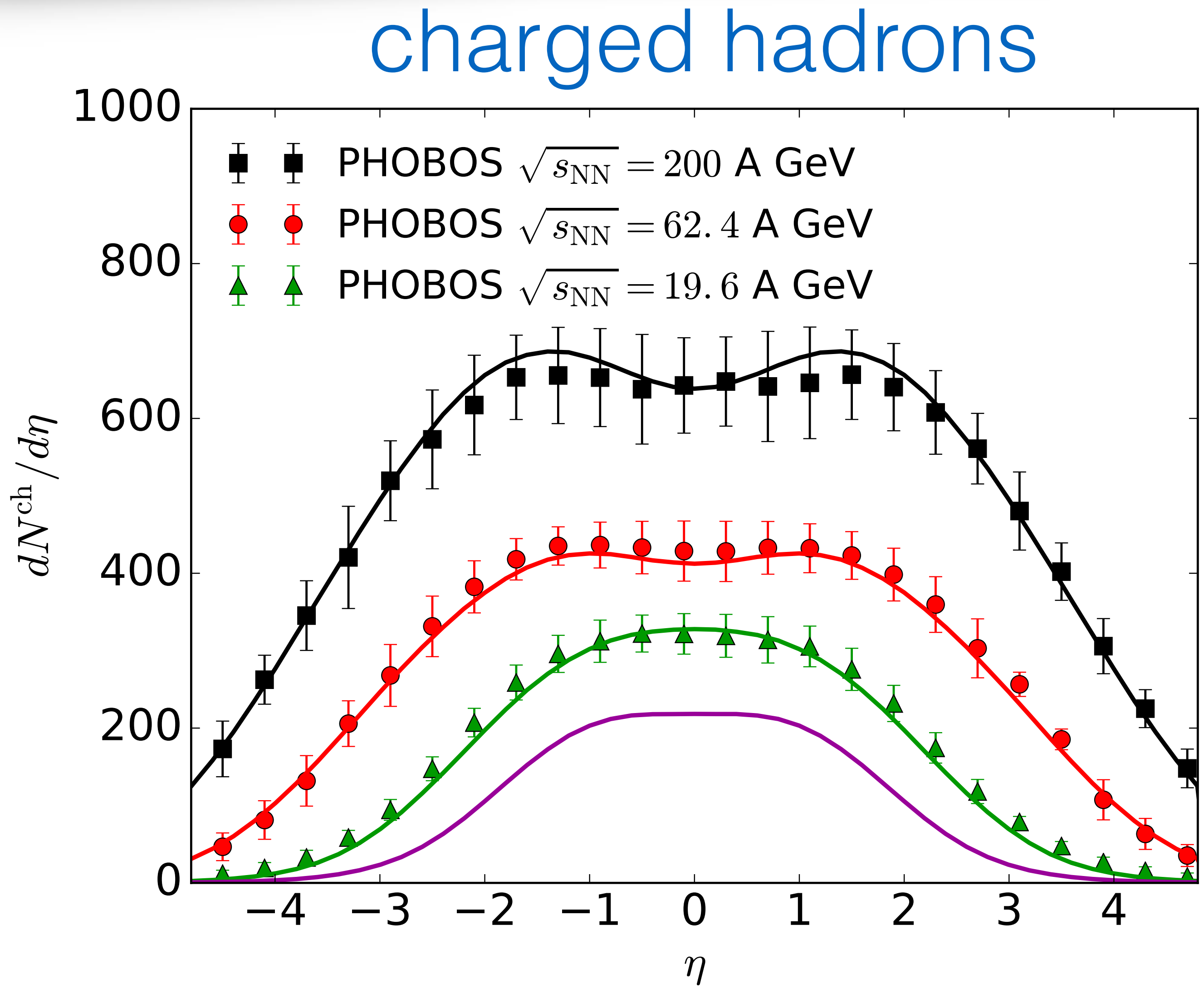

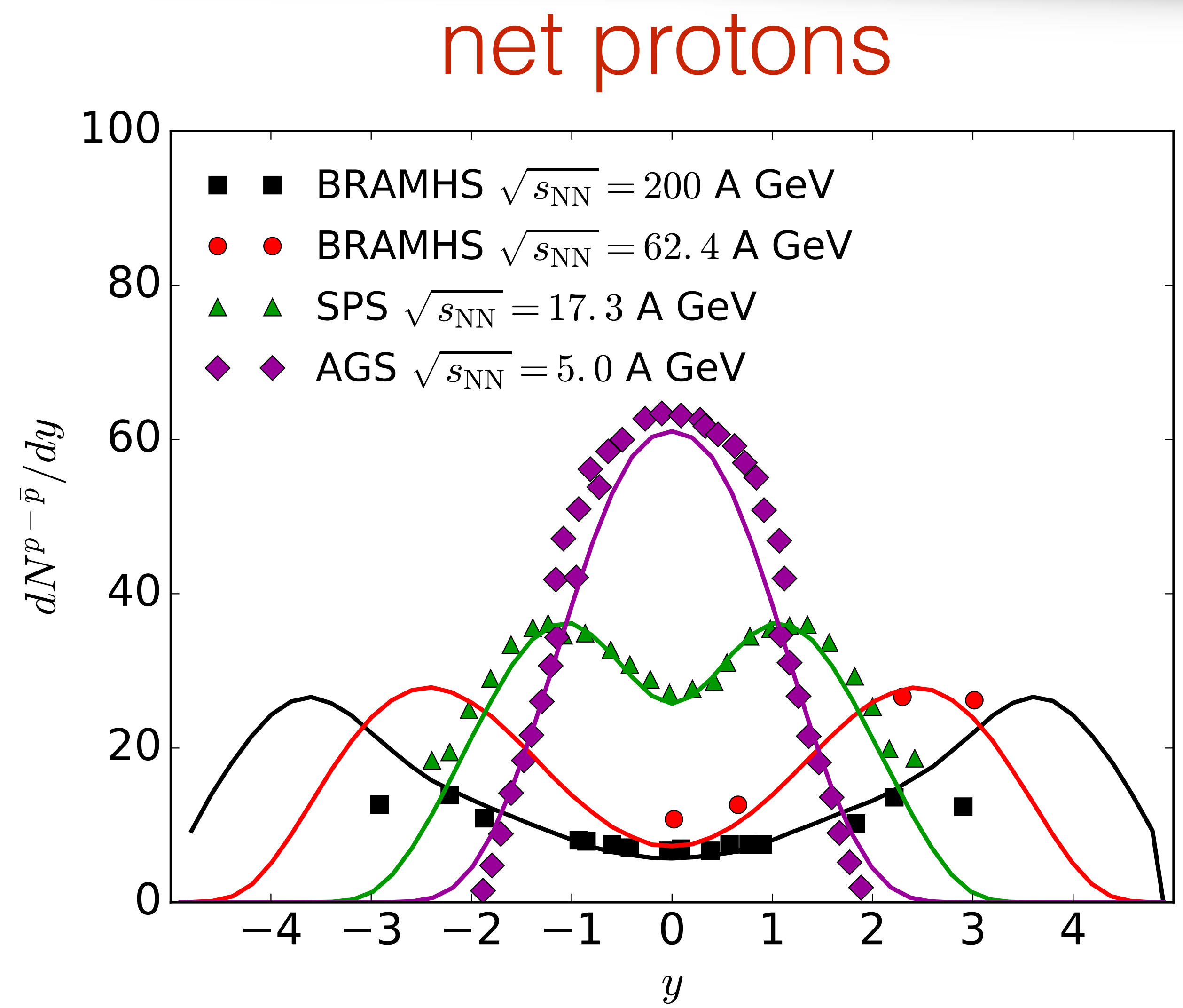

- Full (3+1)-d simulations with net baryon current and its diffusion
- Initial longitudinal profiles are tuned to reproduce the measured (pseudo)-rapidity distributions for charged hadrons and net protons

Effects of net baryon diffusion on pid v_2

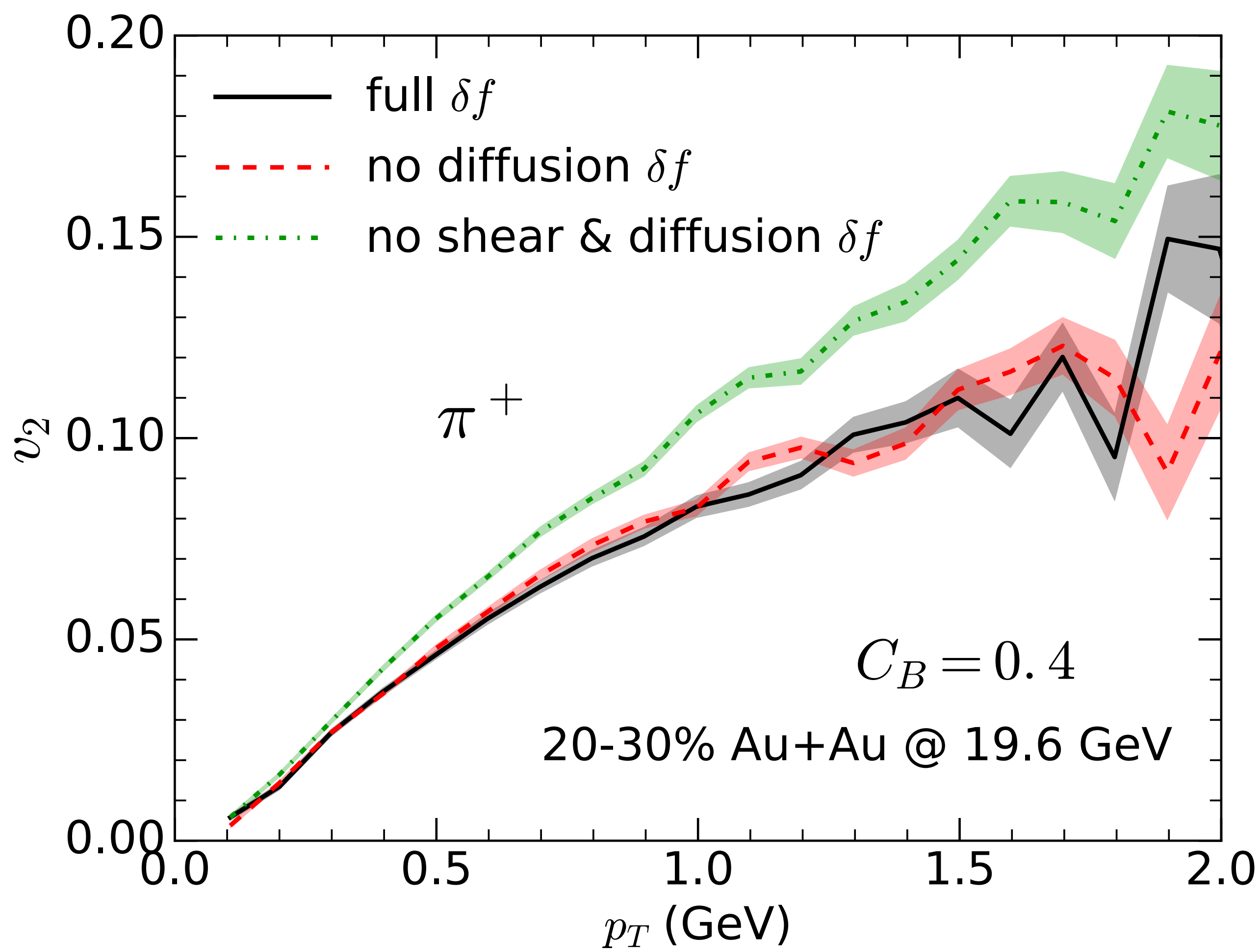

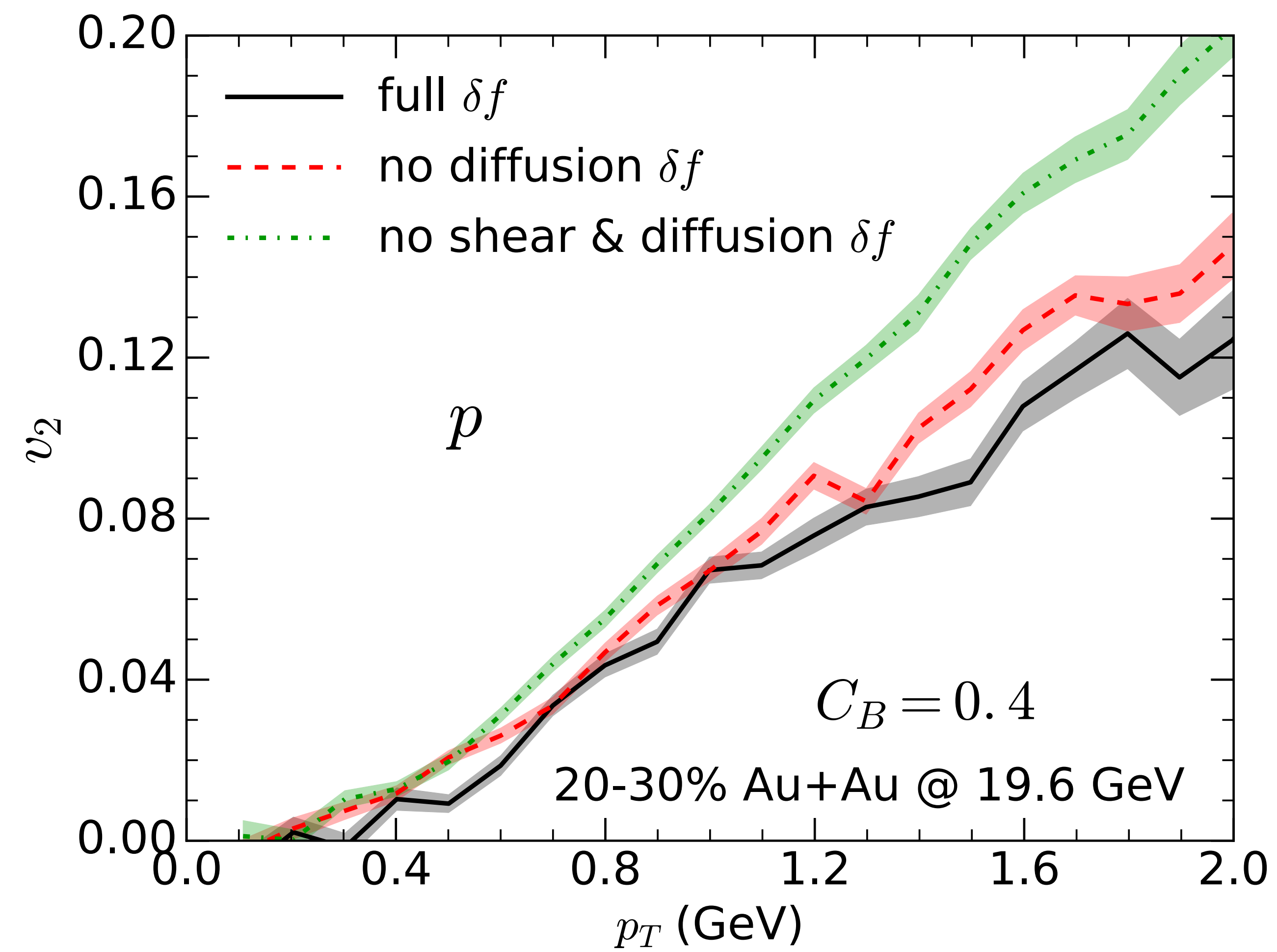

- Identified particles v_2 are more sensitive to shear out-of-equilibrium corrections

Compass for the QCD phase diagram

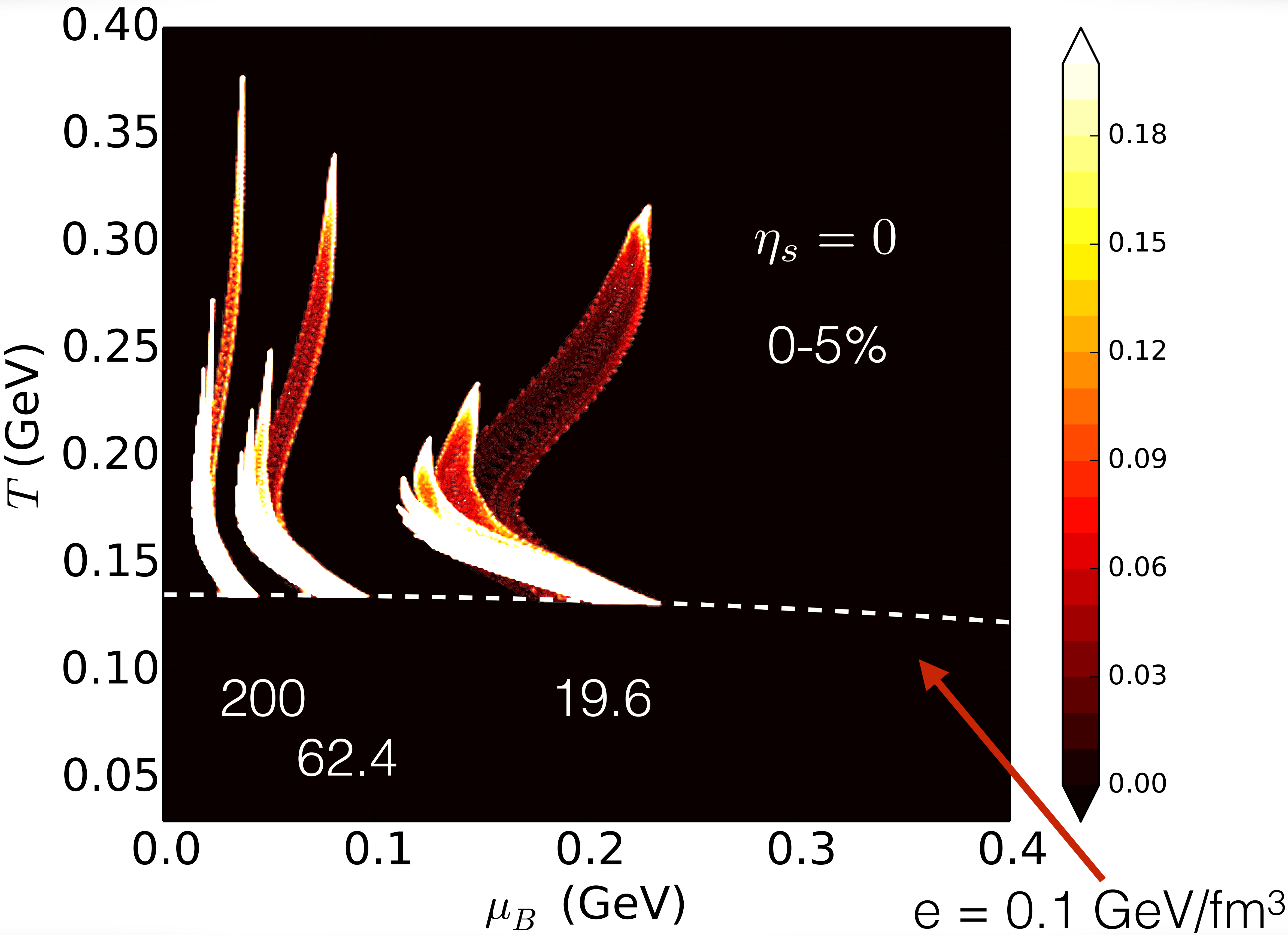

Effects of net baryon diffusion on particle yields

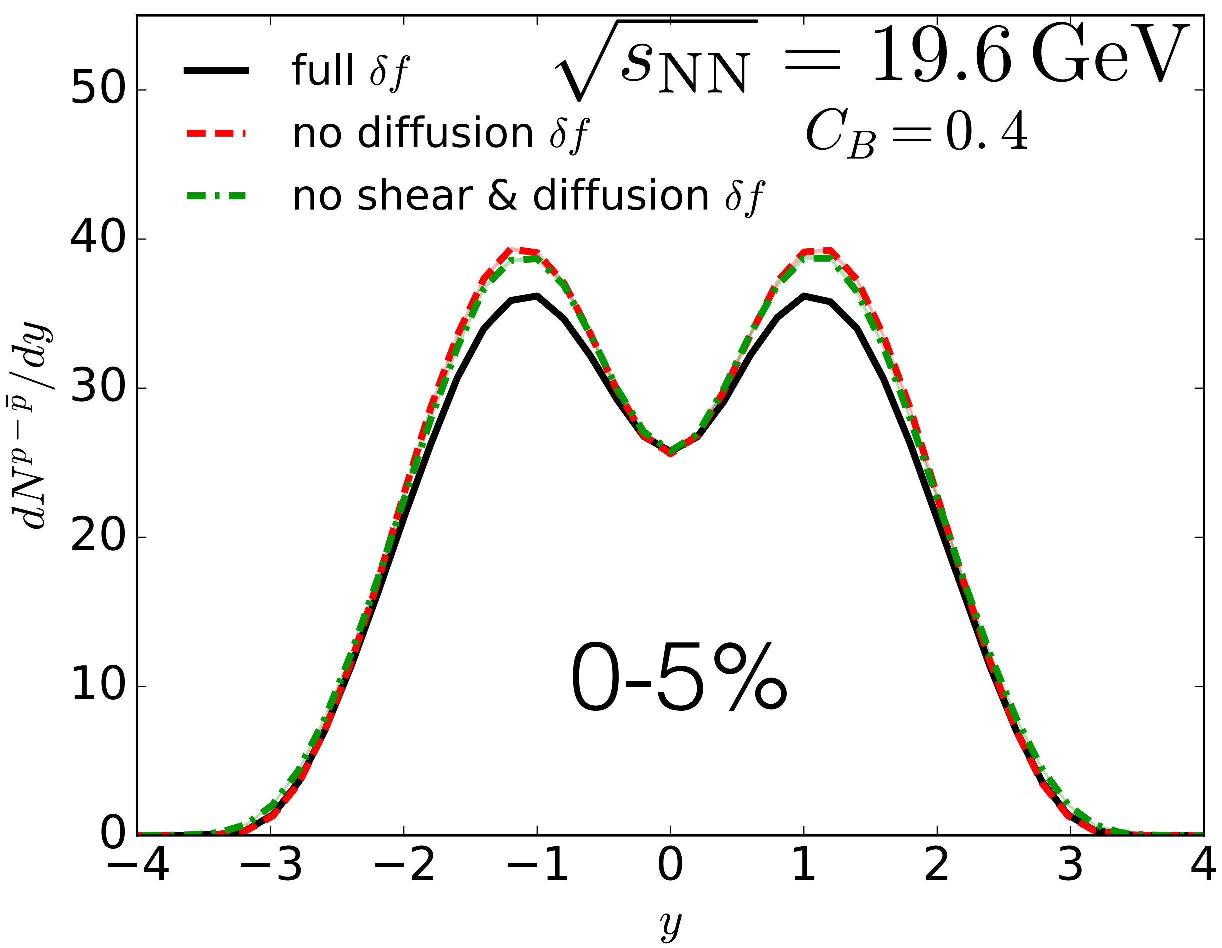

On the switching hyper-surface,

	$C_B = 0.0$	$C_B = 0.4$	$C_B = 1.2$
$\langle \mu_B \rangle$ (GeV)	0.245	0.260	0.276
σ_{μ_B} (GeV)	0.092	0.075	0.069

- The diffusion δf **changes** the net proton number
- Larger diffusion constant results a ~30 MeV larger averaged chemical potential on the switching hyper-surface;
  It reduces the standard deviation of μ_B by ~25%

mapping the QCD phase diagram in precision